

Electrochemical Analyses of Etchants Used to
Detect Sensitization in Marine-Grade
5XXX Aluminum-Magnesium Alloys

A Thesis

Presented to the Faculty of the School of Engineering and Applied Science
University of Virginia

In Partial Fulfillment of the
Requirements for the Degree of
Master of Science (Materials Science and Engineering)

by

Joelle Buczynski

December 2012

APPROVAL SHEET

The dissertation is submitted in partial fulfillment of the
requirements for the degree of
Master of Science (Materials Science and Engineering)

Joelle Buczynski
(Author)

This dissertation has been read and approved by the examining Committee:

Dr. Robert G. Kelly
(Thesis Advisor)

Dr. John R. Scully
(Committee Chair)

Dr. Gary Koenig
(Committee Member)

Dr. Elissa Bumiller
(Committee Member)

Accepted for the School of Engineering and Applied Science:



Dean
School of Engineering and Applied Science

December 2012

ABSTRACT

The 5XXX series aluminum-magnesium alloys (AA5XXX) are susceptible to intergranular corrosion (IGC) in marine environments due to the preferential precipitation and dissolution of the β -phase (Al_3Mg_2) at grain boundaries. Detecting sensitization, or the presence and extent of grain boundary precipitation, contributes to the determination of IGC susceptibility and the prediction of intergranular stress corrosion cracking (IGSCC) propagation in IGC-susceptible materials. Etchants such as concentrated nitric acid, 40 vol% phosphoric acid, and acidified ammonium persulfate are used to detect sensitization in AA5XXX via selective attack of the β -phase. The objective of this work was to characterize the selectivity of these etchants by assessing the corrosion behaviors of the bulk alloy (AA5083) and pure β -phase during etchant exposure. Methods used to analyze corrosion behavior included open circuit potential (OCP) etching, 24-hour mass loss tests according to ASTM G67, and anodic polarization scans. Ammonium persulfate was found to exhibit the highest selectivity amongst the etchants over the range of sensitization conditions, surface orientations (LT, LS), and exposure temperatures considered in this study.

ACKNOWLEDGMENTS

This thesis would not exist without the guidance and encouragement of my advisor, Rob Kelly. I am so grateful for this opportunity, and I can't express enough appreciation for your insight and humor that helped balance the oft-frustrating uncertainties of graduate life. I can move confidently forward to new experiences knowing that I faced and met the challenges of our research with critical thinking, common sense, and a lot of nitric acid. Thank you for your investment. I hope to not depreciate as much as my brand new retirement account already has.

Thank you to my committee – to Dr. Scully, for teaching me electrochemistry and to never underestimate the power of hydrogen – to Dr. Koenig, for lending your time and perspective on short notice even if you asked the most difficult questions – and to Dr. (!) Bumiller, for believing that it was all worth it and worth your while.

Appreciation is also due to Dr. Shiflet, who made our β -phase samples right the very first time he tried, and to Barry Baber, for keeping things running.

And a big thank you goes to the students in CESE: especially to my officemates (Rebecca Schaller, Elissa Bumiller, Mary Lyn Lim, Cindy Shi, and Derek Horton), who reminded me to stop staring out the window and finish my homework, and to those on the AA5XXX project (Mary Lyn Lim, Cortney Crane, Elissa Bumiller, Lei Chen, and Daisuke Mizuno) – thank you for your wisdom and support, and best of luck with the β -phase and beyond.

My work is dedicated to my family, past, present, and future – I would not be where I am without you (and I don't mean in central Virginia). Thank you for your love and good cheer. And most of all, thank you to my three wise men: Jaj, Dad, and Joe. You make hard work look easy and good things possible, and of that, I will always be mindful.

J.B.

12.12.12

TABLE OF CONTENTS

Approval Sheet	ii
Abstract	iii
Acknowledgements	iv
Table of Contents	v
List of Tables	viii
List of Figures	ix
List of Symbols	xiv
1 Background and Objectives	16
1.1 Motivation	16
1.2 Metallurgy of 5XXX Aluminum-Magnesium Alloys (AA5XXX)	16
1.2.1 Composition and Processing	16
1.2.2 β -phase Precipitation	17
1.3 Intergranular Corrosion (IGC) of AA5XXX	18
1.3.1 Thermodynamics of Aluminum and Magnesium Dissolution	18
1.3.2 Preferential Dissolution of β -phase	19
1.4 Detection of Sensitization in AA5XXX	19
1.4.1 Determining IGC Susceptibility via Mass Loss	20
1.4.1.1 ASTM G67 Standard Test Method for Determining Susceptibility to Intergranular Corrosion of 5XXX Series Aluminum Alloys by Mass Loss After Exposure to Nitric Acid (NAMLT Test)	20
1.4.1.2 ASTM B928 Standard Specification for High Magnesium Aluminum-Alloy Sheet and Plate for Marine Service and Similar Environments	21
1.4.2 Determining IGC Susceptibility via Etching	21
1.5 Critical Unresolved Issues	21
1.6 Objectives	23
2 Materials	24
2.1 5XXX Alloys	24
2.1.1 Chemical Composition	24
2.1.2 Microstructure	24
2.1.3 Solution Heat-Treatment	25
2.1.4 Artificial Sensitization and Sensitization Condition	26
2.1.5 Degree of Sensitization (DoS)	26
2.2 β -Phase	27
2.2.1 Synthesis of β -Phase	27
2.2.2 Characterization of β -Phase	28
2.2.2.1 XRD	28

2.2.2.2	Optical Microscopy	29
2.2.2.3	PIXE	30
2.2.2.4	SEM and EDS	31
3	Experimental Methods	33
3.1	Etchant Environments	33
3.1.1	Nitric Acid	33
3.1.2	Phosphoric Acid	33
3.1.3	Ammonium Persulfate	34
3.2	Corrosion Testing and Electrochemical Analyses	34
3.2.1	Short-Term Open Circuit Potential (OCP) Etching of AA5XXX for Screening	34
3.2.1.1	Materials and Sample Preparation	34
3.2.1.2	Etchant Chemistries	35
3.2.1.3	Exposure Temperatures and Times	35
3.2.1.4	Screening Assessment	36
3.2.2	Mass Loss of AA5XXX after 24-Hour Immersion in Etchants to Quantify Degree of Sensitization	36
3.2.2.1	Materials and Sample Preparation	36
3.2.2.2	Exposure Environments	37
3.2.2.3	Grain Fallout and Mass Loss Measurements	37
3.2.2.4	Calculation of Corrosion Current Densities	38
3.2.3	Damage Penetration Assessment of AA5XXX after 24-Hour Immersion in Etchants to Compare Morphology of Attack	39
3.2.3.1	Materials and Damage Morphology	39
3.2.3.2	Quantification of Damage Depth	39
3.2.3.3	ICP Analysis of Etchant Solutions	40
3.2.4	Anodic Polarization of β -Phase and AA5XXX Matrix to Quantify Etchant Selectivity	41
3.2.4.1	Materials and Sample Preparation	41
3.2.4.2	Electrolyte Environment	41
3.2.4.3	Polarization Parameters	42
3.2.4.4	Quantification of Etchant Selectivity	43
4	Results	45
4.1	Short-term Open Circuit Potential Etching of AA5XXX	45
4.1.1	OCP Immersion Etching in Nitric Acid	46
4.1.2	OCP Immersion Etching in Phosphoric Acid	51
4.1.3	OCP Immersion Etching in Ammonium Persulfate	56
4.2	Mass Loss and Damage Penetration in AA5XXX after 24-Hour Immersion in Etchants	59
4.2.1	Mass Loss and Degree of Sensitization	59
4.2.2	Mass Loss Rates / Corrosion Current Densities	60

4.2.3	Damage Morphology	61
4.2.3.1	Material Loss and Damage Penetration in L-Direction	64
4.2.3.2	Material Loss and Damage Penetration in T-Direction	67
4.2.3.3	Material Loss and Damage Penetration in S-Direction	73
4.2.3.4	Average Damage Site Depth and Specimen Dimension Changes	75
4.2.4	Dissolved Species in Etchant Solutions	80
4.3	Anodic Polarization of β -Phase and AA5XXX	83
4.3.1	Anodic Polarization Scans in Nitric Acid	84
4.3.2	Anodic Polarization Scans in Phosphoric Acid	85
4.3.3	Anodic Polarization Scans in Ammonium Persulfate	87
4.3.3.1	pH 1.2 Ammonium Persulfate	87
4.3.3.2	pH 0.7 Ammonium Persulfate	88
4.3.4	Etchant Selectivity (Ratio of Current Densities at the OCP of the matrix)	90
4.4	Summary of Testing and Results	93
4.4.1	Characterization of Etchant Selectivity	93
4.4.2	Selectivity of Nitric Acid	94
4.4.3	Selectivity of Phosphoric Acid	94
4.4.4	Selectivity of Ammonium Persulfate	95
5	Discussion	96
5.1	Material Properties	96
5.1.1	Sensitization Condition	96
5.1.2	Orientation	97
5.1.3	Constituent Particles	98
5.1.4	Surface Finish	99
5.2	Etchant Environment	99
5.2.1	Exposure Temperature	99
5.2.2	Etchant Chemistry	103
5.3	Accuracy, Precision, and Bias of Standardized Testing Methods for IGC Susceptibility	105
6	Conclusions	106
7	Future Work	108
	References	109
	Appendices	112
	Appendix A: β -Phase XRD Characterization Results	112
	Appendix B: Damage Site Depth Distributions and Micrographs	113
	Appendix C: Anodic Polarization Scans in Etchants from 15°C-50°C	128
	Appendix D: Summary of and Ranking of Etchant Selectivity	135

LIST OF TABLES

Table 2.1	Chemical composition of AA5083 (UNS A95083) in wt%	24
Table 2.2	Chemical composition of synthesized β -phase determined via PIXE	30
Table 3.1	Etching duration for AA5083 samples in concentrated nitric acid, phosphoric acid, and ammonium persulfate (pH 1.2) at 22°C, 30°C, and 35°C	35
Table 3.2	Specification detection limits of ICP-OES instrument in parts per million (ppm).....	40
Table 4.1	Summary of mass loss results after immersion in etchants for 24 hours	59
Table 4.2	Current densities calculated from mass loss measurements after exposure to etchants for 24 hours	61
Table 4.3	Summary of mass loss and damage penetration results after exposure to etchants for 24 hours	80
Table 4.4	Average concentration (ppm) and concentration ratios (ppm/ppm) of dissolved species from AA5083 after 24-hour immersion in etchants via ICP spectrometry analysis. NA = nitric acid, PA = phosphoric acid, and AP = 0.7 ammonium persulfate	81
Table 4.5	Electrochemical Properties from Anodic Polarization Data for AA5083-SHTQ and β -Phase Specimens	92
Table 5.1	The activation energy (Q) calculated from the slope of the Arrhenius plots in Figures 5.2-5.4.....	101
Table B.1	Damage site depth distribution data for AA5083 of varying sensitization conditions exposed to nitric acid for 24 hours at 35°C	113
Table B.2	Damage site depth distribution data for AA5083 of varying sensitization conditions exposed to phosphoric acid for 24 hours at 35°C	118
Table B.3	Damage site depth distribution data for AA5083 of varying sensitization conditions exposed to ammonium persulfate for 24 hours at 35°C	123
Table D.1	Summary of results from short-term, OCP etching tests and characterization of etchant selectivity	135
Table D.2	Summary of results from 24-hr mass loss test and characterization of etchant selectivity.....	135
Table D.3	Summary of results from damage assessment following 24-hr mass loss test and characterization of etchant selectivity	136
Table D.4	Summary of results from species dissolution assessment following 24-hr mass loss test and characterization of etchant selectivity	136
Table D.5	Summary of results from anodic polarization tests and characterization of etchant selectivity	137

LIST OF FIGURES

Figure 1.1	The Al-Mg binary phase diagram [ASM] with the β -phase field shaded (~36-38 wt% Mg).....	17
Figure 1.2	Pourbaix diagram of aluminum at 25°C with the stability regions of magnesium superimposed. Regions of passivation and dissolution are highlighted [reproduced from Bumiller].....	19
Figure 2.1	Microstructure of an AA5083-H131 specimen revealed after electrolytic Barker's etching.....	25
Figure 2.2	A section of the Aluminum-Magnesium phase diagram.....	25
Figure 2.3	Average NAMLT mass loss values of AA5083 exposed to nitric acid for 24 hours at 30°C.....	26
Figure 2.4	Induction furnace setup used to synthesize pure β -phase specimens.....	28
Figure 2.5	(a) Powder diffraction file (PDF) of β -phase with α and γ -phase peaks overlaid (b) X-ray diffraction pattern of synthesized β -phase.....	29
Figure 2.6	Optical micrograph of synthesized β -phase specimen after etching with 10vol/vol% phosphoric acid.....	30
Figure 2.7	(a) SEM micrograph of an impurity in synthesized β -phase revealed after electrochemical testing (b) the associated EDS line scan spectra.....	31
Figure 3.1	Schematic of a specimen cut from the center (S/2) of an as-received AA5083 plate for mass loss testing (shown to scale).....	37
Figure 3.2	Schematic of an electrochemical flat cell used in anodic polarization experiments.....	43
Figure 4.1	Organization of post-OCP-immersion micrographs in Figures 4.2 – 4.11.....	45
Figure 4.2	Optical micrographs of LS surface of AA5083 of varying sensitization conditions after 60 minute immersion in nitric acid at: 22°C (a)-(c), 30°C (d)-(f), and 35°C (g)-(i).....	47
Figure 4.3	Optical micrographs of LT surface of AA5083 of varying sensitization conditions after 60 minute immersion in nitric acid at: 22°C (a)-(c), 30°C (d)-(f), and 35°C (g)-(i).....	48
Figure 4.4	Optical micrographs of LS surface of AA5083 of varying sensitization conditions after 90 minute immersion in nitric acid at: 22°C (a)-(c), 30°C (d)-(f), and 35°C (g)-(i).....	49
Figure 4.5	Optical micrographs of LT surface of AA5083 of varying sensitization conditions after 90 minute immersion in nitric acid at: 22°C (a)-(c), 30°C (d)-(f), and 35°C (g)-(i).....	50
Figure 4.6	Optical micrographs of LS surface of AA5083 of varying sensitization conditions after 3 minute immersion in phosphoric acid at: 22°C (a)-(c), 30°C (d)-(f), and 35°C (g)-(i).....	52
Figure 4.7	Optical micrographs of LT surface of AA5083 of varying sensitization conditions after 3 minute immersion in phosphoric acid at: 22°C (a)-(c), 30°C (d)-(f), and 35°C (g)-(i).....	53
Figure 4.8	Optical micrographs of LS surface of AA5083 of varying sensitization conditions after 10 minute immersion in phosphoric acid at: 22°C (a)-(c), 30°C (d)-(f), and 35°C (g)-(i).....	54
Figure 4.9	Optical micrographs of LT surface of AA5083 of varying sensitization conditions after 10 minute immersion in phosphoric acid at: 22°C (a)-(c), 30°C (d)-(f), and 35°C (g)-(i).....	55
Figure 4.10	Optical micrographs of LS surface of AA5083 of varying sensitization conditions after 90 minute immersion in pH 1.2 ammonium persulfate at: 22°C (a)-(c), 30°C (d)-(f), and 35°C (g)-(i).....	57
Figure 4.11	Optical micrographs of LT surface of AA5083 of varying sensitization conditions after 90 minute immersion in pH 1.2 ammonium persulfate at: 22°C (a)-(c), 30°C (d)-(f), and 35°C (g)-(i).....	58

Figure 4.12 Mass loss of AA5083 of varying sensitization conditions exposed to etchants for 24 hours following procedures of ASTM G67	60
Figure 4.13 Organization of post-OCP-immersion micrographs in Figures 4.14 – 4.25	62
Figure 4.14 Digital microscopy images of L-S surface of AA5083 of varying sensitization conditions after 24-hr exposure at 35°C to Nitric Acid, Phosphoric Acid, and Ammonium Persulfate. Grain boundaries along the L-direction (vertical direction) are highly attacked	63
Figure 4.15 Optical micrographs of cross-sectioned AA5083 of varying sensitization conditions after 24-hour exposure at 35°C to etchants: Nitric Acid (a)-(d), Phosphoric Acid (e)-(h), and Ammonium Persulfate (i)-(l). Damage penetration is in the L-direction (vertical direction). The thickness of the 300µm-wide red bar on the top left of each micrograph represents the change in dimension (material loss) from initial measured dimensions.	65
Figure 4.16 Distribution of damage site depths in L-direction after 24-hour exposure to nitric acid at 35°C	66
Figure 4.17 Distribution of damage site depths in L-direction after 24-hour exposure to phosphoric acid at 35°C	66
Figure 4.18 Distribution of damage site depths in L-direction after 24-hour exposure to ammonium persulfate at 35°C	67
Figure 4.19 Optical micrographs of cross-sectioned AA5083 of varying sensitization conditions after 24-hour exposure at 35°C to etchants: Nitric Acid (a)-(d), Phosphoric Acid (e)-(h), and Ammonium Persulfate (i)-(l). Damage penetration is in the T-direction (vertical direction). The thickness of the 300µm-wide red bar on the top left of each micrograph represents the change in dimension (material loss) from initial measured dimensions.	68
Figure 4.20 Optical micrographs of cross-sectioned AA5083 of varying sensitization conditions after 24-hour exposure to Nitric Acid at 30°C and 35°C. Damage penetration is in the T-direction (vertical direction)	69
Figure 4.21 Optical micrographs of cross-sectioned AA5083 after 24-hour exposure at 35°C to nitric acid, phosphoric acid, and ammonium persulfate. SHTQ (a)-(c) and 100°C-30days (d)-(f) samples were etched with Barker’s reagent to highlight the grain structure. Damage penetration is in the T-direction (vertical direction)	70
Figure 4.22 Distribution of damage site depths in T-direction after 24-hour exposure to nitric acid at 35°C	71
Figure 4.23 Distribution of damage site depths in T-direction after 24-hour exposure to phosphoric acid at 35°C	72
Figure 4.24 Distribution of damage site depths in T-direction after 24-hour exposure to ammonium persulfate at 35°C	72
Figure 4.25 Optical micrographs of cross-sectioned AA5083 of varying sensitization conditions after 24-hour exposure at 35°C to etchants: Nitric Acid (a)-(d), Phosphoric Acid (e)-(h), and Ammonium Persulfate (i)-(l). Damage originates in the S-direction (vertical) but follows the L-direction (horizontal). The thickness of the 300µm-wide red bar on the top left of each micrograph represents the change in dimension (material loss) from initial measured dimensions.	74

Figure 4.26 Average damage site depths in L and T-directions as a function of sensitization condition after 24-hour exposure to etchants at 35°C; L-direction series are solid lines, T-direction series are dotted lines	76
Figure 4.27 Average dimension change (material loss) in the L, T, and S-directions as a function of sensitization condition after 24-hour exposure to etchants at 35°C; L-direction series are solid lines, T-direction series are dotted lines, S-direction series are dashed lines	77
Figure 4.28 Average dimension change (material loss) in the L and T-directions as a function of sensitization condition after 24-hour exposure to etchants at 35°C; L-direction series are solid lines, T-direction series are dotted lines	78
Figure 4.29 Average dimension change (material loss) in the L and S-directions as a function of sensitization condition after 24-hour exposure to etchants at 35°C; L-direction series are solid lines, S-direction series are dashed lines	78
Figure 4.30 Average dimension change (material loss) in the S and T-directions as a function of sensitization condition after 24-hour exposure to etchants at 35°C; S-direction series are dashed lines, T-direction series are dotted lines	79
Figure 4.31 Average concentrations (ppm) of dissolved magnesium and aluminum in etchant solutions after 24-hour immersion	82
Figure 4.32 Ratios of dissolved magnesium to dissolved aluminum (ppm/ppm with standard deviations across 12 replicates) in etchant solutions after 24-hour immersion (NA = Nitric Acid, PA = Phosphoric Acid, AP = Ammonium Persulfate). This ratio indicates the extent to which etchants preferentially dissolve magnesium to aluminum and therefore the Mg-rich β -phase relative to the matrix. The ratio of Mg:Al concentrations for congruent, SHTQ-only dissolution is approximately 0.046, while the ratio of Mg:Al concentrations for congruent, β -phase-only dissolution is approximately 0.56-0.61	83
Figure 4.33 Anodic polarization scans of AA5083-SHTQ (LT) and β -phase specimens in Nitric Acid from 15-50°C	84
Figure 4.34 Anodic polarization scans of AA5083-SHTQ specimens in Nitric Acid at 35°C; Scans of the SHTQ LT and LS surfaces after 5 min and 30 min OCP holds are shown	85
Figure 4.35 Anodic polarization scans of AA5083-SHTQ (LT) and β -phase specimens in Phosphoric Acid from 15-50°C	86
Figure 4.36 Anodic polarization scans of AA5083-SHTQ specimens in Phosphoric Acid at 35°C; Scans of the SHTQ LT and LS surfaces after 5 min and 30 min OCP holds are shown	87
Figure 4.37 Anodic polarization scans of AA5083-SHTQ (LT) and β -phase specimens in pH 1.2 Ammonium Persulfate from 15-50°C	88
Figure 4.38 Anodic polarization scans of AA5083-SHTQ specimens in pH 0.7 Ammonium Persulfate at 35°C; Scans of the SHTQ LT and LS surfaces after 5 min and 30 min OCP holds are shown	89
Figure 4.39 Anodic polarization scans of AA5083-SHTQ and β -phase specimens in pH 0.7 Ammonium Persulfate, pH 0.7 Sulfuric Acid, 0.4M Sodium Persulfate, and 0.4M Ammonium Sulfate at 35°C	90
Figure 4.40 Ratios of the current densities of the β -phase and the matrix (SHTQ) at the open circuit potential of the matrix in Nitric Acid, Ammonium Persulfate, and Phosphoric Acid as a function of temperature (15-50°C)	91

Figure 5.1	The change in the difference in open circuit potentials between the matrix and β -phase with increasing temperature, calculated from anodic polarization data. The difference in potentials indicates the thermodynamic driving force for the dissolution of the β -phase at the OCP of the alloy. Phosphoric acid environments have the highest driving force for dissolution and nitric acid environments have the lowest driving force for dissolution. The differences in OCP are relatively stable with temperature in both environments. Ammonium persulfate has a high driving force for dissolution that slightly increase with temperature.....	101
Figure 5.2	Arrhenius plot of the corrosion rates for AA5083-H131-SHTQ and the β -phase in concentrated nitric acid for selected potentials in the passive current region of the anodic polarization curve. The slope of the rates as a function of inverse temperature indicates the activation energy.....	102
Figure 5.3	Arrhenius plot of the corrosion rates for AA5083-H131-SHTQ and the β -phase in phosphoric acid for selected potentials in the passive current region of the anodic polarization curve. The slope of the rates as a function of inverse temperature indicates the activation energy.....	102
Figure 5.4	Arrhenius plot of the corrosion rates for AA5083-H131-SHTQ and the β -phase in pH 1.2 ammonium persulfate for selected potentials in the passive current region of the anodic polarization curve. The slope of the rates as a function of inverse temperature indicates the activation energy.	103
Figure 5.5	Effect of pH on corrosion of aluminium [Reproduced from 14]. (a) acetic acid, (b) hydrochloric acid, (c) hydrofluoric acid, (d) nitric acid, (e) phosphoric acid, (f) sulphuric acid, (g) ammonium hydroxide, (h) sodium carbonate, (i) sodium disilicate, (j) sodium hydroxide.	104
Figure 5.6	Etchant solutions after 24-hour mass loss testing prior to ICP analyses. From left to right in the image: Nitric Acid SHTQ – 7 Days – 14 Days – 30 Days, Phosphoric Acid SHTQ – 7 Days – 14 Days – 30 Days, Ammonium Persulfate SHTQ – 7 Days – 14 Days – 30 Days.	105
Figure A.1	XRD PDFs for (a) γ -phase (b) α -phase and (c) β -phase and the (d) diffraction pattern for synthesized β	112
Figure B.1	Optical images of cross-sectioned AA5083 SHTQ samples showing damage penetration in the: (a) L-direction and (b) T-direction that were used to determine the number of damage sites and their depths after 24-hour exposure to nitric acid at 35°C	114
Figure B.2	Optical images of cross-sectioned AA5083 100°C-7days samples showing damage penetration in the: (a) L-direction and (b) T-direction that were used to determine the number of damage sites and their depths after 24-hour exposure to nitric acid at 35°C.....	115
Figure B.3	Optical images of cross-sectioned AA5083 100°C-14Days samples showing damage penetration in the: (a) L-direction and (b) T-direction that were used to determine the number of damage sites and their depths after 24-hour exposure to nitric acid at 35°C.....	116
Figure B.4	Optical images of cross-sectioned AA5083 100°C-30days samples showing damage penetration in the: (a) L-direction and (b) T-direction that were used to determine the number of damage sites and their depths after 24-hour exposure to nitric acid at 35°C.....	117
Figure B.5	Optical images of cross-sectioned AA5083 SHTQ samples showing damage penetration in the: (a) L-direction and (b) T-direction that were used to determine the number of damage sites and their depths after 24-hour exposure to phosphoric acid at 35°C	119

Figure B.6	Optical images of cross-sectioned AA5083 100°C-7days samples showing damage penetration in the: (a) L-direction and (b) T-direction that were used to determine the number of damage sites and their depths after 24-hour exposure to phosphoric acid at 35°C	120
Figure B.7	Optical images of cross-sectioned AA5083 100°C-14Days samples showing damage penetration in the: (a) L-direction and (b) T-direction that were used to determine the number of damage sites and their depths after 24-hour exposure to phosphoric acid at 35°C	121
Figure B.8	Optical images of cross-sectioned AA5083 100°C-30days samples showing damage penetration in the: (a) L-direction and (b) T-direction that were used to determine the number of damage sites and their depths after 24-hour exposure to phosphoric acid at 35°C	122
Figure B.9	Optical images of cross-sectioned AA5083 SHTQ samples showing damage penetration in the: (a) L-direction and (b) T-direction that were used to determine the number of damage sites and their depths after 24-hour exposure to ammonium persulfate at 35°C	124
Figure B.10	Optical images of cross-sectioned AA5083 100°C-7days samples showing damage penetration in the: a) L-direction and (b) T-direction that were used to determine the number of damage sites and their depths after 24-hour exposure to ammonium persulfate at 35°C	125
Figure B.11	Optical images of cross-sectioned AA5083 100°C-14Days samples showing damage penetration in the: (a) L-direction and (b) T-direction that were used to determine the number of damage sites and their depths after 24-hour exposure to ammonium persulfate at 35°C	126
Figure B.12	Optical images of cross-sectioned AA5083 100°C-30days samples showing damage penetration in the: (a) L-direction and (b) T-direction that were used to determine the number of damage sites and their depths after 24-hour exposure to ammonium persulfate at 35°C	127
Figure C.1	Anodic polarization scans of AA5083-SHTQ and β -phase specimens in Nitric Acid at 15°C	128
Figure C.2	Anodic polarization scans of AA5083-SHTQ and β -phase specimens in Nitric Acid at 22°C	128
Figure C.3	Anodic polarization scans of AA5083-SHTQ and β -phase specimens in Nitric Acid at 30°C	129
Figure C.4	Anodic polarization scans of AA5083-SHTQ and β -phase specimens in Nitric Acid at 35°C	129
Figure C.5	Anodic polarization scans of AA5083-SHTQ and β -phase specimens in Nitric Acid at 50°C	130
Figure C.6	Anodic polarization scans of AA5083-SHTQ and β -phase specimens in Phosphoric Acid at 15°C	130
Figure C.7	Anodic polarization scans of AA5083-SHTQ and β -phase specimens in Phosphoric Acid at 22°C	131
Figure C.8	Anodic polarization scans of AA5083-SHTQ and β -phase specimens in Phosphoric Acid at 35°C	131
Figure C.9	Anodic polarization scans of AA5083-SHTQ and β -phase specimens in Phosphoric Acid at 50°C	132
Figure C.10	Anodic polarization scans of AA5083-SHTQ and β -phase specimens in pH 1.2 Ammonium Persulfate at 15°C	132
Figure C.11	Anodic polarization scans of AA5083-SHTQ and β -phase specimens in pH 1.2 Ammonium Persulfate at 22°C	133
Figure C.12	Anodic polarization scans of AA5083-SHTQ and β -phase specimens in pH 1.2 and pH 0.7 Ammonium Persulfate at 35°C	133
Figure C.13	Anodic polarization scans of AA5083-SHTQ and β -phase specimens in pH 1.2 Ammonium Persulfate at 50°C	134

LIST OF SYMBOLS

α	Alpha phase
β	Beta phase (Al_3Mg_2)
AA5XXX	5XXX-series aluminum alloys
AP	Ammonium persulfate
A_s	Surface area
ASTM	American Society of Testing and Materials
AW_i	Atomic weight of alloying element
$D_{L\text{-dir}}$	Average damage site depth in the L-direction
DoS	Degree of sensitization
$D_{T\text{-dir}}$	Average damage site depth in the T-direction
EDS	Energy dispersive x-ray emission spectroscopy
EQ	Equivalence factor
EW	Equivalent weight of the alloy (grams/equivalent)
F	Faraday's constant
f_i	Weight fraction of alloying element
i_{corr}	Corrosion current density
$i_{\text{corr}}(\text{mass})$	Corrosion current density determined by mass loss
ICP-OES	Inductively coupled plasma optical emission spectrometry
IGC	Intergranular corrosion
IGSCC	Intergranular stress corrosion cracking
i_{pass}	Passive current density
L	Longitudinal (rolling) direction
LS	L x S surface
LT	L x T surface
MSE	Mercury sulfate electrode
n	Equivalent number of transferred electrons
NA	Nitric acid
NAMLT	Nitric Acid Mass Loss Test
OCP	Open circuit potential
PA	Phosphoric acid
PDF	Powder diffraction file
PIXE	Proton-induced x-ray emission spectroscopy
ppm	Parts per million
r	Mass loss rate
R_p	Polarization resistance
S	Short-transverse direction

SEM	Scanning electron microscopy
SHTQ	Solution heat treated and quenched
SSSS	Supersaturated solid solution
ST	S x T surface
T	Long-transverse direction
TEM	Transmission electron microscopy
V_{MSE}	Volts in reference to mercury sulfate electrode
vol%	Volume percent
wt%	Weight percent
XRD	X-ray diffraction
ΔL_{avg}	Average dimension change in the L-direction
Δm	Mass loss
ΔS_{avg}	Average dimension change in the S-direction
ΔT_{avg}	Average dimension change in the T-direction

1 BACKGROUND AND OBJECTIVES

1.1 MOTIVATION

5XXX-series aluminum alloys (AA5XXX) are used in structural components of lightweight Navy vessels. These alloys are prone to sensitization when exposed to standard service temperatures due to the preferential precipitation of the β -phase (Al_3Mg_2) at grain boundaries [1-7, 16-32]. Dissolution of the anodic β -phase from the grain boundaries can initiate intergranular corrosion (IGC), which can progress to intergranular stress corrosion cracking (IGSCC) when the material is under tensile stress [21-25]. Determining the IGC susceptibility of the material is critical to predict and preemptively remediate crack propagation before failure, thereby maintaining the structural integrity of the existing fleet.

IGC susceptibility is often determined by detecting the degree of sensitization (DoS) of the alloy, or the extent of β -phase precipitation at the grain boundaries. ASTM G67 and ASTM B928 specify the utilization of etchants to selectively attack the β -phase relative to the matrix during mass loss testing and surface etching, respectively; measurements of mass loss promoted by grain boundary attack and grain fallout are used to quantify DoS, while surface etching is used to reveal the β -phase decorated grain boundaries upon metallographic examination [6, 7]. However, limited research has been published that investigates the electrochemical bases for these etchants [2, 15]. It is therefore of interest to quantify and characterize etchant selectivity for β -phase dissolution to comprehensively compare the efficacy and applicability for sensitization detection.

1.2 METALLURGY OF 5XXX ALUMINUM-MAGNESIUM ALLOYS (AA5XXX)

Before discussing sensitization detection methods, it is important to review the metallurgy of AA5XXX to understand how sensitization is possible and why it occurs. Metallurgical factors affecting sensitization include composition and processing.

1.2.1 COMPOSITION AND PROCESSING

5XXX aluminum alloys are primarily composed of aluminum (Al) and magnesium (Mg). Commercial alloys contain approximately 4.0 – 5.5 weight percent (wt%) Mg [2, 7]. These alloys derive their strength from cold work and solid solution strengthening. Many of the alloys have a supersaturated solid solution (SSSS) matrix of magnesium and aluminum that is retained through a solutionizing thermal exposure and quenching process [2].

A solutionizing treatment is necessary because a matrix supersaturated with magnesium is not in equilibrium at the temperatures that the alloys experience in service (approximately 10-70°C [39]). This can be seen from the Al-Mg phase diagram in Figure 1.1; at a nominal content of 4.4 wt% Mg, the two-phase field of $\alpha + \beta$ is thermodynamically stable below approximately 260°C.

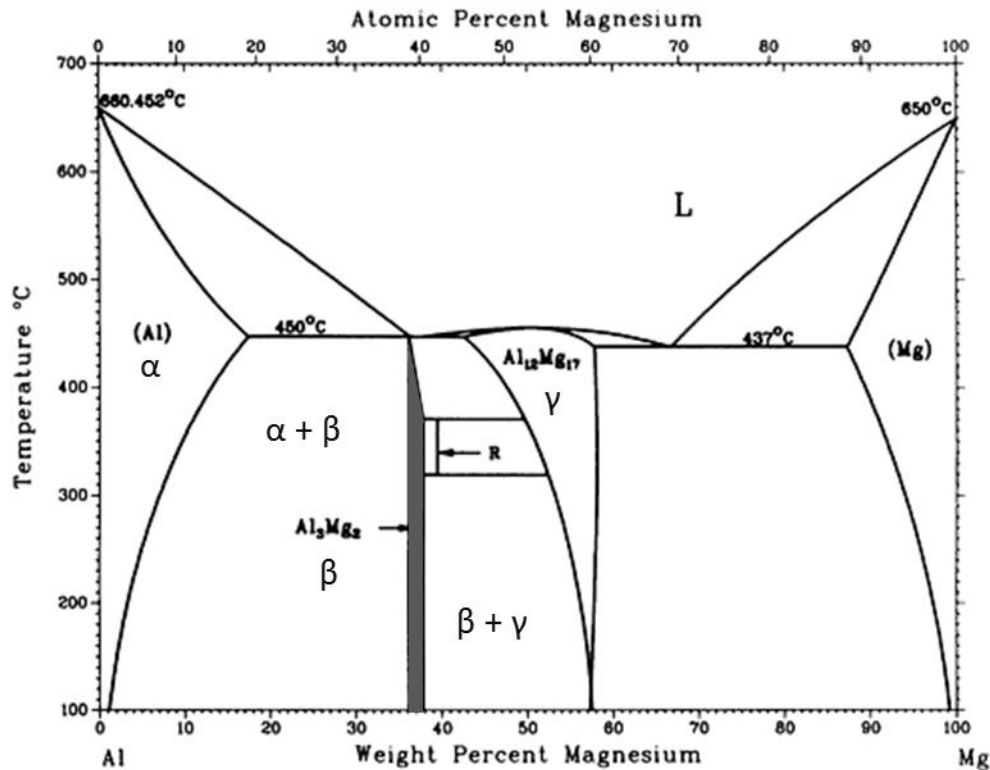


Figure 1.1 The Al-Mg binary phase diagram with the β -phase field shaded (~36-38 wt% Mg) [Modified from 10]

1.2.2 β -PHASE PRECIPITATION

After long exposures at temperatures as low as 50°C, AA5XXX with more than ~3 wt% Mg will experience magnesium diffusion through the SSSS α -Al matrix to low energy sites like grain boundaries [2]. When the local concentration of Mg is high enough, β -phase will precipitate via heterogeneous nucleation and growth to lower the stored energy in the material [1-2, 16-24, 29-30]. The β -phase intermetallic has a variable composition range from ~36 - 38 wt% Mg, and is nominally referred to as Al_3Mg_2 [10].

β -phase precipitation is dependent on both exposure temperature and duration, occurring faster at elevated temperatures (60-180°C) for short durations than at ambient conditions, and is

also influenced by grain boundary misorientation [3, 7, 21-23]. Intragranular precipitation also occurs, but is less relevant to IGC susceptibility.

The equilibrium volume fraction of the β -phase can be calculated using the binary phase diagram in Figure 1.1 and the Lever Rule. Assuming the same nominal Mg content as above (4.4 wt%), a β -phase density of 2.22 g/cm³ [33], an α -phase density of 2.70 g/cm³ (approximated to the density of Al), and a temperature of 100°C, the fraction of the β -phase is approximated to 8.5 vol%. This volume would be similar to the maximum β -phase that would be present in commercial alloys if the system reached equilibrium, but it does not account for other Al or Mg-containing constituent particles.

The size of the β -phase precipitates was observed through transmission electron microscopy (TEM) studies for AA5083 specimens. Coarsening and coalescence of the precipitates occurred as the degree of sensitization increased, and the size varied from 50 – 190 nm and 100 – 1000 nm in width and length, respectively [1, 16-18, 23-25, 29].

The fraction of β -phase at the grain boundaries and the size of the precipitates determine the extent of formation of the network of anodic, β -phase precipitates that provides the pathway for IGC propagation. Both continuous and discontinuous active paths have been shown to undergo dissolution and propagate IGC [1-2].

1.3 INTERGRANULAR CORROSION (IGC) OF AA5XXX

Corrosive environments like chloride-ion-containing seawater must first break down the protective oxide film on AA5XXX material before IGC can occur. The mechanism of intergranular corrosion in AA5XXX begins with breakdown of the passive oxide film, followed by dissolution events at the surface and subsurface where IGC penetrates and can propagate [2].

1.3.1 THERMODYNAMICS OF ALUMINUM AND MAGNESIUM DISSOLUTION

Breakdown of the oxide film on AA5XXX depends on the thermodynamic drivers for electrochemical reactions to proceed. The thermodynamic stability of aluminum and magnesium over a range of pH is captured in the Pourbaix diagram in Figure 1.2 [reproduced from 2]. Aluminum is stable (Al) or passive (Al₂O₃) at neutral pH but dissolves in acidic and alkaline environments as Al³⁺ and AlO₂⁻, respectively. Magnesium is passive as Mg(OH)₂ in alkaline environments but active (Mg⁺) in neutral and acidic environments.

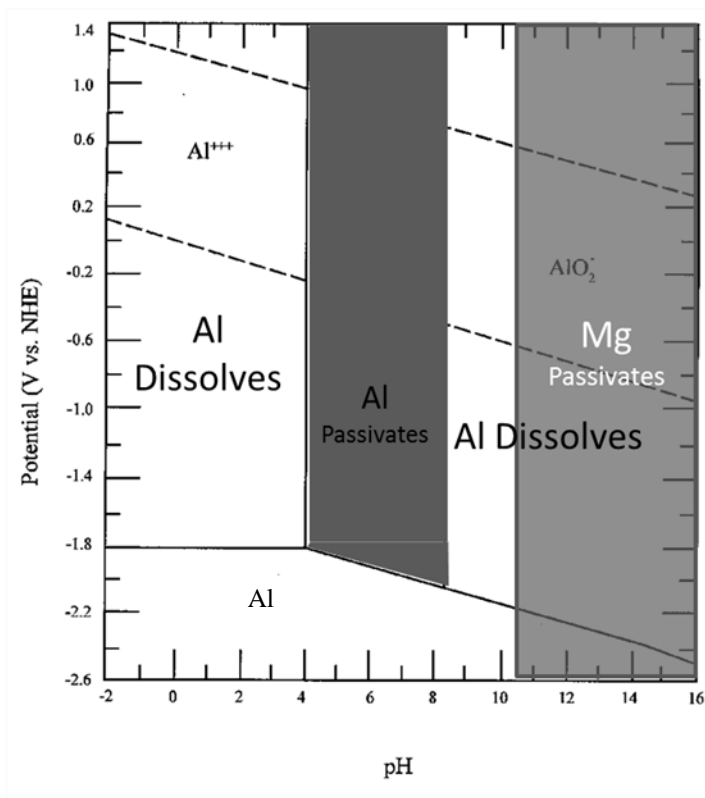


Figure 1.2 Pourbaix diagram of aluminum at 25°C with the stability regions of magnesium superimposed. Regions of passivation and dissolution are highlighted [reproduced from 2].

1.3.2 PREFERENTIAL DISSOLUTION OF β -PHASE

A difference in potential between the β -phase and the alloy matrix provides the driving force for the dissolution of the β -phase precipitates from the grain boundaries [3, 11]. In these occurrences, β -phase is anodic to the alloy matrix. Selective dissolution of the β -phase precipitates leads to IGC and IGC propagation when it spreads to neighboring precipitates and grain boundaries.

1.4 DETECTION OF SENSITIZATION IN AA5XXX

Standardized, accelerated test methods used to detect sensitization and determine DoS include mass loss measurements and OCP etching. The effectiveness of these tests is governed by the test environment's selectivity for the dissolution of the β -phase relative to the matrix. The methods reviewed in the following sections utilize chloride-free etchants to avoid localized pitting of the specimens that could lead to excessive attack on the matrix.

1.4.1 DETERMINING IGC SUSCEPTIBILITY VIA MASS LOSS

Prior to 1980, the Aluminum Association adhered to a combination of etching tests and salt spray tests to evaluate the susceptibility to IGC for AA5XXX. A Federal Specification called for metallographic examination of each commercial production lot using a 40% phosphoric acid etchant at 35°C for 3 minutes to assess if the microstructure was “predominantly free of a continuous grain boundary network of aluminum-magnesium precipitate” [36]. Additionally, the corrosion resistance of AA5XXX was determined by exposing samples for one week to the synthetic seawater acetic acid intermittent salt spray test (SWAAT); salt spray testing caused exfoliation in samples that had experienced exfoliation corrosion in actual service, but did not always cause exfoliation of materials believed to exhibit borderline susceptibility [36]. Errors stemming from difficulties with SWAAT reproducibility induced the transition toward immersion testing, which also better accounted for intergranular corrosion.

In 1972, Craig reported a test method to indicate the resistance of aluminum-magnesium alloys 5086 and 5456 in the H116 and H117 tempers to exfoliation and intergranular corrosion by immersion of specimens of set area into concentrated nitric acid at 30°C for 24 hours [36]. Mass loss resulting from intergranular attack and grain fallout provided a quantitative measurement of precipitate continuity at the grain boundaries. The method was based on the same philosophy as the metallographic examination with phosphoric acid – nitric acid dissolved intermetallic precipitates while not appreciably attacking the solid solution of magnesium in the aluminum matrix [36].

1.4.1.1 ASTM G67 STANDARD TEST METHOD FOR DETERMINING THE SUSCEPTIBILITY TO INTERGRANULAR CORROSION OF 5XXX SERIES ALUMINUM ALLOYS BY MASS LOSS AFTER EXPOSURE TO NITRIC ACID (NAMLT)

The work reported by Craig was adapted by the Aluminum Association and the American Society of Testing and Materials (ASTM) in 1980 for ASTM G67, or the Nitric Acid Mass Loss Test (NAMLT). This standard test method is the primary protocol for quantifying IGC susceptibility today. The same test environment and duration reported by Craig are specified: concentrated nitric acid at 30°C for 24 hours. The grain fallout stemming from the preferentially corroded β -phase at the grain boundaries results in a mass loss per unit surface area, which is used to indicate the degree of sensitization of an AA5XXX specimen [6].

1.4.1.2 ASTM B928 STANDARD SPECIFICATION FOR HIGH MAGNESIUM ALUMINUM-ALLOY SHEET AND PLATE FOR MARINE SERVICE AND SIMILAR ENVIRONMENTS

The current standard that specifies quality-assurance-related production lot acceptance limits for AA5XXX is ASTM B928. This specification uses the NAMLT mass loss values to define levels of sensitization. Specimens with NAMLT mass loss equal to or above 25 mg/cm^2 are considered sensitized, with the grain fallout resulting from a continuous network of preferentially dissolved grain boundary precipitates [7]. Specimens with mass loss values less than or equal to 15 mg/cm^2 are considered unsensitized and IGC resistant, resulting from discontinuous precipitation of β -phase at the grain boundaries [6, 7]. A mass loss value between 15 mg/cm^2 and 25 mg/cm^2 indicates intermediate sensitization resulting from a random distribution of the β -phase at the grain boundaries and in the grains [6, 7].

1.4.2 DETERMINING IGC SUSCEPTIBILITY VIA ETCHING

ASTM B928 also specifies a qualitative assessment of sensitization for alloys of intermediate sensitization via OCP etching of polished specimens in 40% phosphoric acid at 35°C for 3 minutes (mirroring the test environment and duration mentioned in the Federal Specification above) [7, 36]. Metallographic examination after etching allows for the assessment of DoS through the observation of grain boundary continuity, which correlates to the extensiveness of the β -phase precipitate network.

1.5 CRITICAL UNRESOLVED ISSUES

Critical unresolved issues exist concerning the standardized test methodologies, including the applicability of each method for in-situ testing to reduce the cost and time of maintenance associated with detecting and remediating sensitization of structural material. The limitations of these methodologies are outlined below.

ASTM G67 is a destructive evaluation of IGC susceptibility and is not suitable for use on-board navy vessels due to the toxic nature of the strongly oxidizing, concentrated nitric acid, the necessary temperature stability at 30°C , and the 24-hour test duration. Because testing is not completed in-situ, suspect material must be cut from the structures and sent for analysis. If the material is found to be sensitized (mass loss $> 25 \text{ mg/cm}^2$), then more material must be cut from the ship for testing to remediate possible IGC spreading. If the material is found to be unsensitized (mass loss $< 15 \text{ mg/cm}^2$), then replacement material must be welded to the structure to cover the area where the specimens were removed.

Etching material on-board vessels using the ASTM B928 etchant of 40% phosphoric acid would be a less time-consuming and destructive process relative to ASTM G67, but would require an adequately polished surface for metallographic examination, the ability to maintain the temperature of exposure, and an optical microscope that can be used on-board a ship. Given the qualitative nature of the analysis, development of a library of images for comparison with the etching results would be necessary to maintain consistent interpretations of the definitions of grain boundary continuity.

Given the aforementioned limitations of the methodologies, there is interest in non-destructive techniques to detect sensitization and quantitatively determine DoS that are more applicable for in-situ testing. Electrochemical test protocols are valid candidates; they allow for shorter test durations and correspondingly light surface damage after analysis (to avoid replacing unsensitized material after testing), a wider range of test solutions of varying pH, and the ability for the test solutions to be packaged in portable instrumentation.

An electrochemical protocol of open circuit potential and polarization tests to quantify DoS was proposed by Bumiller and Kelly. This methodology utilized alkaline, chloride-free buffers such as sodium phosphate to distinguish trends in electrochemical parameters to indicate the DoS level [2, 5]. As seen in Figure 1.2, alkaline environments passivate magnesium and corrode aluminum, which differs from nitric acid and phosphoric acid which corrode both aluminum and magnesium (though at different rates). Results indicated a distinction in DoS for AA5456 specimens tested in sodium phosphate at room temperature [5].

The temperature sensitivity of the tests should also be considered in the evaluation of their applicability for use outside controlled laboratory settings. Temperature sensitivity of the nitric acid mass loss test (preceding ASTM G67) was reported by Craig such that a ten degree increase in temperature doubled the rate of the chemical reactions; the mass loss approached a limiting ratio of 2.0 for higher DoS specimens but was not observed to double for lower DoS specimens. The temperature sensitivity of the exposure solutions used for OCP etching and polarization tests has not been investigated.

Additionally, the electrochemical bases of the etchants used in the test methodologies briefly described above have not been quantified and compared based on selectivity for β -phase dissolution. This is a key step toward evaluating and optimizing the current test methods for in-situ testing.

1.6 OBJECTIVES

The objective of this work is to characterize and compare the selectivity of AA5XXX etchants by assessing the corrosion behaviors of the bulk alloy (AA5083) and pure β -phase during etchant exposure. The etchants will be compared over a series of tests used to detect sensitization in AA5XXX such as OCP etching and mass loss tests. A range of sensitization conditions, surface orientations, and temperatures will be investigated. Selectivity will be assessed in quantitative terms. Results will contribute to the evaluation of the corrosion susceptibility of AA5XXX both in the lab and on-board Navy vessels.

2 MATERIALS

2.1 5XXX ALLOYS

2.1.1 CHEMICAL COMPOSITION

Samples of aluminum alloy 5083 (AA5083) of the H131 temper were tested in this study. The chemical composition limits for the alloy, specified in ASTM B928, and the composition of the plate¹ used in these experiments are listed in Table 2.1. AA5083 is composed of approximately 4.4 weight percent (wt%) Mg and is susceptible to sensitization (>3 wt% Mg).

Table 2.1 Chemical composition of AA5083 (UNS A95083) in wt% [7]

	Mg	Mn	Fe	Si	Cr	Zn	Ti	Cu	Others	Al
B928 Limits	4.0-4.9	0.4-1.0	≤0.4	≤0.4	0.05-0.25	≤0.25	≤0.15	≤0.1	≤0.15	Remainder ≥92.4
ALCOA Plate	4.4	0.7	0.22	0.1	0.08	0.02	0.02	0.05	<0.01	Remainder ≥94.4

2.1.2 MICROSTRUCTURE

The microstructure of the unrecrystallized alloy and the associated orientation conventions used in this study are shown in Figure 2.1². It can be observed in the micrographs that the grains are longest in the longitudinal, rolling direction (L), followed by the long-transverse direction (T) and the short-transverse direction (S), with average dimensions of 200 μm, 100 μm, and 30 μm, respectively³.

¹ The plate of alloy 5083, which has the Unified Number System (UNS) designation of A95083, and the corresponding chemical composition data were provided by ALCOA.

² Electrolytic etching in Barker's reagent (2.5 vol% HBF₄) causes oxide film growth on the sample surface. Optical micrographs of the etched surface captured using polarized light results in grains with different orientations appearing in different colors. Etching and imaging were done by Mary Lyn Lim at the University of Virginia.

³ Unrecrystallized grain dimensions were measured by Mary Lyn Lim at the University of Virginia.

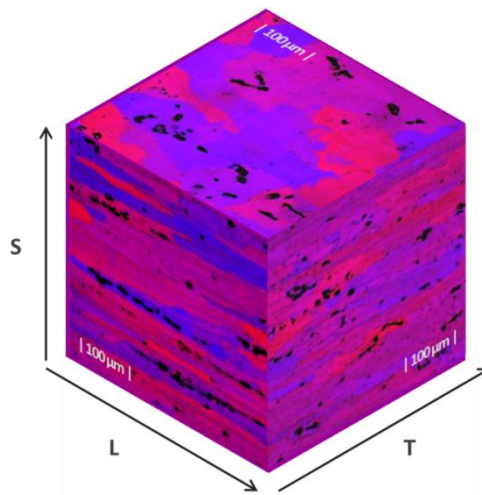


Figure 2.1 Microstructure of an AA5083-H131 specimen revealed after electrolytic Barker's etching². Grains are elongated in the rolling direction (L) and thinnest through the thickness of the plate (S).

2.1.3 SOLUTION HEAT-TREATMENT

AA5083 specimens were cut from a 2.25 inch-thick alloy plate into various geometries and were solution heat-treated at 275°C for 10 hours. This temperature is above the α - β solvus line of the Al-Mg phase diagram; the region of interest is shown in Figure 2.2. During this process, magnesium that has diffused to the grain boundaries and precipitated as β -phase in the as-received material is solutionized. The solution heat-treated specimens were then cold-water quenched to room temperature (SHTQ) to retain the solid solution of aluminum and magnesium.

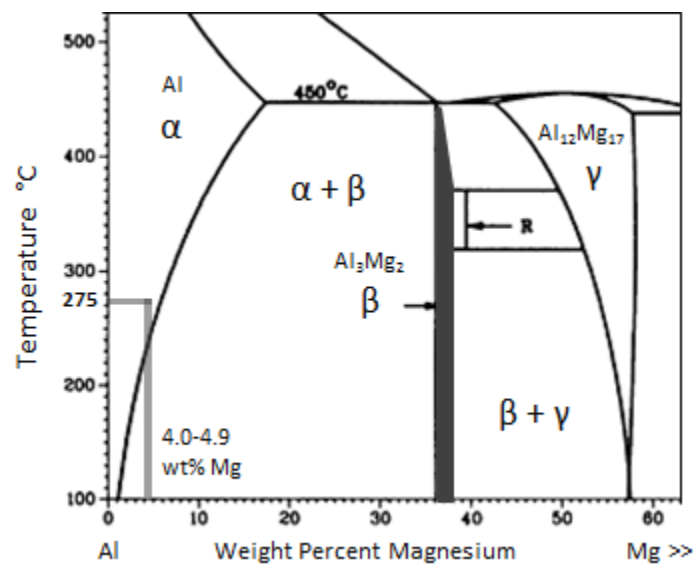


Figure 2.2 A section of the Aluminum-Magnesium phase diagram [Modified from 10]. The β -phase (Al_3Mg_2) stability field between ~36-38 wt% Mg is highlighted, and the solutionizing temperature (275°C) and composition limits of the alloy (4.0-4.9 wt% Mg) are also noted.

2.1.4 ARTIFICIAL SENSITIZATION AND SENSITIZATION CONDITION

Following the SHTQ procedure, some specimens were “sensitized”⁴ at 100°C for varying durations. Thermal exposure of the material at this temperature should promote the formation of β -phase precipitates at the grain boundaries, sensitizing the material in a reproducible manner. Specimens were sensitized for 7 days, 14 days, and 30 days and open-air cooled to room temperature. In this study, the combination of thermal exposure time and temperature (number of days at 100°C) is referred to as the sensitization condition.

2.1.5 DEGREE OF SENSITIZATION (DOS)

To determine their susceptibility to intergranular corrosion (IGC), several SHTQ and sensitized AA5083 specimens were tested according to the procedures in ASTM G67, the Nitric Acid Mass Loss Test (NAMLT) [6]. Duplicate specimens for each sensitization condition were exposed to concentrated nitric acid for 24 hours at 30°C, and the mass loss per unit area for each was measured. The average NAMLT mass loss values⁵ are shown in Figure 2.3.

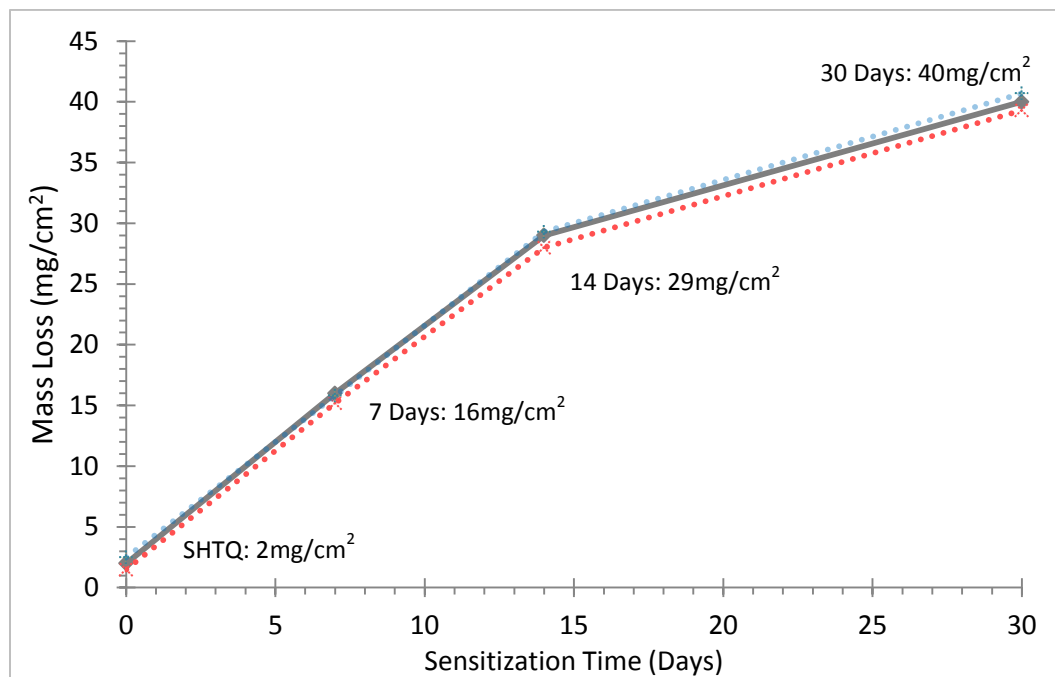


Figure 2.3 Average NAMLT mass loss values of AA5083-H131 exposed to nitric acid for 24 hours at 30°C. Mass loss increased with sensitization condition. The NAMLT values that were averaged are shown in dotted lines.

⁴ AA5083 specimens were solution heat-treated and quenched (SHTQ) and sensitized by Mary Lyn Lim and Wasiu Adedeji at the University of Virginia.

⁵ In this study, the mass loss values from standard G67 testing at 30°C are preceded by the term “NAMLT” to distinguish the values from other mass loss measurements discussed in the Experimental Methods chapter. NAMLT mass loss values were measured and calculated by Mary Lyn Lim and Wasiu Adedeji at the University of Virginia.

The NAMLTL mass loss values are dependent on sensitization condition and indicate the extent or degree of sensitization (DoS) of the material. AA5083 specimens that were only solution heat-treated and quenched were considered unsensitized (NAMLTL < 15 mg/cm²), with an undetectable or relatively insignificant amount of β -phase precipitation. Specimens sensitized at 100°C for 7 days were of intermediate DoS (15 mg/cm² < NAMLTL < 25 mg/cm²). Thermal exposures at 100°C for 14 days and 30 days resulted in highly sensitized material (NAMLTL > 25 mg/cm²) and extensive β -phase precipitation at the grain boundaries [6-7].

2.2 β -PHASE

As previously discussed and shown in the aluminum-magnesium phase diagram in Figure 2.2, the intermetallic β -phase is thermodynamically stable at standard service temperatures in AA5XXX containing more than 3 wt% Mg. However, β -phase is anodic to the alloy matrix when exposed to standard service environments like chloride-containing (Cl⁻) seawater and will preferentially corrode [1-5, 15-17]. Characterizing the corrosion behavior of the β -phase (Al₃Mg₂) is fundamental to the understanding of the IGC behavior of the 5XXX-series aluminum alloys. However, the β -phase precipitates at the grain boundaries are on the size scale of hundreds of nanometers [1, 16-18, 23-25, 29]. Thus, pure β -phase specimens were necessary to avoid interference from the surrounding alloy matrix.

2.2.1 SYNTHESIS OF β -PHASE

Bulk β -phase samples were synthesized via induction melting of high purity aluminum and magnesium (99.999% and 99.95% purity, respectively)⁶. Aluminum shot and magnesium slug were proportioned by weight to the desired final composition ratio of the β -phase. The materials were then combined in a boron-nitride-coated crucible and inductively melted under an Argon atmosphere. The specimen used in this study was cooled and solidified in-crucible and was not homogenized; additional samples were separately cast in pure copper chill blocks into various geometries and homogenized. The setup of the induction furnace used to create the β -phase samples is shown in Figure 2.4.

⁶ β -phase samples were synthesized by Professor Gary Shiflet at the University of Virginia.

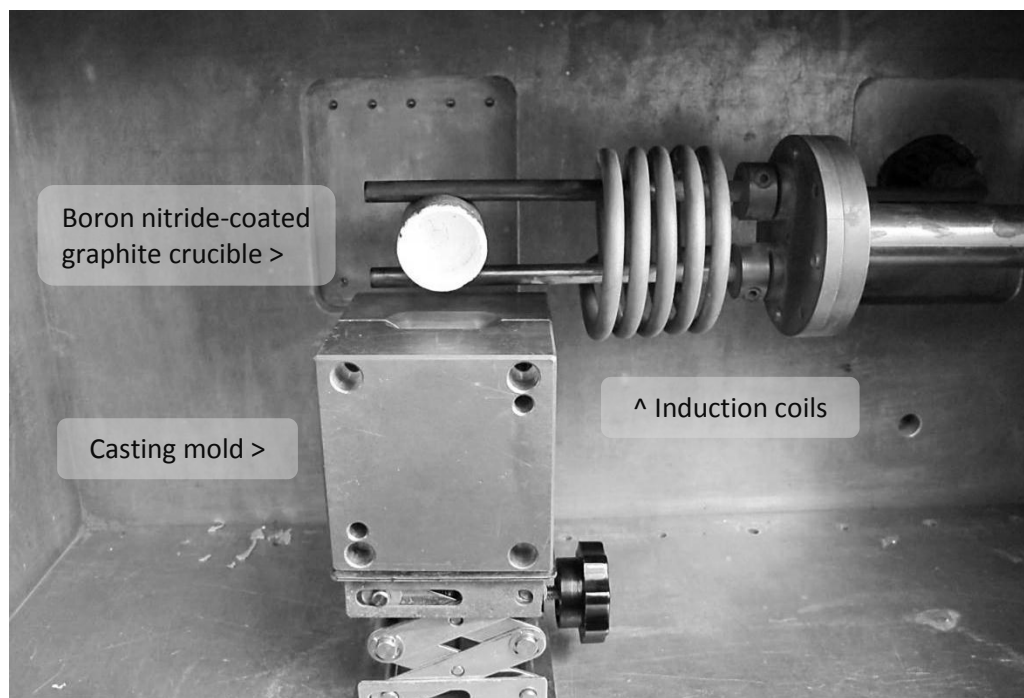


Figure 2.4 Induction furnace setup used to synthesize pure β -phase specimens

2.2.2 CHARACTERIZATION OF β -PHASE

The compositional purity and structural homogeneity of the synthesized β -phase sample was determined using several material characterization techniques. X-ray diffraction (XRD) and optical microscopy were used to detect the presence of secondary phases. Proton induced x-ray emission spectroscopy (PIXE) was used to determine the as-fabricated composition of the sample. Scanning electron microscopy (SEM) and energy dispersive x-ray spectroscopy (EDS) were used to observe and identify trace impurities from precursor materials.

2.2.2.1 XRD

A piece of the β -phase was sectioned from the bulk sample and ground into powder for XRD analysis⁷. The resulting diffraction pattern is shown in Figure 2.5b. This pattern can be compared with the literature powder diffraction file (PDF) for β -phase in Figure 2.5a that has the peaks for the α and γ -phases ($\text{Al}_{12}\text{Mg}_{17}$) overlaid (the literature α and γ -phase diffraction patterns are shown in Figure A.1 in the Appendix). The peaks for the synthesized β -phase sample closely match those in the literature PDF without exhibiting the characteristic peaks for the α or γ -phases, indicating that the synthesized sample is pure β -phase.

⁷ XRD preparation and testing of β -phase was done by Andrew Cheung at the University of Virginia.

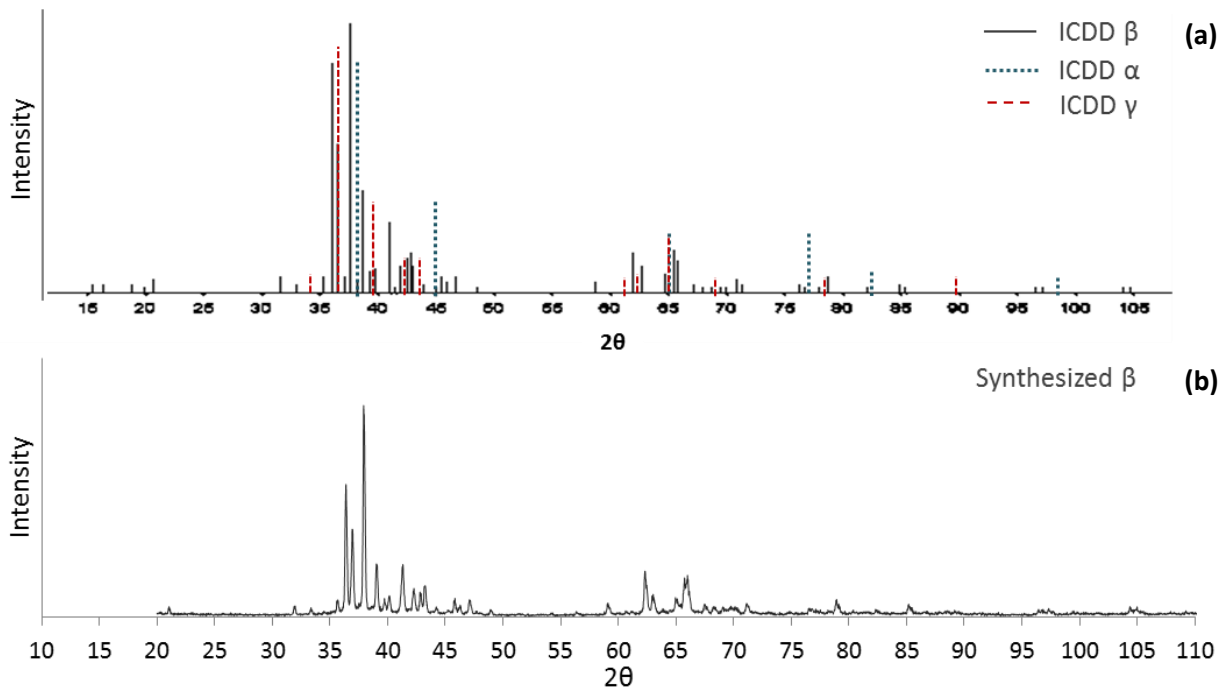


Figure 2.5 (a) Powder diffraction file (PDF) of β -phase with α and γ -phase peaks overlaid [Modified from 9] and **(b)** X-ray diffraction pattern of synthesized β -phase. The peaks for the synthesized specimen match the peaks in the literature PDF without exhibiting peaks for the α or γ -phases [Appendix A].

2.2.2.2 OPTICAL MICROSCOPY

The possibility of compositional variations across the sample was considered because the sample was not homogenized. The microstructure of the sample was therefore analyzed via phosphoric acid etching and optical microscopy to observe any secondary stable (α , γ) or metastable (β' , β'') phases on the surface of the remainder of the specimen⁸. Al-rich secondary phases (α) would be less attacked by the acid environment. Phases that are Mg-rich (γ) would also likely be attacked at a different rate than the bulk β -phase matrix. The β' and β'' phases are compositionally the same as the β -phase, but they have different crystal structures that should be visible upon etching [2].

A micrograph of the etched surface is shown in Figure 2.6. The etching did not reveal any secondary phases, but possible oxide inclusions and impurities were visible. Based on the optical microscopy evaluations, the sample appeared to be pure β -phase.

⁸ Preparation for optical microscopy analysis included the following steps: (1) the specimen was mounted in epoxy and (2) ground to 1200 grit on silicon carbide (SiC) paper in ethylene glycol then (3) polished to 0.1 μm with oil-based diamond suspension. After polishing, the specimen was (4) rinsed in acetone and (5) dried with compressed air, followed by (6) etching in 10 vol/vol% phosphoric acid for 45 seconds at 55°C.

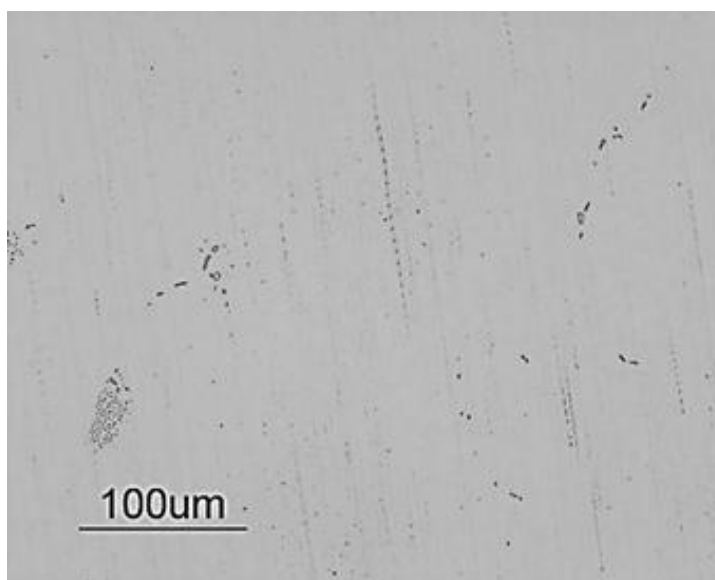


Figure 2.6 Optical micrograph of synthesized β -phase specimen after etching with 10vol/vol% phosphoric acid. Possible oxide inclusions or impurities are visible.

2.2.2.3 PIXE

Because impurities were observed via etching and optical microscopy, additional verification was needed to further confirm the purity of the synthesized β -phase sample beyond the phase matching analysis from XRD. The composition of the sample was determined via PIXE⁹ after polishing the specimen used for optical microscopy to a 0.1 μm finish with ethylene glycol and diamond suspension. The composition of the specimen, listed in Table 2.2, was approximately 36.1 wt% Mg and 63.9 wt% Al, which is in the literature range of approximately 36.1–37.8 wt% Mg for pure β -phase [10]. Trace impurities of Mn, Fe, Zn, and Cu were also detected in parts per million (ppm) quantities, where 10^4 ppm is equivalent to 1 wt%.

Table 2.2 Chemical composition of synthesized β -phase determined via PIXE

Al	Mg	Mn	Fe	Zn	Cu
63.92 wt%	36.06 wt%	119.3 ppm	12.5 ppm	8.9 ppm	4.1 ppm
$\pm 0.64\%$	$\pm 0.36\%$	± 3.4 ppm	± 1.9 ppm	± 0.7 ppm	± 0.6 ppm

⁹ Proton-Induced X-Ray Emission Spectroscopy (PIXE) is a non-destructive compositional analysis technique. The collimator/beam diameter size was 15.875 mm (surface interaction diameter), and the penetration depth was ~ 0.08 mm, or 80 μm . The specimen analyzed had an as-polished surface diameter of 25 mm and a thickness of 8 mm. PIXE was done by Elemental Analysis, Inc. in Lexington, KY.

2.2.2.4 SEM AND EDS

The impurities visible after electrochemical testing¹⁰ of the β -phase were also investigated using electron microscopy. The impurity shown in the SEM micrograph in Figure 2.7a was identified as a silicon/silicide particle via an EDS line scan across the particle (Figure 2.7b).

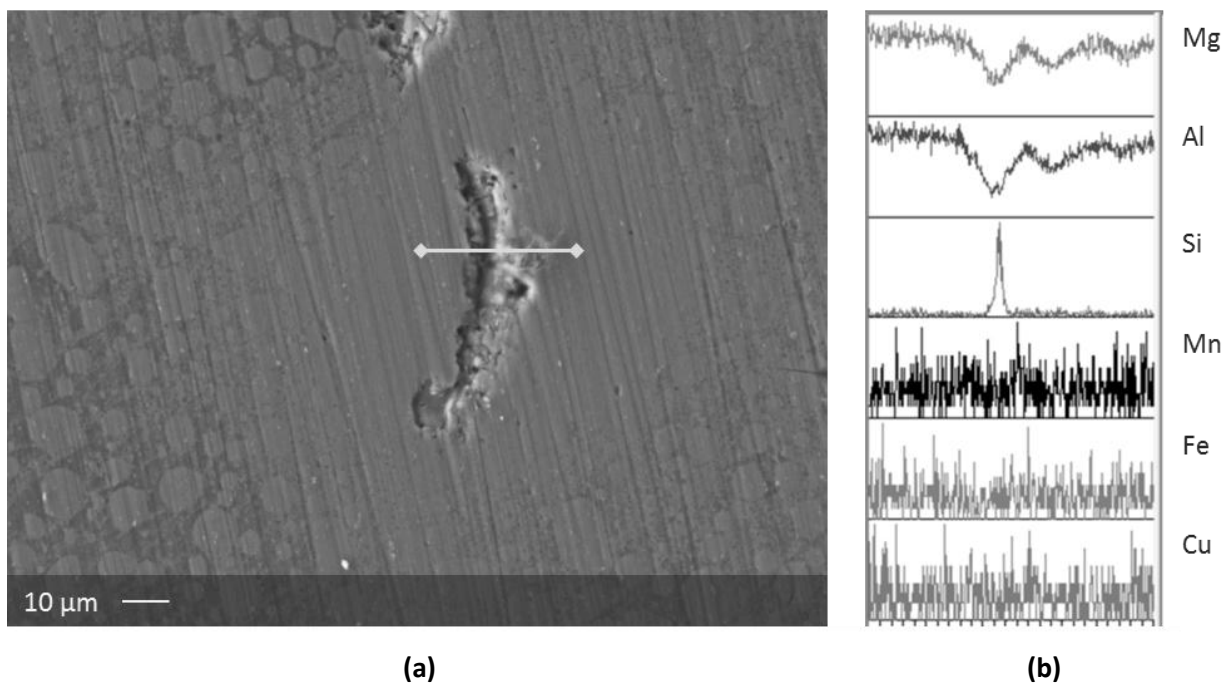


Figure 2.7 (a) SEM micrograph of an impurity in synthesized β -phase revealed after electrochemical testing and (b) the associated EDS line scan spectra that show an increase in silicon content at the impurity and a decrease in both aluminum and magnesium content. The Mn, Fe, and Cu spectra are considered noise.

Silicon was not identified as an impurity during PIXE, but different surfaces were analyzed in the techniques. This inconsistency between EDS and PIXE could be explained by an inhomogeneous distribution of impurities throughout the synthesized sample. The material layers beneath the PIXE-tested surface likely had trace impurities in addition to Si that were not captured by the instrument. The possibility of inhomogeneity was addressed in future sample syntheses, which included a homogenization step after casting. Alternatively, the silicon impurity could also be contamination from grinding the sample with silicon carbide.

Following the series of aforementioned characterization techniques, the purity of the single-phase β specimen was confirmed. The very small area of the impurities relative to the area of the

¹⁰ Electrochemical testing of the β -phase and its corrosion properties are discussed in the Experimental Methods and Results chapters.

bulk β -phase was neither expected to nor observed to interfere with the corrosion properties of the intermetallic¹¹.

¹¹ Neither the open circuit potentials nor the current densities of the β -phase generated during anodic polarization were observed to shift when different areas of the specimen were tested at the same temperature (which would have included varied impurities due to the inhomogeneity of the sample). Anodic polarization results are discussed in the Results chapter.

3 EXPERIMENTAL METHODS

3.1 ETCHANT ENVIRONMENTS

A limited selection of etchant environments are presently used to detect sensitization in 5XXX-series aluminum alloys by researchers across the fields of academia, government, and industry. These environments include the ASTM G67 exposure solution of concentrated nitric acid¹², the ASTM B928 etchant of phosphoric acid, and acidified ammonium persulfate. There are few reports in literature detailing the corrosion behavior of both AA5XXX and pure β -phase in these environments [2, 15]. The corrosion behavior and the associated data are necessary to determine the electrochemical bases of these etchants, quantify their selectivity, and comprehensively compare their efficacy and applicability.

3.1.1 NITRIC ACID

The corrosion behavior of AA5083 and pure β -phase was assessed in concentrated nitric acid, the ASTM G67 test solution to determine susceptibility to IGC¹³. The nitric acid (HNO_3) used for experiments in this study was reagent grade (70 wt%) and was not diluted before immersion or polarization experiments. The pH of the solution was approximately -1.2 (calculated)¹⁴. The general corrosiveness of nitric acid as a strong oxidizer and its ready decomposition into hazardous oxides required handling precautions [34]; all experiments involving concentrated nitric acid were executed in a fume hood or other contained environment with appropriate exhaust ventilation.

3.1.2 PHOSPHORIC ACID

Phosphoric acid (H_3PO_4) is the standard AA5XXX etchant utilized in ASTM B928 to determine the continuity of β -phase precipitation at the grain boundaries¹⁵. The concentration specified in B928 and used in this study is 40 parts by volume (vol/vol%) of reagent grade (85

¹² Concentrated nitric acid is not a common “etchant” in terms of standard use in metallographic examinations. But its designation as the ASTM G67 test solution to determine IGC susceptibility in AA5XXX is based on its preferential dissolution of the β -phase. This mechanism of selective attack of a phase meets the underlying qualification of an etchant, and thus nitric acid will be referred to as an etchant in this study.

¹³ The significance and use of ASTM G67, the Nitric Acid Mass Loss Test (NAMLT), is discussed in more detail in the Background and Objectives chapter. NAMLT methodology is discussed in subsection 3.2.2.

¹⁴ The pH of concentrated nitric acid was not measured for these experiments. pH was calculated using the following equation: $\text{pH} = -\log[\text{H}^+]$, where $[\text{H}^+]$ is the concentration of hydrogen ions. $[\text{H}^+]$ was assumed to be 15.8M (concentration of 70% nitric acid) since nitric acid is a strong acid that is expected to fully dissociate.

¹⁵ The significance and use of ASTM B928, the standard specification for marine-grade Al-Mg alloys, is discussed in more detail in the Background and Objectives chapter. Etching methodology is discussed in subsection 3.2.1.

wt%) phosphoric acid and 60 vol/vol% ultrapure water [7]. The solution was prepared at room temperature and had a pH of ~0.7.

3.1.3 AMMONIUM PERSULFATE

Continuing the use of acidic test environments, ammonium persulfate – an etchant more commonly used in the semiconductor industry for copper alloys [40] – has recently been developed as an effective AA5XXX etchant by Allen and Yang at the University of Wisconsin [8]. Additional work by Chen and Lim at the University of Virginia confirmed those results and showed that acidified ammonium persulfate at a pH of 1.2 was also an effective etchant [35]. In this study, the etchant was prepared by dissolving 30 grams of reagent grade (+98%) ammonium peroxydisulfate ((NH₄)₂S₂O₈) in 300 milliliters (mL) of ultrapure water¹⁶ at room temperature. The 0.4M solution was acidified with sulfuric acid (H₂SO₄) to a pH of 1.2 and 0.7 to more directly compare the ammonium persulfate etching results with the phosphoric acid etching results.

3.2 CORROSION TESTING AND ELECTROCHEMICAL ANALYSES

3.2.1 SHORT-TERM OPEN CIRCUIT POTENTIAL (OCP) ETCHING OF AA5XXX FOR SCREENING

The environments were initially screened to determine their efficacy in etching commercial aluminum-magnesium alloys¹⁷. Parameters included sensitization condition of the material and etchant exposure times and temperatures.

3.2.1.1 MATERIALS AND SAMPLE PREPARATION

Samples of AA5083-H131 cut from a thickness of S/2 were solution heat-treated at 275°C for 10 hours, quenched (SHTQ), and artificially sensitized for 7 days and 30 days at 100°C (NAMLT mass loss of 16 and 40 mg/cm², respectively). The longitudinal by long-transverse (LT) and longitudinal by short-transverse (LS) surfaces were ground to a 1200 grit finish with silicon carbide (SiC) paper and water, and dried with compressed air prior to etching.

¹⁶ Ultrapure Millipore water has a resistivity of 18.2 MΩ·cm at 25 °C and < 10 ppb (parts per billion) total organic carbon.

¹⁷ In other words, the etchants were first tested to make sure they worked as etchants and allowed the β-phase to be distinguished from the alloy matrix in sensitized materials upon viewing with an optical microscope.

3.2.1.2 ETCHANT CHEMISTRIES

The sample surfaces were immersed in concentrated nitric acid (70 wt%), phosphoric acid (40 vol/vol%), and acidified ammonium persulfate (pH 1.2). The matrix is noble to β -phase in all solutions¹⁸, so preferential etching of β -phase was expected at the open circuit potential (OCP or E_{corr}) of the alloy¹⁹. The samples were immersed face-up in each solution, with one sample per beaker. A solution-volume-to-surface-area ratio of $\sim 15 \text{ mL/cm}^2$ was consistent throughout testing to ensure that each specimen was fully submerged. All glassware used for solution preparation and etching was pre-cleaned in a 50 vol/vol% nitric acid/water bath to remove chloride ions (Cl^-) and avoid pitting of the samples, which could obscure the etched grain boundaries.

3.2.1.3 EXPOSURE TEMPERATURES AND TIMES

The samples were immersed at OCP at 22°C (room temperature), 30°C, and 35°C, the temperatures specified for ammonium persulfate etching, nitric acid mass loss testing, and phosphoric acid etching, respectively. The beakers containing the specimens were immersed in a water bath that was temperature-controlled to $\pm 0.1^\circ\text{C}$ ²⁰. The samples were immersed for the durations listed in Table 3.1²¹, and optical micrographs of the surfaces were captured after each time step. It is important to note that the samples were not continuously immersed; rather, the samples were immersed for the initial duration, rinsed in water and dried with compressed air, imaged, and then re-immersed until the next duration listed.

Table 3.1 Etching duration for AA5083 samples [(LT, LS) x (SHTQ, 100°C-7 Days, 100°C-30 Days)] in concentrated nitric acid, phosphoric acid, and ammonium persulfate (pH 1.2) at 22°C, 30°C, and 35°C

Etching Temperature	Nitric Acid	Phosphoric Acid	Ammonium Persulfate
22°C - 30°C - 35°C	60 min & 90 min	3 min & 10 min	90 min

¹⁸ Polarization data confirming that β -phase is anodic to the matrix is shown in the Results chapter.

¹⁹ The samples were etched at open circuit potential, i.e. a potential was not applied to the system.

²⁰ The temperature is controlled, but the pH of the solution is not controlled/buffered. The pH of each solution changes at different rates at each temperature; the final pH of ammonium persulfate and phosphoric acid will be different at the same temperature despite the same initial value, and the final pH of the ammonium persulfate at 22°C will differ from the final pH at 35°C.

²¹ The phosphoric acid etch defined at 35°C in ASTM B928 stipulates that the alloys should be etched for 3 minutes [7].

3.2.1.4 SCREENING ASSESSMENT

Bright-field optical micrographs of the etched surfaces were taken at a magnification of 500x after varying exposure times. The etchants were then compared by the clarity of the etch detected by optical inspection (grain boundary attack versus matrix attack), the time required for etching, and the temperature sensitivity of the etchant. The clarity of the etch was used to qualitatively indicate the selectivity of the etchant.

It was expected that when exposed to a selective etchant, SHTQ samples would not etch (grain boundaries would not be revealed) due to lack of β -phase precipitation, and that samples sensitized for 7 days would show less attack at the grain boundaries than the more heavily sensitized samples thermally exposed for 30 days. It was also expected that the LS surface could etch more quickly than the LT surface due to the elongated and thin grain shapes with longer grain boundaries, meaning a longer continuous network of β -phase precipitates that could be attacked.

3.2.2 MASS LOSS OF AA5XXX AFTER 24-HOUR IMMERSION IN ETCHANTS TO QUANTIFY DEGREE OF SENSITIZATION

Mass loss testing was completed to determine the effects of the test environment on the degree of sensitization of 5XXX-series aluminum alloys. Mass loss testing followed the NAMLT methodology outlined in ASTM G67 that was slightly modified for temperature (35°C in place of 30°C) and environment (nitric acid, phosphoric acid, and ammonium persulfate).

3.2.2.1 MATERIALS AND SAMPLE PREPARATION

Mass loss test specimens of AA5083-H131 were cut from the center of a 2.25 inch-thick plate into pieces with the L x S x T dimensions of 5.0 cm x 2.5 cm x 0.6 cm²², in accordance with ASTM G67 [6]. A schematic of the cut specimens is shown to scale in Figure 3.1. The LS surface represented the largest surface area of the specimens.

²² Samples were cut from the plate using a low-speed band saw - machining was done by Peter Schare at the University of Virginia.

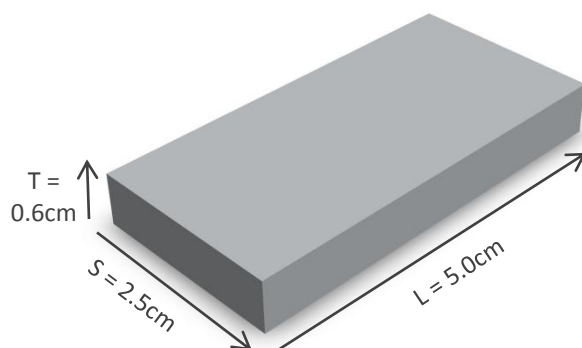


Figure 3.1 Schematic of a specimen cut from the center ($S/2$) of an as-received AA5083 plate for mass loss testing (shown to scale)

The specimens were then solution heat-treated and cold-water quenched (SHTQ) and artificially sensitized at 100°C for 7, 14, and 30 days (NAMLT mass loss²³ of 2, 16, 29, and 40 mg/cm², respectively). They were then ground to a 320 grit finish with silicon carbide (SiC) paper and water, and the edges were smoothed to minimize local stresses. The dimensions were measured to the nearest 0.02 millimeters (mm), and the total surface area was calculated.

The specimens were etched in 5 wt% sodium hydroxide (NaOH) at 80°C for 1 minute, followed by a water rinse and desmutting by immersion in concentrated nitric acid for 30 seconds. The specimens were then rinsed with water, dried with compressed air, and weighed to ± 1 mg [6].

3.2.2.2 EXPOSURE ENVIRONMENT

Duplicate specimens of each sensitization condition were individually immersed in concentrated nitric acid (70 wt%), phosphoric acid (40 vol/vol%), and acidified ammonium persulfate (pH 0.7)²⁴ for 24 hours at 35°C. The beakers containing the specimens were immersed in a water bath that was temperature-controlled to ± 0.1 °C. A solution-volume-to-surface-area ratio of ~ 3 mL/cm² (19 mL/in²) specified in ASTM G67 was consistent throughout testing [6]. PTFE beaker covers were used to reduce evaporation of the solution.

3.2.2.3 GRAIN FALLOUT AND MASS LOSS MEASUREMENTS

After 24 hours of immersion, the specimens were removed from the etchants and ultrasonically cleaned in ultrapure water to allow loosened grains to fall from the surfaces. The

²³ NAMLT mass loss is the degree of sensitization of samples exposed to concentrated nitric acid for 24 hours at 30°C.

²⁴ Solution preparation is described in more detail in Section 3.1.

specimens were air dried, and the final mass was measured to the nearest 1 mg. The average mass loss per unit area for each sensitization condition was calculated, and the final dimensions were measured to calculate the material lost during exposure. The etchant solutions were saved to assess the concentrations of dissolved species.

3.2.2.4 CALCULATION OF CORROSION CURRENT DENSITIES

The corrosion current densities during mass loss measurements, $i_{corr}(\text{mass})$ (Amperes/cm²), were calculated using Equation 3.1, derived from Faraday's Law [14]:

$$r = \left(\frac{1}{t}\right) \left(\frac{\Delta m}{A_s}\right)_{avg} = \frac{[i_{corr}(\text{mass})](EW)}{nF} \quad \text{Equation 3.1}$$

- + r = mass loss rate (grams/cm²·sec)
- + $(\Delta m/A_s)_{avg}$ = average mass loss per initial surface area (grams/cm²)
- + t = time (sec)
- + n = equivalent number of transferred electrons (equivalents/mole)
- + F = Faraday's constant (96485 Coulombs/mole·equivalent)
- + EW = equivalent weight of the alloy (grams/equivalent)

The equivalent weight of the alloy, EW , was calculated using Equation 3.2:

$$EW = \frac{1}{EQ} = \sum \frac{AW_i}{f_i n_i} \quad \text{Equation 3.2}$$

- + EQ = equivalence factor
- + AW_i = atomic weight of alloying element (grams/mole)
- + f_i = weight fraction of alloying element (wt%)
- + n_i = equivalent number of transferred electrons (equivalents/mole)

Based on the AA5083 composition listed in Table 2.1 in the Materials chapter, the two elements of concern when calculating EW are aluminum (94.4 – 95.6 wt%) and magnesium (4.4 wt %), since the other alloying additions combined total to a maximum of 1.2 wt %. Therefore the composition for the dominant elements was simplified, and a weight fraction of 0.956 for Al and 0.044 for Mg was utilized. Assuming congruent dissolution following the reactions listed in Equation 3.3 and Equation 3.4, an equivalent weight of ~9.10 grams/equivalent was calculated.



The equivalent weight was input into Equation 3.1 to solve for current density, which is compared to the corrosion current densities for the SHTQ sensitization condition from anodic polarization experiments (experiments are described in section 3.2.4 and results are described in chapters 4 and 5). Although much attention to detail was employed while following the NAMLT methodology, it is important to note that the corrosion current densities calculated using mass loss measurements are subject to the errors associated with each of those measurements.

3.2.3 DAMAGE PENETRATION ASSESSMENT OF AA5XXX AFTER 24-HOUR IMMERSION IN ETCHANTS TO COMPARE MORPHOLOGY OF ATTACK

Following the mass loss testing, the effects of the test environment on the damage morphology of AA5XXX were assessed and quantified.

3.2.3.1 MATERIALS AND DAMAGE MORPHOLOGY

The LS surfaces of the corroded AA5083 specimens from the 24-hour mass loss tests were imaged using digital microscopy (to allow for focusing on the varying damage depths). All surfaces of the specimens were then mounted in epoxy²⁵ to preserve the damage morphology, and cross-sectioned and polished to a colloidal silica finish with water to reveal the damage penetration in all three directions, L, T, and S. Optical micrographs of the polished cross-sections were then captured.

3.2.3.2 QUANTIFICATION OF DAMAGE DEPTH

Damage penetration in the L and T-directions was measured per damage site from selected optical micrographs that spanned ~3.4 mm across the surface of each specimen (two micrographs taken at 50x magnification). A damage site was defined as any discrete feature where material was lost, such as intergranular fissures or grain fallout voids. The penetration depth of each damage site was measured by hand; a grid of known spacing was overlaid on the micrograph

²⁵ Samples were mounted in a castable epoxy (resin + hardener) under vacuum to remove trapped gas from the fissures. Voids in epoxy coverage could lead to excess damage to the fissures during polishing. The epoxy was cured at standard atmospheric pressure at room temperature (i.e. heat and pressure were not applied that could alter the damage morphology of the specimen).

using GIMP software after calibrating the scale bar with ImageJ software, and the penetration depth was measured to the closest grid line.

In the case of “floating” intergranular fissures that did not appear to have an initiation site: the fissure tips were counted and their distance from the surface was measured. This averages and accounts for fissures traveling perpendicular to the viewing plane that may have been separated by sectioning or started directly beneath the imaged surface. The number of damage sites was counted to generate damage distributions and calculate an average damage site depth for each sensitization condition and etchant.

3.2.3.3 ICP ANALYSIS OF ETCHANT SOLUTIONS

Inductively coupled plasma optical emission spectrometry (ICP-OES) was used to analyze the etchants after 24-hour exposure to ascertain the types and relative amounts of AA5XXX species that dissolved into solution. The solutions from the nitric acid, phosphoric acid, and ammonium persulfate (pH 0.7) exposures of the SHTQ and 100°C-30days sensitization conditions were analyzed²⁶.

The solutions were first decanted – particulates were allowed to settle and the liquid was pipetted into a trace-metal-free, biological-grade container – to measure concentrations in the etchants without additional dissolution by the grain-fallout particulates. The decanted solutions were diluted by a factor of 10, mixed thoroughly, and run through the ICP-OES.

Concentrations were calibrated against standards of Al, Mg, Mn, Fe, and Si; other alloying additions were not calibrated due to their low overall weight percent in the material and the detection limits of the instrument. The specification detection limits of the instrument are listed in Table 3.2. Each of the twelve replicate tests of the etchants was also run against an internal Yttrium (Y) standard to compensate for varying solution viscosities and dilution.

Table 3.2 Specification detection limits of ICP-OES instrument in parts per million (ppm)

Al	Mg	Mn	Fe	Si
0.0041 ppm	0.00001 ppm	0.00007 ppm	0.00025 ppm	<i>Not Available</i>

Concentrations were reported in parts per million (ppm) with individual standard deviations for each specie; these values were not converted to an overall weight percent of the material due

²⁶ ICP analysis was performed by Joseph Hagan at the University of Virginia.

to the unknown weight of the grain fallout residue. It was expected that the ratio of aluminum to magnesium concentrations in solution would indicate the extent to which etchants selectively attacked the β -phase.

3.2.4 ANODIC POLARIZATION OF β -PHASE AND AA5XXX MATRIX TO QUANTIFY ETCHANT SELECTIVITY

Samples of AA5083-H131 (~4.4 wt% Mg) and synthesized, pure β -phase (~36 wt% Mg) were tested in nitric acid, phosphoric acid, and ammonium persulfate to compare their polarization behaviors and quantify etchant selectivity and its dependence on temperature.

3.2.4.1 MATERIALS AND SAMPLE PREPARATION

Solution heat-treated and cold-water quenched (SHTQ) specimens of AA5083 were chosen to represent the bulk AA5XXX matrix for polarization experiments; the material should be a solid solution of aluminum and magnesium and have little if any β -phase precipitation at the grain boundaries, but also contains the cathodic constituent particles that may play a role in the selective attack of the β -phase. The SHTQ material has a NMLT mass loss value of 2 mg/cm² and is considered unsensitized.

The β -phase sample was synthesized via induction melting. It was confirmed to be single phase following several characterization techniques described in Chapter 2 (Materials).

In preparation for electrochemical analysis, the mounted β -phase specimen and the AA5083 samples were ground to 1200 grit using SiC paper and ethylene glycol to limit the dissolution of the β -phase. The samples were rinsed in acetone, dried with compressed air, and stored in a desiccator (when necessary) prior to testing.

3.2.4.2 ELECTROLYTE ENVIRONMENT

The AA5083-SHTQ and β -phase samples were exposed to concentrated nitric acid (70 wt%), phosphoric acid (40 vol/vol%), and acidified ammonium persulfate (pH 1.2 and 0.7). The samples were exposed at 15°C, 22°C (room temperature), 35°C, and 50°C. Nitric acid was additionally exposed at 30°C, the temperature defined in the Nitric Acid Mass Loss Test. The solutions were pre-heated or cooled prior to testing, and the temperature of the exposures was maintained in a controlled ($\pm 0.1^\circ\text{C}$), forced-air temperature chamber.

Additional experiments were run to determine the corrosion-dominating species in ammonium persulfate. Anodic polarization scans of both AA5083-SHTQ and β -phase samples in dilute, pH 0.7 sulfuric acid, 0.4M sodium persulfate, and 0.4M ammonium sulfate were

performed to compare the current densities to those of the materials in pH 0.7 ammonium persulfate.

3.2.4.3 POLARIZATION PARAMETERS

Anodic polarization testing of AA5083-SHTQ in the selected etchants was conducted according to the following protocol: (1) a 5 minute open circuit potential (OCP) measurement to allow for system stabilization and (2) an IR-compensated potentiodynamic scan 200 millivolts (mV) below to at least 400 mV above the OCP. The scan rate was 2 mV/sec.

Additional tests on both the LT and LS surfaces of the SHTQ samples were completed at 35°C (the selected mass loss test temperature) after 5 minute and 30 minute stabilizing OCP holds to determine how the corrosion current density and OCP change with exposure time and surface orientation. The tests were run with the aforementioned polarization parameters with the exception of the longer OCP hold.

Polarization of the β -phase followed a protocol similar to that of the SHTQ tests: (1) a 5 minute OCP measurement to allow for system stabilization and (2) an IR-compensated potentiodynamic scan 200 mV below the OCP of β -phase to 100 mV above the OCP of AA5083-SHTQ in the same solution. The scan rate was 5 mV/sec to limit the exposure time and excessive mass loss during dissolution.

A schematic of the three-electrode cell used in the experiments is shown in Figure 3.2. The area of the sample exposed to the solution was consistently defined by an O-ring. A platinized counter electrode and mercury/mercurous sulfate (Hg/HgSO_4) reference electrode (MSE) was used for all experiments, where MSE is +0.64 volts (V) versus the normal hydrogen electrode (NHE). The solution-volume-to-surface-area ratio was at least 250 mL/cm², and solutions were replaced/refreshed for every test. All glassware was pre-cleaned in nitric acid to remove possible chlorides in solution.

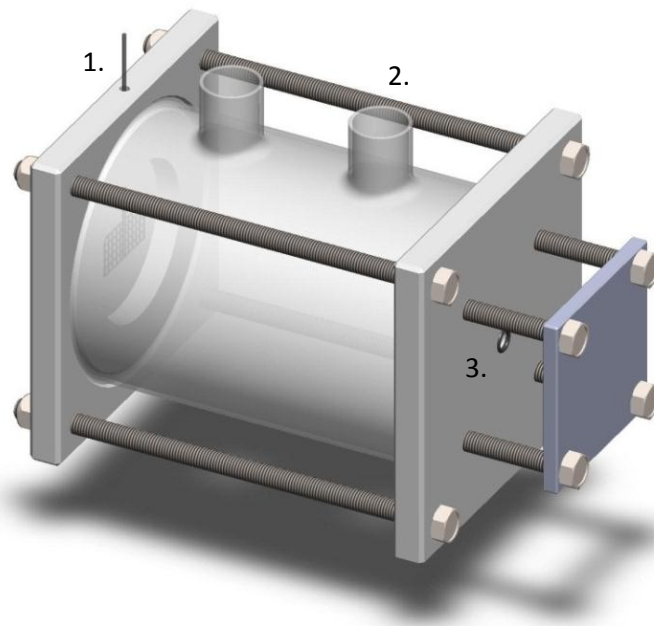


Figure 3.2 Schematic of an electrochemical flat cell used in anodic polarization experiments

- (1.) Platinized niobium counter electrode
- (2.) Opening for MSE reference electrode
- (3.) Working electrode-electrolyte interface. O-ring with inner area of $\sim 0.06\text{cm}^2$ controls surface area of specimen

3.2.4.4 QUANTIFICATION OF ETCHANT SELECTIVITY

Electrochemical variables determined through anodic polarization tests of the β -phase and matrix included open circuit potential, polarization resistance, corrosion current density, and passive current density. The polarization resistance (R_p) was determined from linear plots of potential versus current density at potentials near the OCP, and the corrosion current densities were determined by extrapolating the passive current densities to the OCP.

Comparing the polarization resistances of the β -phase and the matrix at their respective open circuit potentials could indicate how selective an etchant is for Mg dissolution, since the β -phase is more Mg-rich than the matrix (~ 36 wt% Mg for the β -phase relative to 4.4 wt% for the matrix). However, the ratio of current densities at the OCP of the matrix is more representative of the coupled behavior. In sensitized material undergoing etchant exposure, the β -phase is polarized up to the OCP of the surrounding alloy matrix. This occurs since the β -phase present at the grain boundaries represents a very small fraction of the total exposed surface (an approximate maximum of 8.5 vol% β -phase compared to 91.5 vol% α -phase in AA5083²⁷).

²⁷ The volume fractions of the β and α -phases were approximated assuming that material with the nominal Mg content of AA5083 (4.4 wt% Mg) reached equilibrium at 100°C (sensitizing temperature) to precipitate the maximum amount of β -

Therefore etchant selectivity was quantified as the ratio of the current density of the β -phase at the OCP of the alloy to the corrosion current density of the alloy.

phase from the solid solution α -phase, and that the quenching process preserved the equilibrium volume fractions. The calculation is detailed in the Background and Objectives Chapter.

4 RESULTS

4.1 SHORT-TERM OPEN CIRCUIT POTENTIAL ETCHING OF AA5XXX

AA5083 specimens were immersed in concentrated nitric acid, phosphoric acid, and acidified ammonium persulfate at 22°C, 30°C, and 35°C to qualitatively screen the effectiveness of the etchants and their sensitivity to temperature. Optical micrographs of the specimens after OCP etching are shown in Figures 4.2 – 4.11. The micrographs are categorized by etchant, grouped by surface (LS, LT) and time of etch (t_{etch}), and organized by temperature of etch and the sensitization condition/NAMLT value of the specimen. This arrangement of the micrographs follows the hierarchy shown in Figure 4.1.

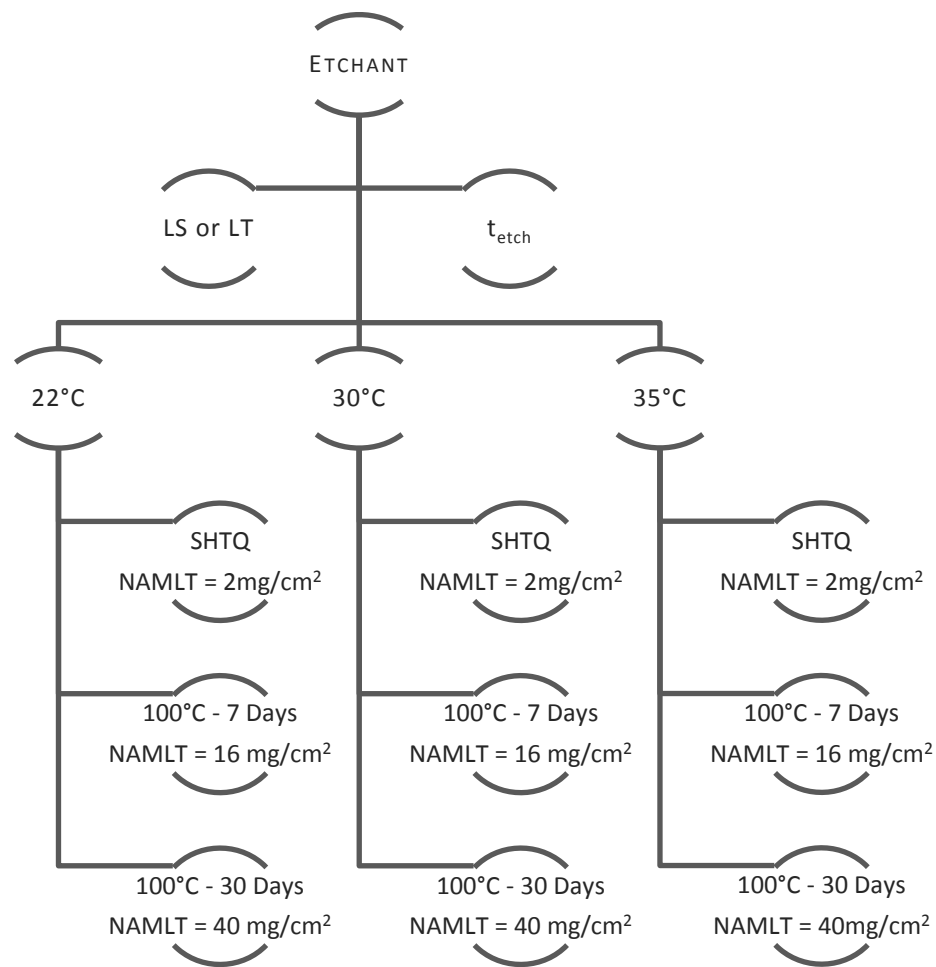


Figure 4.1 Organization of post-OCP-immersion micrographs in Figures 4.2 – 4.11

The specimen surfaces after etching captured in each micrograph are described by the extent and clarity of the etch. The extent of etching refers to the state of grain boundary attack, which

is qualitatively determined based on the corresponding visibility/highlighting of the boundaries – un-etched specimens have no visible grain boundary attack, partially etched specimens have lightly and non-uniformly attacked grain boundaries, etched specimens have uniformly attacked and highlighted grain boundaries²⁸, and over-etched grain boundaries are visibly dark, wide, and continuous. Etch clarity qualitatively refers to the visible differentiation in attack between the grain boundaries and the matrix. The extent and clarity of the etch are linked, such that the extent of grain boundary attack may be obscured by the attack of the matrix. Parameters affecting both the extent and clarity of etching for a given chemistry include surface preparation and temperature of exposure, which in turn determine the time to etch.

4.1.1 OCP IMMERSION ETCHING IN NITRIC ACID

Optical micrographs of AA5083 specimens after immersion in concentrated nitric acid are shown in Figures 4.2 – 4.5. Figures 4.2 and 4.3 show the LS and LT surfaces after 60 minutes of immersion, respectively. Figures 4.4 and 4.5 show the LS and LT surfaces after 90 minutes of immersion, respectively.

The SHTQ (NAMLT = 2 mg/cm²) specimens do not exhibit grain boundary etching on either surface, as expected due to the re-solutionizing of precipitated β -phase before testing. Grain boundary attack increases with sensitization condition; specimens sensitized at 100°C for 30 days (NAMLT = 40 mg/cm²) show higher uniformity of attack at the grain boundaries than the specimens sensitized at 100°C for 7 days (NAMLT = 16 mg/cm²).

Etching was observed to be highly dependent on temperature; specimens sensitized for 30 days and immersed at 22°C are relatively un-etched after 60 minutes, whereas specimens of the same sensitization have etched grain boundaries at 30°C and 35°C for the LS surface, and partially etched and etched grain boundaries at 30°C and 35°C, respectively, for the LT surface.

The edges of the constituent particles are attacked after all exposures, indicating either the presence of β -phase precipitates and/or galvanic coupling interactions with the matrix. The moderate attack of the matrix may have obscured the attack of the grain boundaries at 22°C, which led to the re-immersion of the specimens for a total etching time of 90 minutes.

After 90 minutes of exposure to nitric acid, grain boundary attack was at least partially visible on both surfaces of the 100°C-7days and 100°C-30days specimens. The SHTQ samples remained un-etched, and the sensitized 35°C samples were over-etched.

²⁸ Attacked grain boundaries do not need to appear as continuous to be considered “etched”, since β -phase does not always precipitate continuously along the grain boundaries.

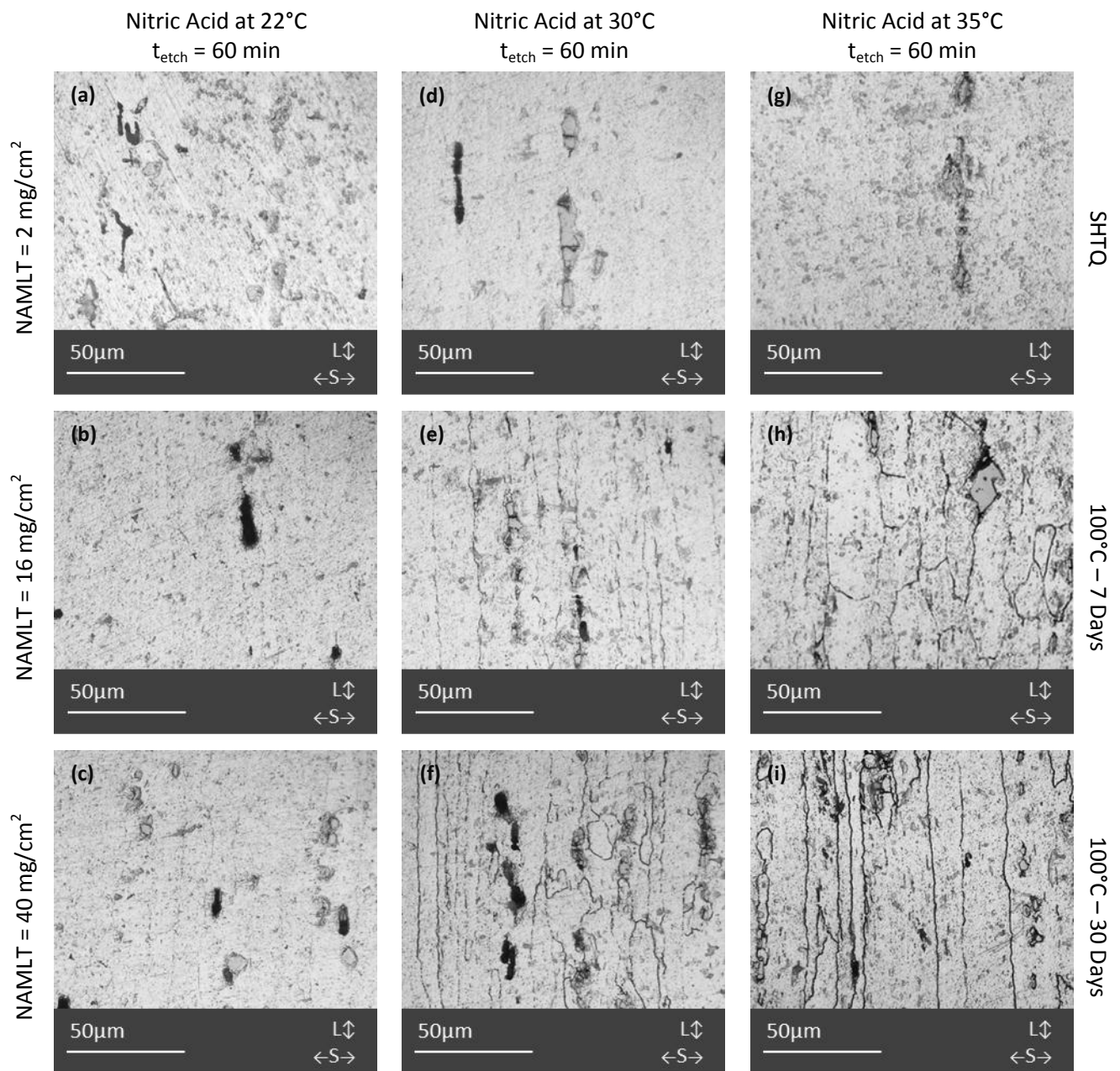


Figure 4.2 Optical micrographs of **LS surface** of AA5083 of varying sensitization conditions after **60 minute immersion in nitric acid** at: 22°C (a)-(c), 30°C (d)-(f), and 35°C (g)-(i).

Extent of etch: (a) un-etched (b) un-etched (c) un-etched/partially etched (d) un-etched (e) partially etched/etched (f) etched (g) un-etched (h) etched (i) etched/over-etched

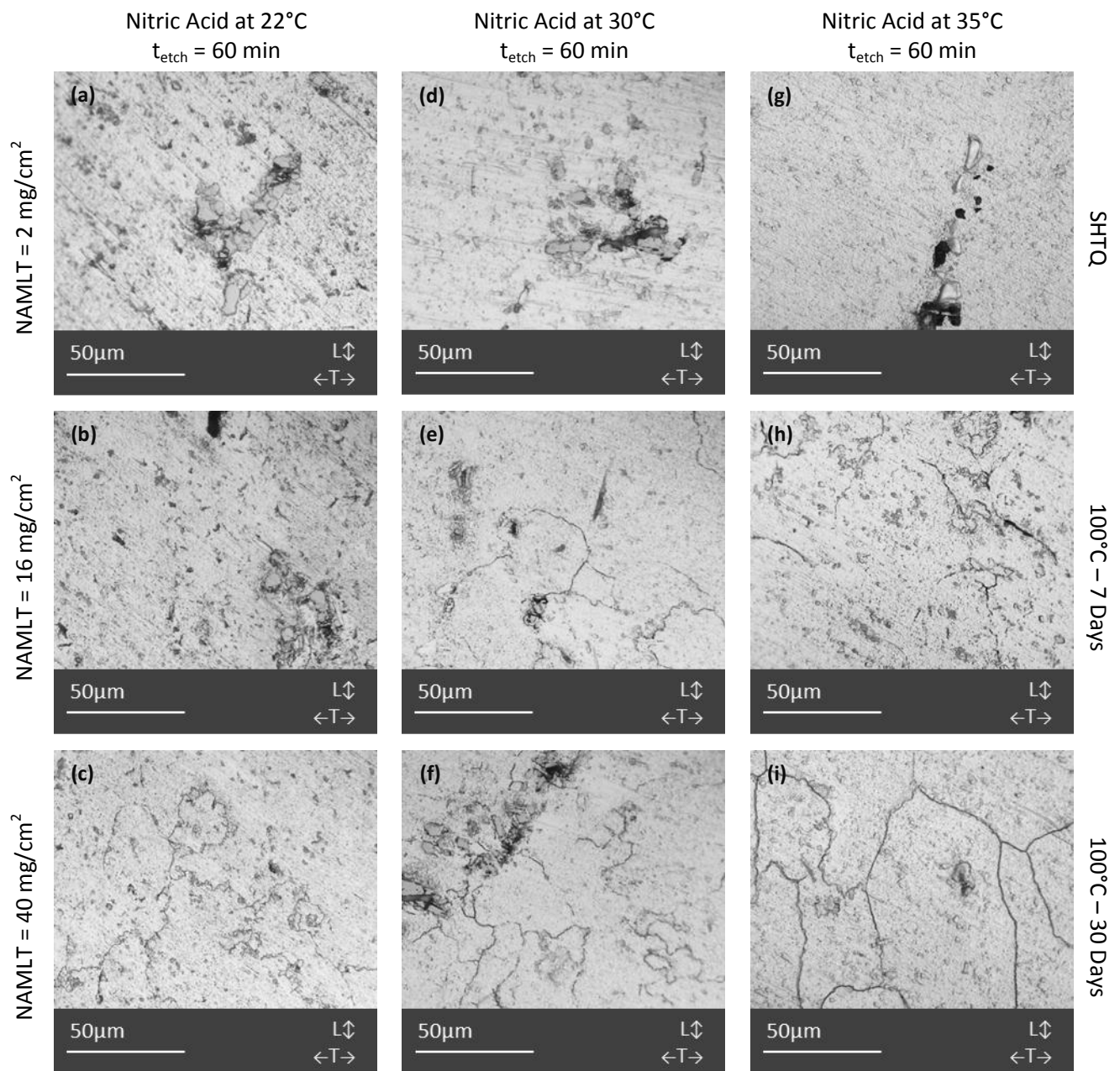


Figure 4.3 Optical micrographs of **LT surface** of AA5083 of varying sensitization conditions after **60 minute immersion in nitric acid** at: 22°C (a)-(c), 30°C (d)-(f), and 35°C (g)-(i).

Extent of etch: (a) un-etched (b) un-etched (c) un-etched/partially etched (d) un-etched (e) partially etched (f) etched (g) un-etched (h) partially etched (i) etched

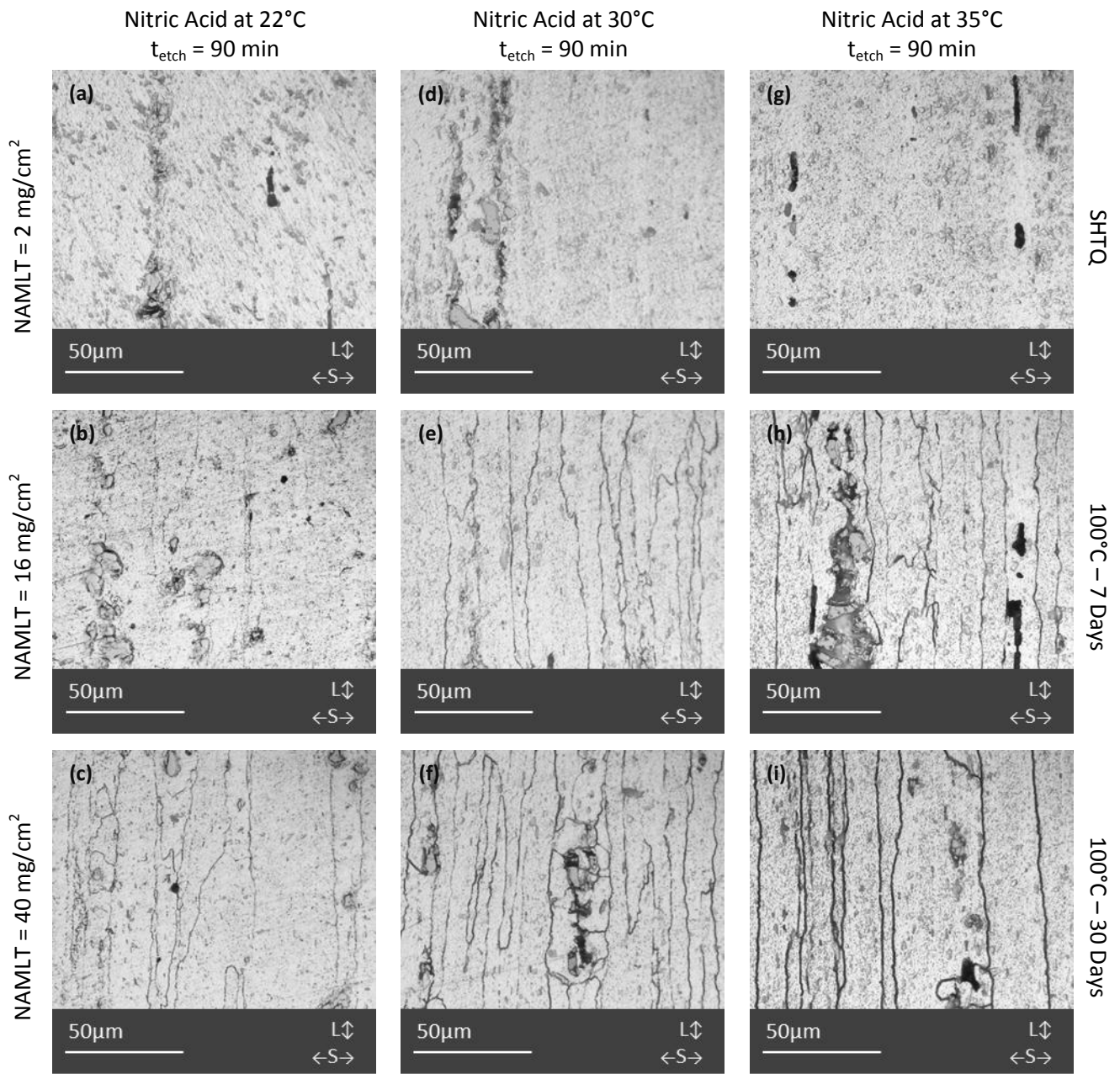


Figure 4.4 Optical micrographs of **LS surface** of AA5083 of varying sensitization conditions after **90 minute immersion in nitric acid** at: 22°C (a)-(c), 30°C (d)-(f), and 35°C (g)-(i).

Extent of etch: (a) un-etched (b) un-etched/partially etched (c) etched (d) un-etched (e) etched (f) etched (g) un-etched (h) etched (i) over-etched

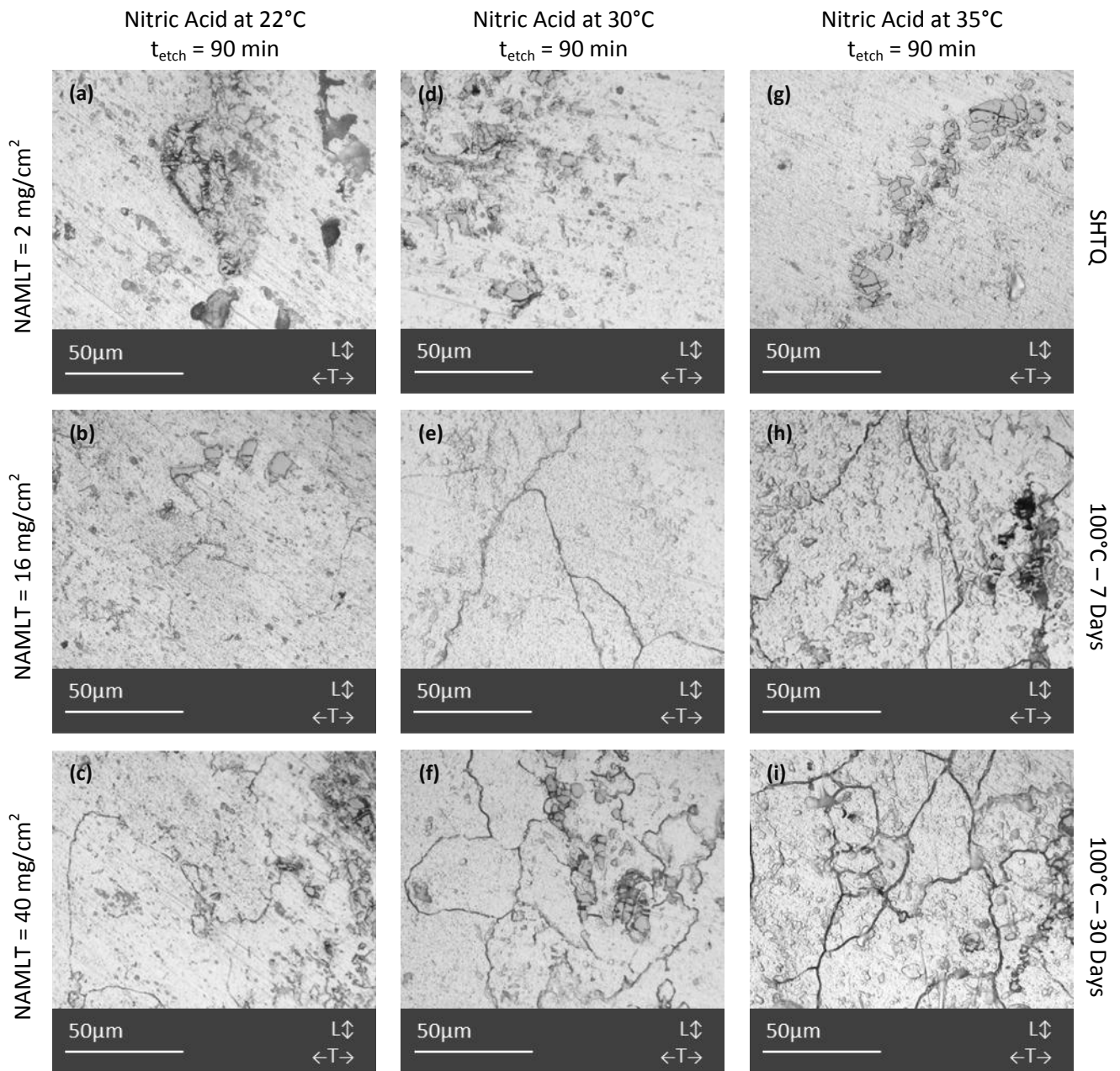


Figure 4.5 Optical micrographs of **LT surface** of AA5083 of varying sensitization conditions after **90 minute immersion in nitric acid** at: 22°C (a)-(c), 30°C (d)-(f), and 35°C (g)-(i).

Extent of etch: (a) un-etched (b) un-etched/partially etched (c) partially etched/etched (d) un-etched (e) etched (f) etched (g) un-etched (h) etched/over-etched (i) over-etched

4.1.2 OCP IMMERSION ETCHING IN PHOSPHORIC ACID

Optical micrographs of AA5083 specimens after immersion in 40 vol% phosphoric acid are shown in Figures 4.6 – 4.9. Figures 4.6 and 4.7 show the LS and LT surfaces after 3 minutes²⁹ of immersion, respectively. Figures 4.8 and 4.9 show the LS and LT surfaces after 10 minutes of immersion, respectively.

Grain boundary attack increased with sensitization condition; SHTQ specimens were not etched, while specimens sensitized at 100°C for 30 days showed higher uniformity of attack at the grain boundaries than the specimens sensitized at 100°C for 7 days.

Etching was observed to be highly dependent on temperature; specimens sensitized for 30 days and immersed at 22°C are relatively un-etched after 3 minutes, whereas specimens of the same sensitization show etched grain boundaries at 30°C and 35°C for the LS and LT surfaces.

The edges of the constituent particles are attacked after all exposures, indicating either the presence of β -phase precipitates and/or galvanic coupling interactions with the matrix. There is relatively high attack of the matrix, which may be obscuring the attack of the grain boundaries of the 100°C-30days specimen at 22°C and the 100°C-7days specimen at all tested temperatures. The specimens were re-immersed up to a total exposure time of 10 minutes to observe the grain boundaries at 22°C.

After 10 minutes of exposure to phosphoric acid, grain boundary attack was at least partially visible on both surfaces of the 100°C-7days and 100°C-30days specimens. The SHTQ samples remained un-etched, and the sensitized 35°C samples were over-etched.

²⁹ ASTM B928 specifies etching AA5XXX samples for 3 minutes at 35°C

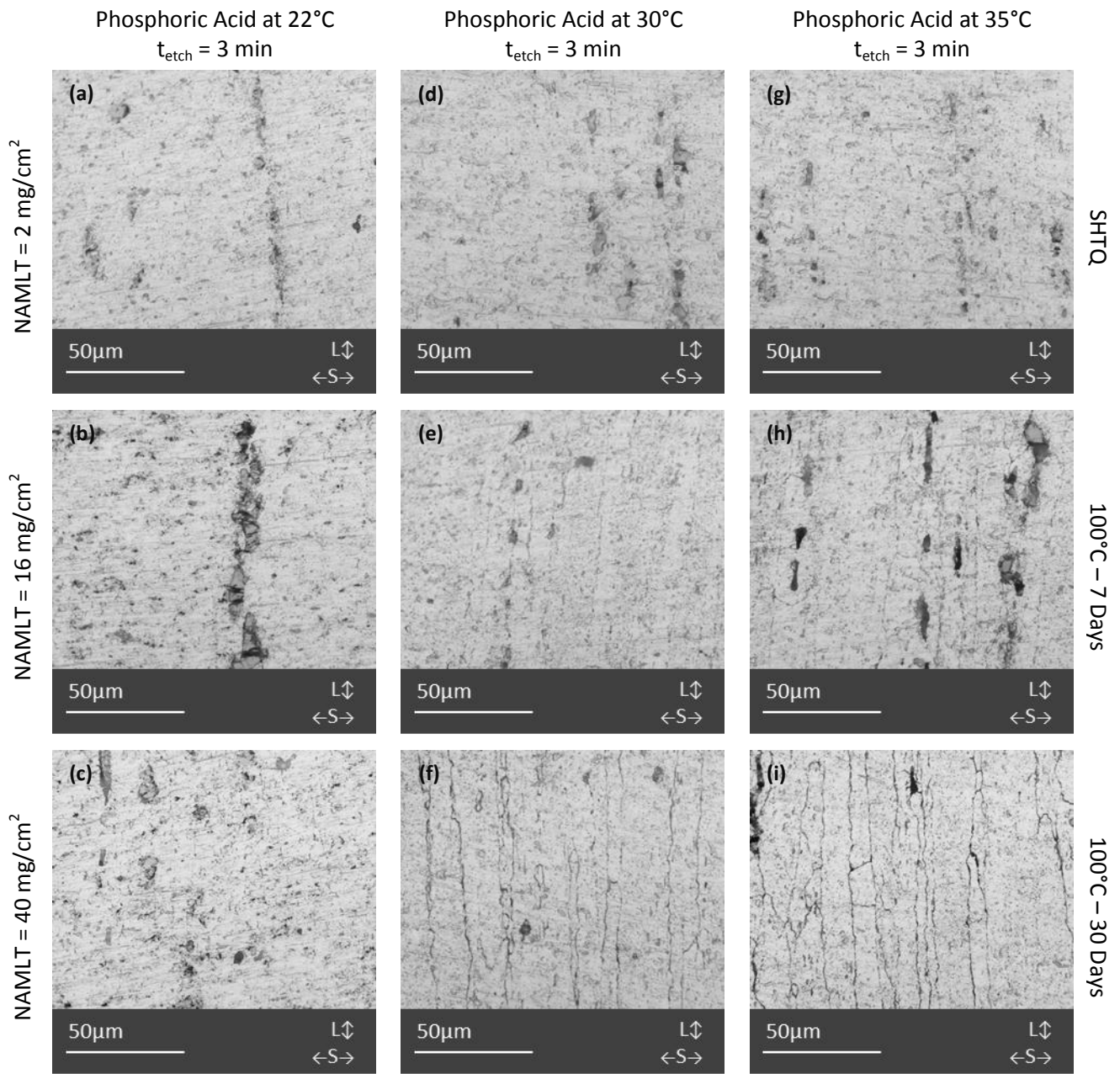


Figure 4.6 Optical micrographs of **LS surface** of AA5083 of varying sensitization conditions after **3 minute immersion in phosphoric acid** at: 22°C (a)-(c), 30°C (d)-(f), and 35°C (g)-(i).

Extent of etch: (a) un-etched (b) un-etched (c) un-etched (d) un-etched (e) un-etched/partially etched (f) partially etched (g) un-etched (h) un-etched/partially etched (i) etched

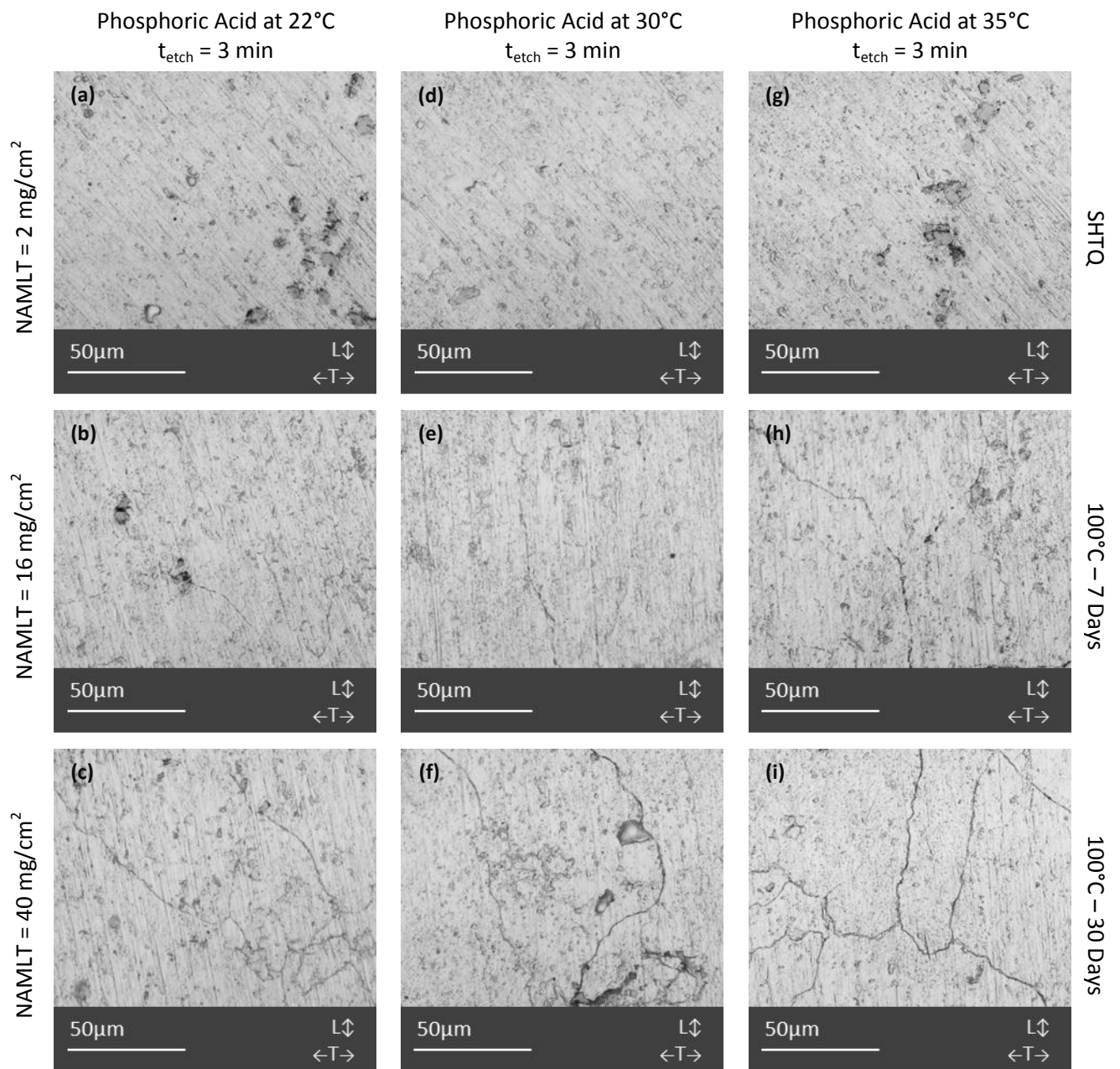


Figure 4.7 Optical micrographs of **LT surface** of AA5083 of varying sensitization conditions after **3 minute immersion in phosphoric acid** at: 22°C (a)-(c), 30°C (d)-(f), and 35°C (g)-(i).

Extent of etch: (a) un-etched (b) un-etched/partially etched (c) partially etched/etched (d) un-etched (e) un-etched/partially etched (f) partially etched/etched (g) un-etched (h) partially etched (i) etched

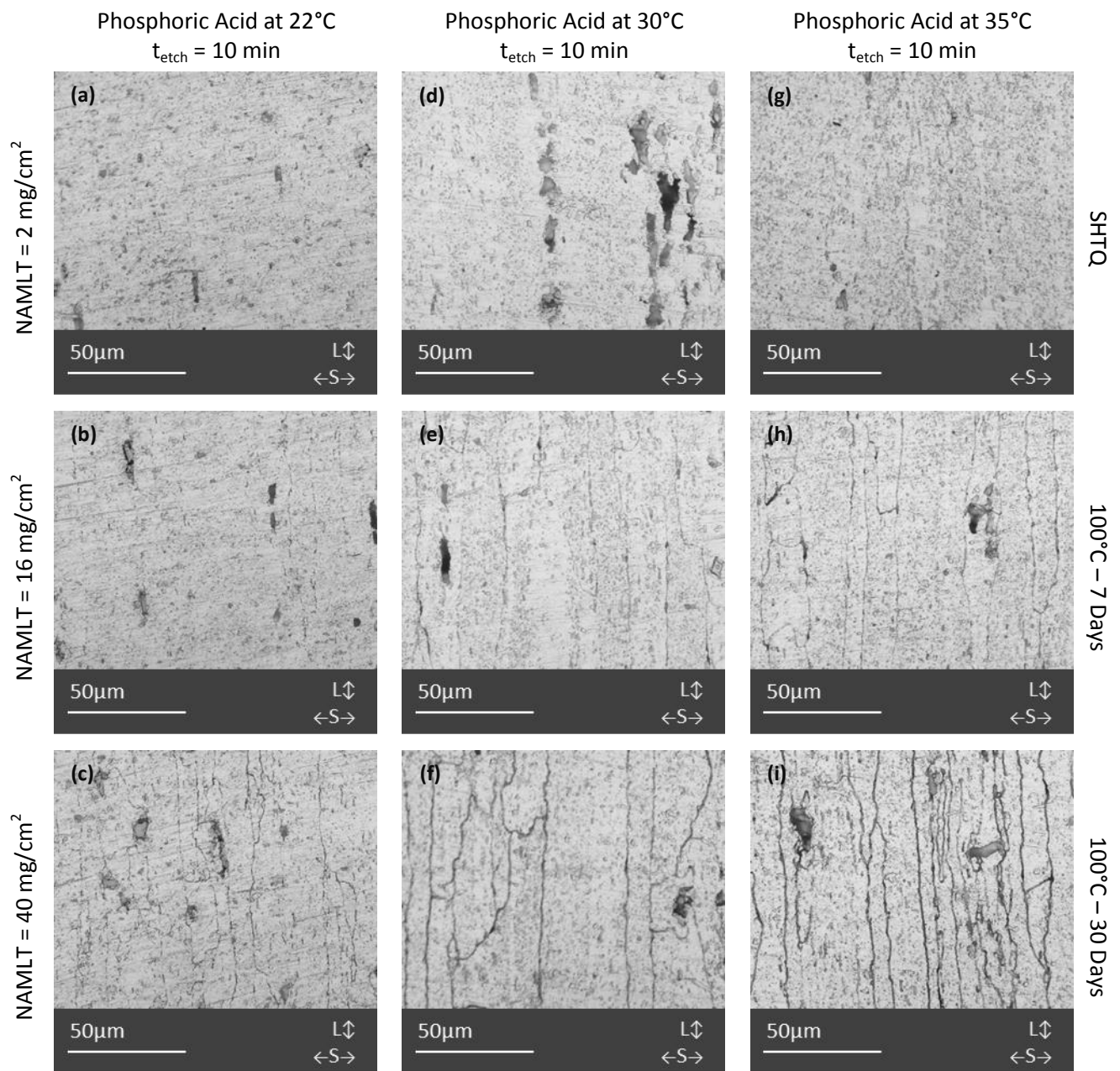


Figure 4.8 Optical micrographs of **LS surface** of AA5083 of varying sensitization conditions after **10 minute immersion in phosphoric acid** at: 22°C (a)-(c), 30°C (d)-(f), and 35°C (g)-(i).

Extent of etch: (a) un-etched (b) un-etched/partially etched (c) partially etched/etched (d) un-etched (e) partially etched (f) etched (g) un-etched (h) etched (i) over-etched

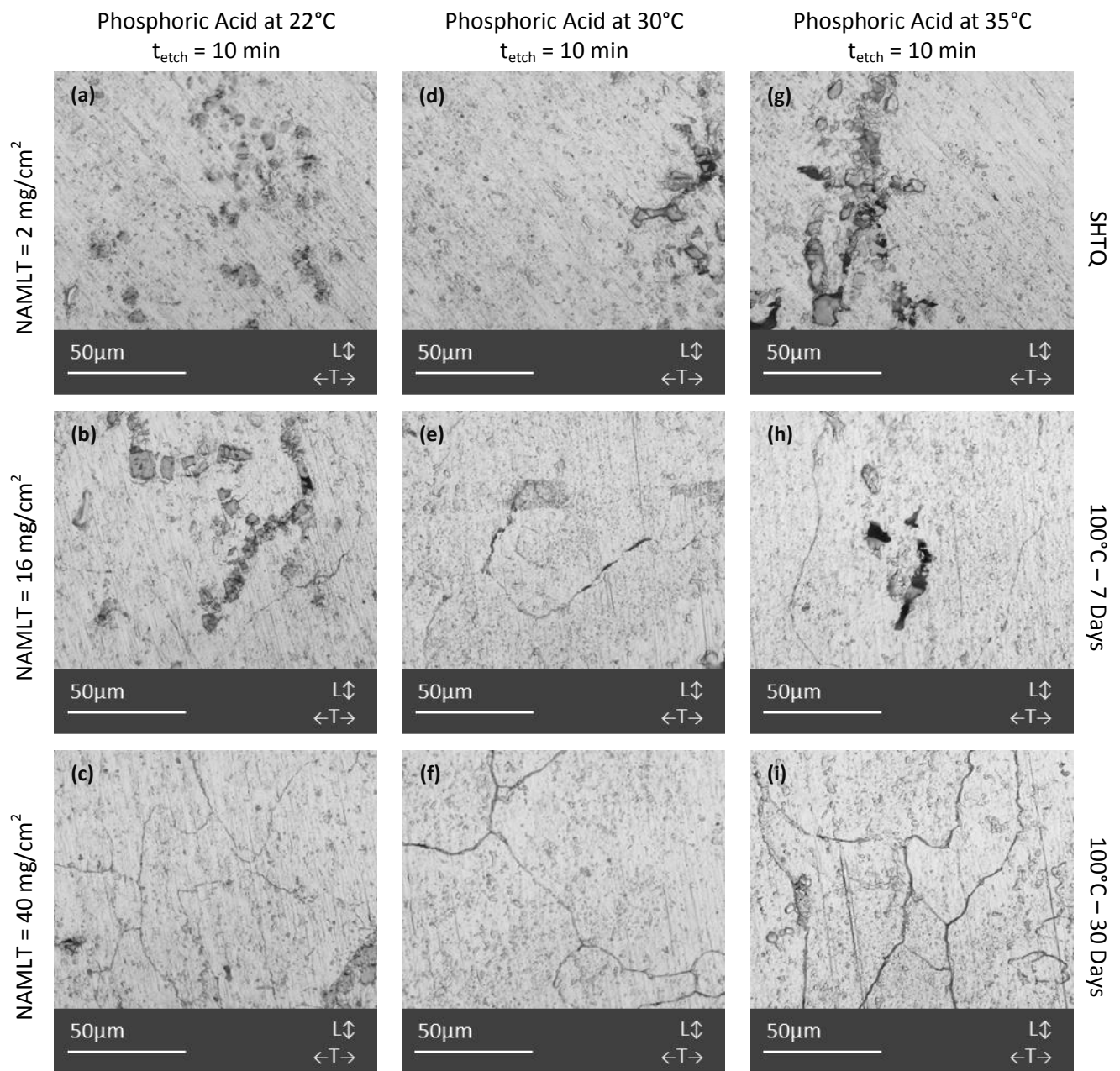


Figure 4.9 Optical micrographs of **LT surface** of AA5083 of varying sensitization conditions after **10 minute immersion in phosphoric acid** at: 22°C (a)-(c), 30°C (d)-(f), and 35°C (g)-(i).

Extent of etch: (a) un-etched (b) un-etched/partially etched (c) partially etched/etched (d) un-etched (e) partially etched (f) etched (g) un-etched (h) partially etched (i) over-etched

4.1.3 OCP IMMERSION ETCHING IN AMMONIUM PERSULFATE

Figures 4.10 and 4.11 show the LS and LT surfaces after 90 minutes³⁰ of immersion in pH 1.2 ammonium persulfate, respectively.

Grain boundary attack increased with sensitization condition; SHTQ specimens were not etched, while specimens sensitized at 100°C for 30 days showed higher uniformity of attack at the grain boundaries than the specimens sensitized at 100°C for 7 days.

Etching was observed to be dependent on temperature; LS surface specimens sensitized for 30 days and immersed at 22°C were etched after 90 minutes, whereas specimens of the same sensitization showed over-etched grain boundaries at 30°C and 35°C for the LS surface.

The edges of the constituent particles are attacked after all exposures, indicating either the presence of β -phase precipitates and/or galvanic coupling interactions with the matrix. There is relatively low to moderate attack of the matrix, which may be obscuring the extent of attack of the grain boundaries of the 100°C-7days specimens at 22°C.

³⁰ Previous work by Lei Chen showed that the time to etch in pH 1.2 ammonium persulfate was approximately 60 minutes at room temperature; grain boundaries were not observed for the highest sensitization level at 22°C after 60 minutes in these experiments. However, the specimens in this work were only ground to 1200 grit and were not further polished, which may account for the longer time to etch used in these experiments.

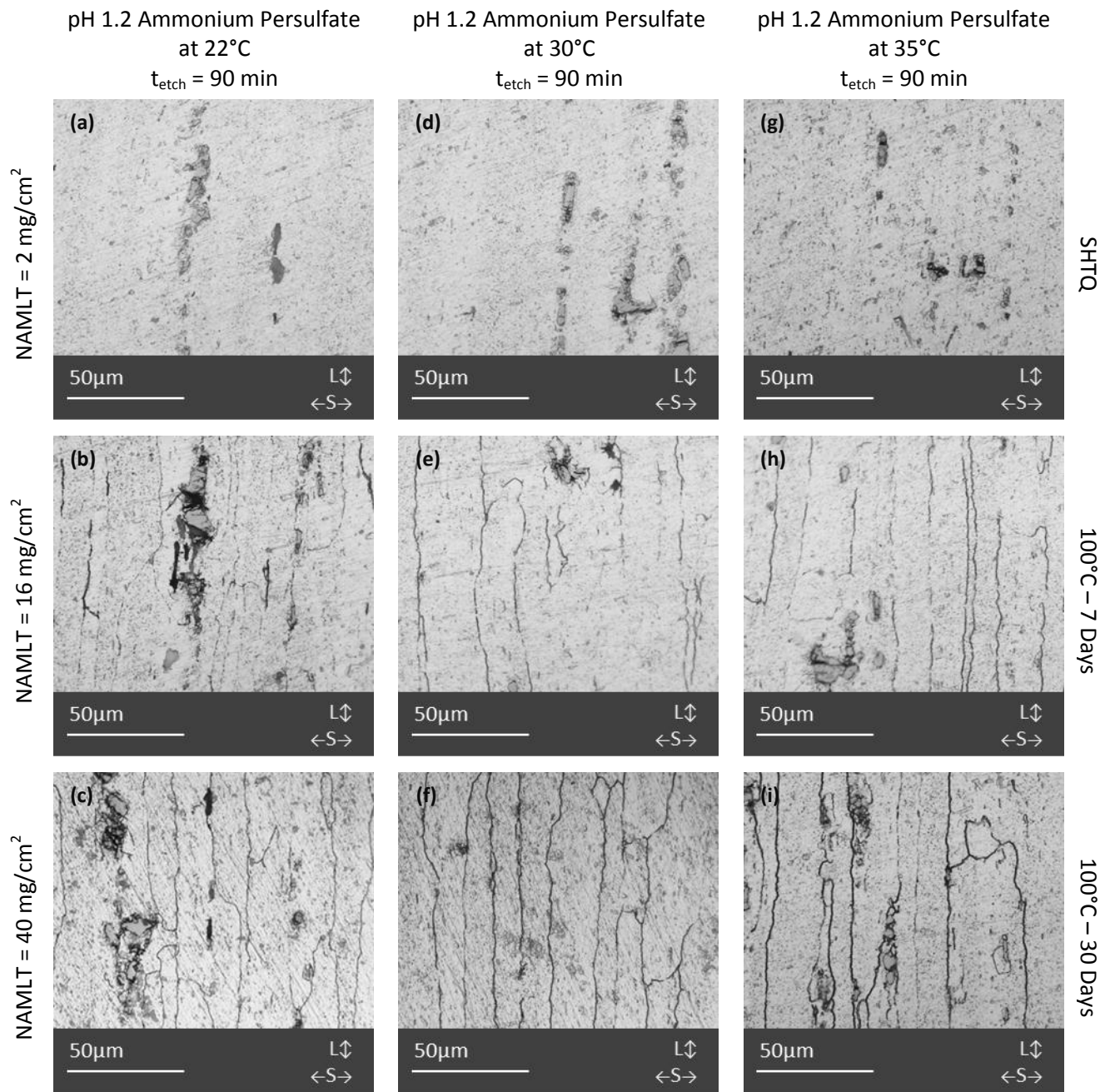


Figure 4.10 Optical micrographs of **LS surface** of AA5083 of varying sensitization conditions after **90 minute immersion in pH 1.2 ammonium persulfate** at: 22°C (a)-(c), 30°C (d)-(f), and 35°C (g)-(i).

Extent of etch: (a) un-etched (b) partially etched/etched (c) etched (d) un-etched (e) partially etched/etched (f) etched/over-etched (g) un-etched (h) partially etched/etched (i) etched/over-etched

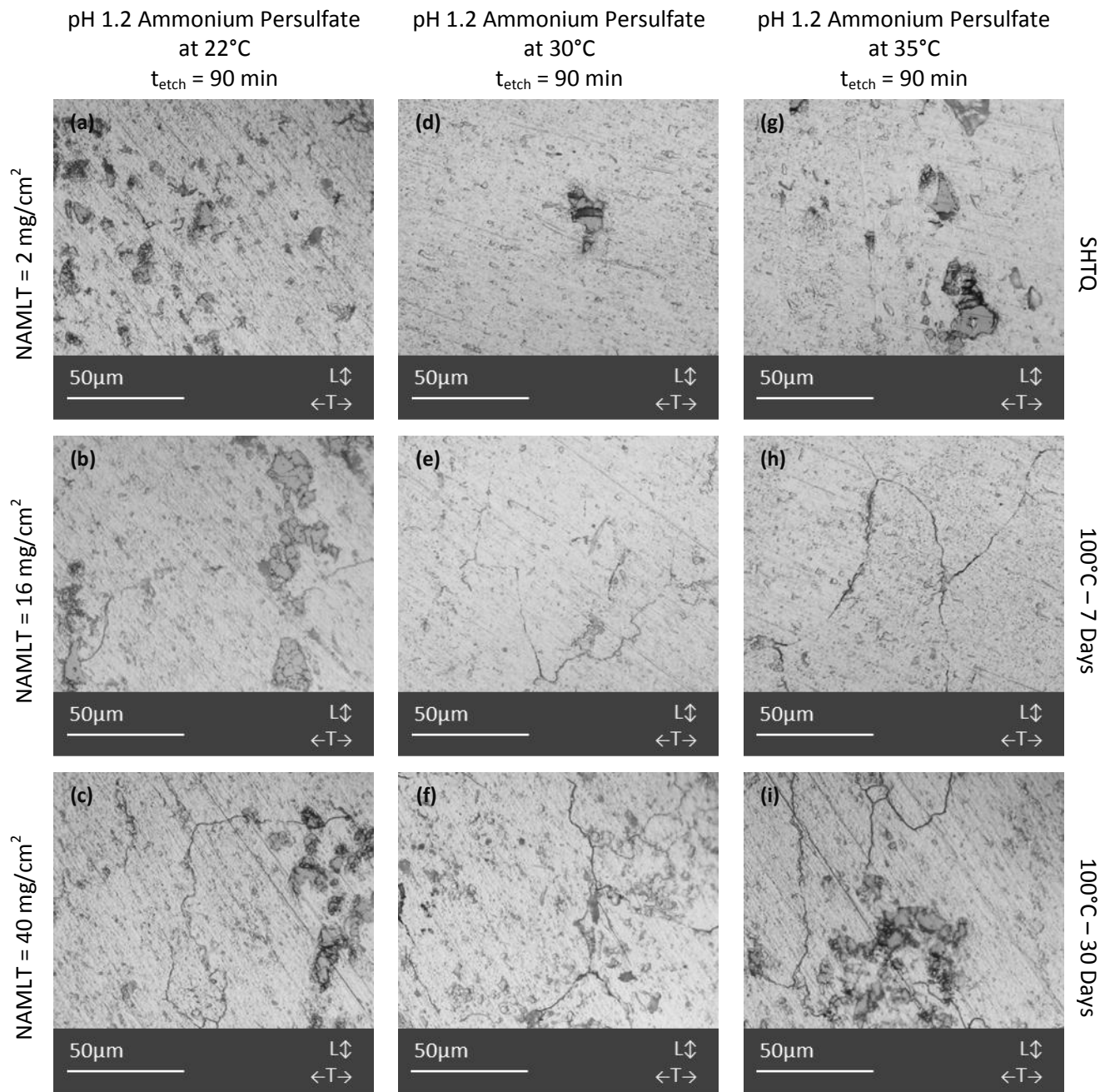


Figure 4.11 Optical micrographs of **LT surface** of AA5083 of varying sensitization conditions after **90 minute immersion in pH 1.2 ammonium persulfate** at: 22°C (a)-(c), 30°C (d)-(f), and 35°C (g)-(i).

Extent of etch: (a) un-etched (b) un-etched/partially etched (c) partially etched (d) un-etched (e) partially etched (f) etched (g) un-etched (h) etched (i) etched

4.2 MASS LOSS AND DAMAGE PENETRATION IN AA5XXX AFTER 24-HOUR IMMERSION IN ETCHANTS

Mass loss tests in concentrated nitric acid, phosphoric acid, and acidified ammonium persulfate were conducted according to the procedures in ASTM G67, the Nitric Acid Mass Loss Test. The results were used to quantify the degree of sensitization (DoS) of the AA5XXX material. The corroded specimens and etchant solutions after exposure were then analyzed to determine the effects of the etchant environment on the damage morphology.

4.2.1 MASS LOSS AND DEGREE OF SENSITIZATION

Mass loss results after 24-hour immersion in concentrated nitric acid, phosphoric acid, and acidified ammonium persulfate at 35°C are shown in Figure 4.1 and summarized in Table 4.1. The average mass loss over 2 samples, expressed per area (mg/cm^2), increases with sensitization condition in each etchant. Phosphoric acid exposures resulted in the highest mass loss across all sensitization conditions, while ammonium persulfate exposures resulted in the lowest mass loss. Nitric acid acted comparably at both 30°C (the specified NAMLT temperature) and 35°C; the mass loss over the range of sensitization conditions increased at both temperatures by similar percent changes. However, the mass lost at 35°C was almost twice as much as that lost at 30°C, which indicates high temperature sensitivity.

Table 4.1 Summary of mass loss results after immersion in etchants for 24 hours

Sensitization Condition	Average Mass Loss (mg/cm^2)			
	30°C Nitric Acid	35°C Nitric Acid	35°C Phosphoric Acid	35°C Ammonium Persulfate
275°C – 10 hrs. (SHTQ)	2	3	64	3
100°C – 7 Days	16	32	113	14
100°C – 14 Days	29	59	129	26
100°C – 30 Days	40	76	138	33

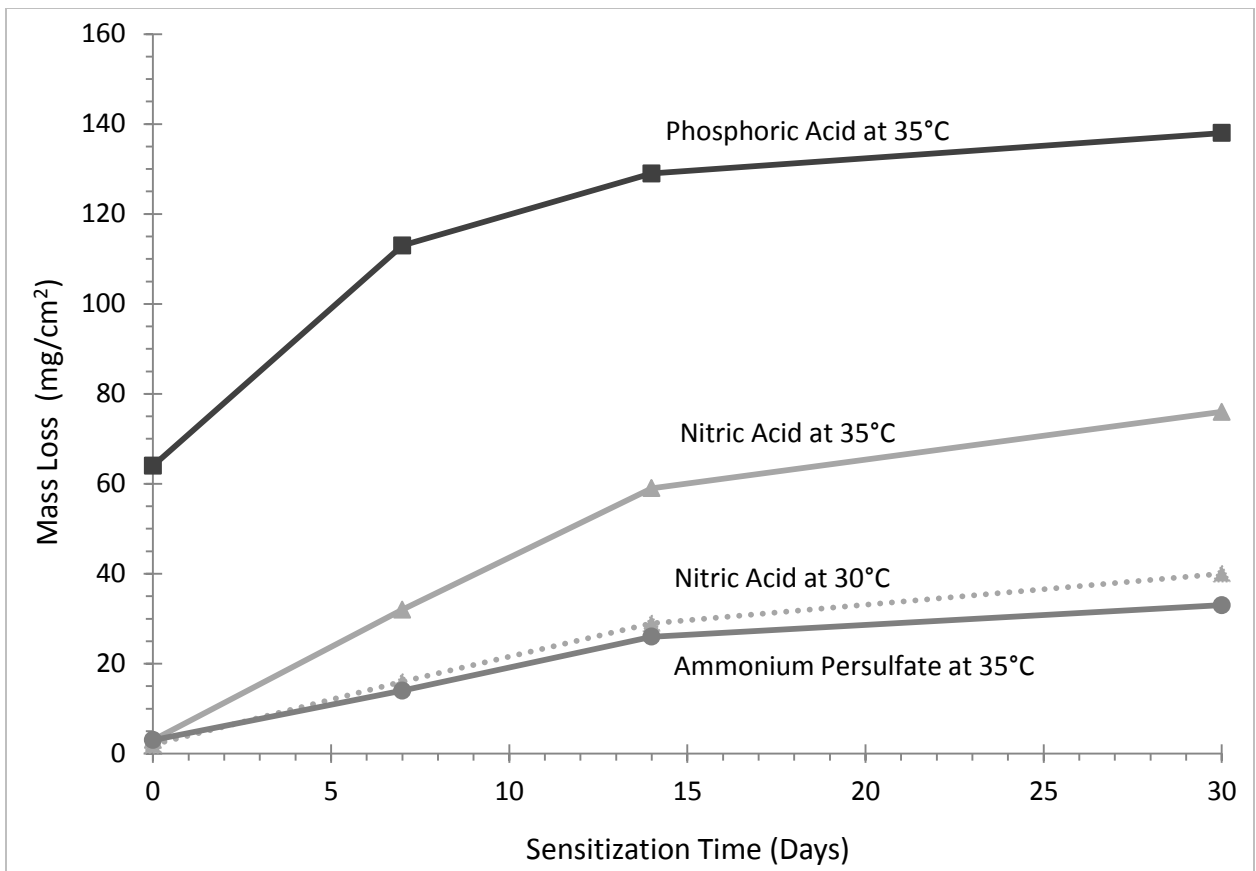


Figure 4.12 Mass loss of AA5083 of varying sensitization conditions exposed to etchants for 24 hours following procedures of ASTM G67³¹

4.2.2 MASS LOSS RATES / CORROSION CURRENT DENSITIES

The average mass loss values from the modified NAMLT testing were used in conjunction with Equations 3.1 – 3.4 to calculate the average corrosion current density for each sensitization condition over 24 hours. Results of the calculations are listed in Table 4.2. These corrosion current densities, which increase with mass loss, are compared to the corrosion current densities for the SHTQ specimens determined via anodic polarization experiments in Section 4.3.

³¹ ASTM G67 procedure and mass loss measurements in Nitric Acid at 30°C were completed by Mary Lyn Lim and Wasiu Adedeji.

Table 4.2 Current densities calculated from mass loss measurements after exposure to etchants for 24 hours

Sensitization Condition	30°C Nitric Acid		35°C Nitric Acid		35°C Phosphoric Acid		35°C Ammonium Persulfate	
	$\Delta m/As$ (mg/cm ²)	$i_{corr}(\text{mass})$ (A/cm ²)	$\Delta m/As$ (mg/cm ²)	$i_{corr}(\text{mass})$ (A/cm ²)	$\Delta m/As$ (mg/cm ²)	$i_{corr}(\text{mass})$ (A/cm ²)	$\Delta m/As$ (mg/cm ²)	$i_{corr}(\text{mass})$ (A/cm ²)
SHTQ	2	0.25×10^{-3}	3	0.37×10^{-3}	64	7.85×10^{-3}	3	0.37×10^{-3}
100°C - 7D	16	1.96×10^{-3}	32	3.93×10^{-3}	113	13.9×10^{-3}	14	1.72×10^{-3}
100°C - 14D	29	3.56×10^{-3}	59	7.24×10^{-3}	129	15.8×10^{-3}	26	3.19×10^{-3}
100°C - 30D	40	4.91×10^{-3}	76	9.33×10^{-3}	138	16.9×10^{-3}	33	4.05×10^{-3}

4.2.3 DAMAGE MORPHOLOGY

After mass loss experiments, the effects of the test environment on damage morphology were assessed and quantified. Digital micrographs of the specimens after 24-hr immersion were captured to observe surface damage (Figure 4.14), and optical micrographs were captured after cross-sectioning to determine the damage penetration depths (Figures 4.15 – 4.25). Most of the micrographs are categorized by surface/direction (L, T, S), grouped by etchant (nitric acid, phosphoric acid, pH 0.7 ammonium persulfate), and organized by the sensitization condition/NAMLT value of the specimen. This arrangement of the micrographs follows the hierarchy shown in Figure 4.13.

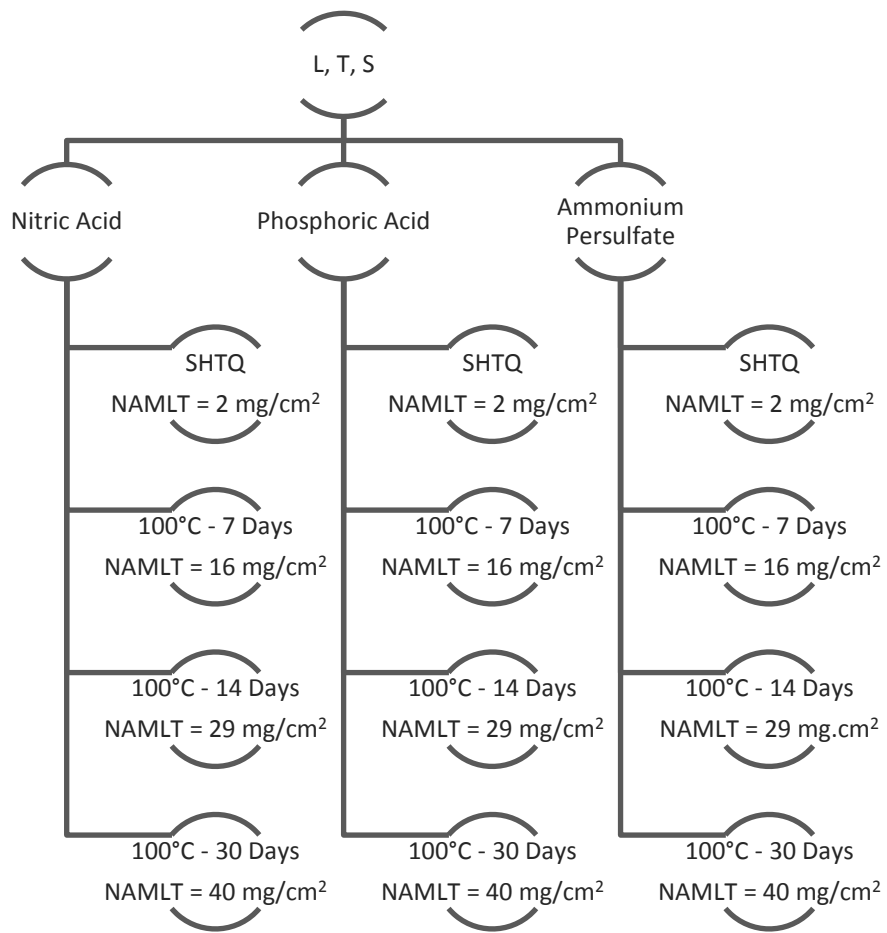


Figure 4.13 Organization of post-OCP-immersion micrographs in Figures 4.14 – 4.25

The damage on the LS surfaces is shown in Figure 4.14. The grains boundaries along the L-direction are highly attacked, and the material loss from grain fallout increases with sensitization condition. Phosphoric acid exposures appear to result in the most grain fallout, which correlates to the highest mass loss determined by G67 testing. Ammonium persulfate exposures appear to result in the least grain fallout, which correlates to the lowest mass loss determined by G67 testing.

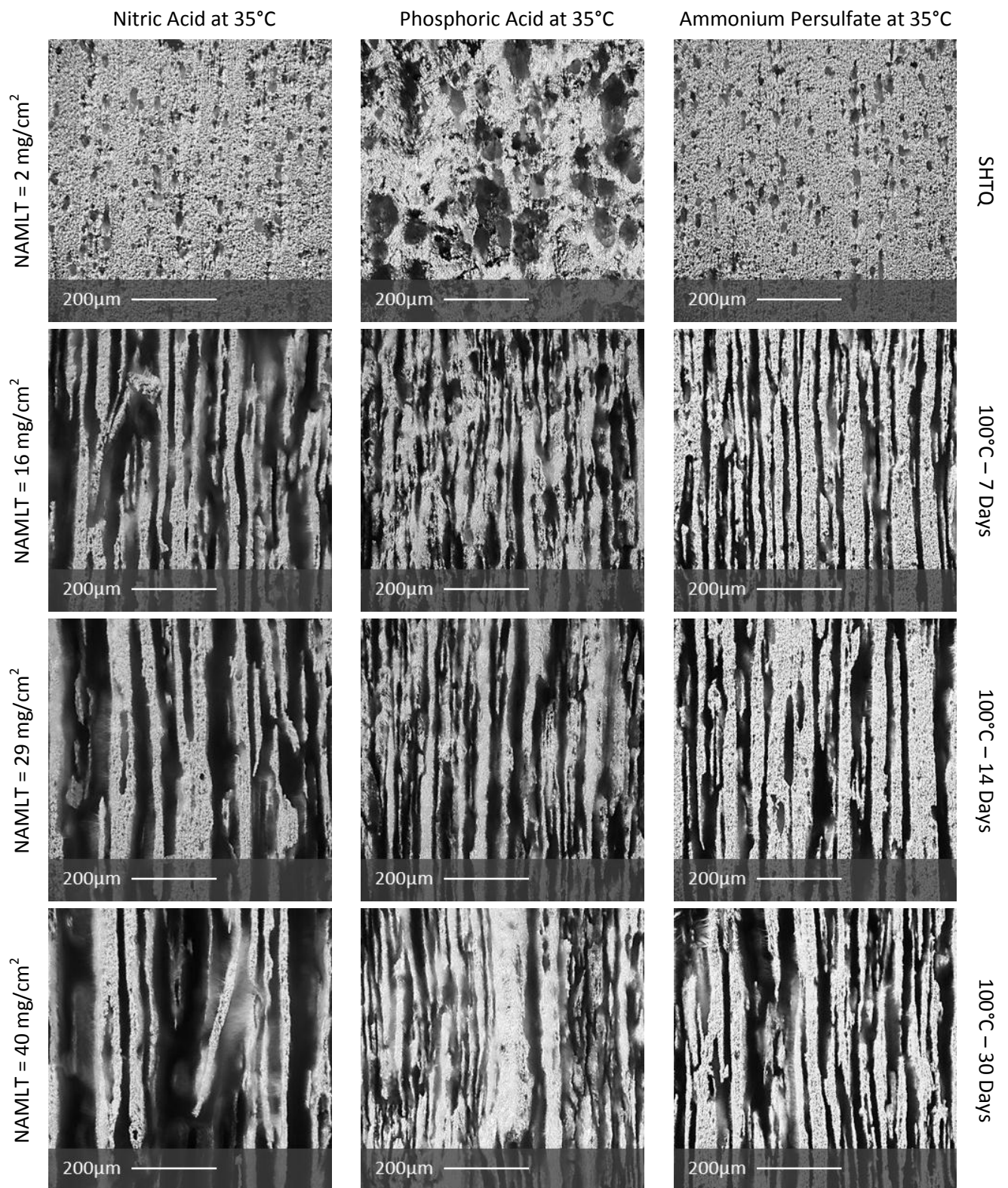


Figure 4.14 Digital microscopy images³² of L-S surface of AA5083 of varying sensitization conditions after 24-hr exposure at 35°C to **Nitric Acid**, **Phosphoric Acid**, and **Ammonium Persulfate**. Grain boundaries along the L-direction (vertical direction) are highly attacked.

³² Focal depths vary for each digitally-compiled micrograph, such that the phosphoric acid-exposed samples involved more focusing steps at intermediate depths due to shallow damage sites than the intergranularly-attacked samples exposed to nitric acid and ammonium persulfate that had relatively flat surfaces at the damage site mouths.

4.2.3.1 DAMAGE PENETRATION IN L-DIRECTION

Damage penetration in the L-direction after mass loss testing is shown in Figure 4.15. The damage sites are relatively fine and intergranular for the sensitized nitric acid and ammonium persulfate exposure specimens. However, the nitric acid exposures result in more penetration in the S-direction, leading to more grain fallout and the visibly wider “mouths” of the fissures. The SHTQ specimens in all three etchants and the sensitized specimens in phosphoric acid appear less intergranular in morphology.

The damage site depths were measured from the micrographs in Appendix B (Figures B.1 – B.12) taken over a set surface length (~3.4mm) of the specimen, and the distributions of depths for each etchant are shown in Figures 4.16 – 4.18. Nitric acid and ammonium persulfate exposures resulted in a higher quantity of deep, fissure-like, damage sites than the phosphoric acid exposures. The appearance of the fissures and distribution of damage site depths correlate well with the measured mass loss values.

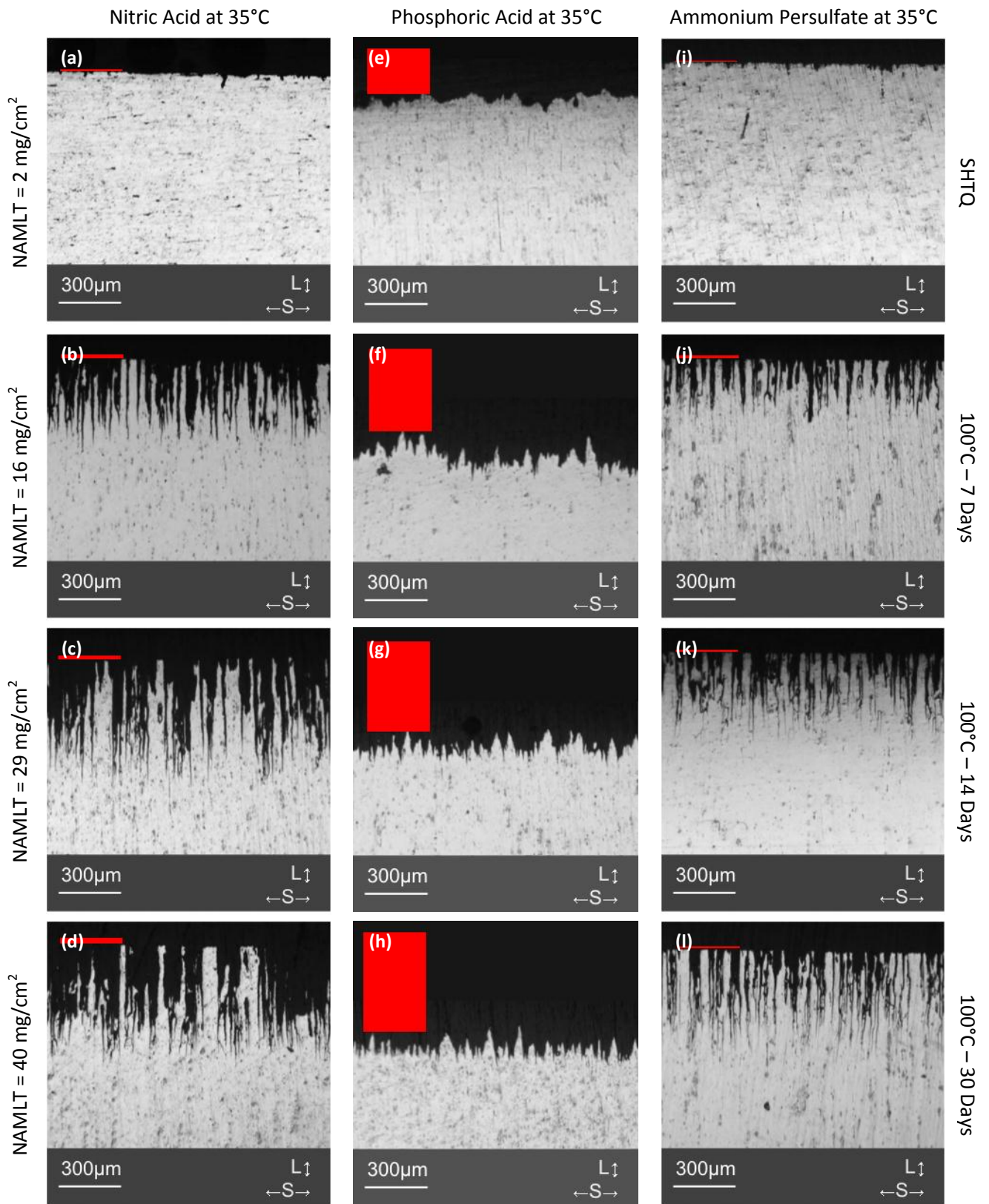


Figure 4.15 Optical micrographs of cross-sectioned AA5083 of varying sensitization conditions after 24-hour exposure at 35°C to etchants: **Nitric Acid** (a)-(d), **Phosphoric Acid** (e)-(h), and **Ammonium Persulfate** (i)-(l). Damage penetration is in the **L-direction** (vertical direction). The thickness of the 300µm-wide red bar on the top left of each micrograph represents the change in dimension (material loss) from initial measured dimensions.

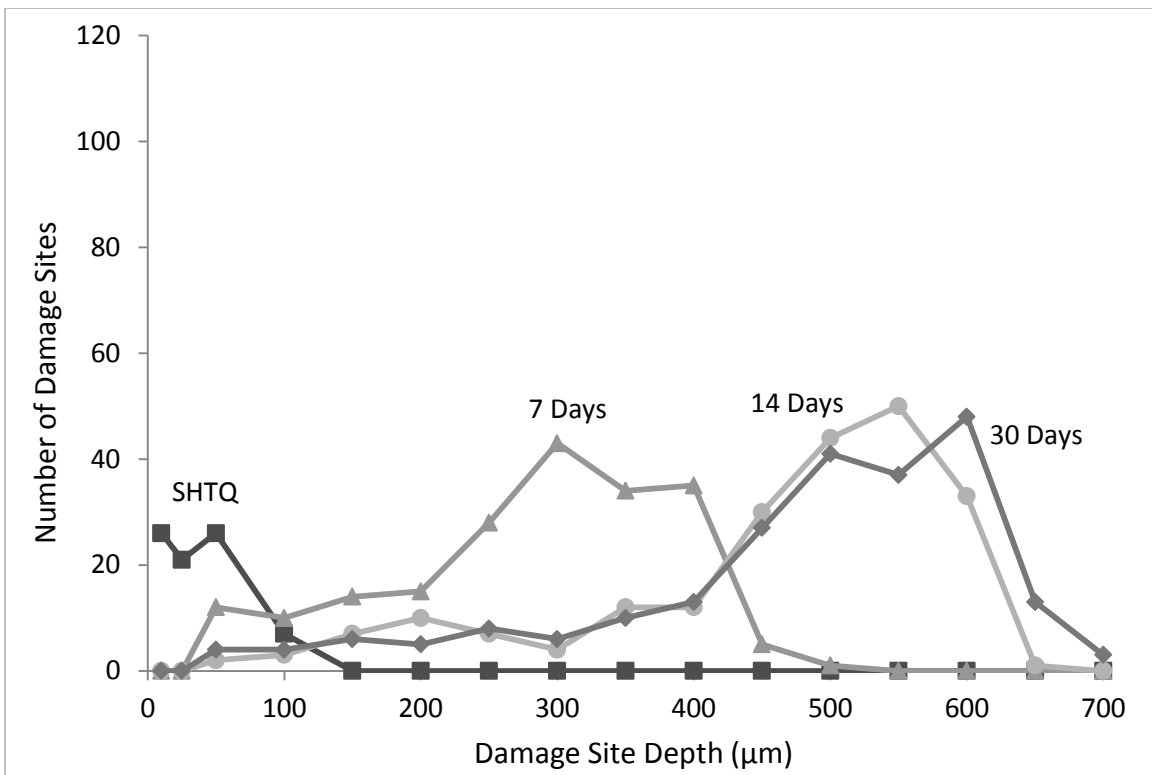


Figure 4.16 Distribution of damage site depths in **L-direction** after 24-hour exposure to **nitric acid** at 35°C

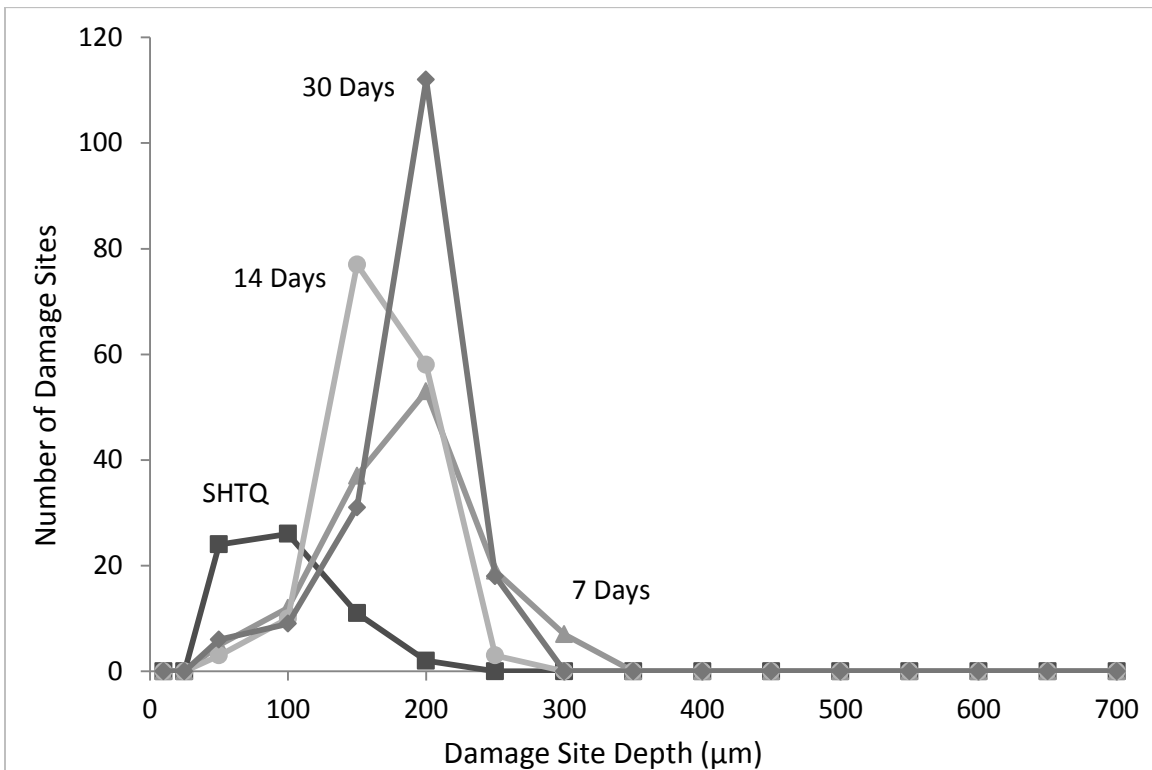


Figure 4.17 Distribution of damage site depths in **L-direction** after 24-hour exposure to **phosphoric acid** at 35°C

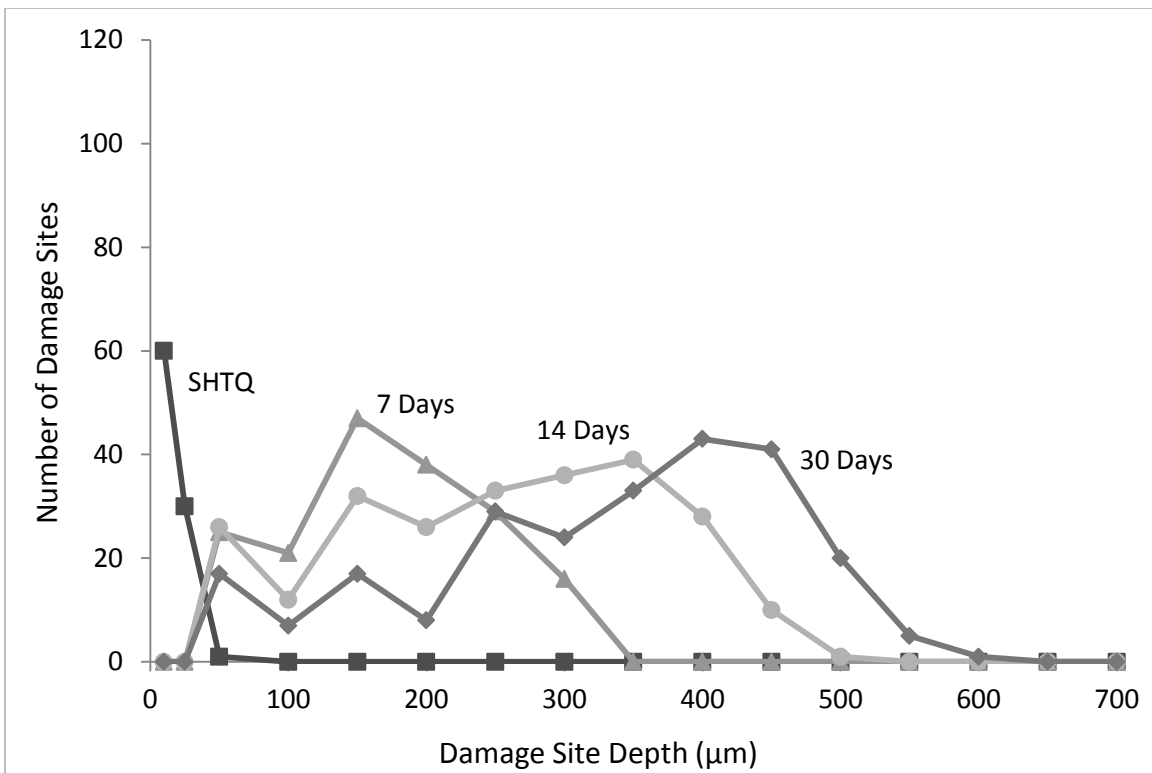


Figure 4.18 Distribution of damage site depths in **L-direction** after 24-hour exposure to **ammonium persulfate** at 35°C

4.2.3.2 DAMAGE PENETRATION IN T-DIRECTION

Damage penetration in the T-direction after mass loss testing is shown in Figure 4.19. The damage sites are not as fine as in the L-direction for the nitric acid and ammonium persulfate exposures. As seen in the L-direction micrographs, the nitric acid exposures result in more penetration in the S-direction than the ammonium persulfate exposures, leading to more grain fallout and the visibly wider fissure mouths. The SHTQ specimens in all three etchants and the sensitized specimens in phosphoric acid do not show damage that is intergranular in morphology.

Figure 4.20 compares the T-direction cross-sections after exposure to nitric acid at 30°C and 35°C. The morphology of attack is essentially the same; however, increasing the temperature increased the severity of the grain fallout, which is also seen after the mass loss tests.

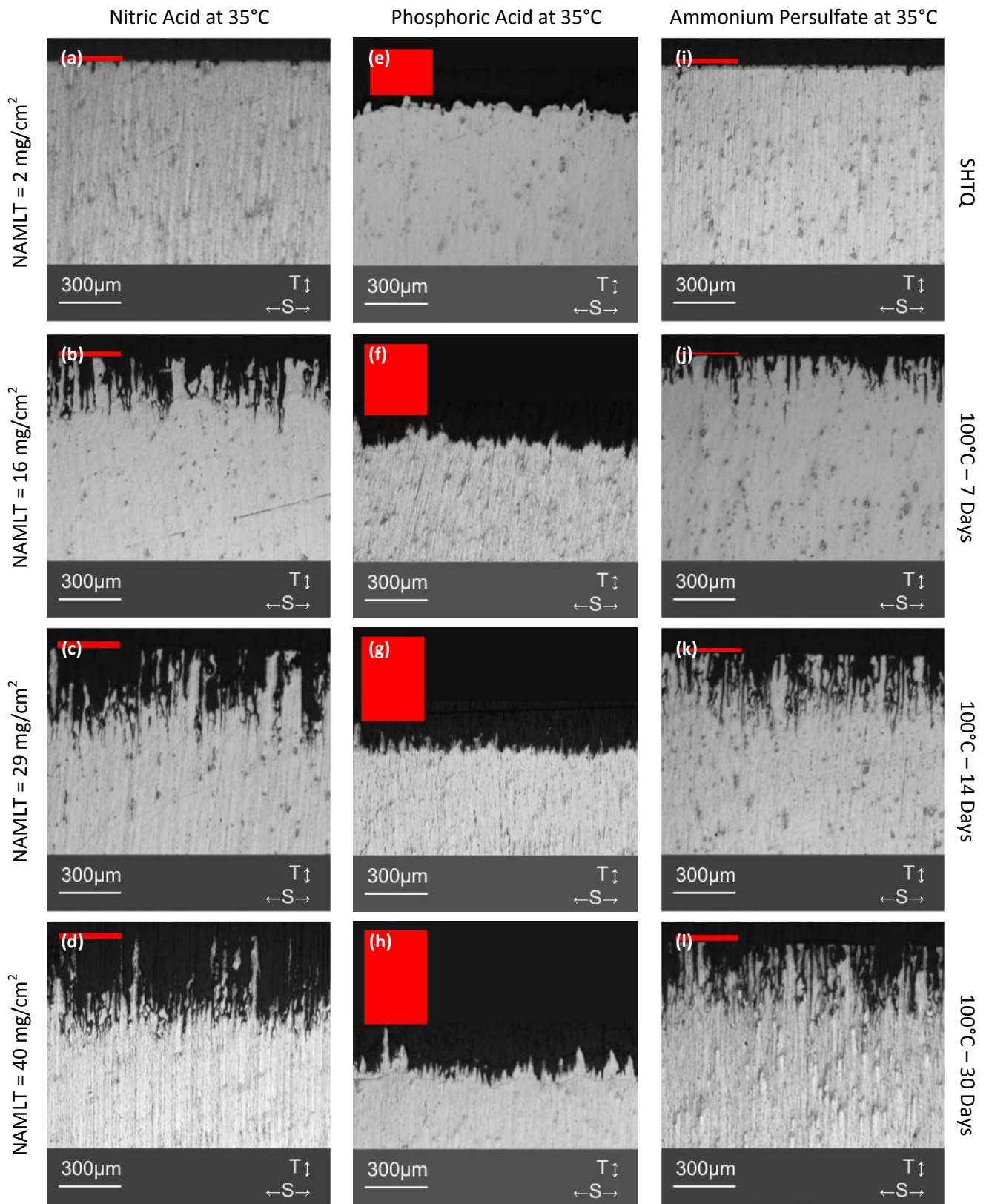


Figure 4.19 Optical micrographs of cross-sectioned AA5083 of varying sensitization conditions after 24-hour exposure at 35°C to etchants: **Nitric Acid** (a)-(d), **Phosphoric Acid** (e)-(h), and **Ammonium Persulfate** (i)-(l). Damage penetration is in the **T-direction** (vertical direction). The thickness of the 300µm-wide red bar on the top left of each micrograph represents the change in dimension (material loss) from initial measured dimensions.

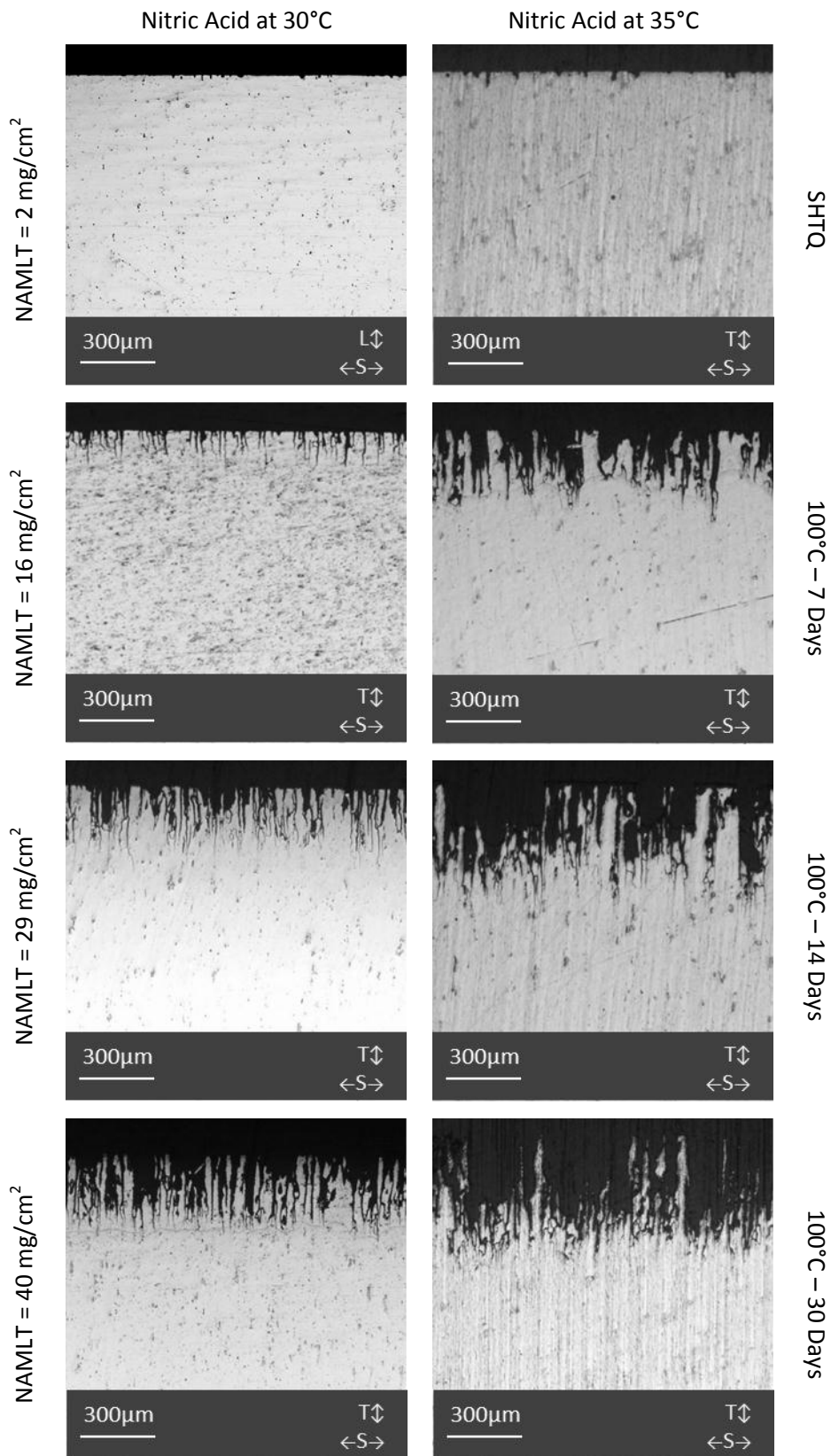


Figure 4.20 Optical micrographs of cross-sectioned AA5083 of varying sensitization conditions after 24-hour exposure to **Nitric Acid** at **30°C** and **35°C**. Damage penetration is in the **T-direction** (vertical direction).

The specimens were etched with Barker's reagent to highlight the grain structure to more closely investigate whether the damage was propagating intergranularly. The etched specimens are shown in Figure 4.21. The damage sites do not appear to originate or propagate from grain boundaries for the SHTQ samples. Specimens with higher sensitization (NAMLT = 30 mg/cm²) appear to have intergranular attack, although the phosphoric acid appears to attack along the width of the damage sites nearly as quickly as it does the depth.

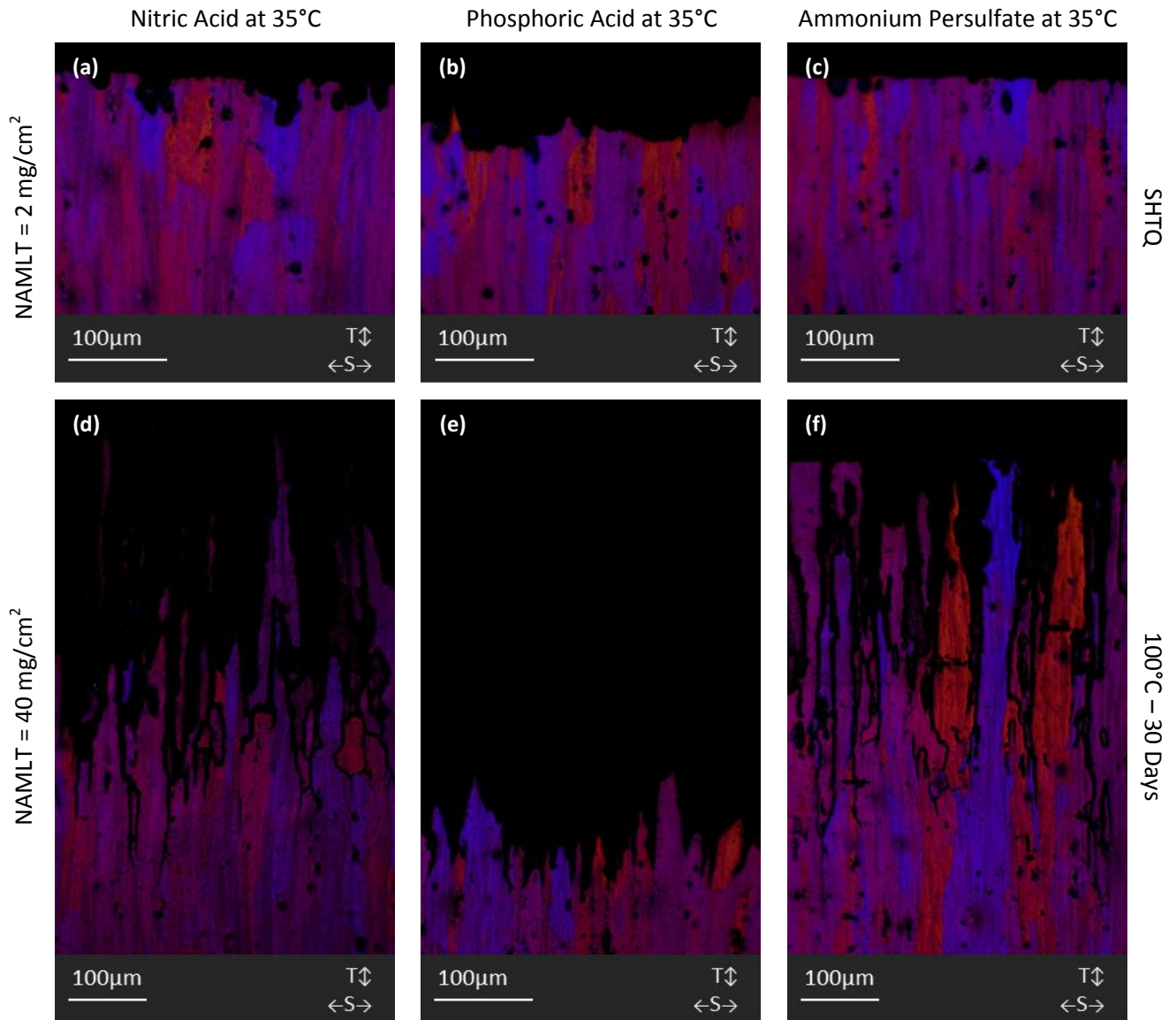


Figure 4.21 Optical micrographs of cross-sectioned AA5083 after 24-hour exposure at 35°C to nitric acid, phosphoric acid, and ammonium persulfate. SHTQ (a)-(c) and 100°C-30days (d)-(f) samples were etched with Barker's reagent to highlight the grain structure. Damage penetration is in the **T-direction** (vertical direction).

The damage site depths were measured from the micrographs in the Appendix B (Figures B.1 – B.12) taken over a set surface length (~3.4mm) of the specimen, and the distributions of depths for each etchant are shown in Figures 4.22 – 4.24. As with the L-direction, nitric acid and ammonium persulfate exposures resulted in a higher quantity of deep, fissure-like, damage sites than the phosphoric acid exposures. The appearance of the fissures and distribution of damage site depths correlate well with the measured mass loss values.

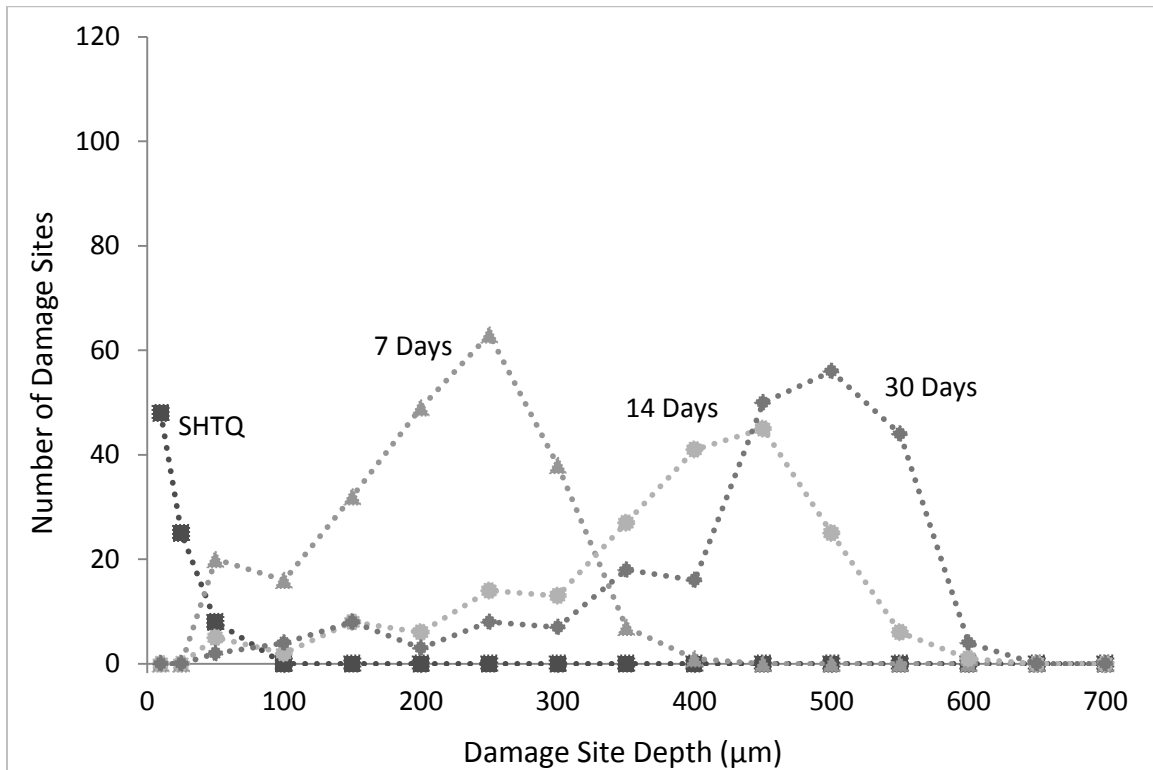


Figure 4.22 Distribution of damage site depths in **T-direction** after 24-hour exposure to **nitric acid** at 35°C

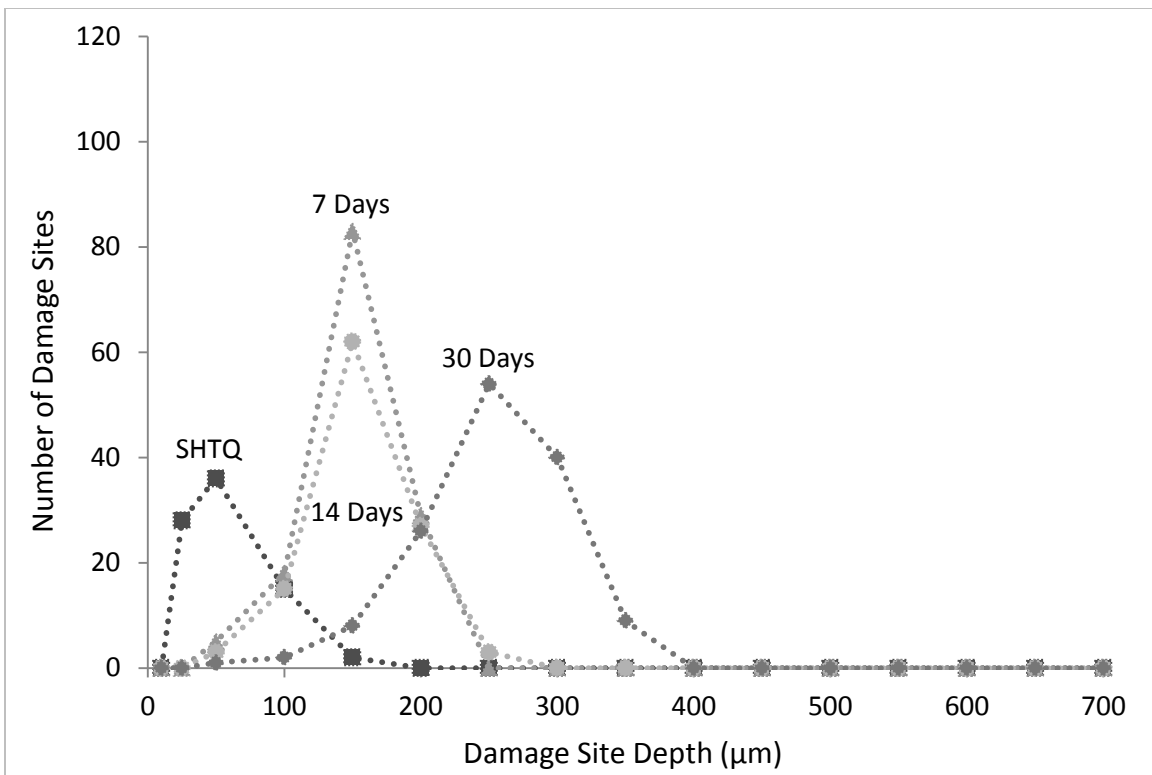


Figure 4.23 Distribution of damage site depths in **T-direction** after 24-hour exposure to **phosphoric acid** at 35°C

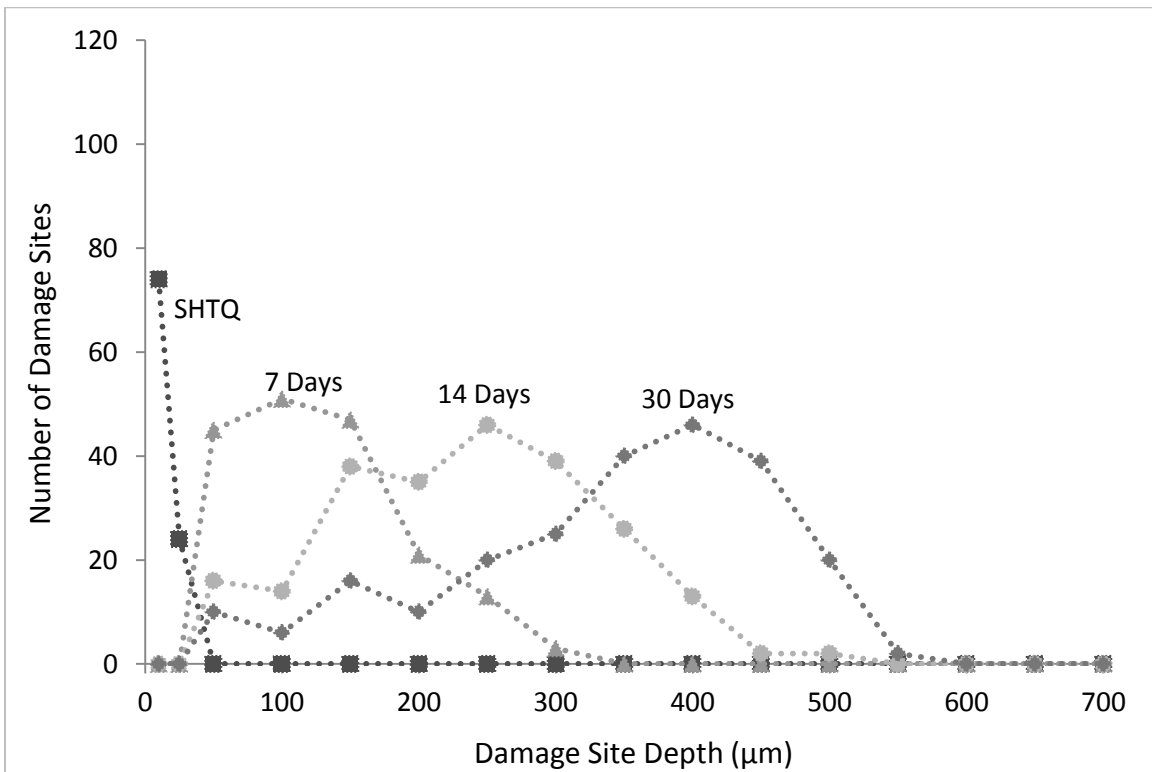


Figure 4.24 Distribution of damage site depths in **T-direction** after 24-hour exposure to **ammonium persulfate** at 35°C

4.2.3.3 DAMAGE PENETRATION IN S-DIRECTION

Damage penetration in the S-direction after mass loss testing is shown in Figure 4.25. The damage appears to originate in the S-direction and then propagate along the L-direction, which has longer grain boundaries (i.e. longer network of β -precipitates). The nitric acid and ammonium persulfate damage sites are more intergranular in morphology than the phosphoric acid sites.

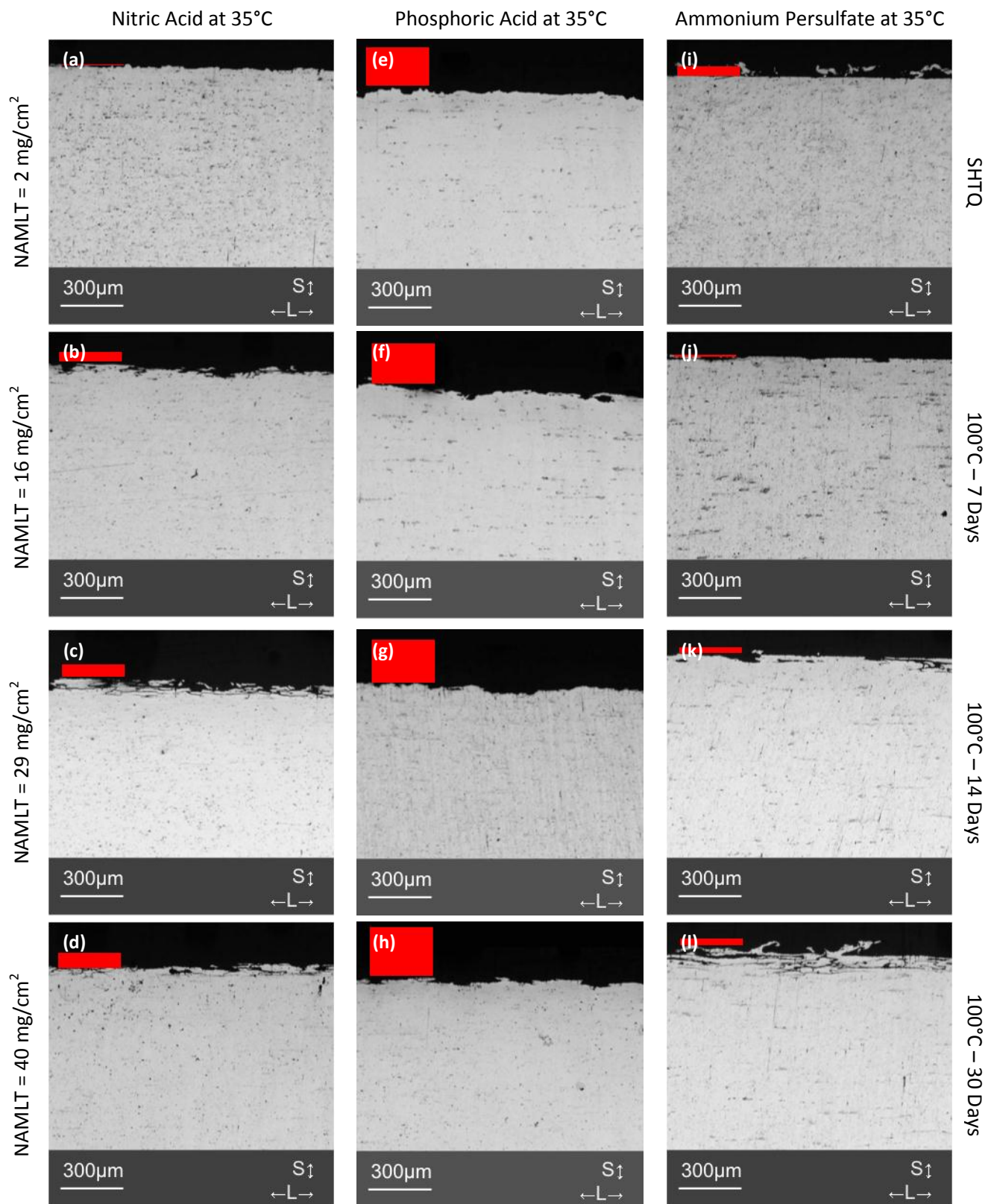


Figure 4.25 Optical micrographs of cross-sectioned AA5083 of varying sensitization conditions after 24-hour exposure at 35°C to etchants: **Nitric Acid** (a)-(d), **Phosphoric Acid** (e)-(h), and **Ammonium Persulfate** (i)-(l). Damage originates in the **S-direction** (vertical) but follows the L-direction (horizontal). The thickness of the 300 µm-wide red bar on the top left of each micrograph represents the change in dimension (material loss) from initial measured dimensions.

4.2.3.4 AVERAGE DAMAGE SITE DEPTH AND SPECIMEN DIMENSION CHANGES

The average damage site depths for the L and T-directions were calculated from the distributions in Appendix B and are shown in Figure 4.26. The dimension changes³³ in the L, T, and S-directions were measured for each specimen after testing, and the averages are shown in Figures 4.27 – 4.30. The averages dimension changes (material loss) are also shown to scale in the micrographs in Figures 4.15, 4.19, and 4.25 for the L, T, and S-direction damage penetration morphologies, respectively³⁴.

Nitric acid exposures of sensitized material resulted in the deepest damage sites amongst the etchants with intermediate dimension changes, indicating deep fissures with low to moderate grain fallout. Ammonium persulfate immersed specimens had intermediate damage depths but the lowest change in dimension, indicating moderate to deep fissures with low grain fallout. Phosphoric acid resulted in the lowest damage depths for sensitized material and the highest depths for unsensitized material (SHTQ); coupling the low damage penetration with the highest change in dimension indicates that the phosphoric acid demonstrates the highest attack of the matrix of the three etchants.

³³ The dimension changes were measured from the mouth of the damage sites, such that the depth of the damage sites is not included unless the grain fallout was wider than the jaws of the digital caliper.

³⁴ The average dimension change values were measured over the entire length, width, and thickness of each specimen. These values are divided in half and represented graphically on Figures 4.15, 4.19, and 4.25 to provide a scale of the initial dimensions of each specimen prior to the damage penetration from one surface, as seen in the micrographs.

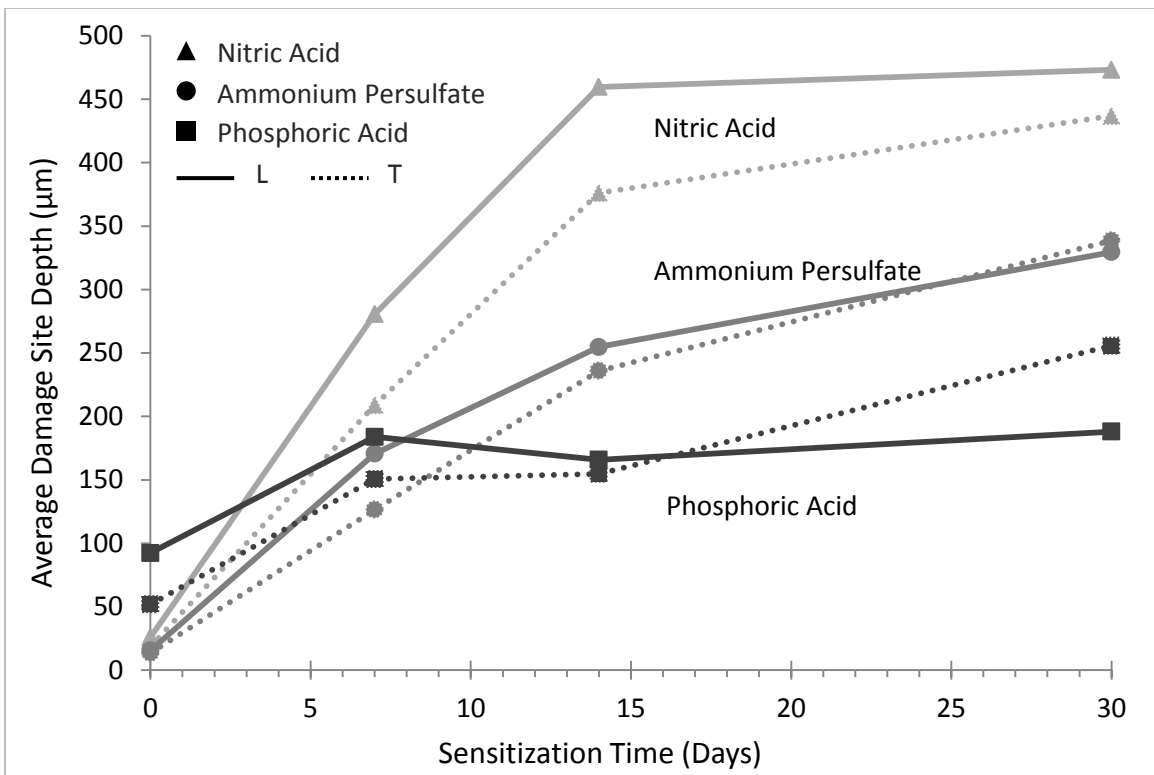


Figure 4.26 Average damage site depths in **L and T-directions** as a function of sensitization condition after 24-hour exposure to etchants at 35°C; L-direction series are solid lines, T-direction series are dotted lines

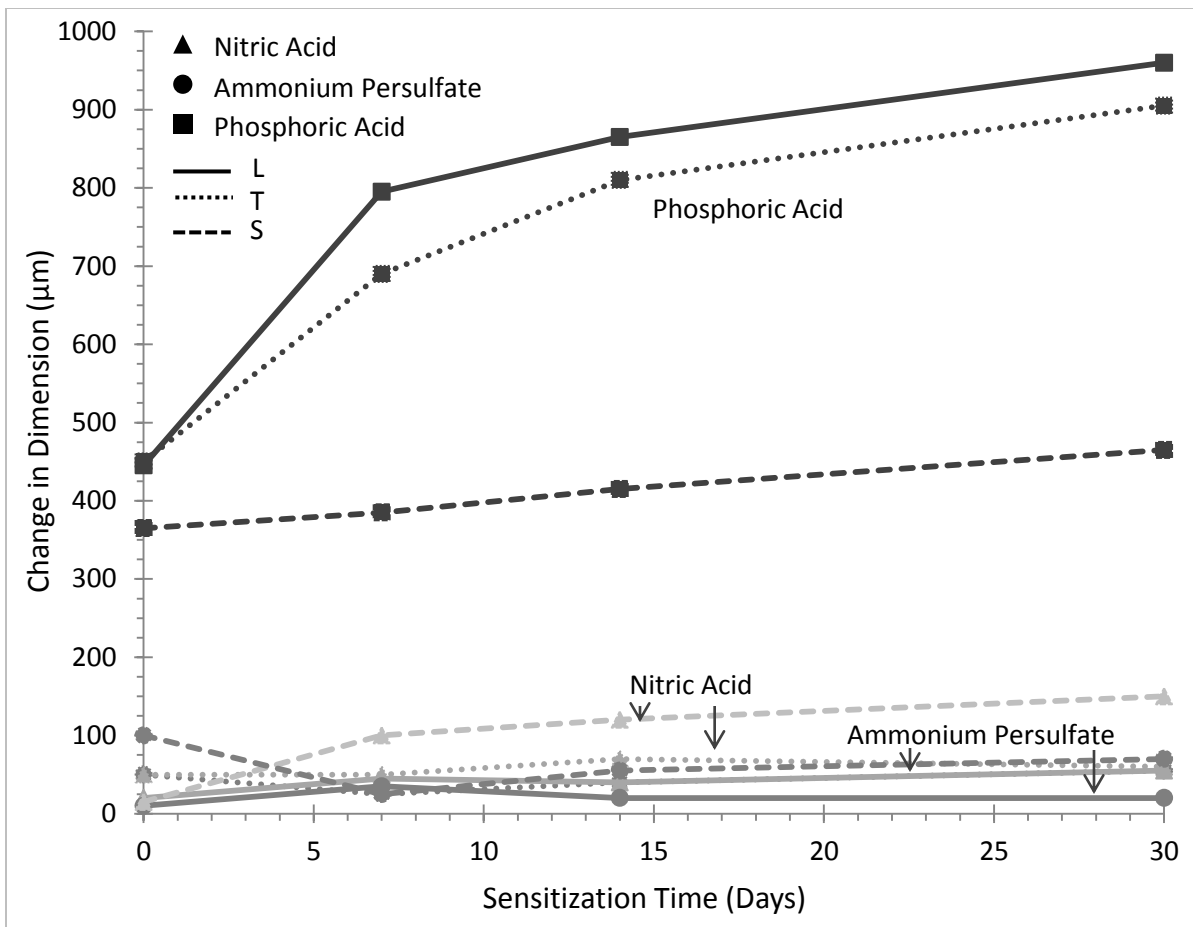


Figure 4.27 Average **dimension change** (material loss) in the **L, T, and S-directions** as a function of sensitization condition after 24-hour exposure to etchants at 35°C; L-direction series are solid lines, T-direction series are dotted lines, S-direction series are dashed lines

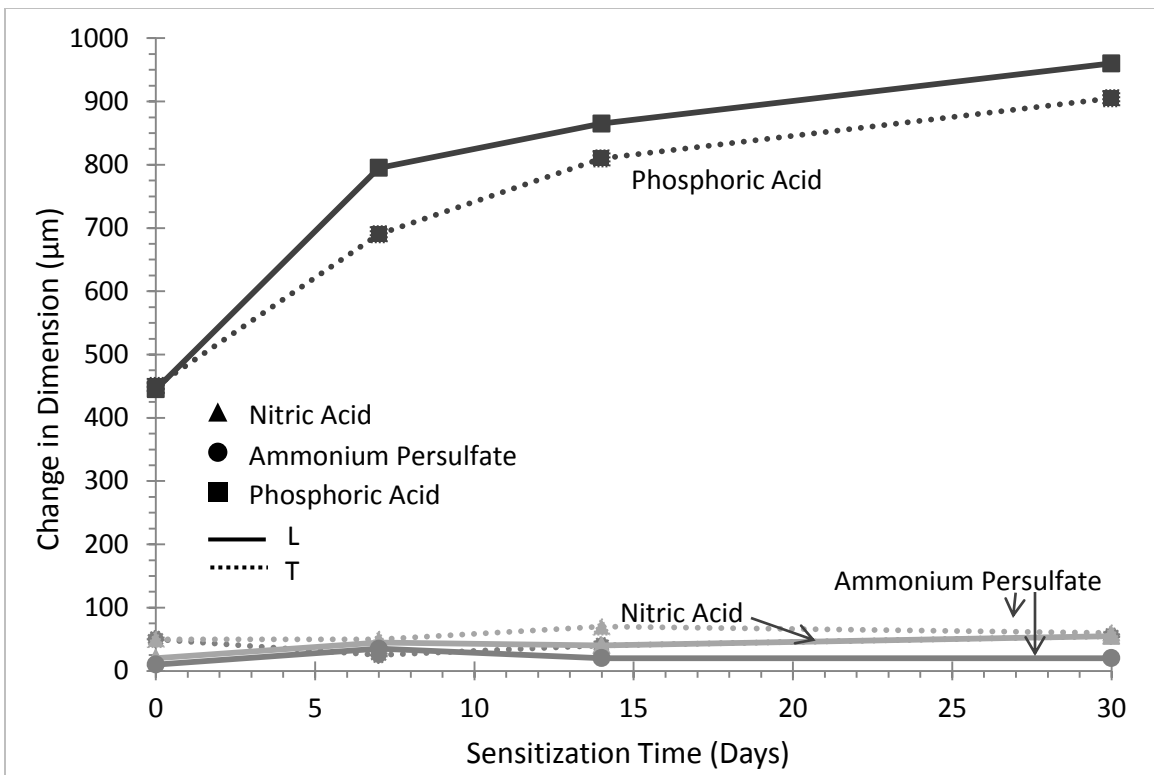


Figure 4.28 Average **dimension change** (material loss) in the **L and T-directions** as a function of sensitization condition after 24-hour exposure to etchants at 35°C; L-direction series are solid lines, T-direction series are dotted lines

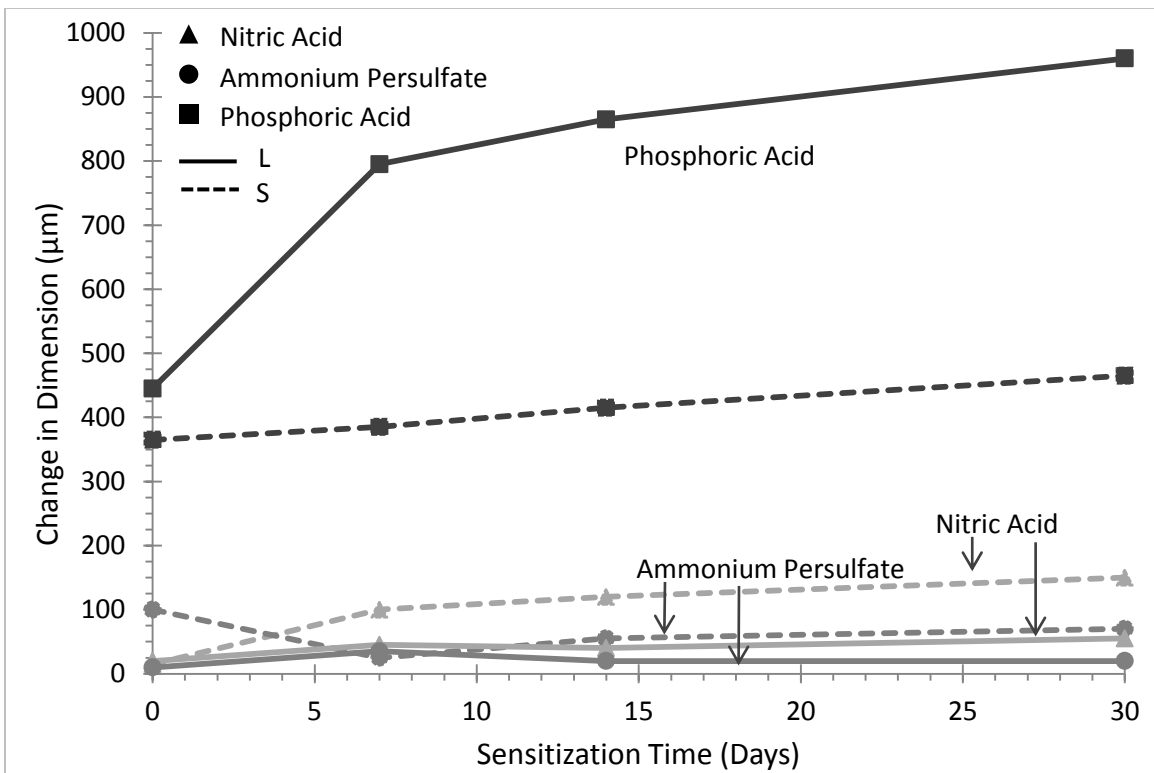


Figure 4.29 Average **dimension change** (material loss) in the **L and S-directions** as a function of sensitization condition after 24-hour exposure to etchants at 35°C; L-direction series are solid lines, S-direction series are dashed lines

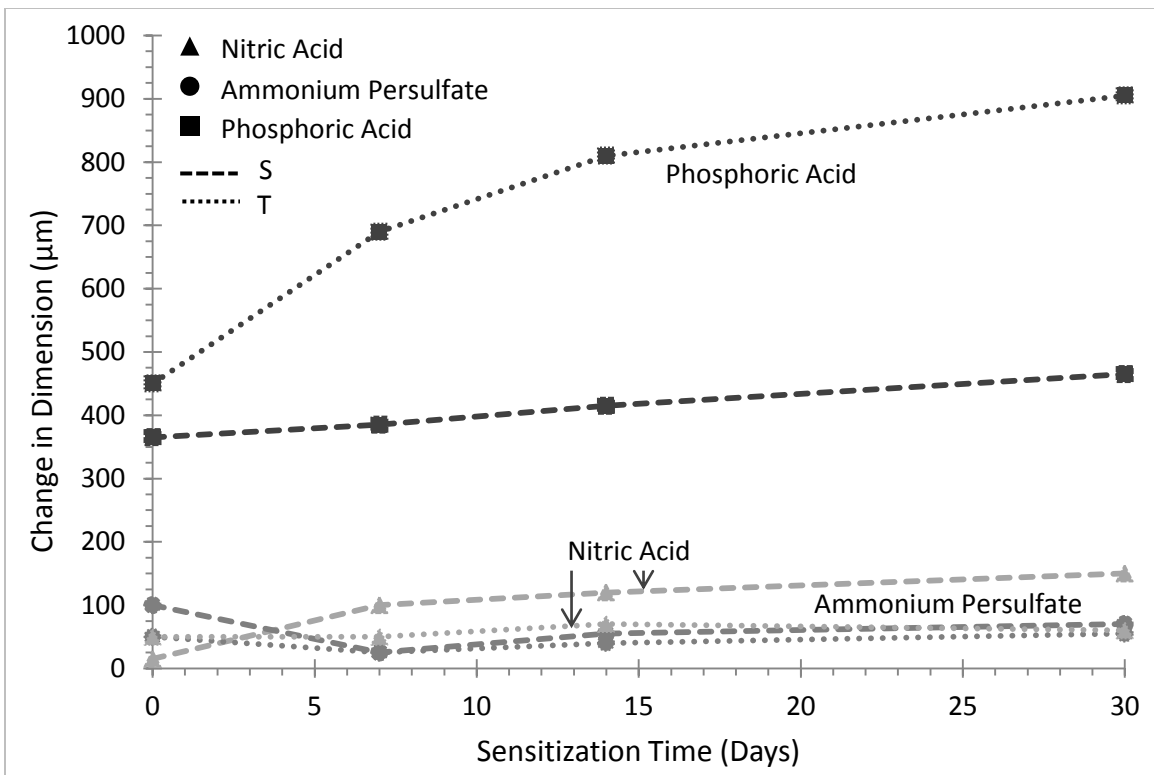


Figure 4.30 Average **dimension change** (material loss) in the **S and T-directions** as a function of sensitization condition after 24-hour exposure to etchants at 35°C; S-direction series are dashed lines, T-direction series are dotted lines

The mass loss measurements and qualitative microstructural analysis support the dimension change and damage depth observations; the relevant measurements and calculations are summarized in Table 4.3.

Table 4.3 Summary of mass loss and damage penetration results after exposure to etchants for 24 hours

Environment	Sensitization Condition		Average Mass Loss [$\Delta m/A_s$] _{AVG} (mg/cm ²)	Dimension Changes			Average Damage Site Depth	
	Temperature (°C)	Time (Days)		ΔL_{AVG} (μm)	ΔT_{AVG} (μm)	ΔS_{AVG} (μm)	D_{L-Dir} (μm)	D_{T-Dir} (μm)
Nitric Acid 30°C	SHTQ	0	2					
	100	7	16	-	-	-	-	-
	100	14	29					
	100	30	40					
Nitric Acid 35°C	SHTQ	0	3	20	50	15	26	18
	100	7	32	45	50	100	281	209
	100	14	59	40	70	120	460	376
	100	30	76	55	60	150	473	437
Phosphoric Acid 35°C	SHTQ	0	64	445	450	365	92	52
	100	7	113	795	690	385	184	151
	100	14	129	865	810	415	166	155
	100	30	138	960	905	465	188	256
Ammonium Persulfate 35°C	SHTQ	0	3	10	50	100	16	14
	100	7	14	35	25	25	171	127
	100	14	26	20	40	55	255	236
	100	30	33	20	55	70	330	339

4.2.4 DISSOLVED SPECIES IN ETCHANT SOLUTIONS

The concentrations of species dissolved in the etchant solutions after 24-hour immersion were determined via ICP spectrometry, and their average across twelve replicates are listed in Table 4.4. Aluminum, magnesium, manganese, iron, and silicon were present in all solutions, as expected based on the alloy composition listed in Table 2.1. Concentrations of chromium, zinc, titanium, and copper were not analyzed due to their lower weight percentage in the alloy and the detection limits of the instrument.

Table 4.4 Average concentration (mass ppm) and concentration ratios (ppm/ppm) of dissolved species from AA5083 after 24-hour immersion in etchants via ICP spectrometry analysis. NA = nitric acid, PA = phosphoric acid, and AP = 0.7 ammonium persulfate.

<i>10x dilution</i>	Average Concentration (mass ppm)						Concentration Ratio	
	Al	Mg	Mn	Fe	Si	Sum	Al:Mg	Mg:Al
NA SHTQ	92.67 ± 0.50	5.97 ± 0.23	0.85 ± 0.08	0.29 ± 0.01	0.05 ± 0.02	99.82	15.53	0.0644
NA 30-Day	2417.79 ± 22.14	140.16 ± 3.20	22.29 ± 1.61	7.57 ± 0.08	0.89 ± 0.04	2588.70	17.25	0.0580
PA SHTQ	2392.62 ± 30.85	152.39 ± 2.86	21.55 ± 1.51	6.60 ± 0.08	1.90 ± 0.04	2575.06	15.70	0.0637
PA 30-Day	4776.42 ± 68.14	283.72 ± 5.60	43.32 ± 2.97	12.52 ± 0.14	3.46 ± 0.07	5119.45	16.83	0.0594
AP SHTQ	89.33 ± 0.37	6.03 ± 0.25	0.62 ± 0.07	0.25 ± 0.01	0.10 ± 0.03	96.32	14.81	0.0675
AP 30-Day	792.73 ± 2.60	67.04 ± 1.36	10.31 ± 1.08	3.96 ± 0.07	1.08 ± 0.04	875.12	11.83	0.0846

The sum of the average concentrations is also listed for each solution in Table 4.3. The total concentration of dissolved species in the etchants increases from the unsensitized condition (SHTQ) to the sensitized condition (100°C-30days) across all solutions, with phosphoric acid dissolving the most material and ammonium persulfate dissolving the least amount of material.

All etchants were found to dissolve more aluminum than magnesium, and the ratios of their respective concentrations are listed in Table 4.4. The magnesium to aluminum concentration ratio indicates how readily the solutions dissolve magnesium relative to aluminum and therefore the more Mg-rich β -phase relative to the matrix. The ratios are shown graphically in Figures 4.31 and 4.32. The stoichiometric ratio for AA5083 given a 4.4 wt% Mg content is 0.046³⁵, so all of the etchant exposures resulted in some selective attack. However, since the stoichiometric ratio for β -phase dissolution (36.1-37.8 wt% Mg) is approximately 0.56-0.61, the aluminum matrix is still shown to dissolve in all etchants³⁶. Ammonium persulfate exposures result in higher concentrations of dissolved magnesium relative to dissolved aluminum, which indicates that the solution would be more preferentially corrosive of the β -phase than the other solutions. Phosphoric acid exposures result in the lowest ratio of dissolved magnesium to aluminum, indicating that it is the least selective toward β -phase dissolution.

³⁵ Stoichiometric ratio of Mg and Al concentrations for SHTQ-only dissolution (wt%/wt%) = $4.4/(100-4.4) = 0.046$.

³⁶ Stoichiometric ratio of Mg and Al concentrations for β -phase-only dissolution (wt%/wt%) = $(36.1 \text{ to } 37.8)/[100-(36.1 \text{ to } 37.8)] = 0.56 \text{ to } 0.61$.

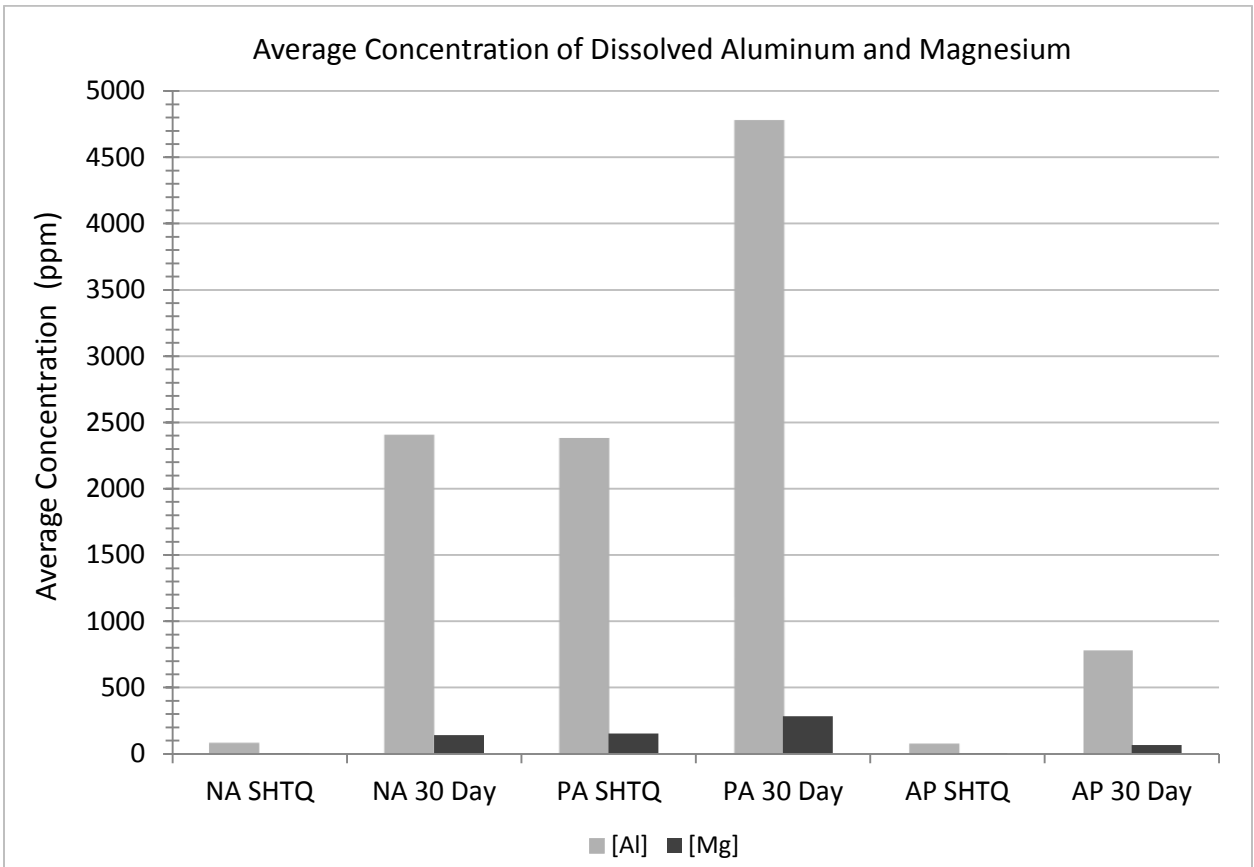


Figure 4.31 Average concentrations (ppm) of dissolved magnesium and aluminum in etchant solutions after 24-hour immersion.

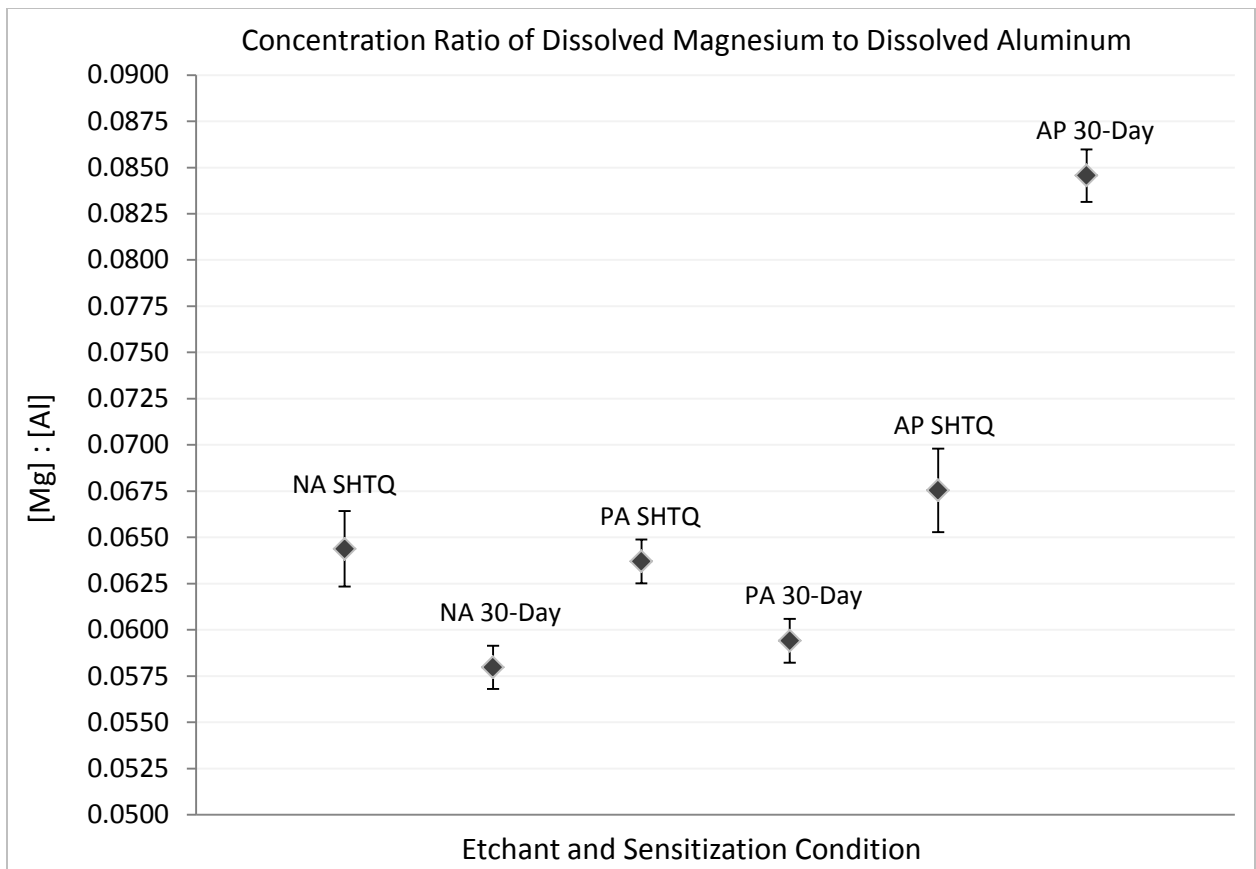


Figure 4.32 Ratios of **dissolved magnesium to dissolved aluminum** (ppm/ppm with standard deviations across 12 replicates) in etchant solutions after 24-hour immersion (**NA = Nitric Acid, PA = Phosphoric Acid, AP = Ammonium Persulfate**). This ratio indicates the extent to which etchants preferentially dissolve magnesium to aluminum and therefore the Mg-rich β -phase relative to the matrix. The ratio of Mg:Al concentrations for congruent, **SHTQ-only dissolution is approximately 0.046**, while the ratio of Mg:Al concentrations for congruent, **β -phase-only dissolution is approximately 0.56-0.61**.

4.3 ANODIC POLARIZATION OF β -PHASE AND AA5XXX MATRIX

Solution-heat-treated-and-quenched AA5083 (representative of the alloy matrix) and pure β -phase specimens were anodically polarized in nitric acid, phosphoric acid, and acidified ammonium persulfate to compare their corrosion behaviors and quantify etchant selectivity. The resulting polarization curves, generated from 15-50°C, comprise Figures 4.33 - 4.39 and are categorized by etchant; the curves are plotted with potential (volts versus MSE electrode) on the y-axis and current density (A/cm^2) on the x-axis. The ratios of current densities at the OCP of the matrix (quantitatively defining etchant selectivity) are plotted in Figure 4.40 and listed in Table 4.5.

4.3.1 ANODIC POLARIZATION SCANS IN NITRIC ACID

Figure 4.33 shows the polarization curves for SHTQ (LT surface) and β -phase specimens in nitric acid from 15-50°C. As expected, the OCP of the matrix is higher (less negative) than that of the β -phase at all temperatures tested³⁷. The β -phase exhibits current densities that are higher than those of the matrix both at their respective OCPs and at the OCP of the matrix (the potential to which the β -phase will be polarized when the alloy is corroding without an applied potential). The higher corrosion current density of the β -phase indicates preferential attack of magnesium rather than aluminum. The corrosion current densities (proportional to corrosion rates) and passive current density increase with temperature for both materials. The polarization curves specific to each test temperature are reproduced for clarity in Figures C.1 – C.5 in Appendix C.

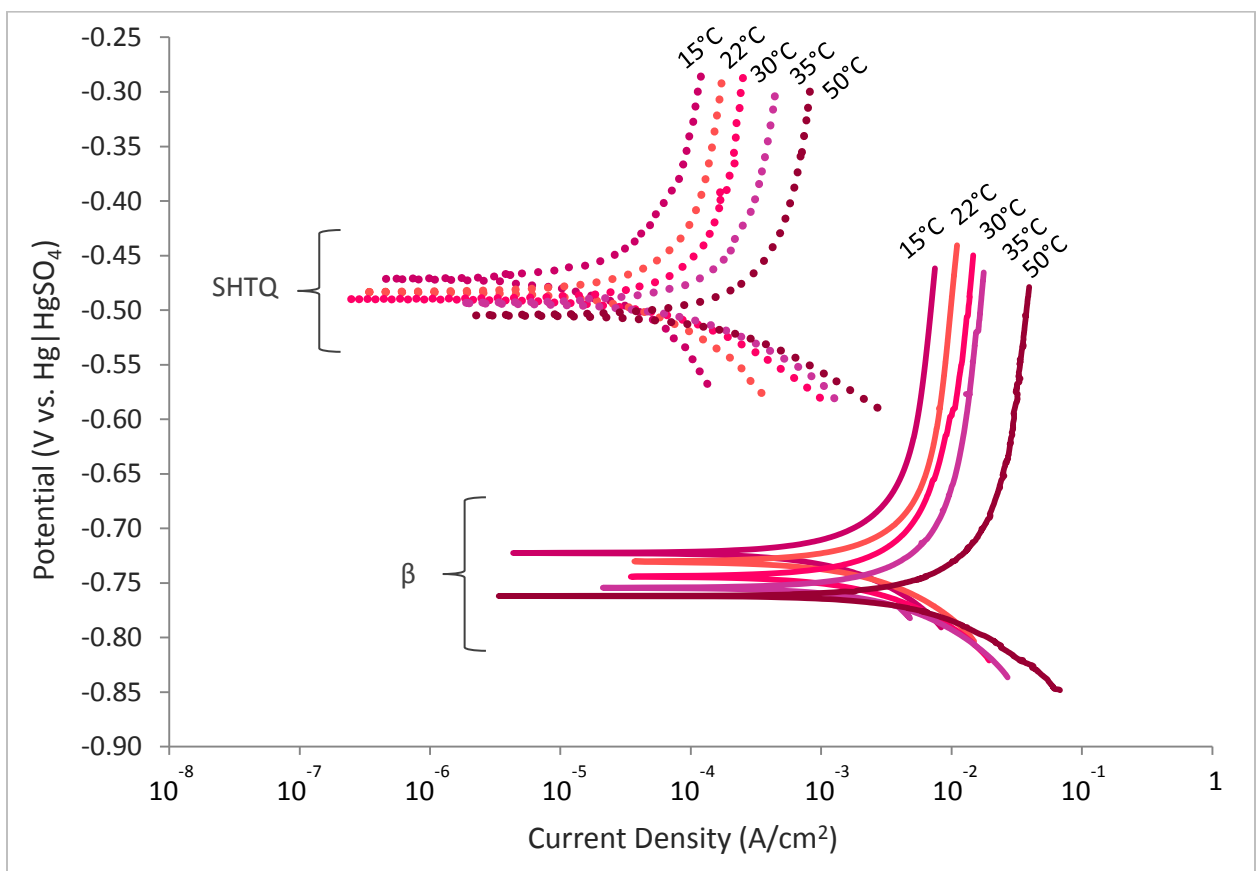


Figure 4.33 Anodic polarization scans of AA5083-SHTQ (LT) and β -phase specimens in **Nitric Acid** from **15-50°C**

³⁷ The potentials were not adjusted for the temperature dependence of the reference electrode; therefore, the open circuit potentials will only be compared within one test temperature and not across the temperature range.

Figure 4.34 shows the polarization curves for the SHTQ LT and LS surfaces in nitric acid at 35°C after 5 minute and 30 minute OCP holds. The open circuit potentials and corrosion rates for the LT samples remain relatively the same after the longer exposure times. The LS surface exhibits similar current densities but a higher OCP after 5 minutes than the LT surface, and the OCP further increases with exposure time. Both surfaces reached relatively the same passive current density despite differences in orientation and exposure time.

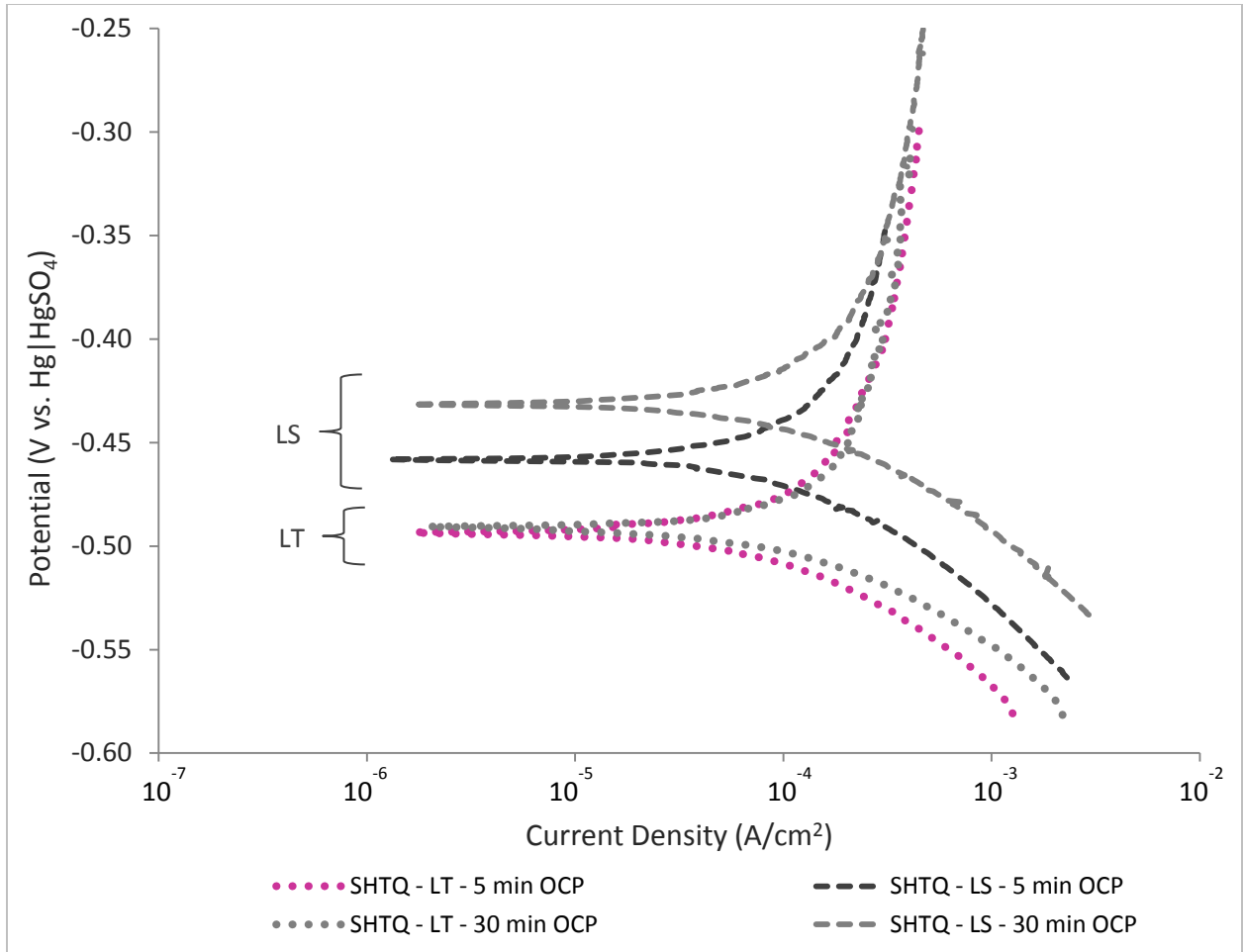


Figure 4.34 Anodic polarization scans of AA5083-SHTQ specimens in **Nitric Acid** at **35°C**; Scans of the **SHTQ LT and LS surfaces** after 5 min and 30 min OCP holds are shown

4.3.2 ANODIC POLARIZATION SCANS IN PHOSPHORIC ACID

Figure 4.35 shows the polarization curves for SHTQ (LT surface) and β -phase specimens in phosphoric acid. As with the nitric acid exposures, the OCP of the matrix is higher than that of the β -phase at all temperatures tested, and the corrosion current densities and passive current densities increase from 15°C to 50°C for both materials. However, the β -phase exhibits current

densities that are lower than those of the matrix at their respective OCPs, indicating that phosphoric acid is less selective for Mg dissolution relative to Al dissolution. The etchant is selective toward β -phase dissolution at the OCP of the matrix, since the passive current density of the β -phase is higher than the corrosion current density of the matrix. The polarization curves specific to each test temperature are reproduced for clarity in Figures C.6 – C.9 in Appendix C.

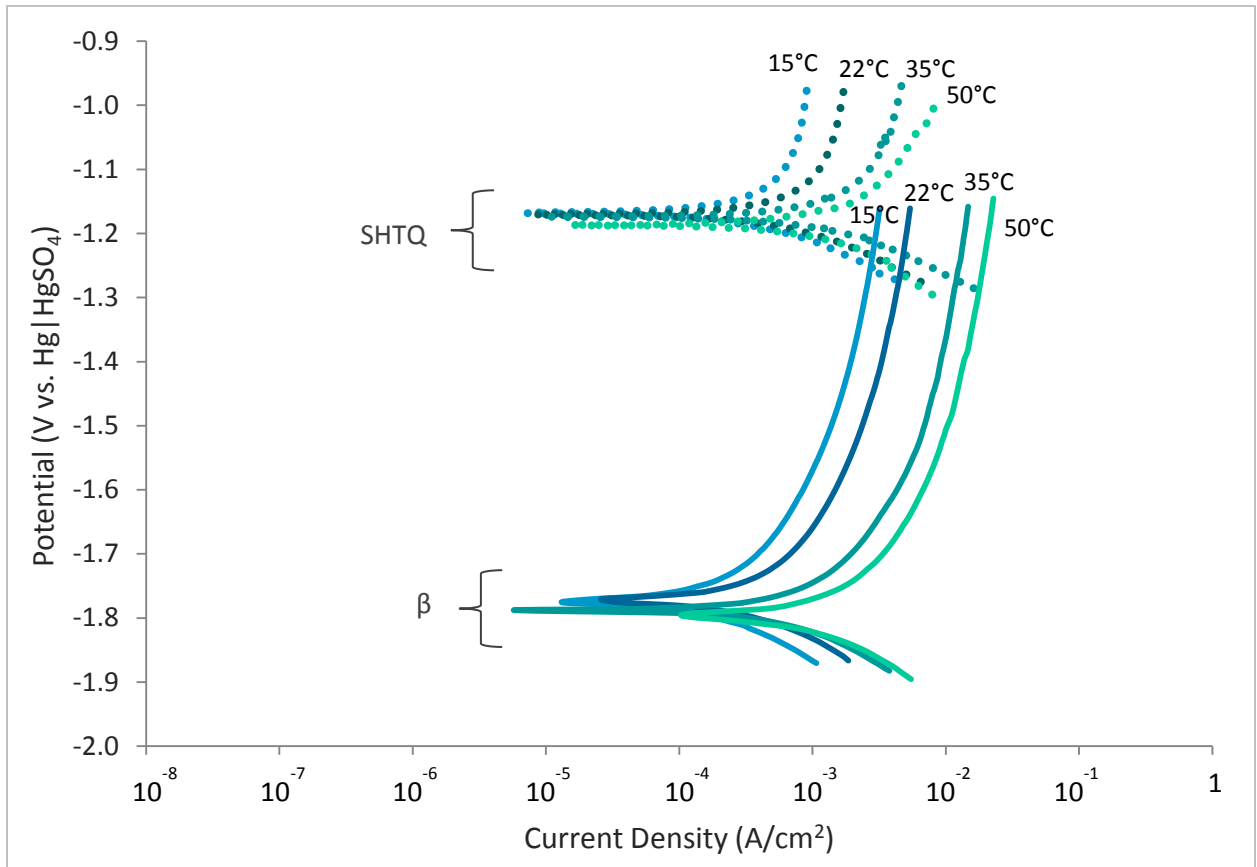


Figure 4.35 Anodic polarization scans of AA5083-SHTQ (LT) and β -phase specimens in **Phosphoric Acid** from **15-50°C**

Figure 4.36 shows the polarization curves for the SHTQ LT and LS surfaces in phosphoric acid at 35°C after 5 minute and 30 minute OCP holds. The open circuit potentials increase with exposure time for both surfaces. The LS surface exhibits similar corrosion current densities and the same passive current densities after both OCP durations, and higher OCPs than the LT surface. The corrosion current density and passive current density for the LT surface increases over the exposure times tested.

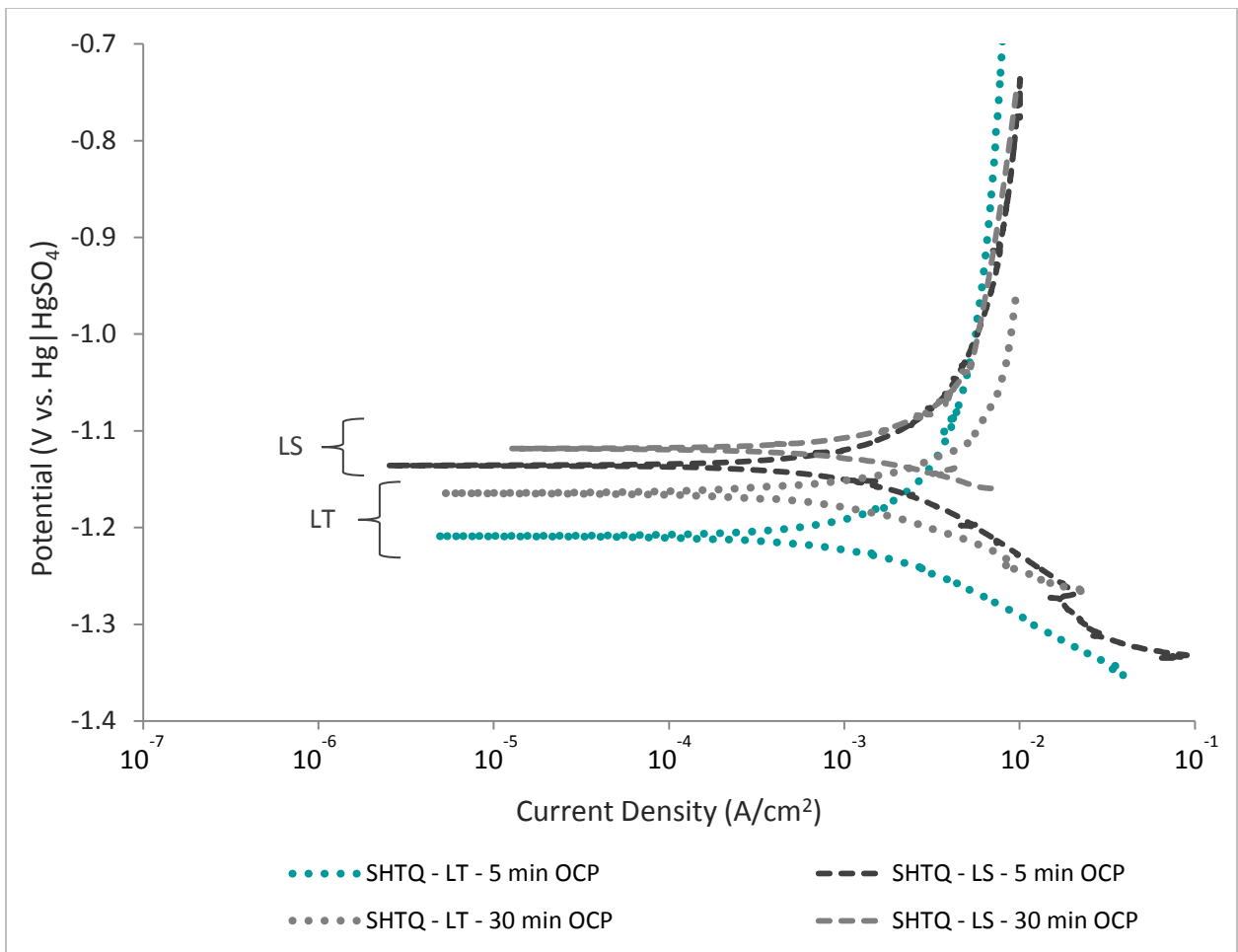


Figure 4.36 Anodic polarization scans of AA5083-SHTQ specimens in **Phosphoric Acid** at **35°C**; Scans of the **SHTQ LT and LS surfaces** after 5 min and 30 min OCP holds are shown

4.3.3 ANODIC POLARIZATION SCANS IN AMMONIUM PERSULFATE

The AA5083-SHTQ and β -phase specimens were polarized in both pH 1.2 (OCP etching pH) and pH 0.7 (mass loss testing pH) ammonium persulfate. Tests in pH 1.2 ammonium persulfate were run from 15-50°C, and tests in pH 0.7 ammonium persulfate were run at 35°C (mass loss testing temperature).

4.3.3.1 PH 1.2 AMMONIUM PERSULFATE

Figure 4.37 shows the polarization curves for SHTQ (LT surface) and β -phase specimens in ammonium persulfate from 15-50°C. Similar to both the nitric acid and phosphoric acid exposures, the OCP of the matrix is higher than that of the β -phase at all temperatures tested. The OCP of the β -phase appears to be more temperature sensitive than that of the matrix when considering the percent decrease with increasing temperature. The β -phase exhibits current

densities that are higher than those of the matrix both at their respective OCPs and at the OCP of the matrix. As with the nitric acid exposures, the higher corrosion current density of the β -phase indicates preferential attack. The corrosion current densities and passive current densities increase with temperature for both materials. The polarization curves specific to each test temperature are reproduced for clarity in Figures C.10 – C.13 in Appendix C.

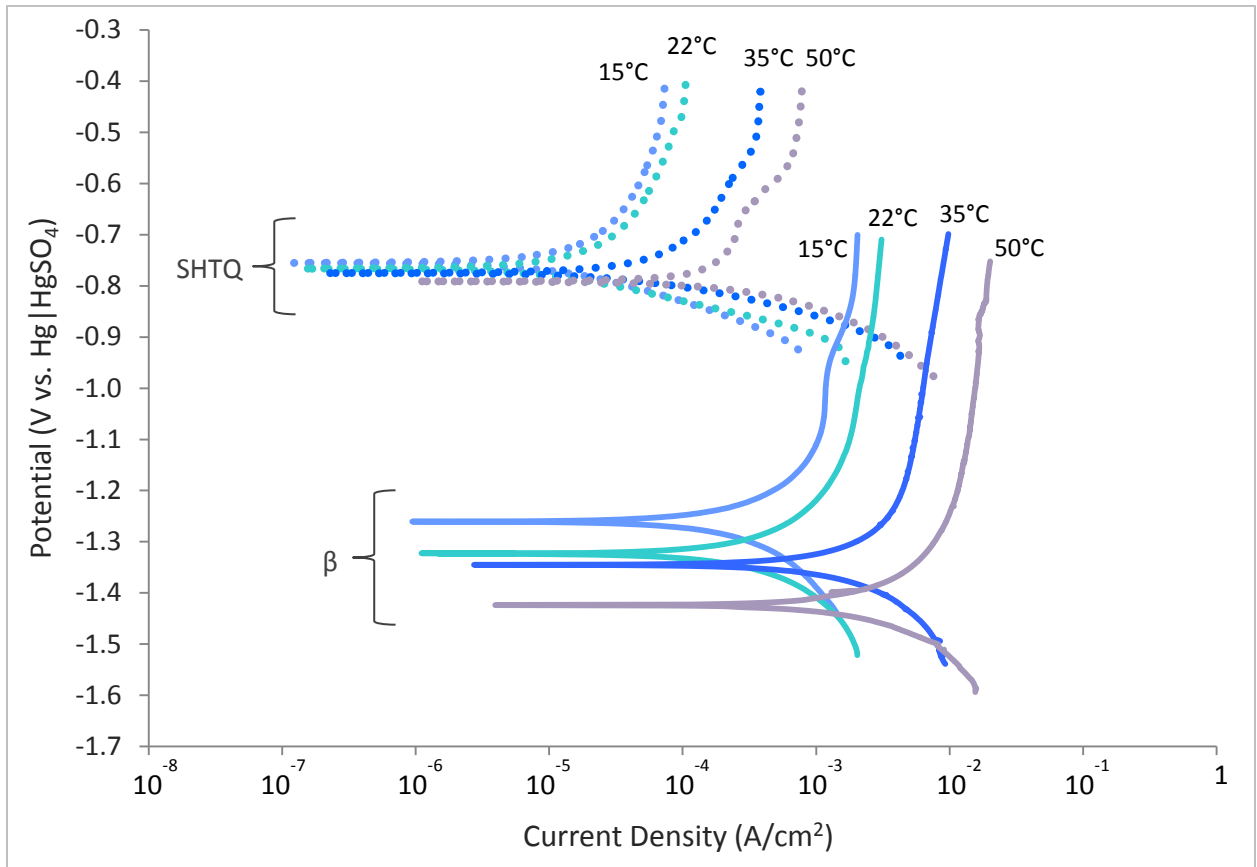


Figure 4.37 Anodic polarization scans of AA5083-SHTQ (LT) and β -phase specimens in **pH 1.2 Ammonium Persulfate** from **15-50°C**

4.3.3.2 PH 0.7 AMMONIUM PERSULFATE

Figure 4.38 shows the polarization curves for the SHTQ LT and LS surfaces in ammonium persulfate at 35°C after 5 minute and 30 minute OCP holds. The open circuit potentials and corrosion rates for the LT samples slightly increase after the longer exposure times. The LS surface exhibits an increased OCP but decreased current densities after the longer exposure time. The LS surface also has higher OCPs than the LT surface after both exposure durations.

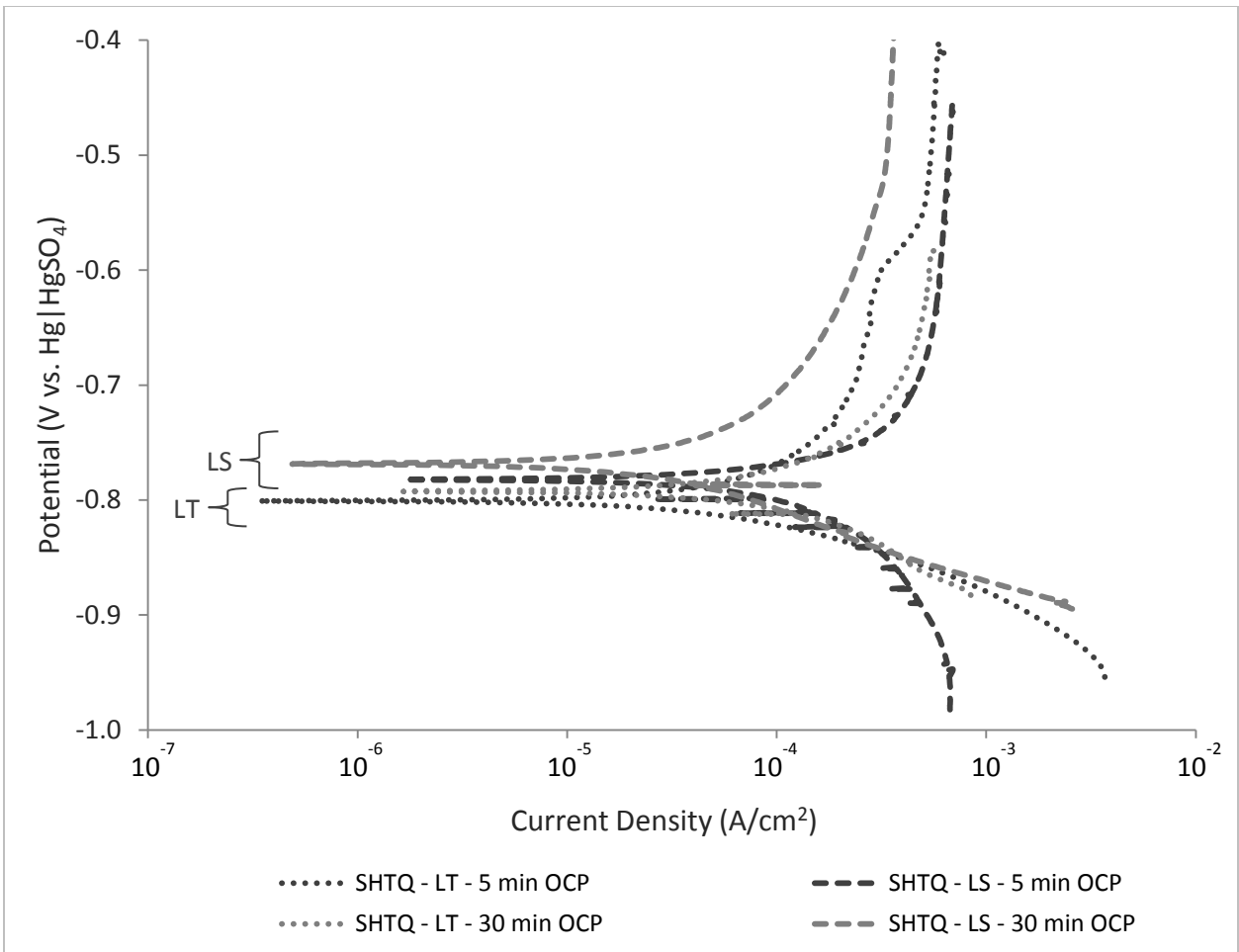


Figure 4.38 Anodic polarization scans of AA5083-SHTQ specimens in **pH 0.7 Ammonium Persulfate** at **35°C**; Scans of the **SHTQ LT and LS surfaces** after 5 min and 30 min OCP holds are shown

Polarization tests were also performed at 35°C to determine the dominant species affecting the selectivity of the acidified ammonium persulfate etchant. Figure 4.39 shows the polarization curves for the SHTQ (LT) and β -phase specimens in 0.4M, pH 0.7 ammonium persulfate, 0.4M ammonium sulfate, 0.4M sodium persulfate, and pH 0.7 sulfuric acid. Results indicate that the oxidizing persulfate ions are the dominant species, since the unacidified sodium persulfate tests yielded the most similar current densities and open circuit potentials to the ammonium persulfate exposures.

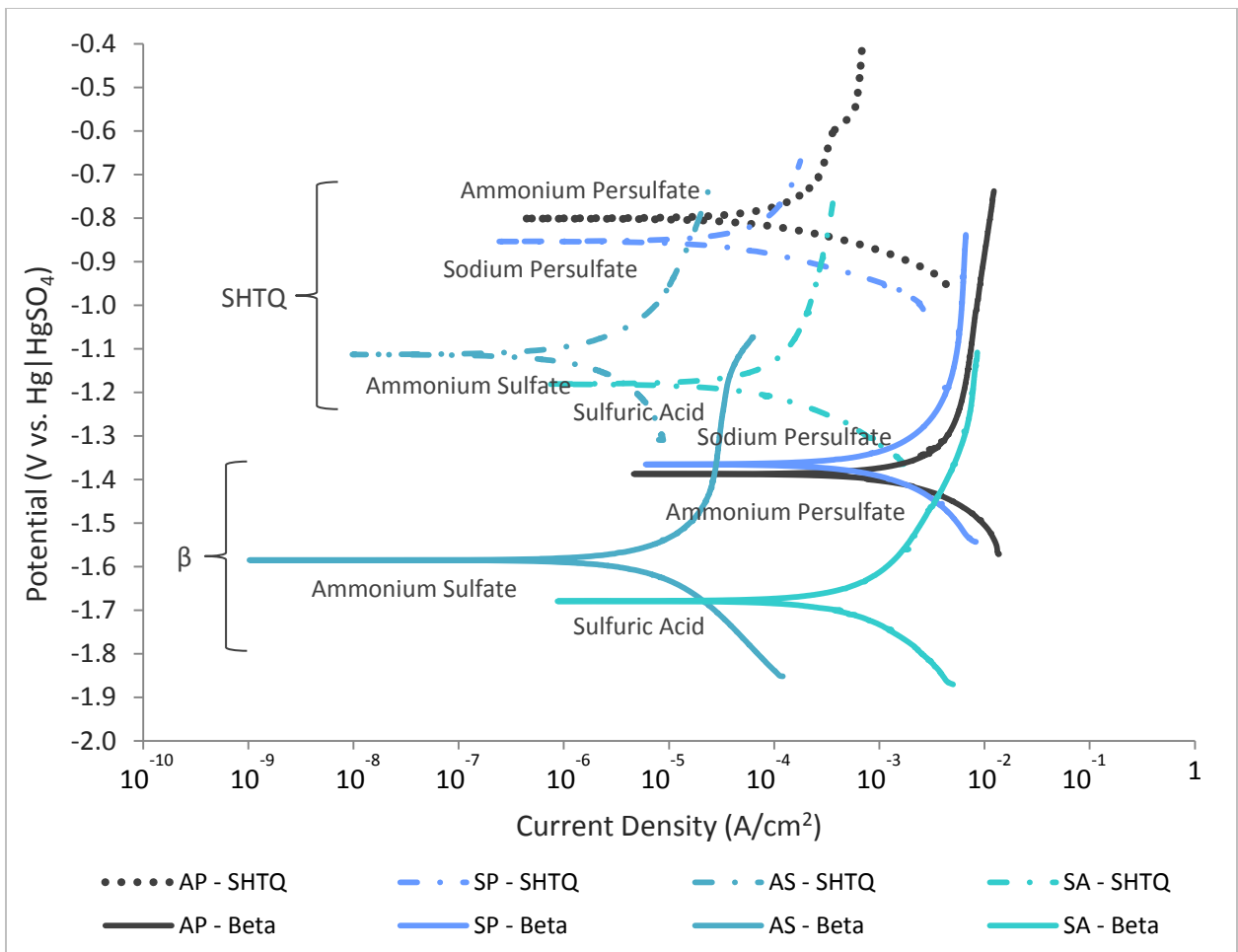


Figure 4.39 Anodic polarization scans of AA5083-SHTQ and β -phase specimens in **pH 0.7 Ammonium Persulfate**, **pH 0.7 Sulfuric Acid**, **0.4M Sodium Persulfate**, and **0.4M Ammonium Sulfate** at **35°C**

4.3.4 ETCHANT SELECTIVITY (RATIO OF CURRENT DENSITIES AT THE OCP OF THE MATRIX)

The open circuit potentials and current densities (after a 5 min OCP hold) were determined from the polarization data and are recorded in Table 4.5. The polarization resistance (R_p) was determined from the slope of the linearly plotted polarization curve near the open circuit potential. The current density at the corrosion potential for the SHTQ specimens was estimated by extrapolating the passive current density to the OCP. The ratio of the current density of the β -phase at the OCP of the matrix ($i(\beta)_{\text{SHTQ}}$) to the corrosion current density of the matrix at its OCP ($i(\text{SHTQ})_{\text{corr}}$) indicates the selectivity of the etchants and is shown graphically as a function of temperature in Figure 4.40.

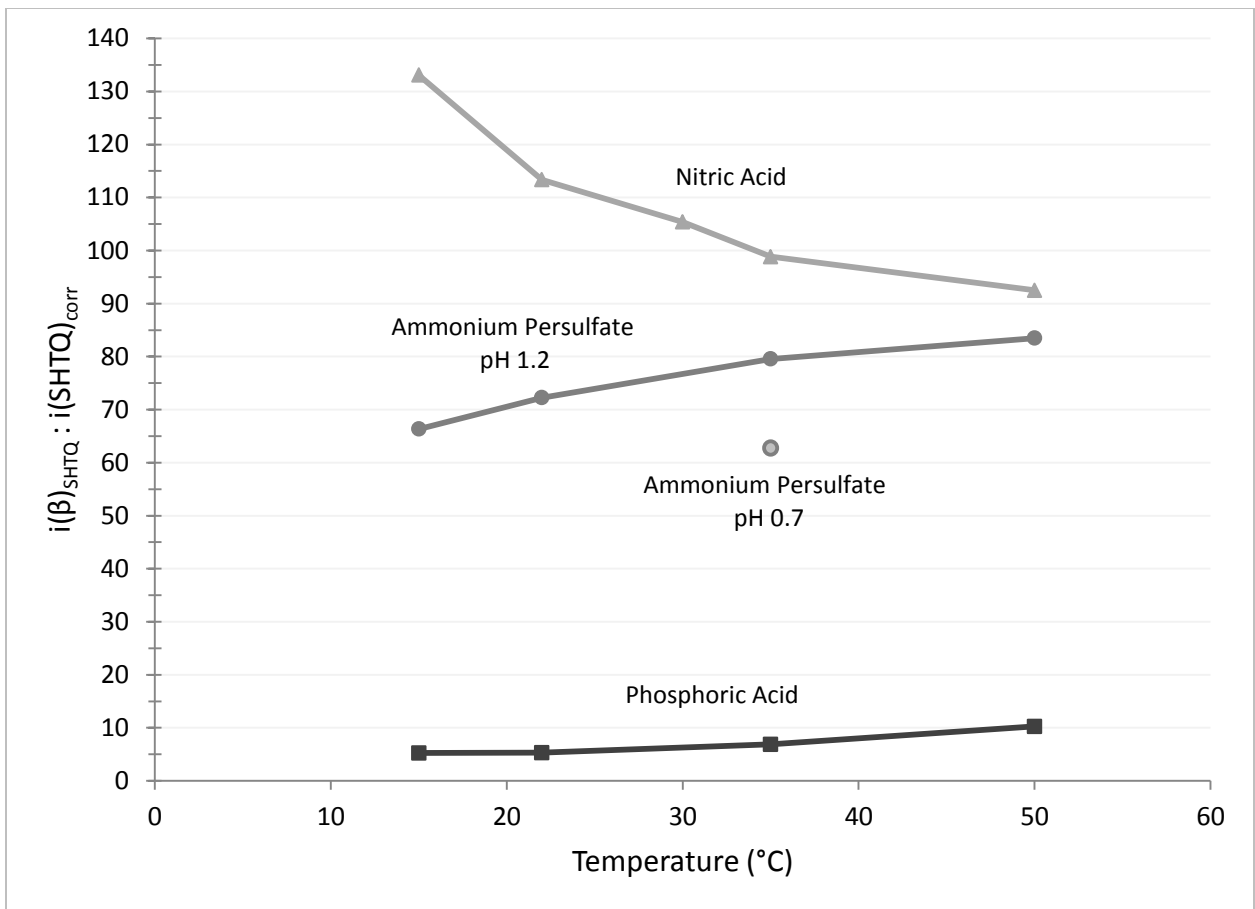


Figure 4.40 Ratios of the current densities of the β -phase and the matrix (SHTQ) at the open circuit potential of the matrix in Nitric Acid, Ammonium Persulfate, and Phosphoric Acid as a function of temperature (15-50°C)

Etchant selectivity was highest for nitric acid and lowest for phosphoric acid. Selectivity decreased significantly for nitric acid from 15°C to 50°C (ratio change from 133 to 93), and increased moderately for ammonium persulfate (ratio change from 66 to 84) and slightly for phosphoric acid (ratio change from 5 to 10) across the same temperature range. These results correlate well with the OCP etching assessments, damage site depth measurements, and ICP analyses that indicate that phosphoric acid is less selective for β -phase dissolution than nitric acid and ammonium persulfate. Based on the polarization results, ammonium persulfate of pH 0.7 was less selective than at a pH of 1.2. Deviations from the trends seen with the etching and mass loss tests are discussed in Chapter 5.

Table 4.5 Electrochemical Properties from Anodic Polarization Data for AA5083-SHTQ and β -Phase Specimens

Etchant	T _{exposure} (°C)	OCP _{SHTQ} (V vs. MSE)	OCP _{β} (V vs. MSE)	Δ OCP (V)	R _p (SHTQ) ($\Omega \cdot \text{cm}^2$)	R _p (β) ($\Omega \cdot \text{cm}^2$)	i(SHTQ) _{corr, cathodic} (A/cm ²) *	i(SHTQ) _{corr, anodic} (A/cm ²) **	i(β) _{SHTQ} (A/cm ²)	i(β) : i(SHTQ) at OCP _{SHTQ} ***
Nitric Acid	15	-0.47	-0.72	0.251	851	11	1.7×10^{-5}	5.5×10^{-5}	7.3×10^{-3}	133
	22	-0.48	-0.73	0.248	450	7.2	2.0×10^{-5}	9.0×10^{-5}	1.0×10^{-2}	113
	30	-0.49	-0.74	0.254	253	6.6	7.0×10^{-5}	1.3×10^{-4}	1.4×10^{-2}	105
	35	-0.49	-0.76	0.261	163	5.0	8.0×10^{-5}	1.7×10^{-4}	1.7×10^{-2}	99
	50	-0.51	-0.76	0.257	89	2.6	1.3×10^{-4}	4.0×10^{-4}	3.7×10^{-2}	93
Phosphoric Acid	15	-1.17	-1.77	0.605	65	156	3.0×10^{-4}	6.0×10^{-4}	3.2×10^{-3}	5.3
	22	-1.17	-1.77	0.602	37	82	5.0×10^{-4}	1.0×10^{-3}	5.3×10^{-3}	5.3
	35	-1.17	-1.79	0.617	18	37	1.0×10^{-3}	2.1×10^{-3}	1.4×10^{-2}	6.9
	50	-1.19	-1.80	0.613	19	25	1.1×10^{-3}	2.1×10^{-3}	2.2×10^{-2}	10
Ammonium Persulfate (pH 1.2)	15	-0.76	-1.26	0.506	1692	123	1.3×10^{-5}	3.0×10^{-5}	2.0×10^{-3}	66
	22	-0.77	-1.32	0.556	1508	91	1.3×10^{-5}	4.0×10^{-5}	2.9×10^{-3}	72
	35	-0.78	-1.35	0.571	390	20	6.0×10^{-5}	1.1×10^{-4}	8.8×10^{-3}	80
	50	-0.79	-1.42	0.634	92	13	3.0×10^{-4}	2.3×10^{-4}	1.9×10^{-2}	84
Ammonium Persulfate (pH 0.7)	35	-0.80	-1.39	0.587	249	14	9.0×10^{-4}	1.8×10^{-4}	1.1×10^{-2}	63
Notes:	<p>* i(SHTQ)_{corr, cathodic} was extrapolated from the cathodic current densities to the OCP of SHTQ</p> <p>** i(SHTQ)_{corr, anodic} was extrapolated from the anodic passive current densities to the OCP of SHTQ</p> <p>*** i(SHTQ)_{corr, anodic} was used for i(SHTQ)_{corr} for ratio calculations</p>									

4.4 SUMMARY OF TESTING AND RESULTS

4.4.1 CHARACTERIZATION OF ETCHANT SELECTIVITY

Etchants are used to detect sensitization and subsequently determine IGC susceptibility in the 5XXX Al-Mg alloys via the preferential attack of β -phase precipitates primarily located at the grain boundaries. The goal of this work was to assess the extent of preferential attack after etchant exposure to characterize the degree of etchant selectivity for nitric acid, phosphoric acid, and ammonium persulfate.

Several methods were used to characterize etchant selectivity³⁸. OCP surface etching tests were performed to qualitatively confirm that the solutions worked as etchants and to determine their selectivity based on etching clarity (the visible distinction of the β -decorated grain boundaries). Mass loss after 24-hour exposure was measured to quantify the degree of sensitization as a function of a specified set of sensitization conditions, and the corresponding damage morphology and damage-site-depth measurements were used to assess the intergranular nature of the attack.

The concentrations of species dissolved in the solutions after mass loss tests were determined via ICP analyses and were used to calculate a Mg-to-Al dissolution ratio for each etchant; a higher ratio indicated a higher affinity for dissolution of the Mg-rich β -phase. Etchants that attacked the specimens intergranularly during exposure resulting in deep damage sites and a relatively high Mg-to-Al dissolution ratio were considered highly selective³⁹.

Etchant selectivity was also defined by the ratio of current densities of the β -phase and the matrix at the OCP of the matrix which was calculated from anodic polarization data. Etchants with high current density ratios were considered more selective, since the current densities indicated that the β -phase at the grain boundaries corroded more rapidly than the surrounding matrix.

Comparing the results from these tests allows for a more comprehensive assessment of etchant selectivity, which is detailed per etchant in the following sections and summarized and ranked in Appendix D.

³⁸ Standardized detection methods utilizing etchants are described in detail in Chapter 1: Background and Objectives

³⁹ A relatively high Mg:Al concentration ratio is still less than 1. Since both the matrix (~94 wt% Al) and the β -phase (~64 wt% Al) are dissolving, there remains a higher total concentration of Al in solution (though this does not indicate the rate of dissolution specific to each species)

4.4.2 SELECTIVITY OF NITRIC ACID

Nitric acid was an effective etchant during short-term OCP etching tests with low to moderate attack of the matrix and visibly etched grain boundaries for the sensitized specimens. Mass loss test exposures of sensitized material resulted in the deepest damage sites amongst the etchants with intermediate dimension changes, and damage morphology analysis identified deep, intergranular fissures with low to moderate grain fallout. These results, which correlate with the mass loss measurements, indicate that nitric acid is a highly selective etchant. Exposures in nitric acid also yielded the highest etchant selectivity during anodic polarization.

The low selectivity determined via the concentration ratio of dissolved magnesium to dissolved aluminum conflicts with the results from other tests; it was expected that the dissolved sensitized sample would have larger Mg to Al concentrations than the unsensitized sample. The ICP analysis showed that all of the etchants dissolved the alloys with higher Mg to Al concentration ratios than defined by the stoichiometric ratio of the matrix; this indicates that the β -phase dissolution is raising the Mg concentration, and/or that the alloys and the β -phase are dissolving in a non-stoichiometric manner. Additionally, substantial grain fallout provided more surface area of the Al-rich matrix available for dissolution by the etchants. It should be noted that the sample size was limited (multiple replicates of only one etchant sample per sensitization condition), and in some instances the concentrations approached the background values; thus there exists a higher probability for error in some of the measurements. Additional data are necessary to confirm any of the aforementioned trends described in previous sections.

The polarization behavior of the β -phase in concentrated nitric acid also contradicts that observed by Searles, who reported that the β -phase did not show passivity when tested at room temperature [15]. However, this passive behavior does support the observation of only slight increases in corrosion rate with DoS from polarization results reported by Bumiller [2].

4.4.3 SELECTIVITY OF PHOSPHORIC ACID

Phosphoric acid was evaluated to be the least selective of the etchants tested. Immersion for 24 hours resulted in the lowest damage depths for sensitized material and the highest depths for unsensitized material (SHTQ); coupling the low damage penetration with the highest change in dimension indicates that the phosphoric acid demonstrated the highest attack of the matrix. Both OCP surface etching and polarization tests indicated moderate selectivity, due to high attack of

the matrix. Similar to the nitric acid exposures, the concentration ratio of dissolved Mg to Al was also lower for the unsensitized sample than that for the sensitized sample.

4.4.4 SELECTIVITY OF AMMONIUM PERSULFATE

Ammonium persulfate was ranked as the most selective etchant based on the data from the majority of the tests. OCP surface etching resulted in high etching clarity with less attack on the matrix than the other solutions. Specimens had intermediate damage depths but the lowest change in dimension after 24-hr immersion and exhibited deep fissures with low grain fallout and mass loss. Ammonium persulfate exposures also resulted in higher concentrations of dissolved magnesium relative to dissolved aluminum, which indicates that the solution is more preferentially corrosive of the β -phase than the other solutions. The ratio of Mg to Al concentrations for the sensitized sample was much higher relative to the SHTQ sample than in the nitric acid and phosphoric acid exposures, and the margin of error and potential for overlap was also lower. High selectivity was shown for the anodic polarization behavior; as with the nitric acid exposures, the higher corrosion current density of the β -phase over the matrix indicates preferential attack of magnesium rather than aluminum.

The results presented in Chapter 4 and further explained in Chapter 5 (Discussion) are summarized with etchant selectivity rankings (1 = highest selectivity) in Appendix D (Tables D.1 – D.5).

5 DISCUSSION

The degree of etchant selectivity was expected to be dependent on the material properties of the AA5083 specimens (sensitization condition, orientation, constituent particles, specimen preparation) and the exposure environment (temperature, etchant chemistry). The associated trends and effects are compiled in Sections 5.1 (Material Properties) and 5.2 (Etchant Environment).

5.1 MATERIAL PROPERTIES

5.1.1 SENSITIZATION CONDITION

AA5083 specimens that were solution heat-treated, quenched, and sensitized for 7, 14, and 30 days were assessed via OCP etching, 24-hr mass loss testing, and ICP analysis. The damage site depths and damage morphology after 24-hr immersion were also noted. A similar trend was observed throughout the range of tests – attack from etchant exposure increased with sensitization condition.

OCP etching results, shown in Figures 4.2 - 4.11, were a function of DoS. The SHTQ (NAMLT = 2 mg/cm²) specimens did not exhibit grain boundary etching on either the LT or LS surface for all tests. This was expected due to the SHTQ process which re-solutionized β -phase precipitates before testing. Grain boundary attack increased with sensitization condition; specimens sensitized at 100°C for 30 days (NAMLT = 40 mg/cm²) showed higher uniformity of attack at the grain boundaries than the specimens sensitized at 100°C for 7 days (NAMLT = 16 mg/cm²). These results are similar to the guidelines in ASTM B928 for phosphoric acid, which associate the visible continuity of the grain boundaries after etching with the degree of sensitization of the alloy.

The average mass loss after 24-hr immersion increased with sensitization condition (SHTQ through 100°C-30days) in each etchant (Figure 4.12). The higher mass loss with increasing DoS relationship was expected due to the increasing network of β -phase precipitates at the grain boundaries; dissolution of the β -phase precipitates and inter- β -phase ligaments resulted in more grain fallout. The results follow the trends observed for the NAMLT exposure at 30°C.

Intergranular attack morphology was also seen to increase between the SHTQ specimens and the sensitized specimens after 24-hr immersion. The damage sites did not appear to originate or propagate from the grain boundaries for the SHTQ samples, but rather appeared as localized pits (e.g. Figure 4.21). Sensitized specimens (NAMLT = 30 mg/cm²) experienced intergranular,

fissure-like attack, although the phosphoric acid exposures resulted in wider damage sites with much smaller length to width ratios than the other etchant exposures (as approximated qualitatively from Figures 4.15, 4.19-4.21).

The average concentrations of dissolved Al and Mg after 24 hours were measured via ICP analysis and are shown in Figure 4.31. The total concentration of dissolved species in the etchants increased from the unsensitized condition (SHTQ) to the sensitized condition (100°C-30days) across all solutions, with phosphoric acid dissolving the most material and ammonium persulfate dissolving the least amount of material (5119 ppm to 875 ppm for the sensitized sample, respectively). Sensitized samples experienced extensive grain fallout, which increased the surface area available for dissolution and reduced the rate-limiting effects of the diffusion of species to and from the advancing damage site tips.

5.1.2 ORIENTATION

The LT and LS surfaces of AA5083 specimens were assessed via OCP etching and anodic polarization tests, and the damage morphology in the L, T, and S-directions were noted after 24-hr mass loss testing. Similar trends were observed for each surface and direction across the range of etchants – the LS surfaces tended to etch/corrode faster than the LT surfaces, and the damage penetration was most extensive along the L and T-directions.

In short-term OCP etching tests, it was observed that the LS surfaces tended to etch more quickly than the LT surfaces for sensitized samples (this can be seen in Figures 4.2 and 4.3 for nitric acid exposures and Figures 4.10 and 4.11 for ammonium persulfate exposures). This is likely due to a higher number of grain boundaries with longer networks of β -phase precipitates. The orientation was not observed to significantly affect the etching clarity.

After 24 hours, nitric acid and ammonium persulfate exposures resulted in many deep, fissure-like, damage sites in the L and T-directions for sensitized specimens (Figures 4.15 and 4.19). The nitric acid exposures resulted in more penetration in the S-direction than the ammonium persulfate exposures, which led to more grain fallout and the visibly wider “mouths” of the fissures (Figures 4.15-d and 4.15-i). Damage penetration originating along the S-direction tended to propagate along the L and T-directions (Figure 4.25), which had longer grain boundaries and thus a longer network of β -phase precipitates. The SHTQ specimens in all three etchants and the sensitized specimens in phosphoric acid showed less intergranular attack (Figure 4.21).

Anodic polarization tests were used to determine the corrosion behavior of the matrix and the β -phase during etching and mass loss tests. Surface orientation of the matrix was considered, since the area of the LS surfaces was much greater than that of the LT surfaces during the mass loss tests (following the procedures of ASTM G67). The open circuit potentials of the LS surfaces were higher than those of the LT surfaces in all three etchants (Figures 4.34, 4.36, and 4.38). This is likely due to a higher density of cathodic constituent particles on the LS surface. The higher OCP of the LS surface may also indicate that the β -phase would corrode at a marginally faster rate at the OCP of the LS surface than at the OCP of the LT surface. The passive current densities and OCPs seen in polarization tests did not change appreciably with longer (30 min) OCP holds.

5.1.3 CONSTITUENT PARTICLES

The effects of the constituent particles on etchant selectivity were investigated via OCP etching and polarization tests. It was observed that the constituent particles did not affect etching clarity but did affect the OCPs of the AA5083-SHTQ specimens polarized in the three etchants.

The edges of the constituent particles in AA5083 SHTQ and sensitized specimens were attacked after all etching exposures (e.g. Figure 4.9 for phosphoric acid exposures and Figure 4.10 for ammonium persulfate exposures). This indicates either the presence of β -phase precipitates and/or galvanic coupling interactions with the matrix. However, the clarity of the etch was more affected by the attack on the matrix relative to the β -phase, which is observed in Figures 4.6 and 4.8 for phosphoric acid etching.

The OCP of SHTQ samples was dependent on the density and types of cathodic constituent particles. In some replicate polarization tests, the OCP of the SHTQ sample (specific to one orientation and at one temperature of interest) varied as much as 200 mV from the initial tests, though similar corrosion and passive current densities were observed. The variability in OCP could affect the driving force for the dissolution of the β -phase; however, since both materials (AA5083-SHTQ and β -phase) demonstrate passivity at the potentials investigated in this work, a change in matrix OCP would only marginally increase the corrosion rate of the β -phase at the OCP of the alloy matrix.

5.1.4 SURFACE FINISH

The effects of the specimen preparation process were notable regarding the time to etch. The time to etch in the ammonium persulfate solutions was previously shown to take 60 minutes at room temperature⁴⁰. However, grain boundaries were not observed for the highest sensitization level at 22°C after 60 minutes in these experiments. The specimens in this work were only ground to 1200 grit and were not further polished, which may account for the longer time to etch used in these experiments. It is possible that the “peaks and valleys” formed by the grinding process formed micro-galvanic couples that interfered with the attack of the β -phase at the grain boundaries. The etching time in phosphoric acid was not affected by the surface finish; based on the results from the mass loss and polarization tests, it is likely that the etchant is much more aggressive to the matrix and effectively attacked and dissolved the grinding ridges that may have obscured the underlying grain boundaries.

The effects of further polishing the samples to 1 μ m for polarization experiments were also considered – however, there was no significant change in the polarization data between the 1200 grit and 1 μ m-finished surfaces. Additionally, the effects of polishing the alloy samples in water versus ethylene glycol were considered nil after etching and polarizing the specimens and achieving the same results for both polishing processes.

5.2 ETCHANT ENVIRONMENT

5.2.1 EXPOSURE TEMPERATURE

The temperature sensitivity of etchant selectivity was assessed via OCP etching, mass loss tests, and polarization tests. The attack of the specimens (both the matrix and β -phase) was observed to increase with temperature (from 15°C to 50°C).

Etching was observed to be highly dependent on temperature. In some occurrences, specimens sensitized for 30 days and immersed at 22°C were relatively un-etched after 60 minutes (e.g. Figure 4.2c), whereas specimens of the same sensitization revealed etched or over-etched grain boundaries at 30°C and 35°C after the same time in solution (Figures 4.2f and 4.2i, respectively). These inconsistencies could pose challenges for etching experiments that are not in temperature-controlled environments, since etching for a set period of time but with variable temperature could result in a sensitized sample appearing unsensitized, or a lightly sensitized sample appearing highly sensitized.

⁴⁰ Etching experiments performed by Lei Chen and Mary Lyn Lim at the University of Virginia.

Mass loss measurements were also very sensitive to temperature. ASTM G67 tests in concentrated nitric acid were performed at 30°C and 35°C. The resulting corrosion behaviors were similar when comparing the trendlines on the mass loss versus sensitization time graph in Figure 4.12. But the mass lost at 35°C (3, 32, 59, and 76 mg/cm² for SHTQ to 100°C-30 day specimens) was almost twice as much as that lost at 30°C (2, 16, 29, and 40 mg/cm²), which indicates high temperature sensitivity. The morphology of the attack at both temperatures was intergranular (Figure 4.20); however, testing at 35°C increased the width of the damage sites and augmented the severity of the grain fallout. The temperature sensitivity of mass loss measurements contributes to potential error in calculations; test temperature variance by five degrees can misrepresent whether a sample is considered of intermediate sensitization or sensitized (100°C-7D condition).

The thermodynamic driving force for the dissolution of the β -phase is the difference in potential between β -phase and the matrix. This driving force is plotted as a function of temperature in Figure 5.1 below. Phosphoric acid environments have the highest driving force for dissolution while nitric acid environments have the lowest driving force for dissolution. The differences in OCP are relatively stable with temperature in both environments. Ammonium persulfate has a high driving force for dissolution that slightly increases with temperature. However, the difference in potential as a driving force for dissolution reactions to occur does not account for kinetics; this explains why the phosphoric acid has low selectivity, since exposures result in high corrosion rates of the matrix. This is seen in the mass loss and polarization data.

The polarization behavior of the specimens is also dependent on temperature of exposure. The corrosion current densities and passive current densities increased with temperature for both the matrix and the β -phase (Figures 4.33, 4.35, 4.37). The ratio of current densities decreased from 133 to 93 for the nitric acid exposures as temperature increased from 15°C - 50°C (Figure 4.40). Over the same range of temperatures, ammonium persulfate selectivity increased from 66 to 84, while phosphoric acid exposures had the lowest selectivity (ranging from 5.3 to 10) that was not as dependent on temperature.

Plotting the natural log of the passive current densities at selected potentials as a function of $1/T$ allows for the determination of the activation energy from the slopes of the trendlines⁴¹, as shown in Figures 5.2-5.4 below. The activation energies calculated from the plots are listed in Table 5.1 below.

⁴¹ Activation energy (Q) is calculated from the following equation: $\ln(\text{corrosion rate}) = -Q/RT + \ln(A)$, where $R = 8.314$ J/mol·K, T is temperature in Kelvin, and A is a rate constant [14]

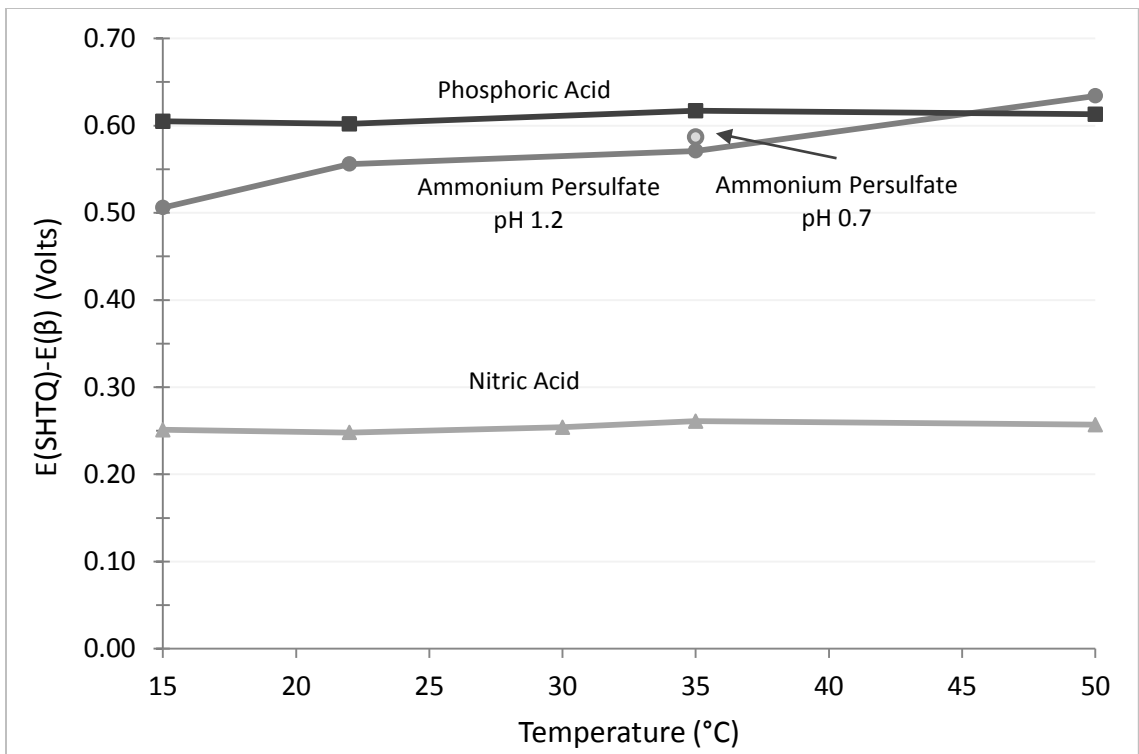


Figure 5.1 The change in the difference in open circuit potentials between the matrix and β -phase with increasing temperature, calculated from anodic polarization data. The difference in potentials indicates the thermodynamic driving force for the dissolution of the β -phase at the OCP of the alloy.

The activation energy was found to be highest for the SHTQ specimens exposed to ammonium persulfate, which corresponds to the slowest corrosion rate of the matrix seen in the mass loss tests. Nitric acid exposures resulted in the largest difference in activation energies between the β -phase and the SHTQ samples, which indicates high selectivity. Phosphoric acid had lower activation energies that were similar for both the β -phase and the matrix, indicating lower resistance to dissolution.

Table 5.1 The activation energy (Q) calculated from the slope of the Arrhenius plots in Figures 5.2-5.4

	Sample	Potential (V vs. MSE)	Slope	Q (KJ/mol)
Nitric Acid	SHTQ	-0.3	-5425	45.1
	SHTQ	-0.4	-5938	49.4
	β -phase	-0.5	-4413	36.7
Phosphoric Acid	SHTQ	-1.0	-5994	49.8
	SHTQ	-1.1	-5010	41.6
	β -phase	-1.2	-5287	44.0
Ammonium Persulfate pH 1.2	SHTQ	-0.5	-7171	59.6
	SHTQ	-0.6	-6483	53.9
	SHTQ	-0.7	-6769	56.3
	β -phase	-0.8	-6265	52.1

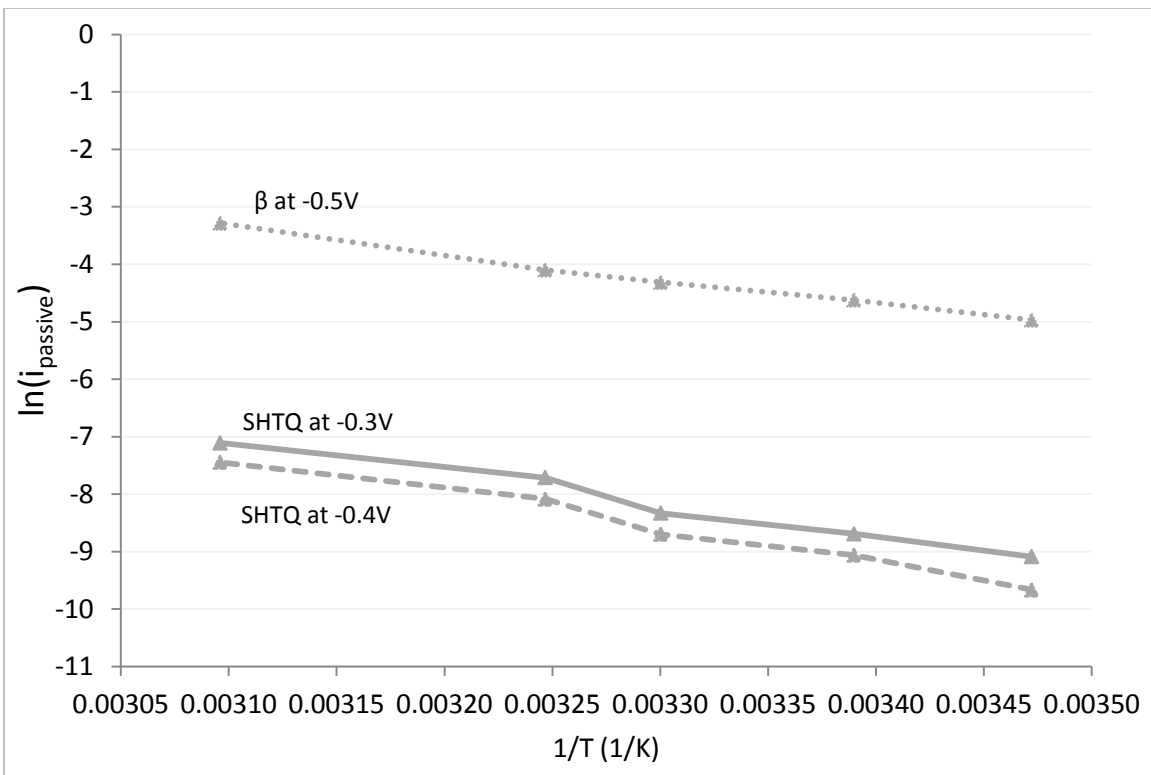


Figure 5.2 Arrhenius plot of the corrosion rates for AA5083-H131-SHTQ and the β -phase in concentrated nitric acid for selected potentials in the passive current region of the anodic polarization curve. The slope of the rates as a function of inverse temperature indicates the activation energy.

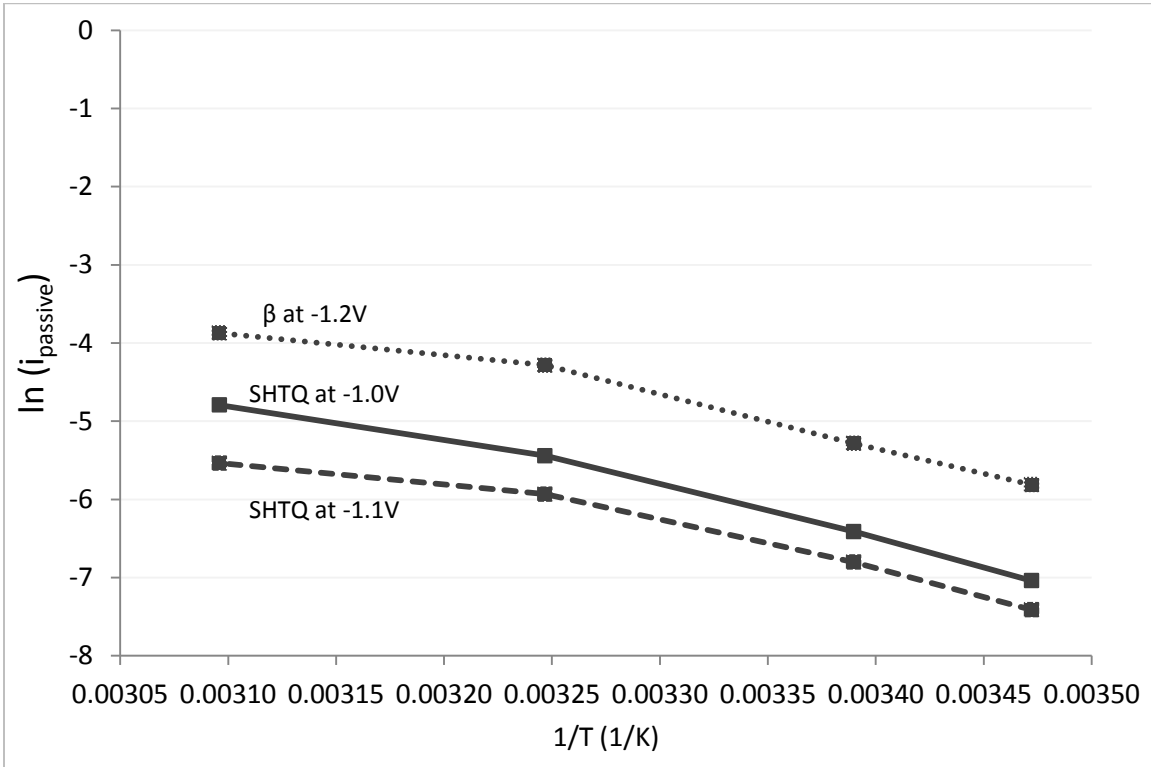


Figure 5.3 Arrhenius plot of the corrosion rates for AA5083-H131-SHTQ and the β -phase in phosphoric acid for selected potentials in the passive current region of the anodic polarization curve. The slope of the rates as a function of inverse temperature indicates the activation energy.

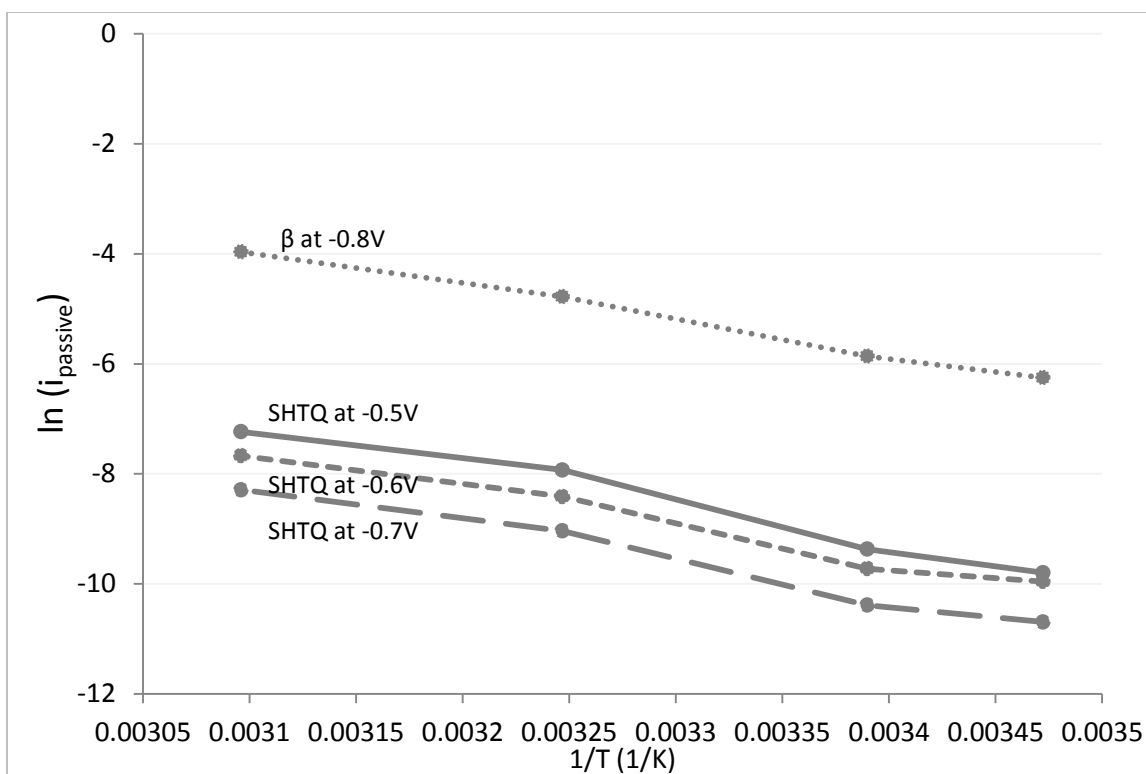


Figure 5.4 Arrhenius plot of the corrosion rates for AA5083-H131-SHTQ and the β -phase in pH 1.2 ammonium persulfate for selected potentials in the passive current region of the anodic polarization curve. The slope of the rates as a function of inverse temperature indicates the activation energy.

5.2.2 ETCHANT CHEMISTRY

The effects of pH on the polarization behavior of the matrix and the β -phase were examined for ammonium persulfate at 35°C. Both materials were more active in the lower pH solution – current densities for pH 0.7 ammonium persulfate were higher than those for pH 1.2 ammonium persulfate, and the OCPs were lower (Figure C.12). However, etchant selectivity decreased with pH, with the pH 0.7 solution being more aggressive toward matrix dissolution than the pH 1.2 solution (Figure 4.40).

Jones reports the effects of pH on the dissolution of aluminum in nitric and phosphoric acid (Figure 5.5 below). In the plot, it can be observed that the phosphoric acid exposures result in more mass loss at acidic pH than the nitric acid exposures, and that both show passivity near neutral conditions. These results are also seen in the mass loss tests in this study.

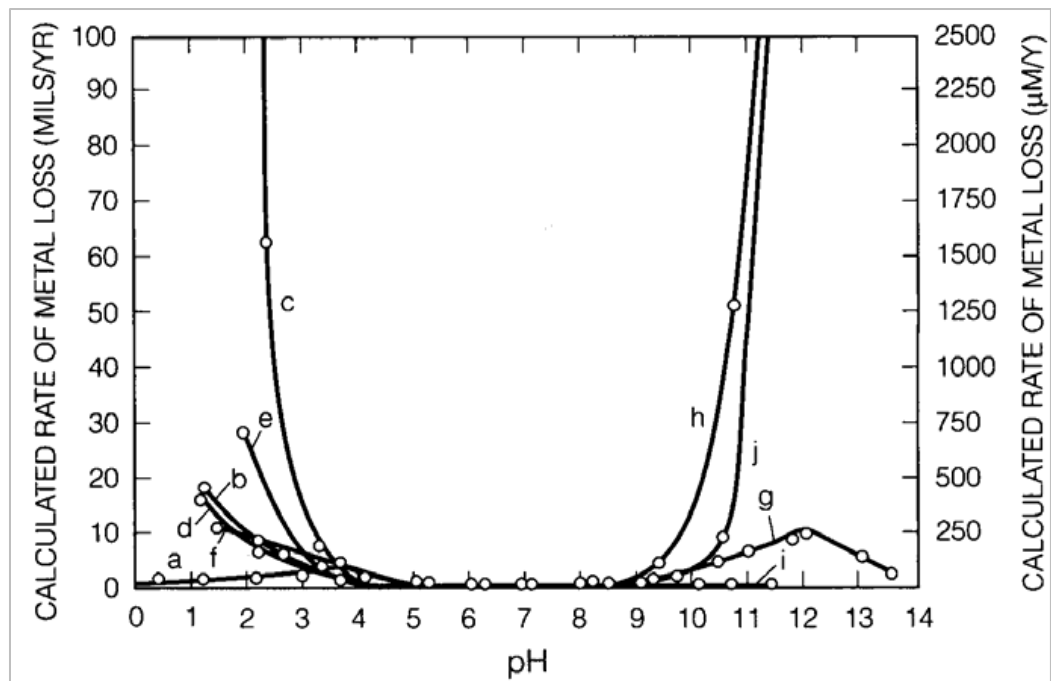


Figure 5.5 Effect of pH on corrosion of aluminium [Reproduced from 14]. (a) acetic acid, (b) hydrochloric acid, (c) hydrofluoric acid, **(d) nitric acid**, **(e) phosphoric acid**, (f) sulphuric acid, (g) ammonium hydroxide, (h) sodium carbonate, (i) sodium disilicate, (j) sodium hydroxide.

However, pH (or the corresponding concentration of hydrogen ions) is not believed to be the major chemical driver for the dissolution reactions to occur since etchant selectivity did not show trends with pH (nitric acid with a negative pH was more selective than phosphoric acid with an intermediate acidic pH but less selective than ammonium persulfate at pH 1.2). Rather it is speculated that the chemical activity, speciation, solubility, and complexation involving the anions in solution have the dominant effect in the ability to break down the passive oxide film on the alloy and selectively dissolve the β -phase. The cation was not found to be as critical for β -phase dissolution, as evidenced in the similar polarization results between ammonium persulfate and sodium persulfate (Figure 4.39).

Additionally, changes in the color of the etchant solutions after 24-hour mass loss testing, seen in Figure 5.6 below, implies that complexation events are occurring that govern the reaction rates. The nitric acid exposures turned brown in appearance, likely due to the formation of nitrous oxides. The phosphoric acid solutions turned aquamarine in color, and the ammonium persulfate solutions acquired a pink tint. Investigation into the speciation of these solutions is beyond the scope of this work, but is recommended for future analyses.

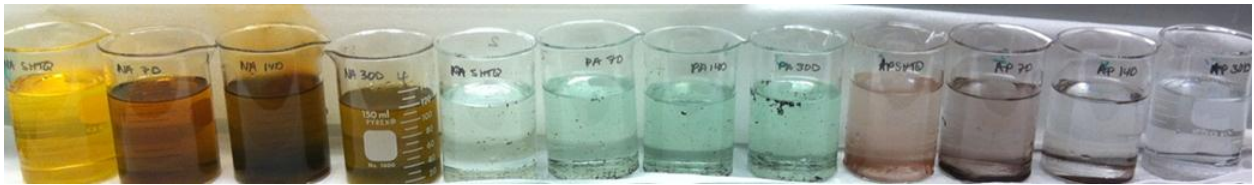


Figure 5.6 Etchant solutions after 24-hour mass loss testing prior to ICP analyses. From left to right in the image: Nitric Acid SHTQ – 7 Days – 14 Days – 30 Days, Phosphoric Acid SHTQ – 7 Days – 14 Days – 30 Days, Ammonium Persulfate SHTQ – 7 Days – 14 Days – 30 Days.

5.3 ACCURACY, PRECISION, AND BIAS OF STANDARDIZED TESTING METHODS FOR IGC SUSCEPTIBILITY

Mass loss tests in concentrated nitric acid and etching tests in phosphoric acid specified in ASTM G67 and B928, respectively, were shown to be highly sensitive to temperature. Although these tests are each defined at a single temperature (30°C for mass loss and 35°C for etching), poor thermal control and stability could result in measurements that are both inaccurate and imprecise. Compounding the error are possible inconsistencies in measuring specimen dimensions, monitoring time of exposure, and cleaning the corroded surfaces after immersion.

Implications of IGC-susceptibility stemming from erroneous mass loss measurements can be misappropriated due to the definitions of sensitization levels in the standards (unsensitized material is defined at mass loss $<15\text{mg}/\text{cm}^2$ and sensitized material is defined at mass loss $>25\text{mg}/\text{cm}^2$). As seen in this study, a specimen of intermediate sensitization (100°C-7days) could be classified as sensitized if the exposure temperature is higher than specified (and result in unnecessarily rejecting new material or prematurely replacing in-service material). Potentially more dangerous is the misrepresentation of sensitized material as unsensitized or of low sensitization if the temperature is lower than specified and less grain fallout is induced.

Etching in phosphoric acid poses a concern due to the qualitative nature and the subjective interpretations of the standard's definition of sensitization (a continuous network of grain boundary precipitation). As shown by IGC penetration experiments reported by Bumiller and Lim, and as seen in the etching and mass loss tests in this study – discontinuous precipitate networks can also corrode given suitable grain boundary dissolution chemistry [1-2]. An IGC-susceptible material would not need to exhibit continuous grain boundary attack upon etching to propagate IGC.

6 CONCLUSIONS

The objective of this work was to characterize the selectivity of nitric acid, phosphoric acid, and acidified ammonium persulfate by assessing the corrosion behaviors of the bulk alloy (AA5083) and pure β -phase during etchant exposure. Open circuit potential (OCP) etching, 24-hour mass loss tests, and anodic polarization scans were performed over a range of sensitization conditions, surface orientations, and exposure temperatures. The following conclusions can be made:

+ *All three etchants demonstrated selectivity for β -phase dissolution*

OCP surface etching tests qualitatively confirmed that the solutions worked as etchants; the grain boundaries were not attacked in unsensitized SHTQ specimens but were corroded in high DoS specimens.

+ *The attack of the matrix determined etch clarity and damage morphology characteristics*

The etchants are all acids, which are thermodynamically driven to attack both aluminum and magnesium. In some etching experiments (primarily phosphoric acid exposures), visible attack of the matrix obscured the grain boundaries, making it more difficult to discern the extent of etching. Matrix attack that was observed upon cross-sectioning specimens after 24-hour exposure appeared to significantly contribute to the mass loss in addition to the grains dislodged after dissolution of the β -decorated grain boundaries.

+ *Etchant selectivity is highly dependent on exposure temperature*

Attack of the SHTQ specimens and the β -phase was observed to increase with temperature (from 15°C to 50°C) in all of the etchants throughout each method of testing considered. The rates of matrix and β -phase attack in relation to each other, defining selectivity, varied significantly with exposure temperature in OCP etching and mass loss tests. For several tests, comparing the etched surfaces for a set sensitization condition (100°C-7days) and duration of exposure showed that the grain boundaries were not etched at 22°C but were etched at 35°C; mass loss for that same sensitization condition doubled with only a five degree increase in temperature for the nitric acid exposure.

- + *Ammonium persulfate was the most selective etchant tested and phosphoric acid was the least selective*

Ammonium persulfate was ranked as the most selective etchant based on exposure results of high etching clarity, low grain fallout but intermediate damage depth penetration, higher dissolved magnesium to dissolved aluminum concentration ratio, and intermediate selectivity during anodic polarization. Nitric acid was ranked intermediately, but also displayed high selectivity during etching and anodic polarization tests. Phosphoric acid was the least selective based on high attack of the matrix during etching, mass loss, and polarization tests.

- + *As they are currently defined, the standardized test methods used to detect sensitization are limited in applicability beyond controlled laboratory environments*

Mass loss tests in concentrated nitric acid and etching tests in phosphoric acid specified in ASTM G67 and B928, respectively, were shown to be highly sensitive to temperature. Poor control over exposure temperature could result in measurements that are both inaccurate and imprecise. As seen in this study for either test, a specimen of intermediate sensitization could be classified as sensitized if the temperature is not properly controlled and vice versa. In addition to temperature sensitivity, the long exposure durations, a hazardous etchant environment, and the destructive nature associated with extensive material dissolution render ASTM G67 a laboratory-specific experiment. Phosphoric acid etching is also most suited for the laboratory given the need for metallographic examination instrumentation (i.e. polishing equipment and microscopes). Similar restrictions would apply if ammonium persulfate were used to detect sensitization via these same methods.

7 FUTURE WORK

Given the data generated in this study, it is recommended that future work focus on test methods alternate to mass loss and surface etching to detect and quantify sensitization and determine IGC-susceptibility. Moving away from the use of concentrated nitric acid and mass loss tests is highly suggested due to the precautions necessary for handling and the time needed for testing. Electrochemical test protocols are attractive due to the relative speed with which data can be generated and analyzed. Optimizing any of the discussed etchants regarding concentration, pH, and exposure temperature would be a logical starting place, with particular emphasis on investigating the speciation of the solutions to better understand the dissolution reactions that occur during etching. Based on the high selectivity for β -phase dissolution, utilization of ammonium persulfate or sodium persulfate as a test environment is recommended. The electrochemical test protocol would also require the development of more applicable definitions of sensitization and how it contributes to IGC susceptibility.

REFERENCES

1. M.L.C. Lim, J.R. Scully, R.G. Kelly, "Intergranular Corrosion Penetration in an Al-Mg Alloy as a Function of Electrochemical and Metallurgical Conditions," *Corrosion*, online at <http://dx.doi.org/10.5006/0722> (2012).
2. E. Bumiller, "Intergranular Corrosion in AA5XXX Aluminum Alloys with Discontinuous Precipitation at the Grain Boundaries", (Ph.D. dissertation, The University of Virginia: Charlottesville, VA, 2011).
3. E. Bumiller, M. Shedd, B. Kazerooni, W. Adedeji, and R.G. Kelly, "The Electrochemistry of Intergranular Corrosion and Sensitization in 5XXX Aluminum Alloys," 2009 DoD Corrosion Conference (2009)
4. E. Bumiller, R Reudisueli, *Correlation of ASTM Tests in the Behavior of 5XXX Aluminum Alloys*, in *Corrosion 2008*. 2008, NACE International: Atlanta, GA.
5. E. Bumiller, R.G. Kelly, work presented at ECS 2008. (Honolulu, HI: Electrochemical Society).
6. ASTM G 67-04, "Standard Test Method for Determining the susceptibility to intergranular corrosion of 5XXX series aluminum alloys by mass loss after exposure to nitric acid (NAMLT Test)," (West Conshohocken, PA: ASTM International, 2004).
7. ASTM B928: Standard Specification for High Magnesium Aluminum-Alloy Sheet and Plate for Marine Service and Similar Environments, ASTM International
8. T.R. Allen, "Grain Boundary Engineering to Improve Corrosion Resistance of 5XXX Series Al Alloys," University of Wisconsin, presented at ONR program review (2010).
9. *Powder Diffraction File Card Number 00-029-0048*. (2010) International Center for Diffraction Data.
10. ASM Handbook, Volume 3: Binary Phase Diagrams, ASM International (2002)
11. J. Moran, "Effects of Metallurgical Variables on the Corrosion of Aluminum Alloys," *Corrosion: Fundamentals, Testing, and Protection*, Vol 13A, ASM Handbook, ASM International (2003) p275-278
12. M. Pourbaix, *Atlas of Electrochemical Equilibria in Aqueous Solutions*. 1974: NACE International.
13. M. Pourbaix, *Journal of the Less Common Metals*. 28 (1972) 51.
14. D.A. Jones, *Principles and Prevention of Corrosion*, 2nd ed. Prentice Hall, 1995
15. J.L. Searles, *The Electrochemical Characteristics of Al₃Mg₂ and Stress Corrosion Cracking Behavior of AA5083 (Al-4.5Mg-1.0Mn)*, M.S. Thesis, Ohio State University, 2000.
16. J.L. Searles, P.I. Guoma, R.G. Buchheit, *Metall. Mater. Trans. A*. 32, 11 (2001): p. 2859-2867.
17. J.L. Searles, P.I. Guoma, R.G. Buchheit, *Mater. Sci. Forum* 396-405 (2002): p. 1437-1442.

18. A.J. Davenport, Y. Yuan, R. Ambat, B.J. Connolly, M. Strangwood, A. Afseth, G. Scamans, *Mater. Sci. Forum.* 519-521 (2006): p. 641-646.
19. I.N.A. Oguocha, O.J. Adigun, S. Yannacopoulos, *J. Mater. Sci.* 43, 12 (2008): p. 4208–4214.
20. D.R. Baer, C.F. Windisch Jr., M.H. Engelhard, M.J. Danielson, R.H. Jones, J.S. Vetrano, *J. Vac. Sci. Technol. A* 18, 1 (2000): p. 131-136.
21. G.M. Scamans, N.J.H. Holroyd, C.D.S. Tuck, *Corros. Sci.* 27, 4 (1987): p. 329-347.
22. G. Scamans. “Low temperature sensitization of AA5XXX alloys”. Technical Report IR07-197, Innoval, Oxon, UK, 2008.
23. R.H. Jones, D.R. Baer, M.J. Danielson, J.S. Vetrano, *Metall. Mater. Trans. A.* 32, 7 (2001): p. 1699-1711.
24. J.S. Vetrano, R.E. Williford, S.M. Bruemmer, R.H. Jones, “Influence of microstructure and thermal history of the corrosion susceptibility of AA5083” in *Aluminum Alloys*, ed. S.K. Das, (Orlando, FL: TMS,1997).
25. R.H. Jones, J.S. Vetrano, C.F. Windisch Jr., *Corrosion.* 60, 12 (2004): p. 1144-1154.
26. R.H. Jones, V.Y. Gertsman, J.S. Vetrano, C.F. Windisch Jr., *Scripta Mater* 50, 10 (2004): p. 1355-1359.
27. J.A. Van Der Hoeven, L. Zhuang, B. Schepers, P. De Smet, J.P. Baekelandt, *Aluminum* 78 (2002): p. 750-754.
28. E.C.W. Perryman, S.E. Hadden, *J. Inst. Metals* 77 (1950): p. 207.
29. R. Goswami, G. Spanos, P.S. Pao, R.L. Holtz, *Mater. Sci. and Eng. A.* 527, 4-5 (2010): p. 1089-1095.
30. R. Goswami, G. Spanos, P.S. Pao, R.L. Holtz, *Metall. Mater. Trans. A.* 42, 2 (2010): p. 348-355.
31. J.C. Chang, T.H. Chuang, *Metall. Mater. Trans. A.* 30, 12 (1999): p. 3191-3199.
32. E. H. Jr. Dix, A. Anderson, M.B. Shumaker, *Corrosion* 15, 2 (1959): p. 55-62.
33. S. Samson, “The Crystal Structure of the Phase beta Mg₂Al₃.” *Acta Crystallographica*, 19, 401-412 (1965) in *Pearson’s Handbook of Crystallographic Data* (1991)
34. *Material Safety Data Sheet: Nitric Acid (65-70%)*. Fisher Scientific (2011).
35. L. Chen, “Thesis Image Fusion and An Outlier Detection Framework for Hierarchical Modeling with Application to Corrosion Prediction,” Ph.D. dissertation, The University of Virginia: Charlottesville, VA (2012).
36. H.L. Craig, Jr., “Nitric Acid Weight Loss Test for the H116 and H117 Tempers of 5086 and 5456 Aluminum Alloys,” *Localized Corrosion – Cause of Metal Failure, ASTM STP 516*, American Society for Testing and Materials, 1972, pp. 17-37.
37. *Powder Diffraction File Card Number 04-003-7061*. International Center for Diffraction Data (2010).
38. *Powder Diffraction File Card Number 04-007-1274*. International Center for Diffraction Data (2010).

39. C. Wong, "Calculating Behavior of 5xxx Al Alloys in Marine Service," Naval Surface Warfare Center Carderock Division, presented at ONR program review (2010).
40. D. Madhav and L.T. Romankiw, "Application of Chemical and Electrochemical Micromachining in the Electronics Industry," *Journal of the Electrochemical Society* 136, no. 6 (1989): 285C-292C.

APPENDIX A: β -Phase XRD Characterization Results

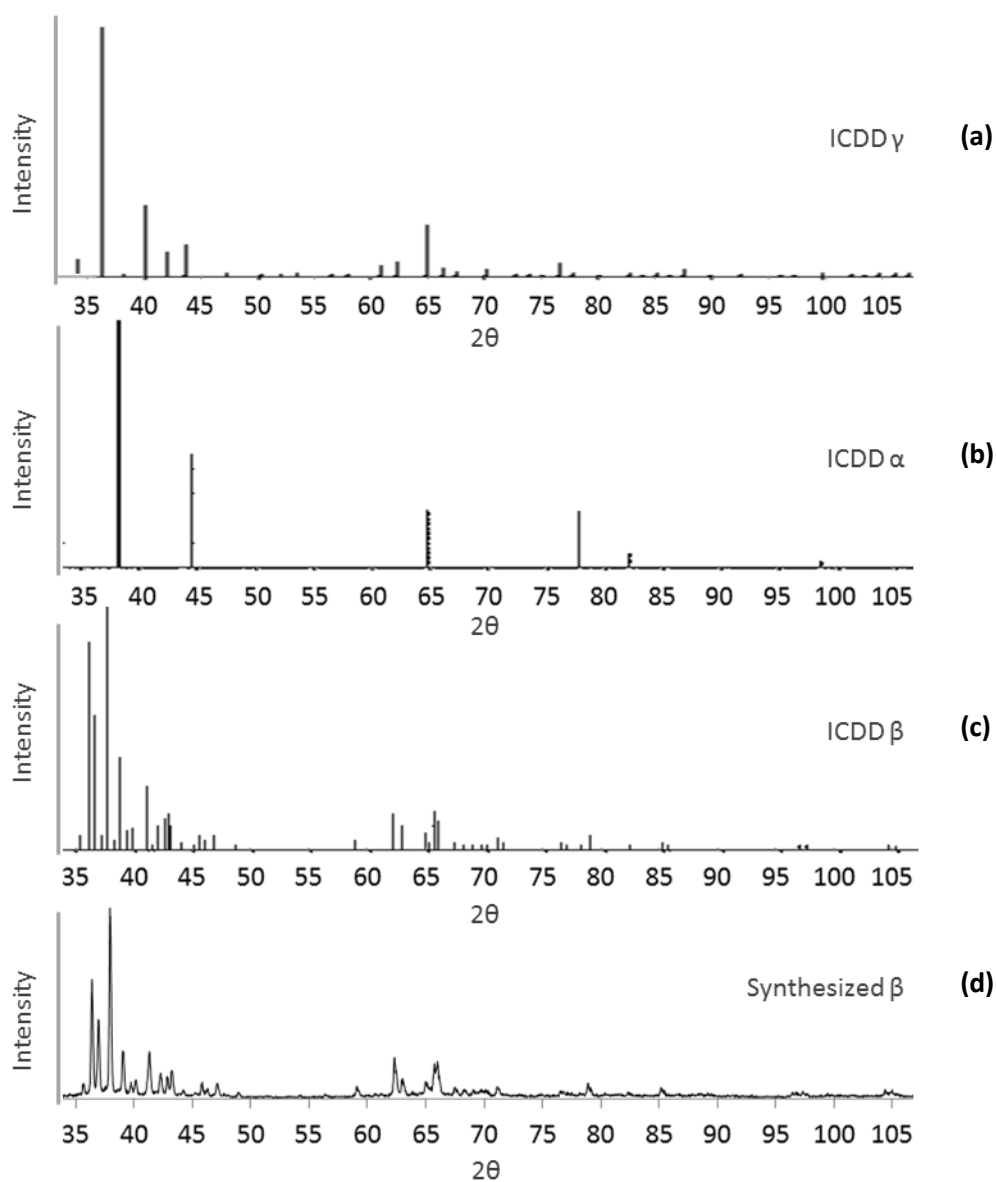


Figure A.1 XRD PDFs for (a) γ -phase (b) α -phase and (c) β -phase and the (d) diffraction pattern for synthesized β

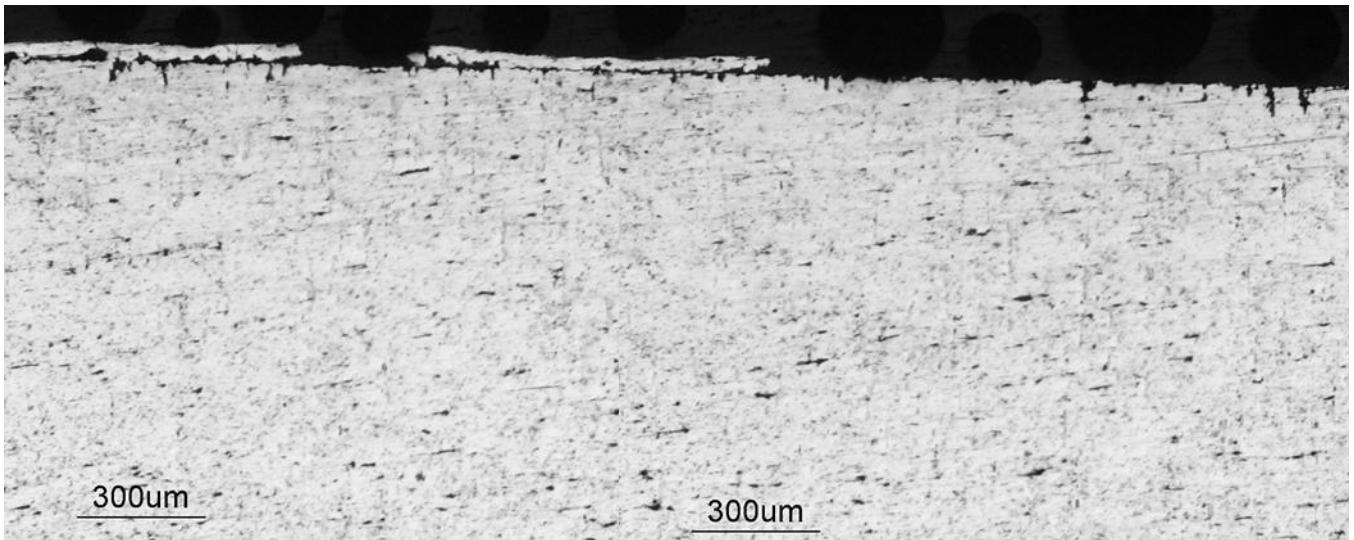
Note: The partial PDFs are modified from literature diffraction PDFs to show diffraction behavior from 35°-105° 2θ [Modified from 9, 37-38]

APPENDIX B: Damage Site Depth Distributions and Micrographs

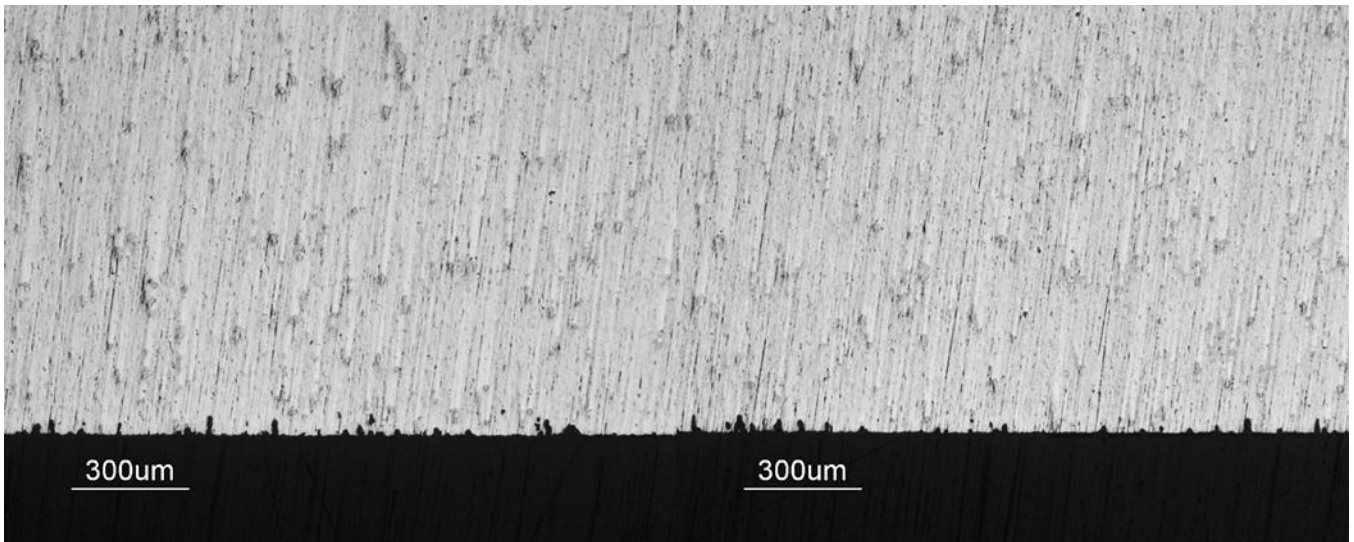
Table B.1 Damage site depth distribution data for AA5083 of varying sensitization conditions exposed to **nitric acid** for 24 hours at 35°C

Damage Site Depth (µm)	Number of Damage Sites*							
	SHTQ		100°C-7 Days		100°C-14 Days		100°C-30 Days	
	<i>L</i>	<i>T</i>	<i>L</i>	<i>T</i>	<i>L</i>	<i>T</i>	<i>L</i>	<i>T</i>
10	26	48	0	0	0	0	0	0
25	21	25	0	0	0	0	0	0
50	26	8	12	20	2	5	4	2
100	7	0	10	16	3	2	4	4
150	0	0	14	32	7	8	6	8
200	0	0	15	49	10	6	5	3
250	0	0	28	63	7	14	8	8
300	0	0	43	38	4	13	6	7
350	0	0	34	7	12	27	10	18
400	0	0	35	1	12	41	13	16
450	0	0	5	0	30	45	27	50
500	0	0	1	0	44	25	41	56
550	0	0	0	0	50	6	37	44
600	0	0	0	0	33	1	48	4
650	0	0	0	0	1	0	13	0
700	0	0	0	0	0	0	3	0

*Number of damage sites per ~0.34cm-long cross-section of exposed surface

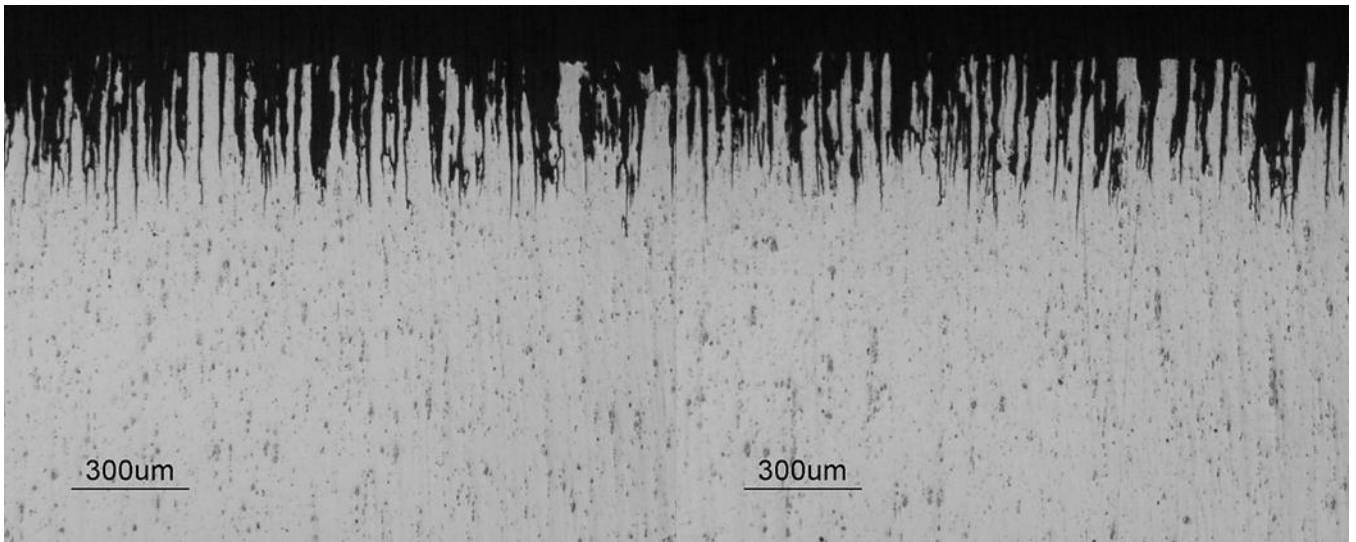


(a)

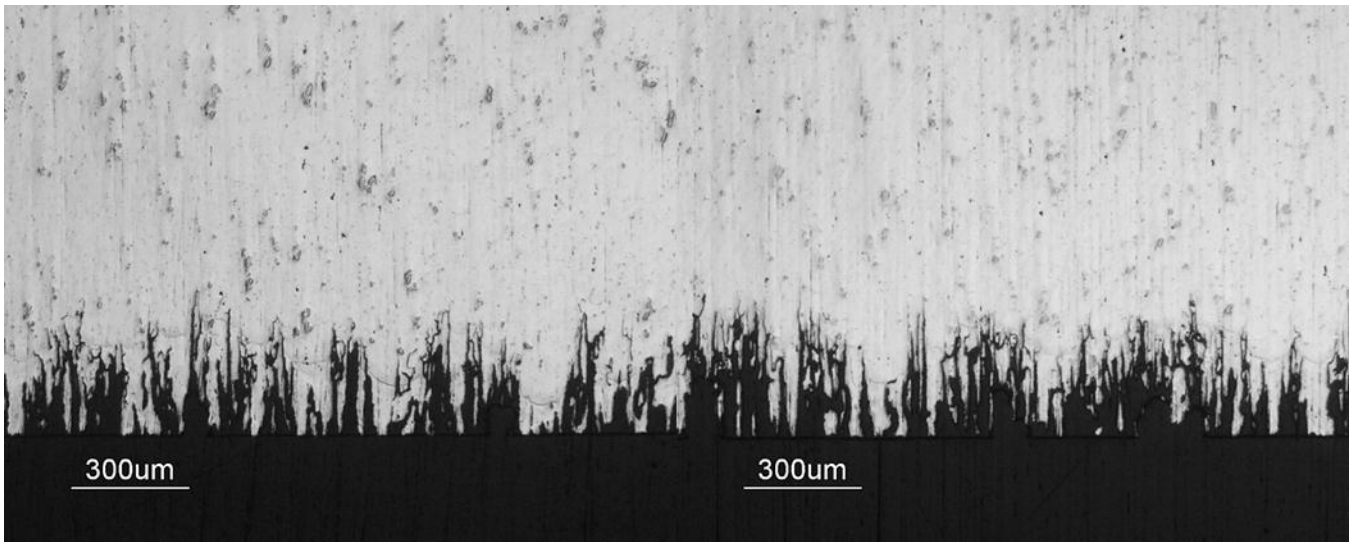


(b)

Figure B.1 Optical images of cross-sectioned AA5083 **SHTQ** samples showing damage penetration in the: (a) **L-direction** and (b) **T-direction** that were used to determine the number of damage sites and their depths after 24-hour exposure to **nitric acid** at 35°C

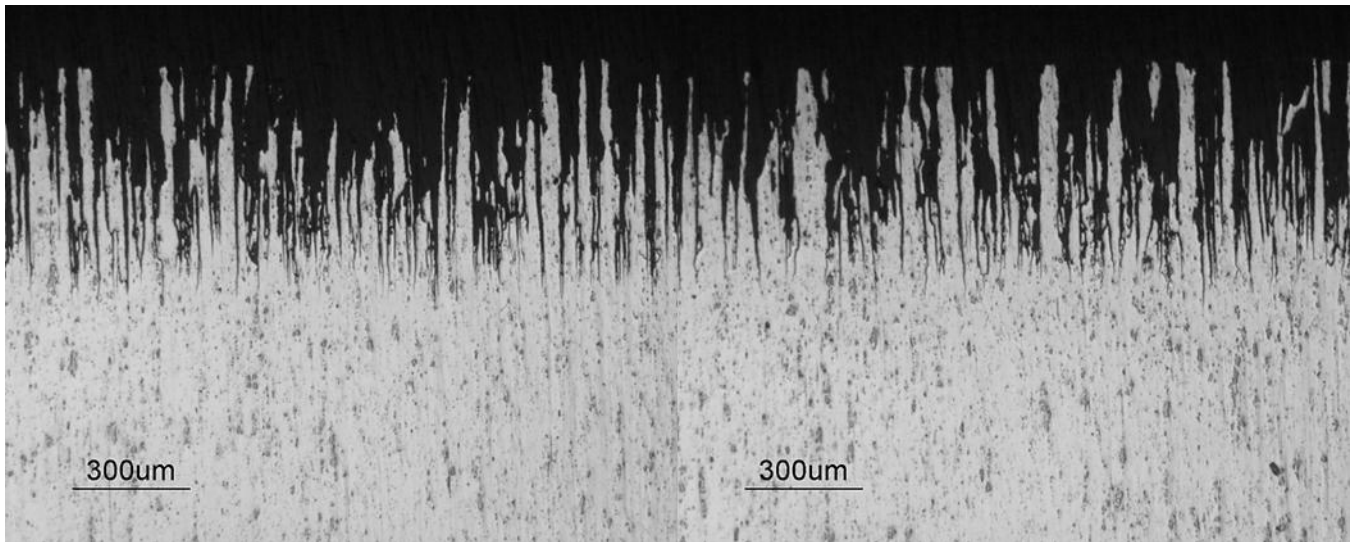


(a)

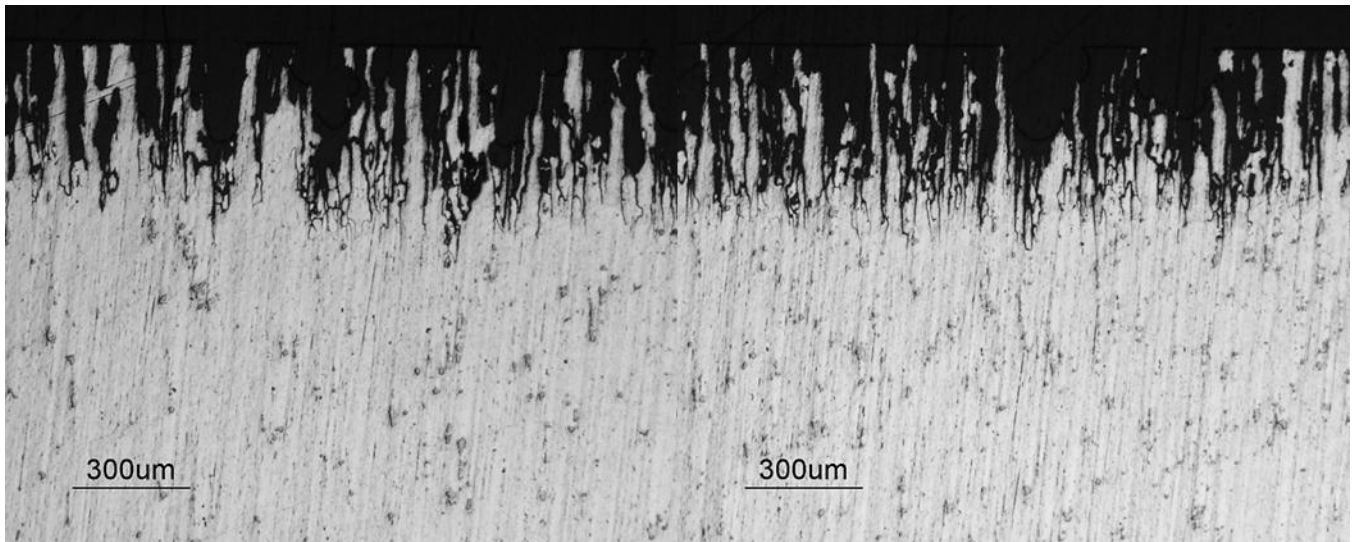


(b)

Figure B.2 Optical images of cross-sectioned AA5083 **100°C-7days** samples showing damage penetration in the: (a) **L-direction** and (b) **T-direction** that were used to determine the number of damage sites and their depths after 24-hour exposure to **nitric acid** at 35°C

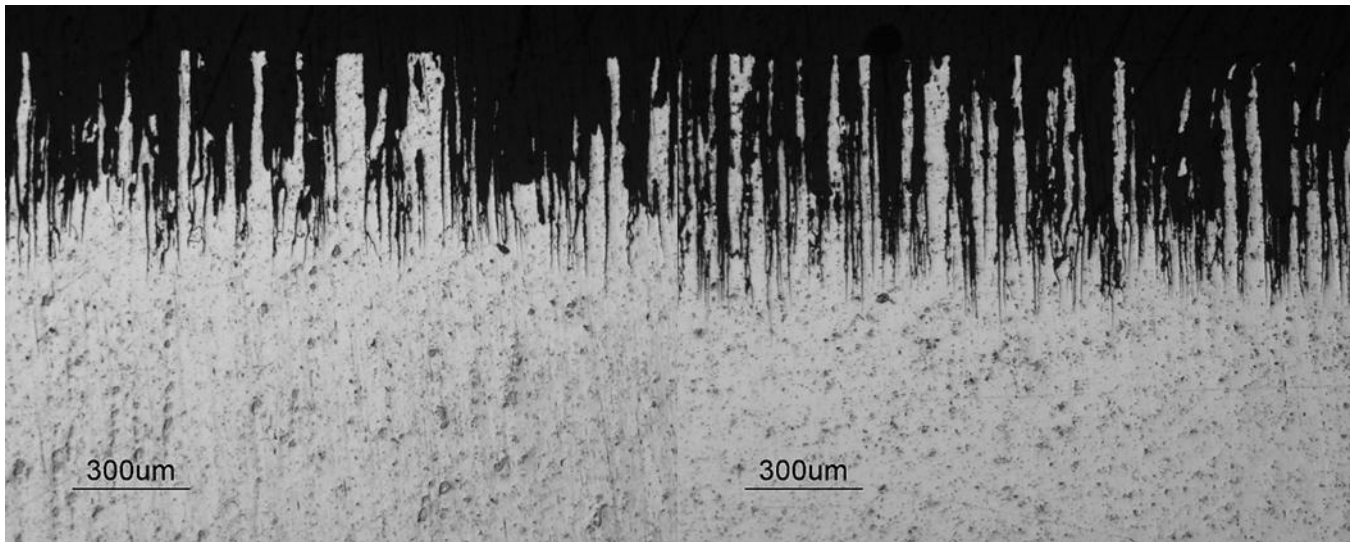


(a)

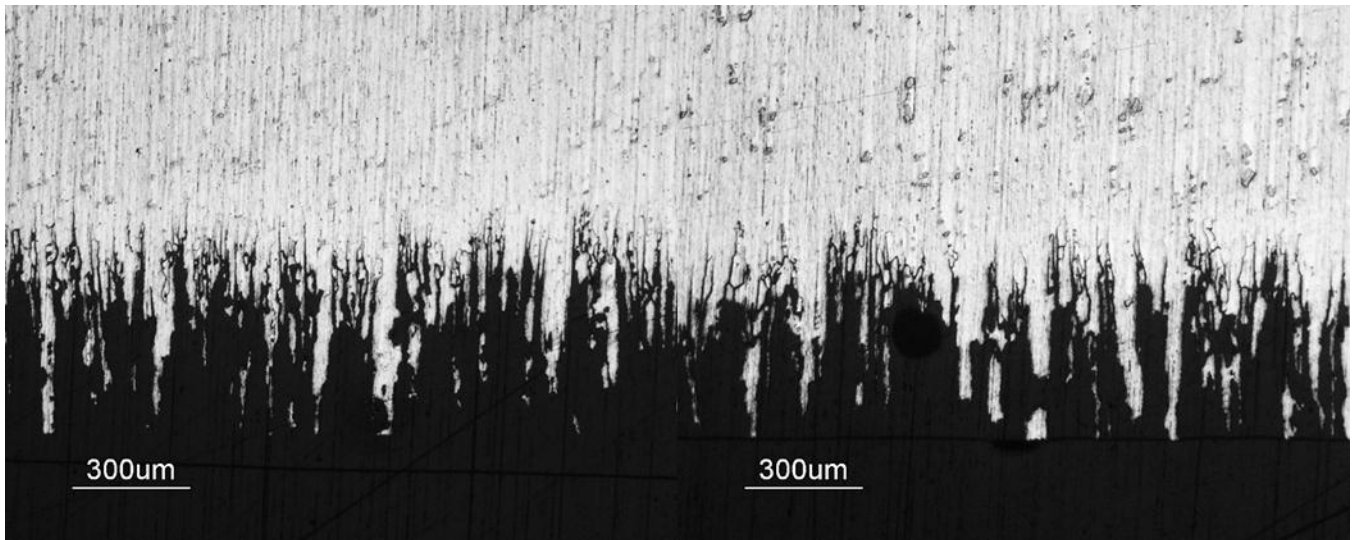


(b)

Figure B.3 Optical images of cross-sectioned AA5083 **100°C-14Days** samples showing damage penetration in the: (a) **L-direction** and (b) **T-direction** that were used to determine the number of damage sites and their depths after 24-hour exposure to **nitric acid** at 35°C



(a)



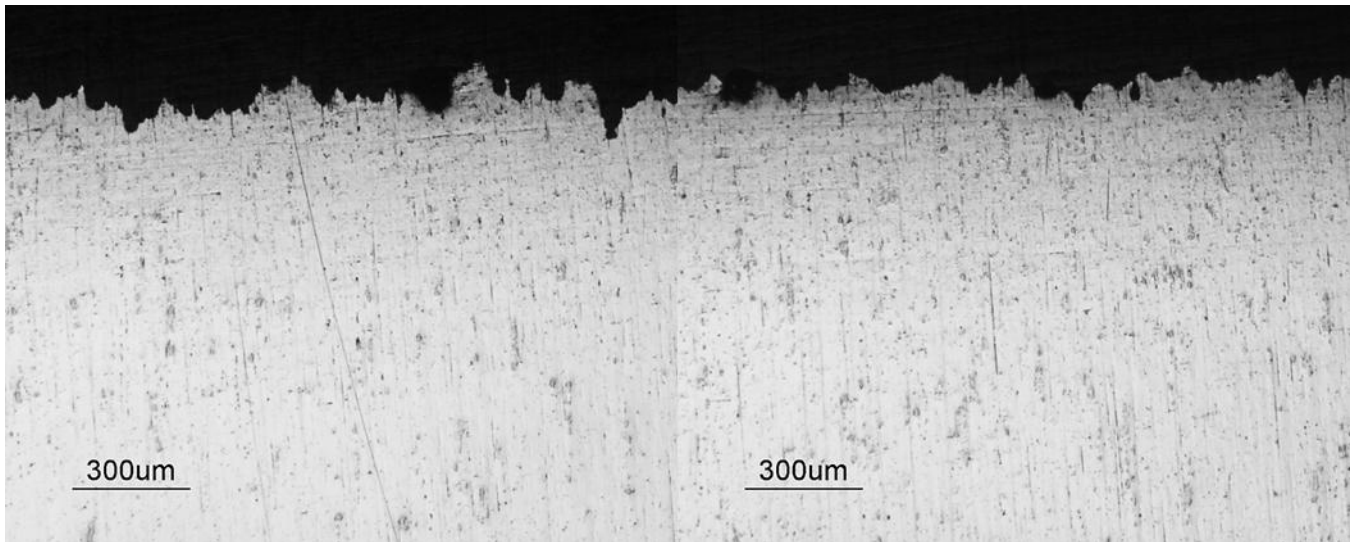
(b)

Figure B.4 Optical images of cross-sectioned AA5083 **100°C-30days** samples showing damage penetration in the: (a) **L-direction** and (b) **T-direction** that were used to determine the number of damage sites and their depths after 24-hour exposure to **nitric acid** at 35°C

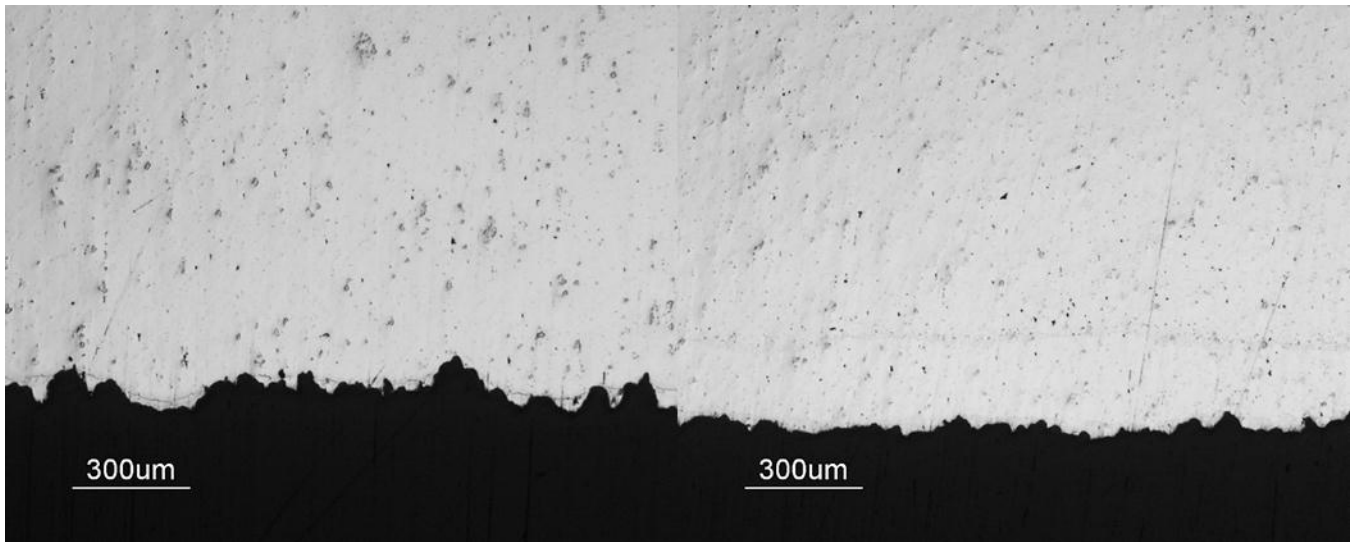
Table B.2 Damage site depth distribution data for AA5083 of varying sensitization conditions exposed to **phosphoric acid** for 24 hours at 35°C

Damage Site Depth (µm)	Number of Damage Sites*							
	SHTQ		100°C-7 Days		100°C-14 Days		100°C-30 Days	
	<i>L</i>	<i>T</i>	<i>L</i>	<i>T</i>	<i>L</i>	<i>T</i>	<i>L</i>	<i>T</i>
10	0	0	0	0	0	0	0	0
25	0	28	0	0	0	0	0	0
50	24	36	5	5	3	3	6	1
100	26	15	12	18	10	15	9	2
150	11	2	37	83	77	62	31	8
200	2	0	53	29	58	27	112	26
250	0	0	19	0	3	3	18	54
300	0	0	7	0	0	0	0	40
350	0	0	0	0	0	0	0	9
400	0	0	0	0	0	0	0	0
450	0	0	0	0	0	0	0	0
500	0	0	0	0	0	0	0	0
550	0	0	0	0	0	0	0	0
600	0	0	0	0	0	0	0	0
650	0	0	0	0	0	0	0	0
700	0	0	0	0	0	0	0	0

**Number of damage sites per ~0.34cm-long cross-section of exposed surface*

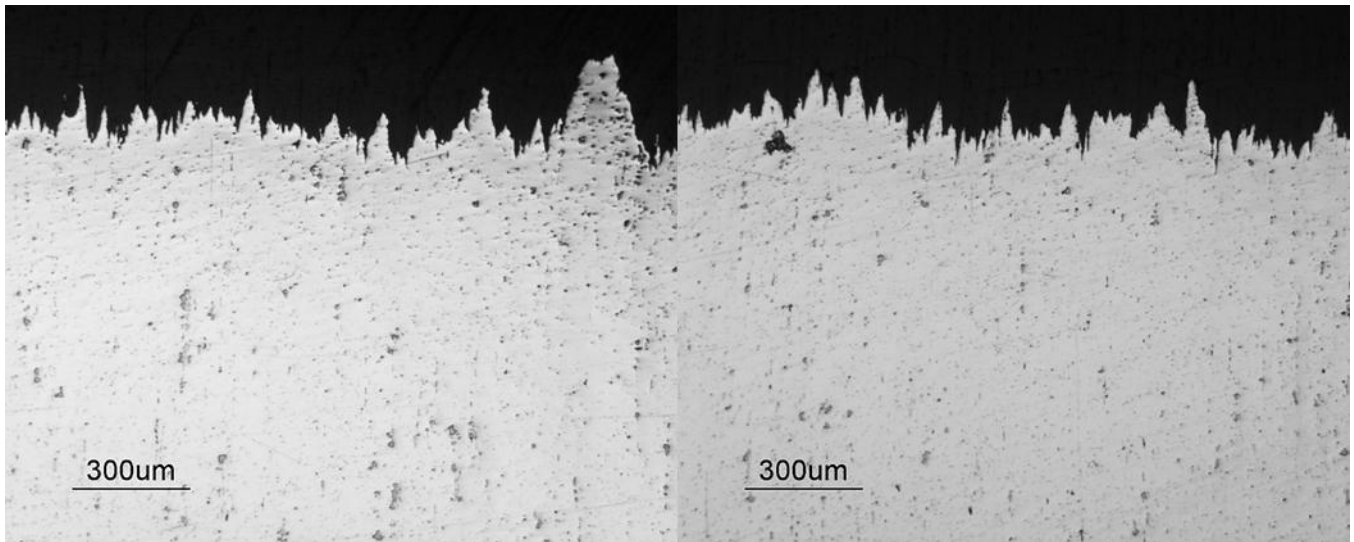


(a)

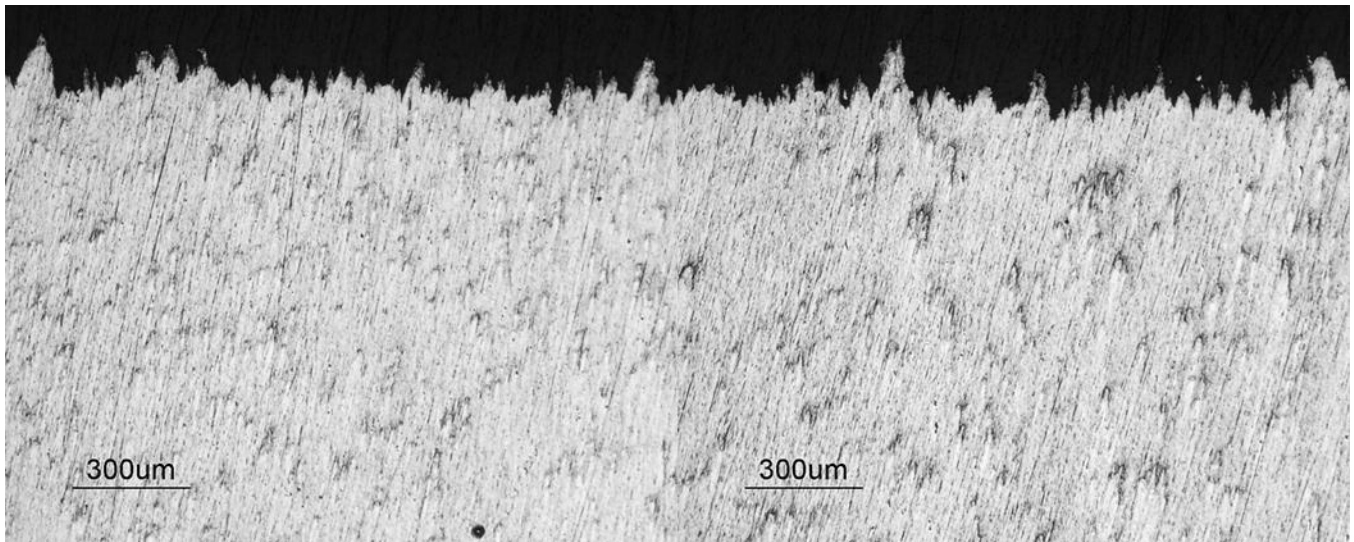


(b)

Figure B.5 Optical images of cross-sectioned AA5083 **SHTQ** samples showing damage penetration in the: (a) **L-direction** and (b) **T-direction** that were used to determine the number of damage sites and their depths after 24-hour exposure to **phosphoric acid** at 35°C

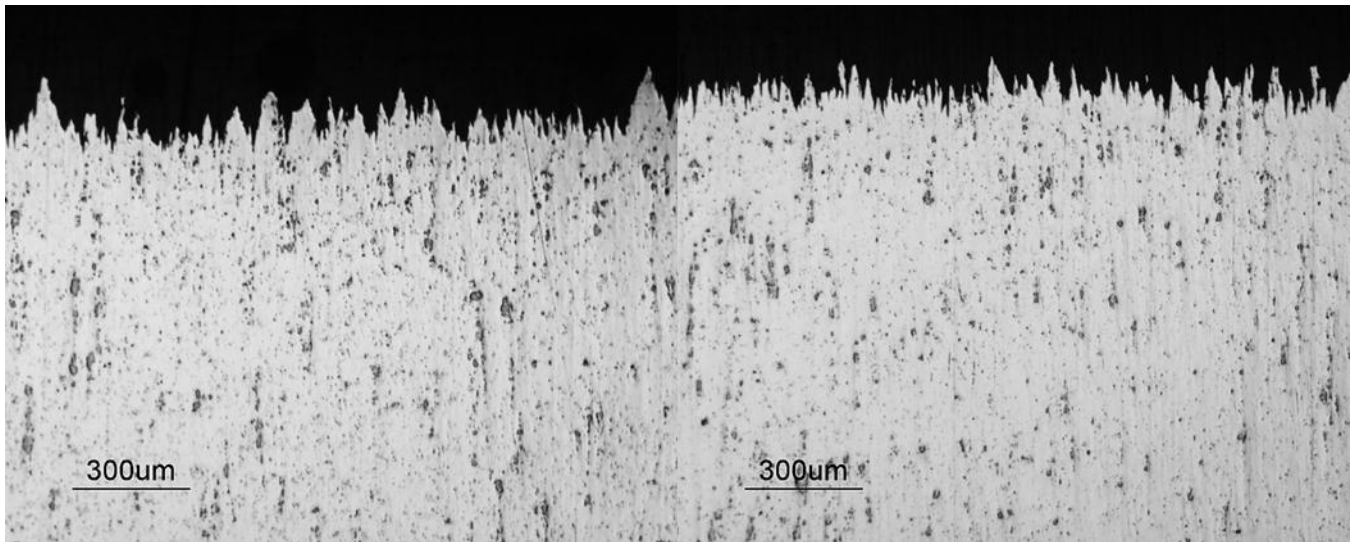


(a)

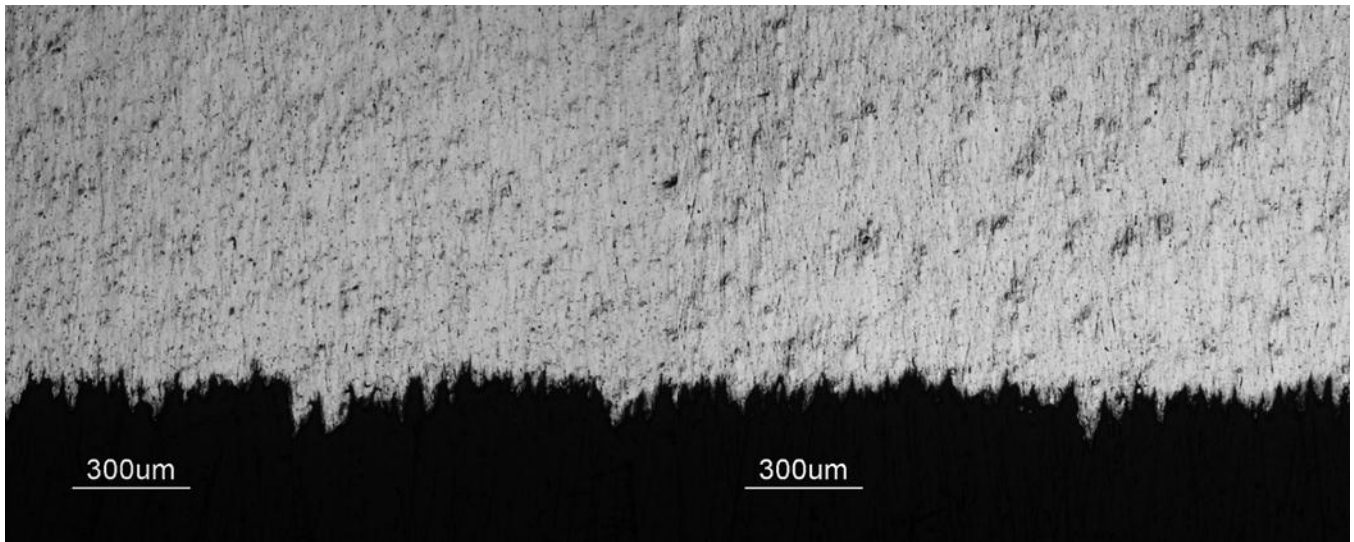


(b)

Figure B.6 Optical images of cross-sectioned AA5083 **100°C-7days** samples showing damage penetration in the: (a) **L-direction** and (b) **T-direction** that were used to determine the number of damage sites and their depths after 24-hour exposure to **phosphoric acid** at 35°C

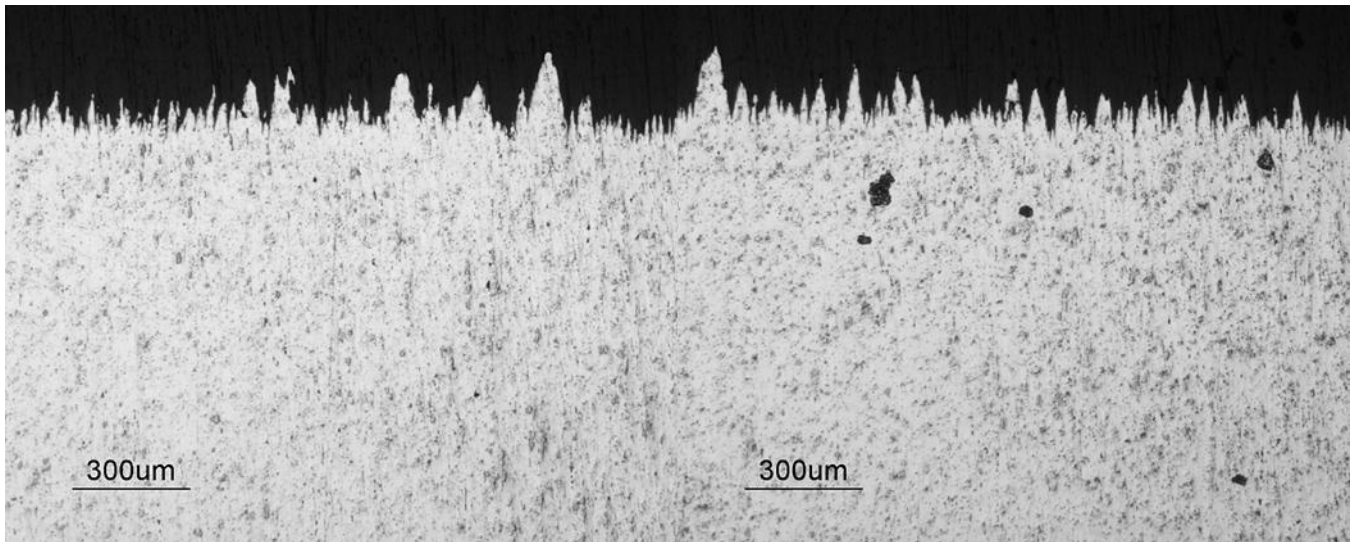


(a)

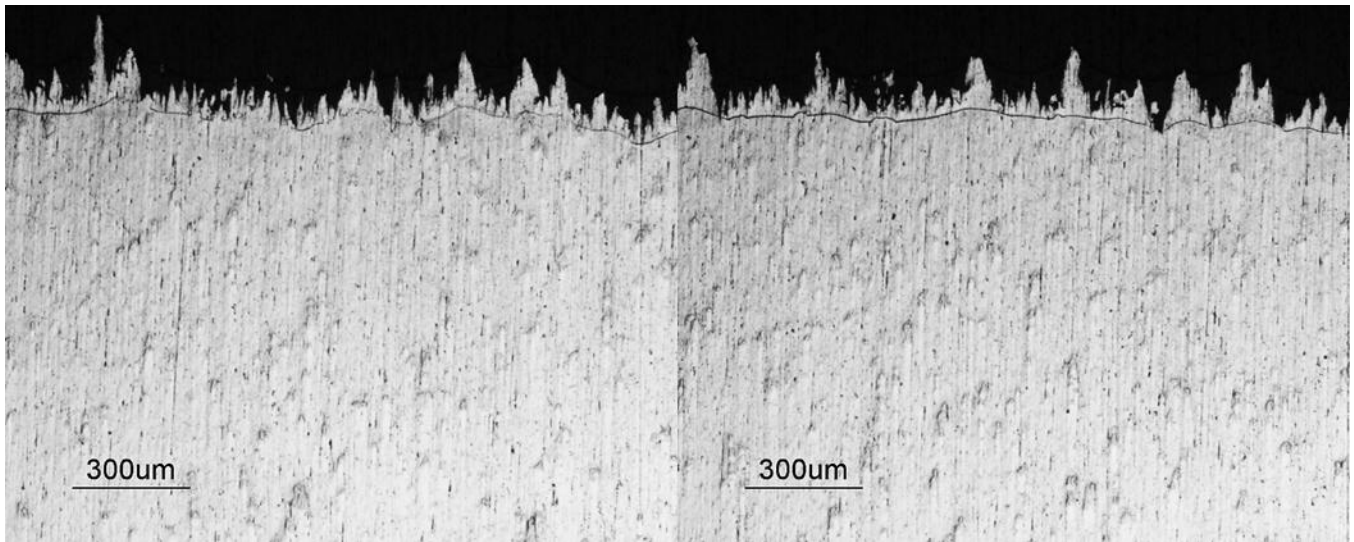


(b)

Figure B.7 Optical images of cross-sectioned AA5083 **100°C-14Days** samples showing damage penetration in the: (a) **L-direction** and (b) **T-direction** that were used to determine the number of damage sites and their depths after 24-hour exposure to **phosphoric acid** at 35°C



(a)



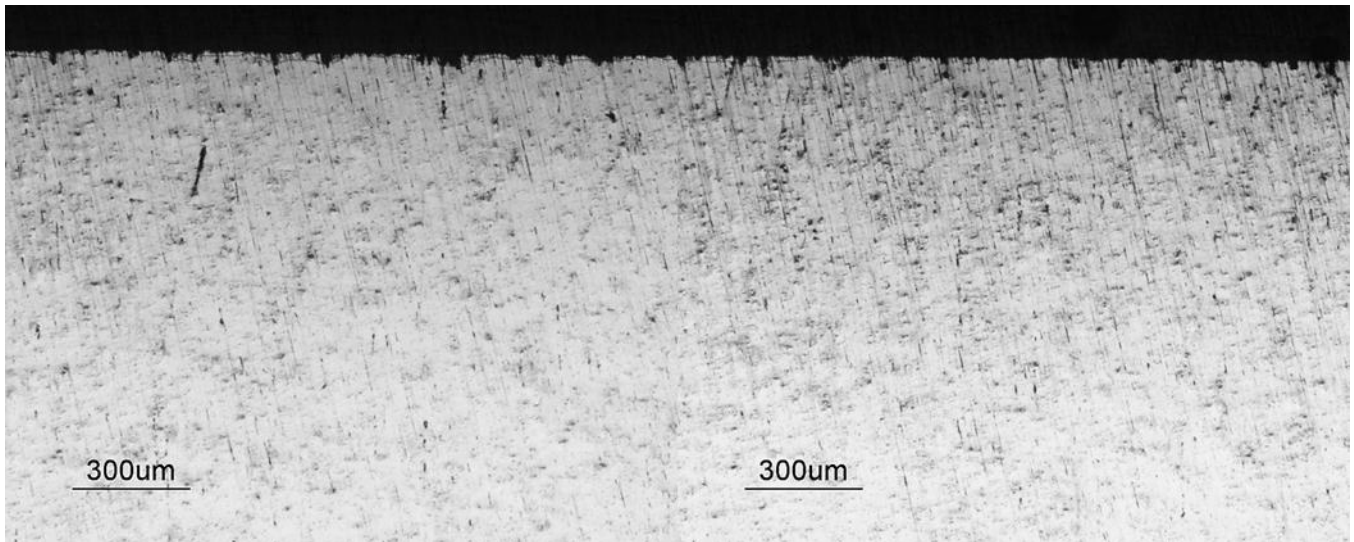
(b)

Figure B.8 Optical images of cross-sectioned AA5083 **100°C-30days** samples showing damage penetration in the: (a) **L-direction** and (b) **T-direction** that were used to determine the number of damage sites and their depths after 24-hour exposure to **phosphoric acid** at 35°C

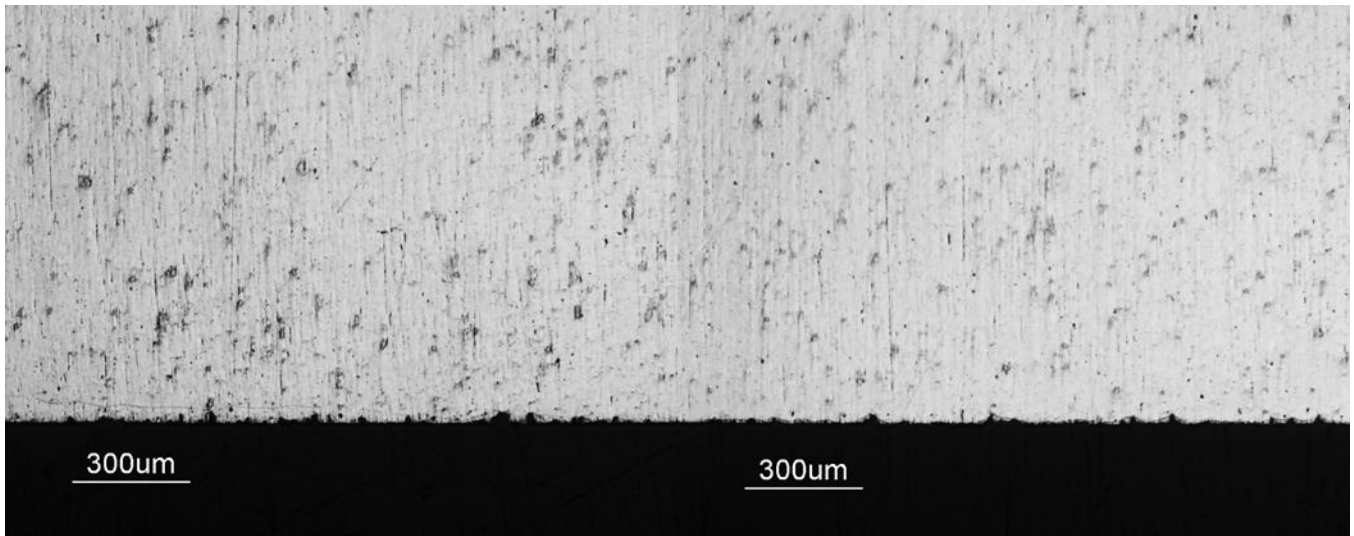
Table B.3 Damage site depth distribution data for AA5083 of varying sensitization conditions exposed to **ammonium persulfate** for 24 hours at 35°C

Damage Site Depth (µm)	Number of Damage Sites*							
	SHTQ		100°C-7 Days		100°C-14 Days		100°C-30 Days	
	<i>L</i>	<i>T</i>	<i>L</i>	<i>T</i>	<i>L</i>	<i>T</i>	<i>L</i>	<i>T</i>
10	60	74	0	0	0	0	0	0
25	30	24	0	0	0	0	0	0
50	1	0	25	45	26	16	17	10
100	0	0	21	51	12	14	7	6
150	0	0	47	47	32	38	17	16
200	0	0	38	21	26	35	8	10
250	0	0	29	13	33	46	29	20
300	0	0	16	3	36	39	24	25
350	0	0	0	0	39	26	33	40
400	0	0	0	0	28	13	43	46
450	0	0	0	0	10	2	41	39
500	0	0	0	0	1	2	20	20
550	0	0	0	0	0	0	5	2
600	0	0	0	0	0	0	1	0
650	0	0	0	0	0	0	0	0
700	0	0	0	0	0	0	0	0

**Number of damage sites per ~0.34cm-long cross-section of exposed surface*

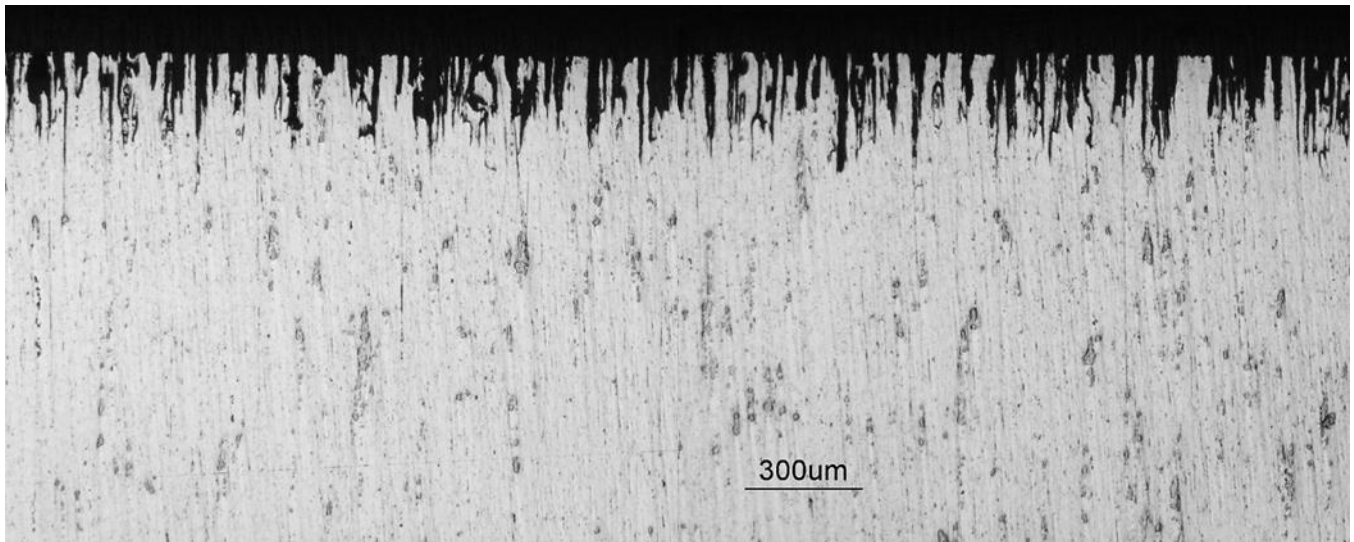


(a)

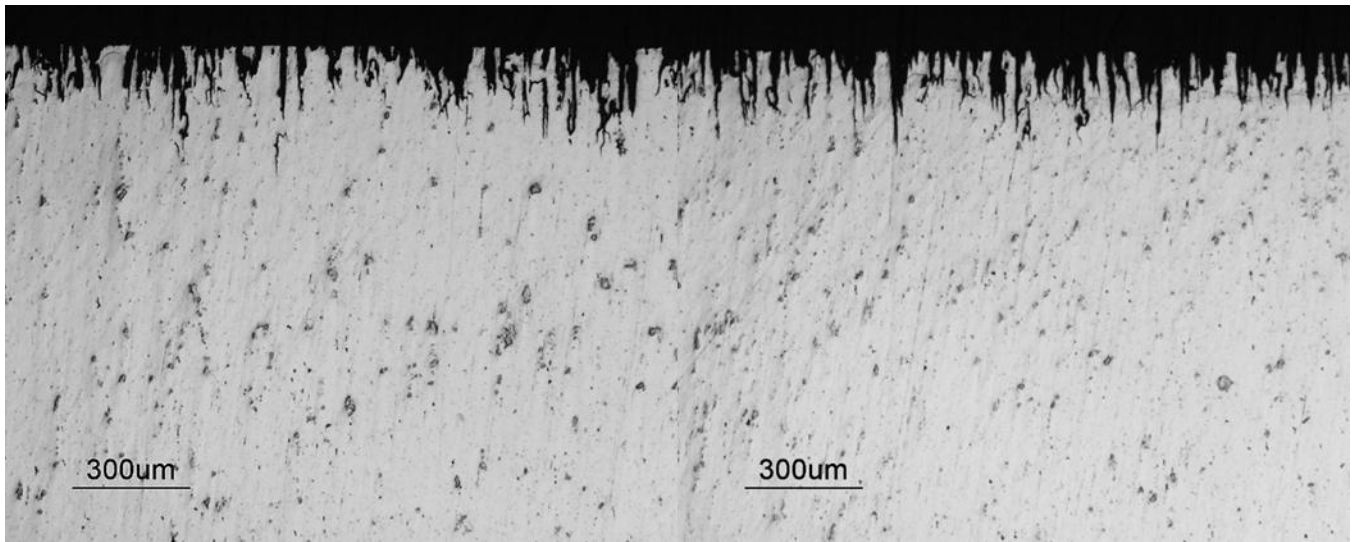


(b)

Figure B.9 Optical images of cross-sectioned AA5083 **SHTQ** samples showing damage penetration in the: (a) **L-direction** and (b) **T-direction** that were used to determine the number of damage sites and their depths after 24-hour exposure to **ammonium persulfate** at 35°C

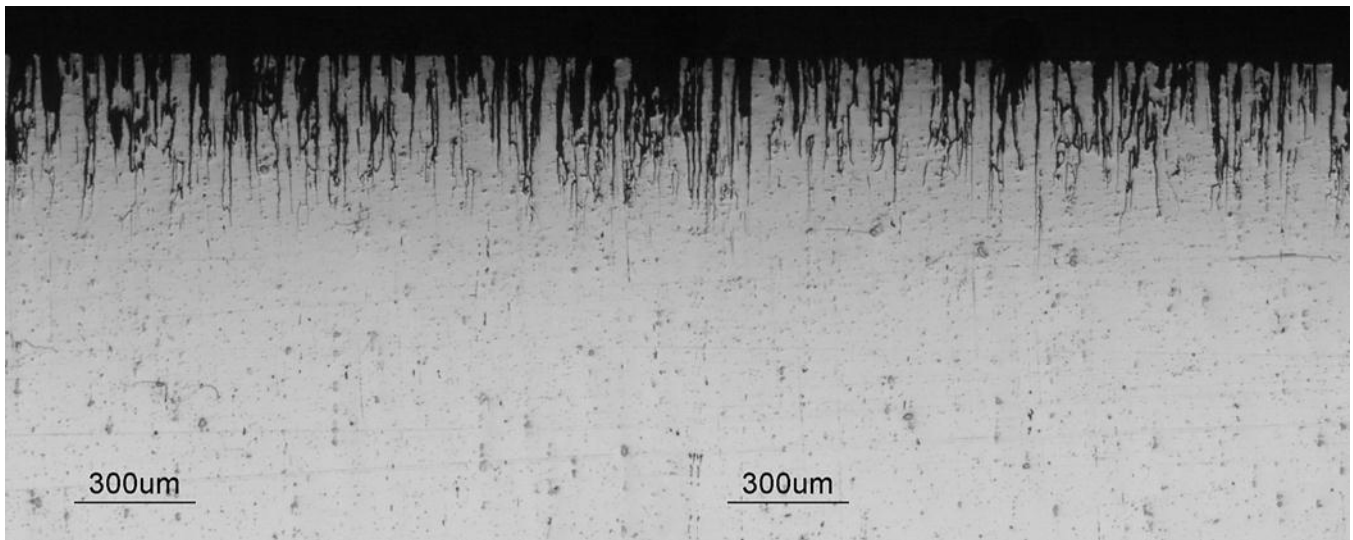


(a)

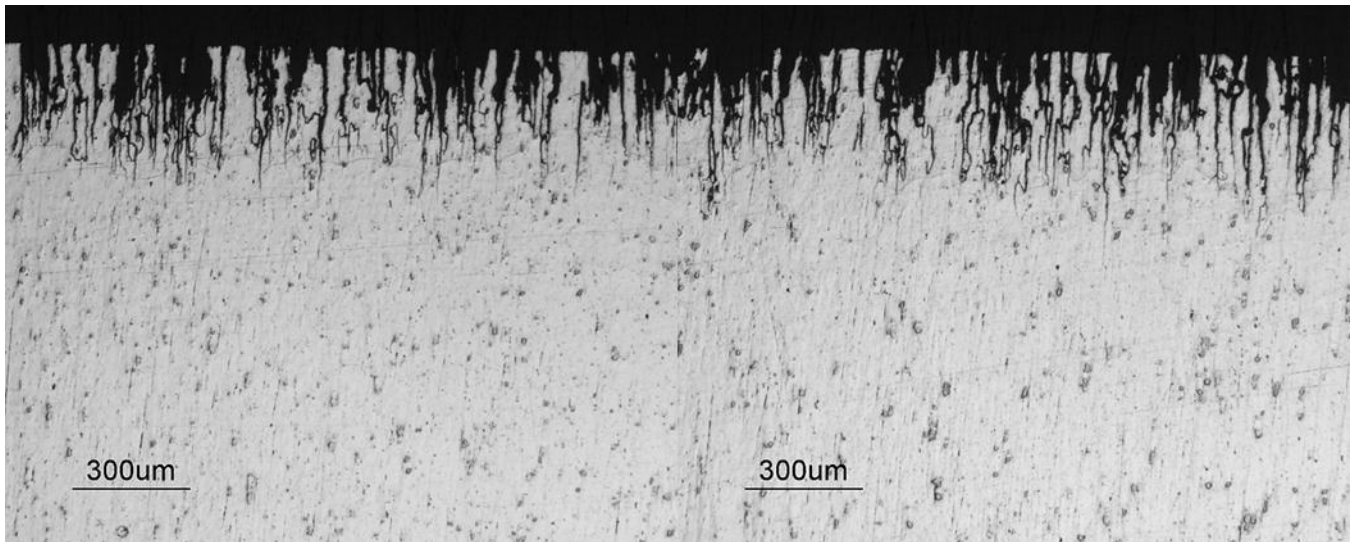


(b)

Figure B.10 Optical images of cross-sectioned AA5083 **100°C-7days** samples showing damage penetration in the: a) **L-direction** and (b) **T-direction** that were used to determine the number of damage sites and their depths after 24-hour exposure to **ammonium persulfate** at 35°C

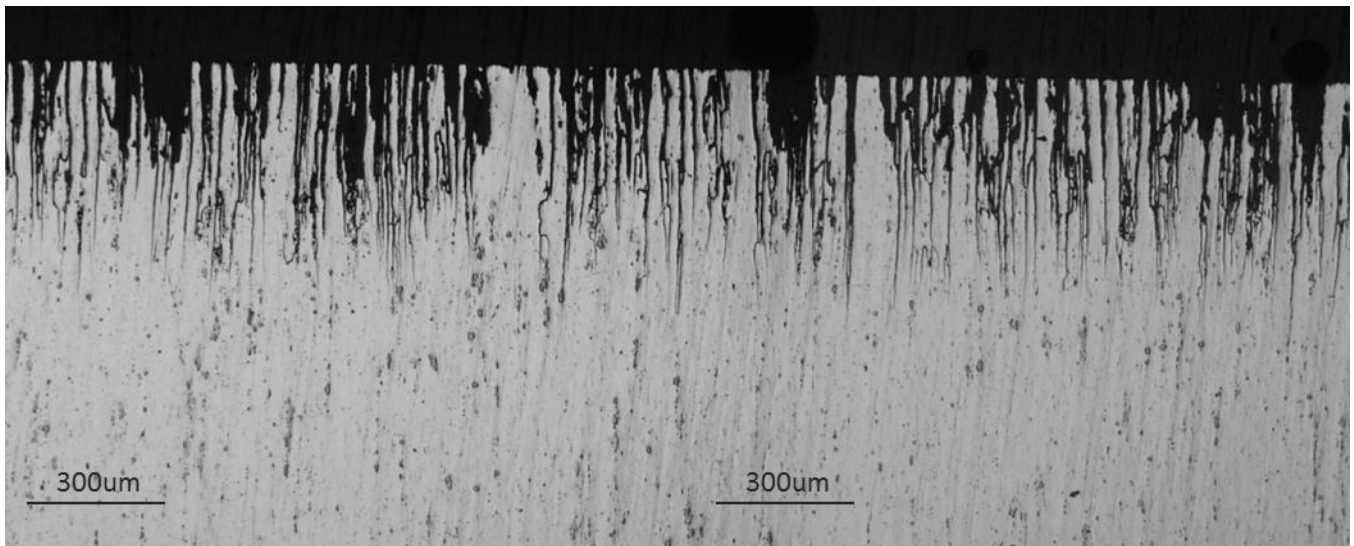


(a)

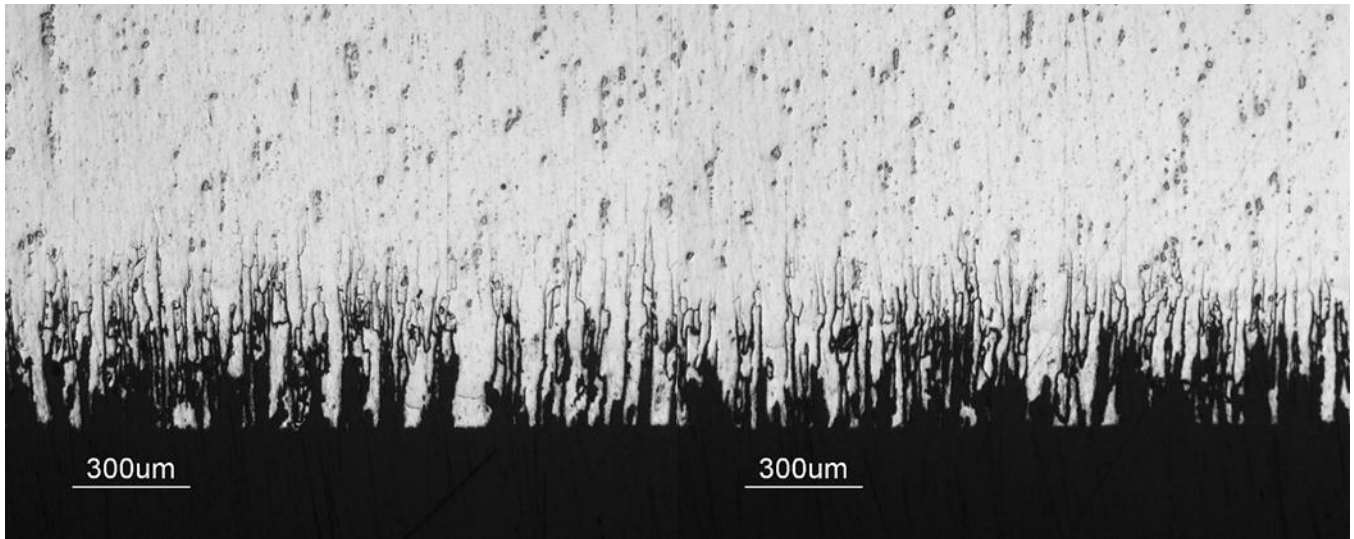


(b)

Figure B.11 Optical images of cross-sectioned AA5083 **100°C-14Days** samples showing damage penetration in the: (a) **L-direction** and (b) **T-direction** that were used to determine the number of damage sites and their depths after 24-hour exposure to **ammonium persulfate** at 35°C



(a)



(b)

Figure B.12 Optical images of cross-sectioned AA5083 **100°C-30days** samples showing damage penetration in the: (a) **L-direction** and (b) **T-direction** that were used to determine the number of damage sites and their depths after 24-hour exposure to **ammonium persulfate** at 35°C

APPENDIX C: Anodic Polarization Scans in Etchants from 15°C-50°C

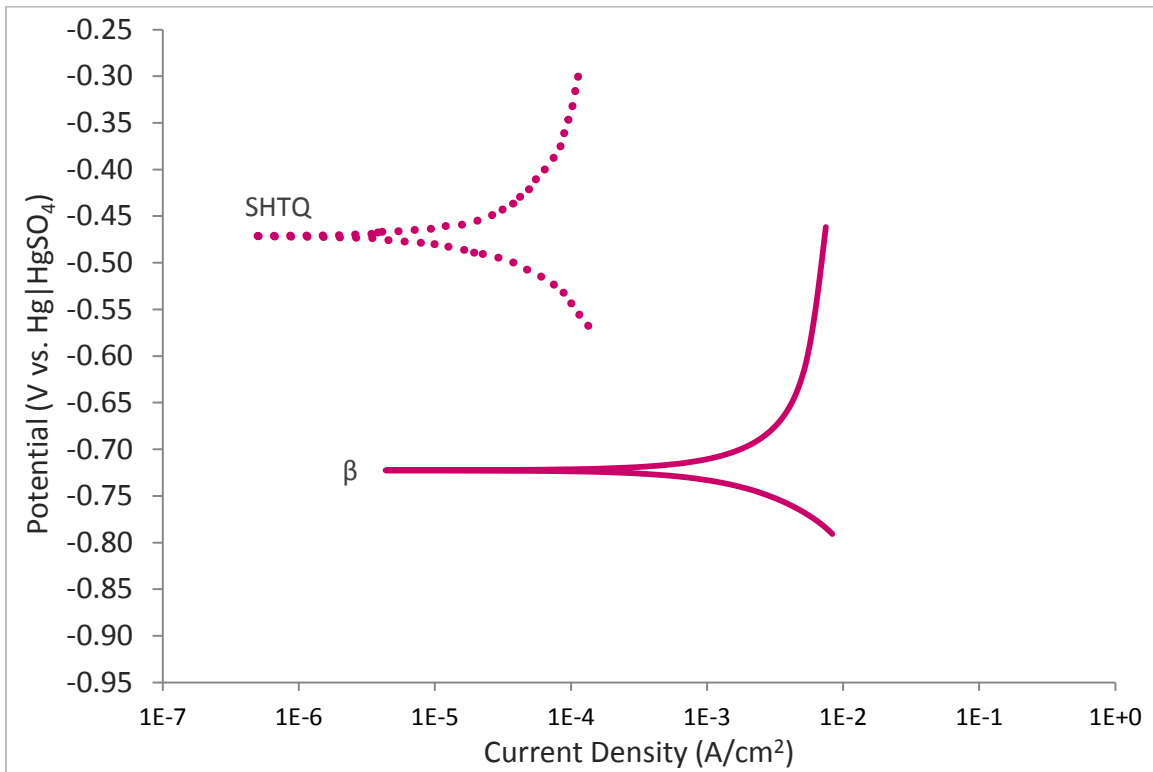


Figure C.1 Anodic polarization scans of AA5083-SHTQ and β -phase specimens in Nitric Acid at 15°C

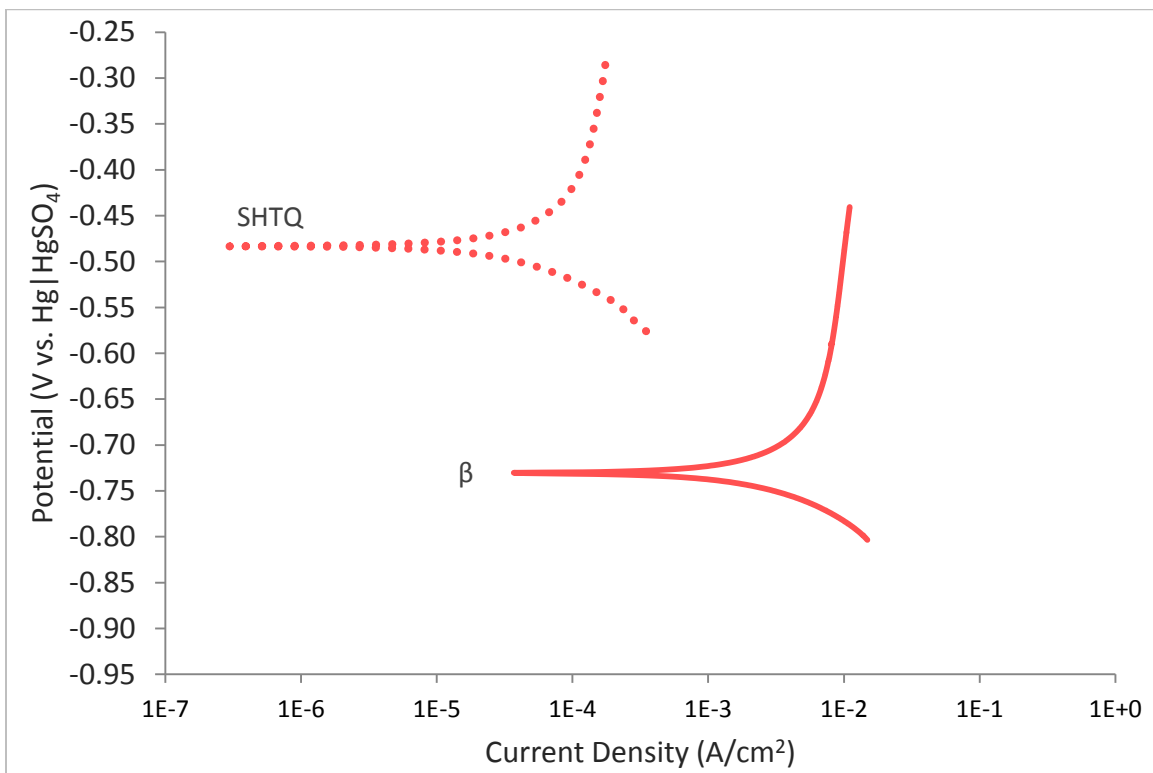


Figure C.2 Anodic polarization scans of AA5083-SHTQ and β -phase specimens in Nitric Acid at 22°C

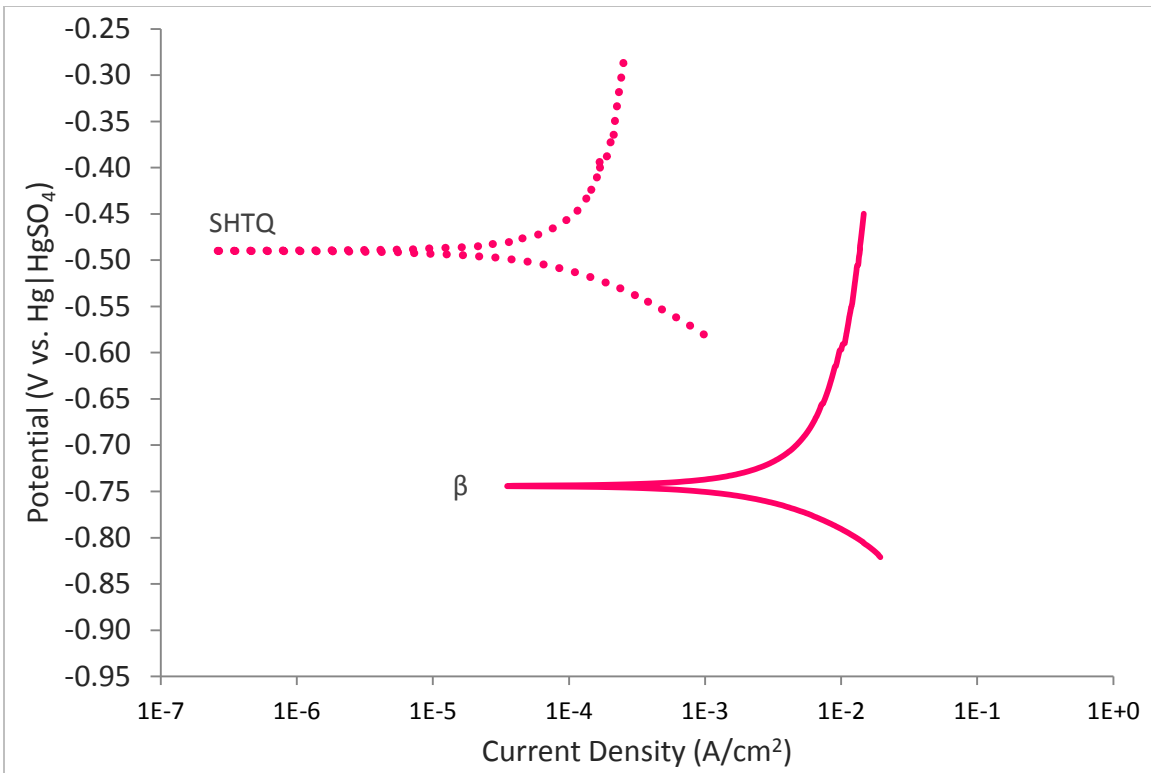


Figure C.3 Anodic polarization scans of AA5083-SHTQ and β-phase specimens in Nitric Acid at 30°C

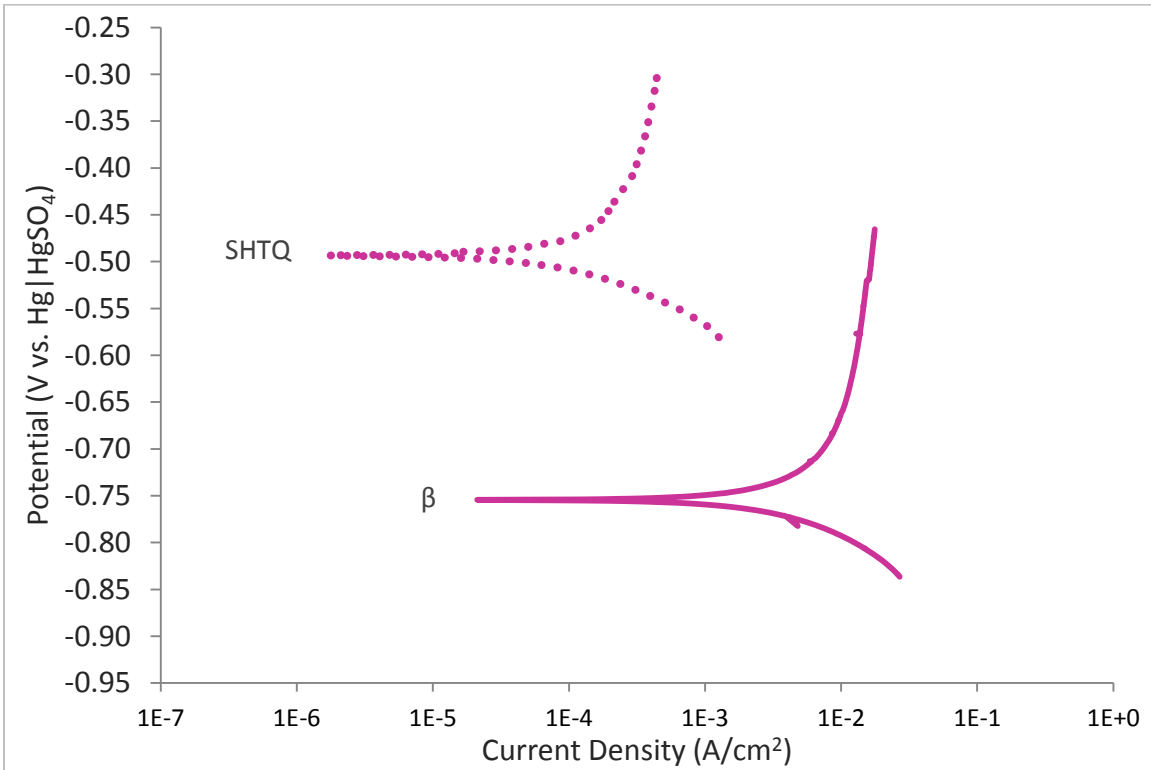


Figure C.4 Anodic polarization scans of AA5083-SHTQ and β-phase specimens in Nitric Acid at 35°C

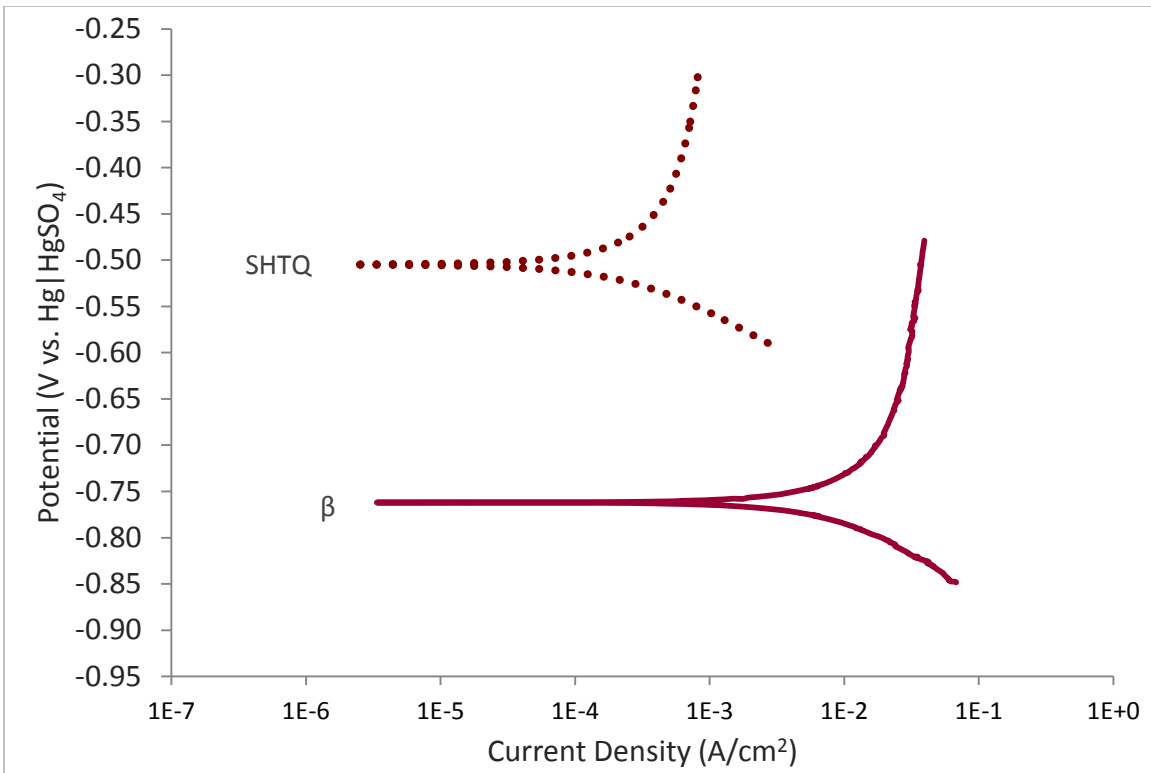


Figure C.5 Anodic polarization scans of AA5083-SHTQ and β -phase specimens in **Nitric Acid** at **50°C**

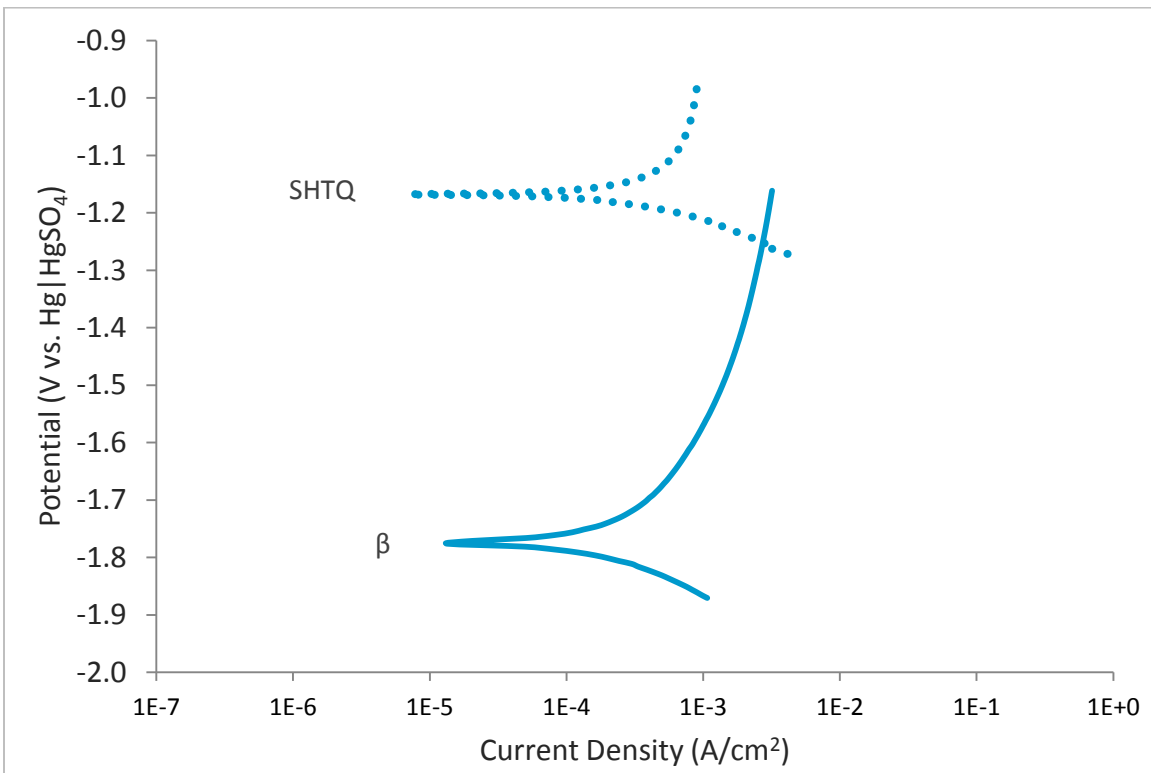


Figure C.6 Anodic polarization scans of AA5083-SHTQ and β -phase specimens in **Phosphoric Acid** at **15°C**

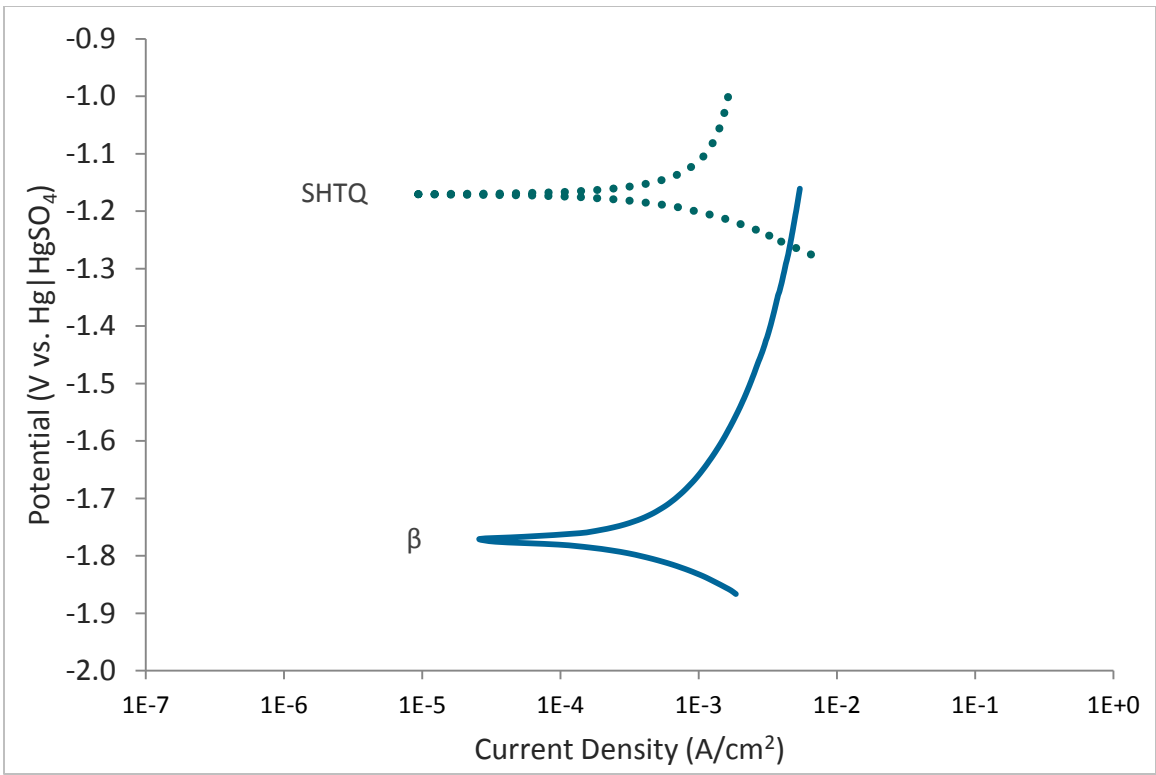


Figure C.7 Anodic polarization scans of AA5083-SHTQ and β -phase specimens in **Phosphoric Acid** at **22°C**

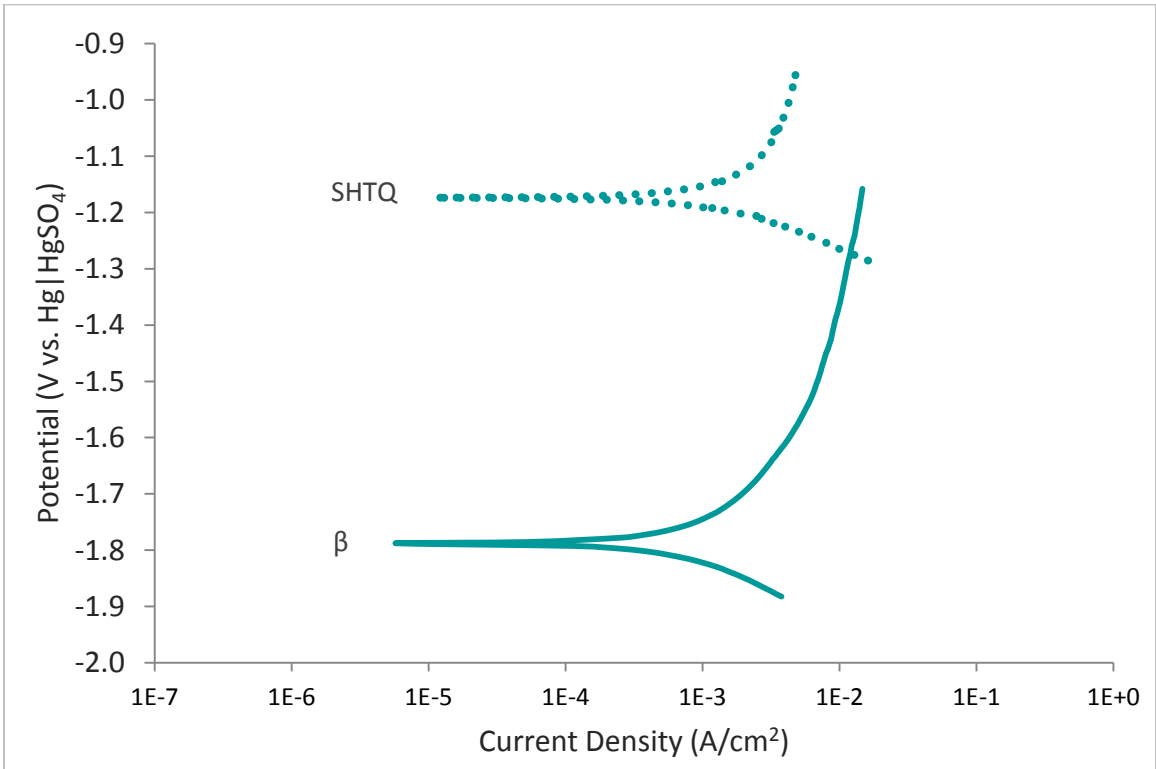


Figure C.8 Anodic polarization scans of AA5083-SHTQ and β -phase specimens in **Phosphoric Acid** at **35°C**

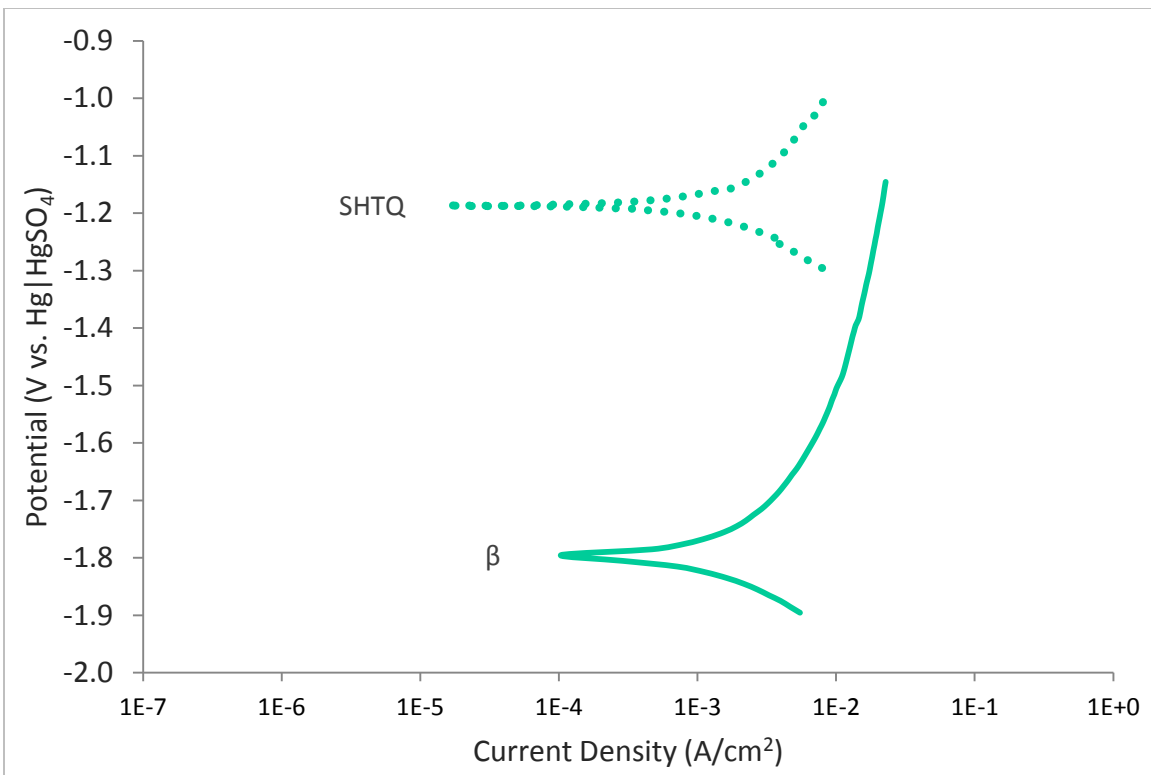


Figure C.9 Anodic polarization scans of AA5083-SHTQ and β-phase specimens in **Phosphoric Acid** at **50°C**

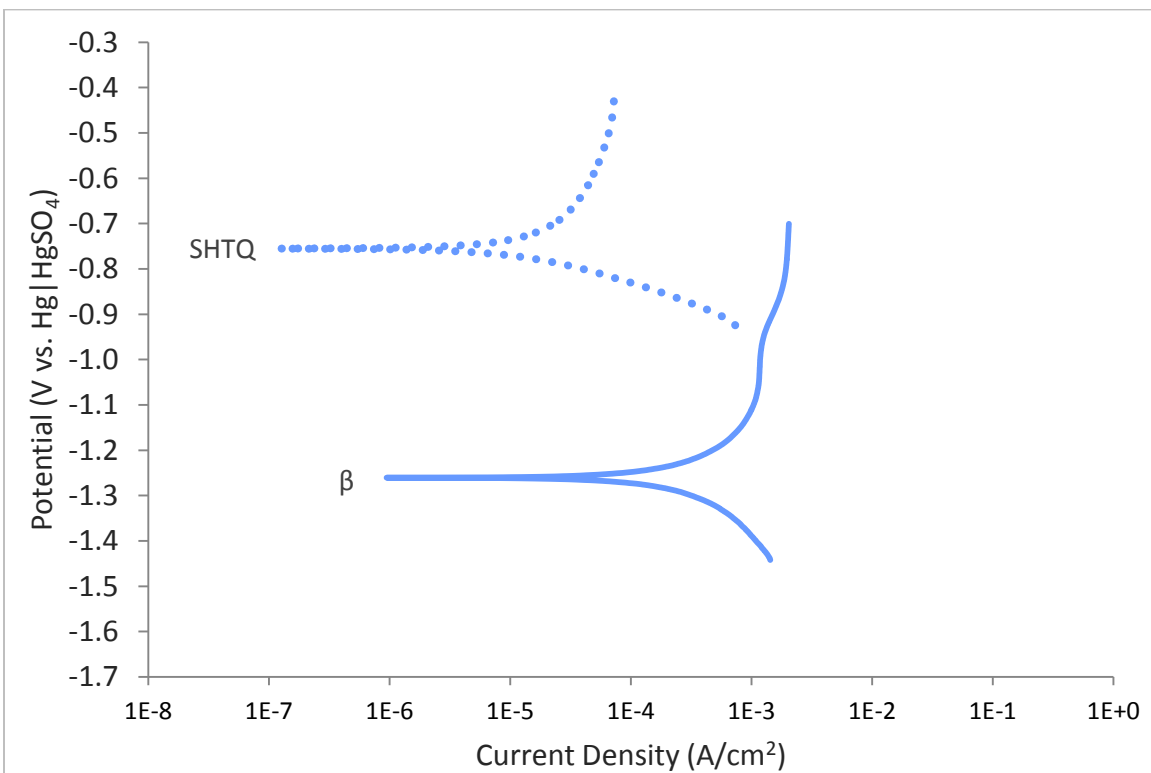


Figure C.10 Anodic polarization scans of AA5083-SHTQ and β-phase specimens in **pH 1.2 Ammonium Persulfate** at **15°C**

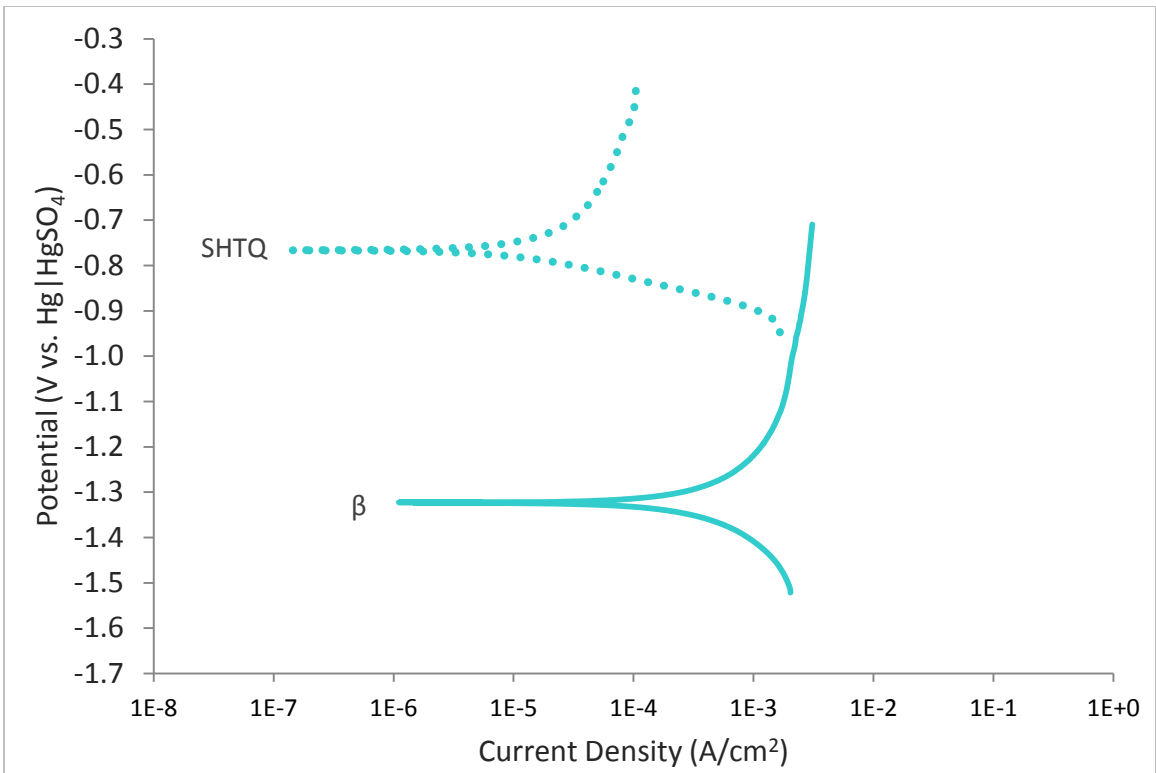


Figure C.11 Anodic polarization scans of AA5083-SHTQ and β -phase specimens in **pH 1.2 Ammonium Persulfate** at **22°C**

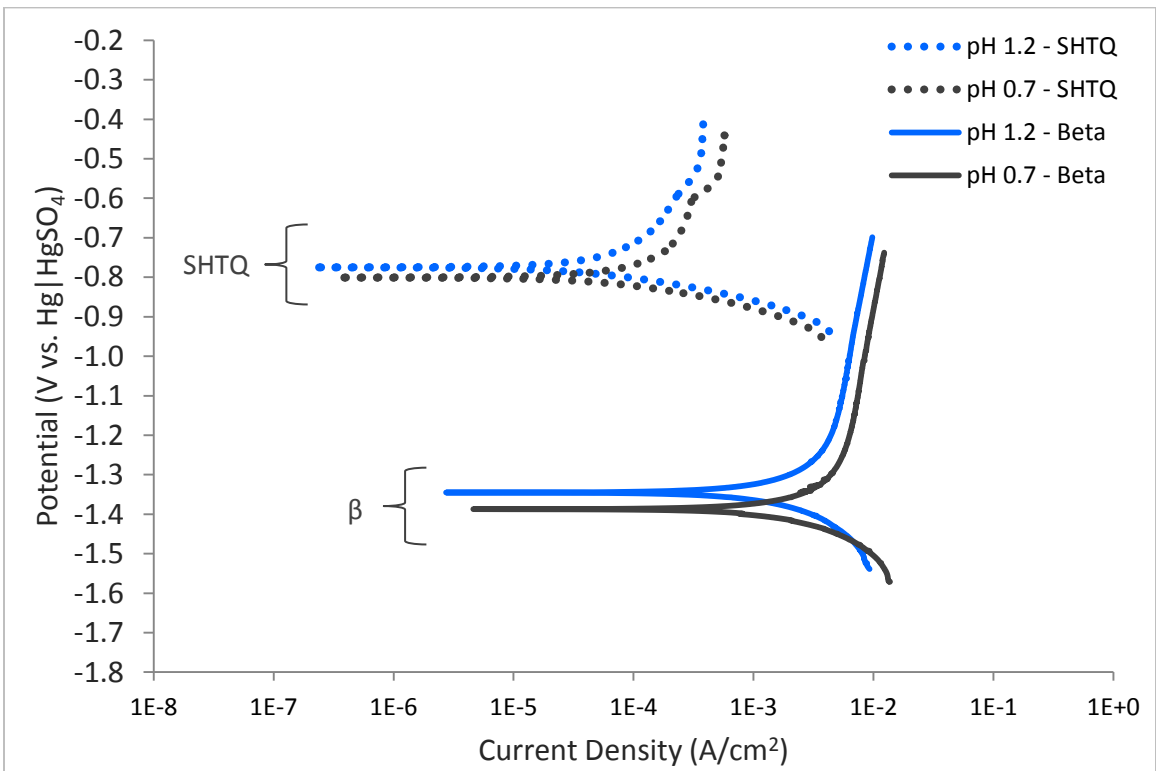


Figure C.12 Anodic polarization scans of AA5083-SHTQ and β -phase specimens in **pH 1.2 and pH 0.7 Ammonium Persulfate** at **35°C**

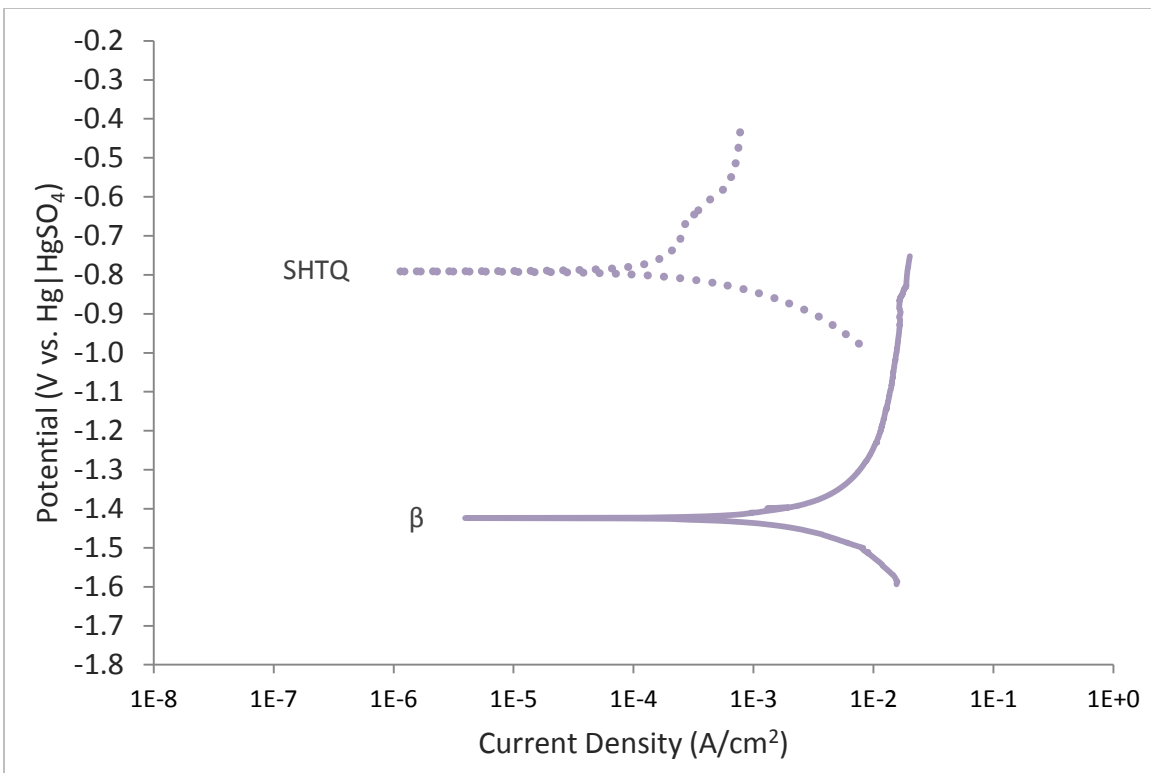


Figure C.13 Anodic polarization scans of AA5083-SHTQ and β -phase specimens in **pH 1.2 Ammonium Persulfate** at **50°C**

APPENDIX D: Summary and Ranking of Etchant Selectivity

Table D.1 Summary of results from short-term, OCP etching tests and characterization of etchant selectivity

OCP Etching from 22°C-35°C			
Etchant	Grain boundary etching	Etch clarity	Etchant selectivity (rank: 1 = highest)
Nitric Acid	<ul style="list-style-type: none"> * SHTQ specimens: un-etched * Sensitized specimens: etched * Time to etch: high temperature dependence 	Attack of matrix: moderate	Moderate to high selectivity (2)
Phosphoric Acid	<ul style="list-style-type: none"> * SHTQ specimens: un-etched * Sensitized specimens: etched * Time to etch: high temperature dependence 	Attack of matrix: moderate to high	Low to moderate selectivity (3)
Ammonium Persulfate (pH 1.2)	<ul style="list-style-type: none"> * SHTQ specimens: un-etched * Sensitized specimens: etched * Time to etch: mild temperature dependence, high surface finish dependence 	Attack of matrix: low to moderate	High selectivity (1)

Table D.2 Summary of results from 24-hr mass loss test and characterization of etchant selectivity

Mass Loss after 24-hr Etchant Exposure at 35°C				
Etchant	Mass loss	Incremental changes in mass loss	Dimension change	Etchant selectivity (rank: 1 = highest)
Nitric Acid	Intermediate	Mass loss increases with sensitization condition	Intermediate	High selectivity (2)
Phosphoric Acid	Highest	Mass loss increases with sensitization condition	Highest	Low selectivity (3)
Ammonium Persulfate (pH 0.7)	Lowest	Mass loss increases with sensitization condition	Lowest	High selectivity (1)

Table D.3 Summary of results from damage assessment following 24-hr mass loss test and characterization of etchant selectivity

Damage Assessment after 24-hr Etchant Exposure at 35°C				
Etchant	Number of damage sites	Damage site depth	Damage morphology	Etchant selectivity (rank: 1 = highest)
Nitric Acid	More damage sites with increasing sensitization condition	* Deeper damage sites with increasing sensitization condition * Highest average damage site depth	* Deep intergranular fissures * Low to moderate grain fallout	High selectivity (2)
Phosphoric Acid	More damage sites with increasing sensitization condition	* Deeper damage sites with increasing sensitization condition * Lowest average damage site depth	* Shallow to moderate damage depths * Less intergranular in appearance * High grain fallout	Low selectivity (3)
Ammonium Persulfate (pH 0.7)	More damage sites with increasing sensitization condition	* Deeper damage sites with increasing sensitization condition * Intermediate average damage depth	* Deep intergranular fissures * Low grain fallout	High selectivity (1)

Table D.4 Summary of results from species dissolution assessment following 24-hr mass loss test and characterization of etchant selectivity

Dissolution of Species after 24-hr Etchant Exposure at 35°C			
Etchant	Sum concentration of dissolved species	[Mg]:[Al]	Etchant selectivity (rank: 1 = highest)
Nitric Acid	* Total concentration increases from SHTQ to 100°C-30 Day specimens * Intermediate total concentration of dissolved species	* Low ratio of concentrations * Lower ratio for sensitized specimens than for unsensitized specimens ⁴²	Lower selectivity (3)
Phosphoric Acid	* Total concentration increases from SHTQ to 100°C-30 Day specimens * Highest total concentration of dissolved species	* Low ratio of concentrations * Lower ratio for sensitized specimens ⁴² than for unsensitized specimens	Lower selectivity (2)
Ammonium Persulfate (pH 0.7)	* Total concentration increases from SHTQ to 100°C-30 Day specimens * Lowest total concentration of dissolved species	* Highest ratio of concentrations * Higher ratio for sensitized specimens than for unsensitized specimens	High selectivity (1)

⁴² The ratio should increase for sensitized specimens since there would be Mg-rich β -phase dissolving at the grain boundaries; however, more grain fallout is also expected, which would increase the area of matrix available for dissolution. Non-stoichiometric dissolution is also a possible explanation for the higher ratios.

Table D.5 Summary of results from anodic polarization tests and characterization of etchant selectivity

Anodic Polarization from 15°C - 50°C				
Etchant	$R_p(\beta) : R_p(\text{SHTQ})$	$i(\beta)_{\text{SHTQ}} : i(\text{SHTQ})_{\text{corr}}$	Comparison of current densities from mass loss and polarization tests ⁴³	Etchant selectivity (rank: 1 = highest)
Nitric Acid	β corrodes faster at its OCP than the matrix at its OCP	<ul style="list-style-type: none"> * β corrodes faster than the matrix at the OCP of the matrix * Highest ratio of current densities * Ratio of current densities decreases with temperature 	$i(\text{SHTQ})_{\text{corr}}$ from polarization data is lower than that calculated from mass loss after 24-hr exposure at both 30°C and 35°C, but is within the same order of magnitude	High selectivity (1)
Phosphoric Acid	β corrodes slower at its OCP than the matrix at its OCP	<ul style="list-style-type: none"> * β corrodes faster than the matrix at the OCP of the matrix * Lowest ratio of current densities * Ratio of current densities slightly increases with temperature 	$i(\text{SHTQ})_{\text{corr}}$ from polarization data is lower than that calculated from mass loss after 24-hr exposure at 35°C, but is within the same order of magnitude	Low selectivity (3)
Ammonium Persulfate (pH 1.2)	β corrodes faster at its OCP than the matrix at its OCP	<ul style="list-style-type: none"> * β corrodes faster than the matrix at the OCP of the matrix * Intermediate ratio of current densities * Ratio of current densities fluctuates with temperature 	<i>Data not available</i>	Moderate selectivity (2)
Ammonium Persulfate (pH 0.7)	β corrodes faster at its OCP than the matrix at its OCP	<ul style="list-style-type: none"> * β corrodes faster than the matrix at the OCP of the matrix * Intermediate ratio of current densities * Current densities are higher for pH 0.7 than for pH 1.2 ammonium persulfate 	$i(\text{SHTQ})_{\text{corr}}$ from polarization data is lower than that calculated from mass loss after 24-hr exposure at 35°C, but is within the same order of magnitude	Moderate selectivity

⁴³ The average corrosion current density of the specimens after 24-hr exposure at OCP was calculated from the mass loss values. The corrosion current densities during polarization experiments were generated after 5 and 30 minute OCP holds.

